Technische Universität
Berlin

OPERATIONAL PLANNING, MODELING AND CONTROL OF VIRTUAL POWER PLANTS WITH ELECTRIC VEHICLES

vorgelegt von
Dipl.-Ing. Andreas Franz Alois RAAB
geb. in Freyung

von der Fakultät IV - Elektrotechnik und Informatik
der Technischen Universität Berlin

zur Erlangung des akademischen Grades
Doktor der Ingenieurwissenschaften
- Dr.-Ing. -

genehmigte Dissertation

Promotionsausschuss:

Vorsitzender	Prof. Dr.-Ing. Ronald Plath
Gutachter:	Prof. Dr.-Ing. Kai Strunz
	Prof. Antonello Monti, Ph.D.
	Prof. Dr. Olav B. Fosso

Tag der wissenschaftlichen Ausschprache: 26. Oktober 2017

Berlin 2018

ABSTRACT

The paradigm shift towards a more sustainable energy supply with a less detrimental environmental impact successively changes the energy sector from a polycentric towards a more distributed energy system. The presence of distributed and renewable energy sources combined with the anticipated electrification of the transport sector results in changes along the entire value chain. This so-called transformation process is accompanied by energy market deregulation and restructuring of the power system. However, in order to increase energy efficiency and improve environmental protection, investigations are needed to establish reliable and secure infrastructures. This will be accompanied by the development of suitable computer aided software solutions for energy market participants and system operators. With further advances in information and communication technology and system automation, there are significant opportunities for realizing such a sustainable energy future.

In this context, the thesis provides a comprehensive discussion of the potential application and deployment of Virtual Power Plants. Here, the aggregation concept serves as a vehicle for the implementation of coordinated and optimized control decisions by means of interconnected and interoperable solutions. The developed methodologies and functionalities are implemented through the service-oriented design and control scheme of the Virtual Power Plant for the determination of economic and technical feasible solutions in energy market and power system operations. Following the framework conditions of liberalized energy markets, an energy management algorithm for joint market operations is established which aims to integrate various distributed, renewable and mobile energy sources. A mixed integer linear programming formulation is proposed for solving the unit commitment and dispatch problem of the Virtual Power Plant operator in multi-period optimization processes. The presented methodology allows trading of various market products with variable time increments capable of solving real-time market transactions.

By providing a uniform model architecture for scalable power plant portfolios, deterministic planning methods and comprehensive investigations are performed. In particular, electric vehicles are considered as additional sources of energy in joint market operations for the provision of service-oriented operations. Furthermore, multilateral transactions are reflected in the hierarchically structured optimization

problem formulation for enhancing the allocation of power system services. The simulation results of the market-related interactions serve to identify the temporal and spatial effects in power system operations. Within this framework, a coordinated voltage control is proposed which combines both local droop controls with remote control algorithms. This allows the additional flexibilities provided by a comprehensive set of distributed, renewable and mobile energy sources to be exploited to mitigate time-varying voltage variations. In addition, the modeling of an active network management is carried out for the purpose of conducting control algorithms for electric vehicles charging in distribution systems. Appropriate evaluation functions and programming indicators are presented to determine the simulation results.

KURZFASSUNG

Der Paradigmenwechsel hin zu einer nachhaltigeren Stromversorgung mit möglichst geringen Umweltauswirkungen verändert den Energiesektor sukzessive von einem polyzentrischen zu einem dezentralistischen Energiesystem. Die Anwesenheit einer Vielzahl dezentraler und erneuerbarer Energieanlagen in Verbindung mit einer antizipierten Elektrifizierung des Verkehrssektors führt zu Veränderungen entlang der gesamten Wertschöpfungskette. Dieser sogenannte Transformationsprozess ist gekennzeichnet durch eine Deregulierung des Energiemarktes und einer Umstrukturierung des Energieversorgungssystems. Um jedoch die Energieeffizienz zu steigern und Verbesserungen im Umweltschutz zu erreichen, sind Untersuchungen zum Aufbau zuverlässiger und sicherer Infrastrukturen erforderlich. Dies geht einher mit der Entwicklung geeigneter computergestützter Softwarelösungen für Energiemarktteilnehmer und Systembetreiber. Darüber hinaus ergeben sich mit weiteren Fortschritten in der Informations- und Kommunikationstechnologie und Systemautomatisierung erhebliche Chancen für eine nachhaltige Gestaltung einer solchen zukünftigen Energieversorgung.

In diesem Zusammenhang erörtert die Arbeit in einer ausführlichen Diskussion Anwendungs- und Einsatzmöglichkeiten von virtuellen Kraftwerken. Hier dient das Aggregationskonzept als Instrument für die Umsetzung koordinierter und optimierter Kontrollentscheidungen durch die Bereitstellung interkonnektiver und interoperabler Lösungsansätze. Die entwickelten Methoden und Funktionalitäten werden in einem service-orientierten Design und Regelschema des virtuellen Kraftwerks eingebunden, um damit umsetzbare ökonomische und technische Lösungen für den Energiemarkt und das Energieversorgungssystem zu determinieren. Die Analysen zur Entwicklung ergänzender Implementierungsmethoden basieren auf numerischen Simulationen zur Ermittlung ökonomisch und technisch umsetzbarer Lösungen für die Teilnahme an den Energiemärkten sowie im operativen Netzbetrieb. Unter Einhaltung der Rahmenbedingungen liberalisierter Energiemärkte wird ein Energie-Management-Algorithmus für integrierte Marktoperationen vorgestellt, mit dem Ziel verschiedenartige verteilte, erneuerbare und mobile Energieanlagen berücksichtigen zu können. Hierfür wird eine gemischt-ganzzahlige lineare Programmierformulierung vorgestellt, um die Kraftwerkseinsatzplanung des Virtuellen Kraftwerksbetreibers in

einem Mehrperiodenoptimierungsprozess lösen zu können. Die entwickelte Methodik erlaubt den Handel von verschiedenen Marktprodukten mit variabler zeitlicher Auflösung bis hin zur Ausführung von Echtzeit-Markttransaktionen.

Durch die Bereitstellung einer einheitlichen Modellarchitektur für skalierbare Kraftwerks-Portfolios werden deterministische Planungsmethoden und umfassende Untersuchungen durchgeführt. Dabei werden besonders Elektrofahrzeuge als zusätzliche Energiequellen in gemeinsamen Marktoperationen für die Bereitstellung von serviceorientierten Operationen berücksichtigt. Darüber hinaus werden multilaterale Transaktionen für die Allokation von Systemdienstleistungen in eine hierarchisch strukturierte Formulierung des Optimierungsproblems einbezogen. Die Simulationsergebnisse der marktorientierten Interaktionen dienen zur Identifikation der zeitlichen als auch räumlichen Effekte im Netzbetrieb. In diesem Rahmen wird eine koordinierte Spannungsregelung vorgeschlagen, welche sowohl lokale als auch statische Proportionalregler mit Fernsteuerungsalgorithmen miteinander kombiniert. Dies ermöglicht die Nutzung zusätzlicher Flexibilitäten, die durch eine Vielzahl verteilter, erneuerbarer und mobiler Energieanlagen zur Verfügung gestellt werden, um zeitveränderliche Spannungsschwankungen abzuschwächen. Ergänzend wird ein aktives Netzmanagement modelliert, welches es unter anderem ermöglicht, Steuerungsalgorithmen für das Lademanagement von Elektrofahrzeugen in Verteilnetzen zu testen. Zur Bestimmung der Simulationsergebnisse werden entsprechende Auswertungsfunktionen und Programmierindikatoren vorgestellt.

ACKNOWLEDGMENTS

First and foremost, I would like to thank Prof. Dr. Kai Strunz who has advised me over the last years. I am very grateful to him for taking care of the work and for his advice as a researcher and scientist in the area of sustainable electric networks and sources of energy. My special thanks also go to Prof. Antonello Monti and Prof. Dr. Olav B. Fosso for supporting the thesis and for undergoing the evaluation and defense process.

I would like to express my gratitude to Prof. Dr. Nikos Hatziargyriou, Prof. Dr. João Peças Lopes, Dr. Spyros Skarvelis-Kazakos, Evangelos Karfopoulos, Anthony Walsh, Marius Ellingsen, and Michael Rivier whose cooperation in the MERGE project accompanied me all the way through my work dealing with electric vehicles.

I would like to thank Prof. Dietmar Göhlich, Prof., Dr. Jan Kaiser, Daniel Freund, Enrico Lauth, Dr. Sven Gräbener, Dr. Olga Levina, Simone Torzynski, Dr. Kristina Bognar, Johannes Sigulla, Mauricio Rojas, Robert Schmidt and Robert Demmig for a close collaboration during the projects Berlin Elektromobil, Berlin-Brandenburg International Showcase for Electromobility and Research Campus Mobility2Grid.

I am thankful to my colleagues, especially Dr. Arnaldo Arancibia, Dr. Maren Kuschke, Despina Koraki, Flavio Gromann, Dr. Felix Klein, Dr. Ehsan Abbasi who helped with advice and fruitful discussion. I would like to especially thank Peter Teske and Markus Gronau for the cooperation in our laboratory developments, and for providing the necessary time and resource toward our applications and hardware-in-the-loop experiments. Thanks also go to the student associates, exchange students and graduates working on different topics related to the results of the thesis, amongst them Jan Heinekamp, Marc Oertel, Jingwei Jia, Christine Hesse, Roman Sikora, Remo Amendola, Simon Spelzhausen, Niklas Prieß, and Laurin Vierrath.

I am very grateful to Stefan Mischinger, Dr. Johannes Richter, Marius Podwyszynski, Dr. Martin Kessler and Björn Krüger for encouragement and their contagious enthusiasm for science and friendship. Finally I would like to thank my family for the love and support during this long process. Thanks to all other people not mentioned here explicitly. They also contributed to the work as it evolved.

Contents

1. INTRODUCTION

1.1. Background and Motivation

The recent United Nations Framework Convention on Climate Change has adopted a range of policies and measures to limit global warming below 2 °C relative to the pre-industrial level [1]. One policy, among others, is the promotion of environmental protection by meeting the Kyoto objectives [2]. This can be achieved through the substitution of high carbon emission intensity power sources, characterized by combustion and fossil fuel-fired processes, with alternative sources of energy [3]. With regard to the policy in energy transitions, the European Union already introduced a series of reform directives in 1996, 2003 and 2009 [4]. As a result of market liberalization, modifications in the power plant portfolio and its composition are evident, which already have a considerable influence on the operational management and control strategies. The gradual phase-out of large-scale and controllable power generation, for example, impacts the present power system operation, security as well as the reliability of power supply. To mitigate these effects, conventional power plant technologies are transferred into capacity reserves and emergency standby reserves [5,6]. Therefore, expansions and innovations in power systems are required to prevent overloading of power system devices and violations of permitted operational limits [7]. Additionally, there is a need for adequate energy market frameworks with non-discriminatory and technology-neutral access for distributed and renewable energy sources [8].

Those transformation processes can be synergistically complemented with changes in the transportation sector where vehicles with combustion engines are substituted by electric vehicles. Here, diversification of the individual traffic and development of mobility concepts are noticeable. This applies in particular to mega-cities and mega-urban regions, which are impacted by high smog and air pollution [9, 10]. The electrification of the transport sector means on the one hand an increase in the energy demand which has to be served. On the other hand, this offers the opportunity to make use of those additional mobile energy sources for energy market participation and power system operation. Therefore, a set of appropriate technical and organizational measures are required to consider the spatial and temporal

availability of electric vehicles and reflect the level of controllability of these load or generation units. Accordingly, the Virtual Power Plant concept is adopted as part of this thesis and extended in this respect.

1.2. Thesis Statement and Primary Research Objectives

The purpose of this thesis is to explore the conceptual requirements for the development and application of Virtual Power Plants in liberalized and unbundled energy markets. The primary objective of this thesis involves the derivation of a methodology to establish a means to:

> Facilitate the energy and mobility transition through the deployment of enhanced operational planning, modeling and control methods for the coordination of distributed, renewable and mobile energy sources. Extend conventional programs and algorithms for modeling and analyzing power plant portfolios to achieve optimized, reliable and affordable energy supply.

Special focus is placed on the issues of forecast uncertainties and compensation of power imbalances in joint market operations and control algorithm for coordinated voltage regulation to support power system operations. In order to achieve these objectives, the proposed framework covers the following methodological aspects:

- examine the market framework conditions, incorporate electric vehicles and combine the unit commitment and dispatch problem with appropriate optimization models in accordance with the operational strategy of the Virtual Power Plant
- develop suitable model architectures that reduce the amount of information and data handling and establish an energy management algorithms to solve hierarchically structured optimization problems under consideration of forecast uncertainties
- investigate real-time balancing mechanisms to mitigate power imbalances and improve voltage profiles in distribution systems through active and reactive power adjustments and provide flexibilities for power system operations

- categorize, model, implement and control various distributed, renewable and mobile energy sources, perform simulations and analyzes the results

The Virtual Power Plant is developed under Matlab environment and applies numerical algorithms and software to solve the optimization problems. A variety of real-data sets consisting of descriptive unit type model attributes and sets of profiles obtained from historical measured data are incorporated. The implications of the developed control concepts for the localization and provision of ancillary services and coordinated redispatch measures are simulated and explored in steady-state analysis.

1.3. Outline of the Thesis

The thesis is organized in six chapters that are divided into three main parts. The first part provides an introduction and background of the thesis and identifies the overall framework conditions (Chapter 1 and 2). The second part discusses the development of an unified model architecture that integrates multiple unit types of energy sources including electric vehicles. Energy management solutions for trading various market products within multi-period optimization processes are investigated capable of solving real-time market transactions in joint market operations (Chapter 3 and 4). The third part establish service-oriented functions for enhanced power system operations through coordinated voltage regulation. Potential impacts and benefits arising from the developed coordinated voltage control regulation are investigated in steady-state power system simulations (Chapter 5). The final part (Chapter 6) summarizes the key findings and discusses perspectives for further developments and improvements. The contents of each chapter are outlined in the following paragraphs.

Chapter 2 investigates the legal, organizational and technical aspects related to the operational planning of Virtual Power Plants. First, the implication of the increasing share of renewable energy sources on the future energy supply is assessed in scenarios for 2030, 2040, and 2050, using Germany as an example. Then, the background and state of the art of Virtual Power Plant deployments is provided. As an example, the interoperability and operating schemes of a physically realized Virtual Power Plant with Microgrid architectures is described as part of a research and laboratory environment. Finally, the energy market characteristics and participation opportunities of Virtual Power Plants are briefly discussed.

Chapter 3 introduces a unified model architecture and develops a nodal-based aggregation and energy management algorithm for Virtual Power Plants, considering

the presented framework characteristics of liberalized energy markets in Chapter 2. Comprehensive mathematical formulations of the model architecture and coordination algorithm with integrated optimization functions are detailed. Based on stochastic simulation methods, the effects of forecast uncertainties on the determination of the optimized scheduling processes in joint market operations are assessed. Here, a method for the modeling of synthetic forecast profiles for the intermittent power generation of renewable energy sources is proposed.

Chapter 4 shows the extension of the unified model architecture to incorporate also unit types of mobile energy sources in terms of electric vehicles suggests an organizational framework for the large-scale integration of electric vehicles. Additional market entities which are involved in the charging and aggregation process of theses mobile energy sources are introduced. Under consideration of state-of-the art charging infrastructures and standards, a SoE-based charging and tarification model is developed and combined with price-based charging in Chapter 3. Different charging strategies are presented along with implications of the optimized charging strategies embedded in the control decision of the Virtual Power Plant through a hierarchically structured optimization. Simulation and computational studies exposes the viability of the extended optimized charging strategies in scenarios for optimized energy procurements and nodal redispatch measures.

Chapter 5 proposes a coordinated voltage regulation based on enhanced voltage droop control modes. The interactions and control schemes of the Virtual Power Plant and system operator are substantiated in mathematical formulations. Different possible operation modes are integrated in an European 20 kV distribution network benchmark. The results of the AC power flow analysis show the implications of the combined local and remote control approach for multiple power sources and system devices. The evaluated control schemes, including steady-state operations of on-load tap-changing transformer, demonstrate the applicability for the localization and provision of ancillary services of the Virtual Power Plant.

Chapter 6 contains the concluding remarks and a summary of the main results achieved and gives an outlook for possible future work.

The Appendix provides comprehensive assessments of the analyzed energy markets and an overview of power plant portfolio parameters. Further, details of the unit type models, attributes and profile characteristics are provided. The European 20 kV distribution network benchmark used throughout the research is detailed by mathematical models and control parameters. Supplementary specifications and simulation results are summarized.

2. FRAMEWORK REQUIREMENTS FOR VIRTUAL POWER PLANTS AND DEPLOYMENTS IN LIBERALIZED ENERGY MARKETS

Abstract – In order to facilitate the deployment of Virtual Power Plants in liberalized energy markets, potential applications are investigated. The potentials are discussed in terms of the transformation change of the power plant portfolio in Germany over the last decades. Based on the governmental goals of Germany in 2030, 2040 and 2050, the implications on the future energy supply with renewable energy sources are estimated. The legal, organizational and technical aspects related to the Virtual Power Plant concept are identified. In this context, smart grid frameworks and deployments are presented. Details on the interoperability and operating schemes of a physical realized Virtual Power Plant with Microgrid architectures as part of a research and laboratory environment are provided. Based on comprehensive statistical assessments, participation opportunities in liberalized energy markets are presented.

Keywords – actor analysis, energy economics, information and communication technology, market deregulation, market participation, power plant portfolios, supervisory control system, supplier/aggregator.

2.1. Introduction

With the increasing share of distributed and renewable energy sources in power systems and energy markets, the operation of fossil-fulled power plants become unprofitable due to less operating hours and lower wholesale market prices. This is caused by the merit order effect of renewable energy sources [11, 12]. Hence, the demand of electricity generated by power plants with conventional energy sources is decreasing [13, 14]. The effect is especially reflected in terms of the wholesale energy prices. Figure 2.1 shows an example of the decreasing average auction prices on the day-ahead market of the German-Austrian bidding zone. The listed average hourly index prices are derived from published information of the European Energy

Exchange and the European Power Exchange for spot market auctions. The daily average price in per unit refers to the absolute values provided on the right hand side. Particularly in times of high power injection of renewable energy sources, represented by the predicted average power provided by wind power plants (wind) and photovoltaic power plant (pv), the daily average prices dropped significantly. Appendix A.1 provides further assessments of the energy market characteristics.

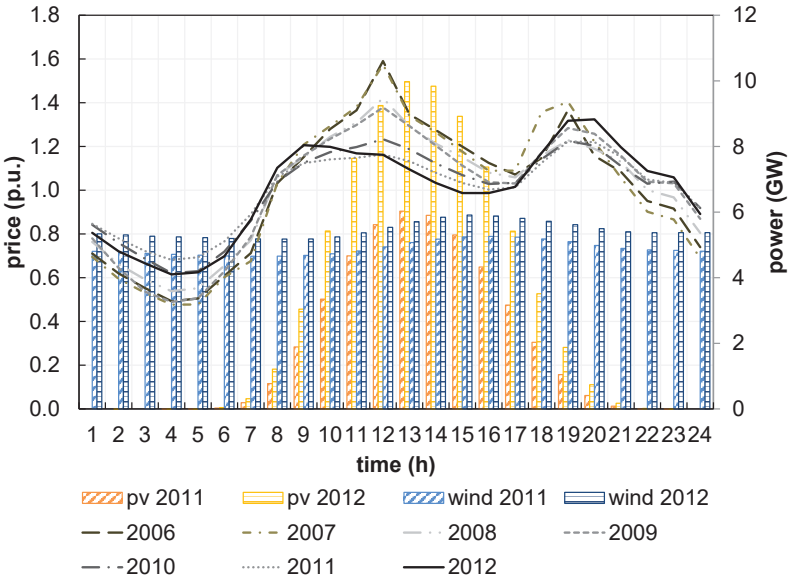

year	daily average price (EUR/MWh)
2008	65.76
2009	38.85
2010	44.49
2011	51.12
2012	42.60

Fig. 2.1.: Average day-ahead auction prices (2006-2012) in the German-Austrian bidding zone in correlation with foretasted power injection of renewable energy sources (2011-2012).

As a result of decreasing market prices, power plant operators take less efficient and unprofitable power plants out of service. This also includes fast controllable power plants, which actually contribute to the provision of ancillary services [15]. In regard to power system stability, the decommissioning of large-scale power plants leads to reductions of immediately available kinetic energy of rotating masses as well as loss of reactive and short circuit power for static and dynamic voltage control [7]. Therefore, power system operations become more complicated by the fact that a considerable number of small-scale power plants will play a much greater role in the energy supply. Through the aggregation and coordinated action of various small-scale generation, load and storage systems the integration process in power systems and energy markets can be facilitated [16–18]. Therefore, the Virtual Power Plant concept is applied and further investigated with regard to the development of advanced control and planning methods. In general, the Virtual Power Plant concept can be used by Supplier/Aggregator (S/A) as intermediary between a large number of units or unit clusters, system operators and market participants [19]. Supplier/Aggregator is the entity which manages generation and load demands, sells or purchases electricity with the purpose of offering demand side management and other possible ancillary services. In the following sections, the Virtual Power

Plant concept is further detailed. Specifications and applications within liberalized energy market framework are provided.

2.2. Decentralization and Transformation Process

The development of appropriate Virtual Power Plant concepts requires the identification of legal, organizational and technical aspects for the application in future energy systems. Here, three sets of power plant technologies with corresponding unit types are differentiated, namely the set of conventional technologies H_{ces} , renewable technologies H_{res} , and storage technologies H_{stor} :

$$\begin{aligned} H_{\text{ces}} &= \{\text{nuclear}, \text{lignite}, \text{hard}, \text{coal}, \text{gas}, \text{chp}, \text{dg}\}\,, \\ H_{\text{res}} &= \{\text{wind}, \text{pv}, \text{bio}, \text{hydro}\}\,, \text{ and } H_{\text{stor}} = \{\text{ps}, \text{bat}, \text{ev}\}\,. \end{aligned} \tag{2.1}$$

The categorization of the unit types is based on the used source of energy or the respective power plant technology. The unit types are defined as follows:

> nuclear:= nuclear power plant, lignite:= lignite-fired power plant, hard coal:= hard-coal-fired power plant, gas:= gas-fired power plant, chp:= combined heat and power plant, dg:= distributed generators with internal combustion engines, wind:= wind power plant, pv:= photovoltaic power plant, bio:= biomass and bio-gas power plant, hydro:= hydro power plant, ps:= pumped-storage system, bat:= stationary battery system, ev:= electric vehicles.

The transformation process in the energy sector is assessed by means of the following elaborations that focus on the cross energy supply, installed capacities and number of installed power plants. The data originate from the Federal Ministry for the Environment, Nature Conservation, Building and Nuclear Safety [20], the German Federal Network Agency [21], the German section of the International Solar Energy Society [22] and the German Federal Ministry of Economics and Technology. The data set is enriched with information from the International Solar Energy Society to supplement power plants with installed capacities of 20 MW and lower.

2.2.1. Power Plant Portfolio Composition and Changes

Alongside a steady decline of power plants with conventional energy sources in Germany, the power plant capacity of decentralized and renewable energy sources has increased significantly in the last decades. The total amount of power plants in Germany covers more than 1.5 million decentralized and renewable energy sources across all voltage levels. A summary of the composition of the power plant portfolio for 1990 and 2014 is given in Appendix B. According to [23], the total capacity of large-scale power plants with conventional energy sources, namely nuclear, lignite, and hard coal was ∼86 GW in 1990 and decreased to ∼62 GW in 2014. In terms of power plants with more than 20 MW installed capacity, Fig. 2.2 shows the differences of the rated power in 1990 compared to 2014. The black dashed line shows the log-normal distribution. The capacities of large-scale power plants more than 100 MW installed capacity changed in the probability distribution of the overall power plant portfolio, and displacements at lower installed capacities can be denoted. The presence of small-scale power plants in the overall power plant portfolio results in a leftward shift and densification in the lower capacity ranges. The changes are highlighted with red rectangles in Fig. 2.2b.

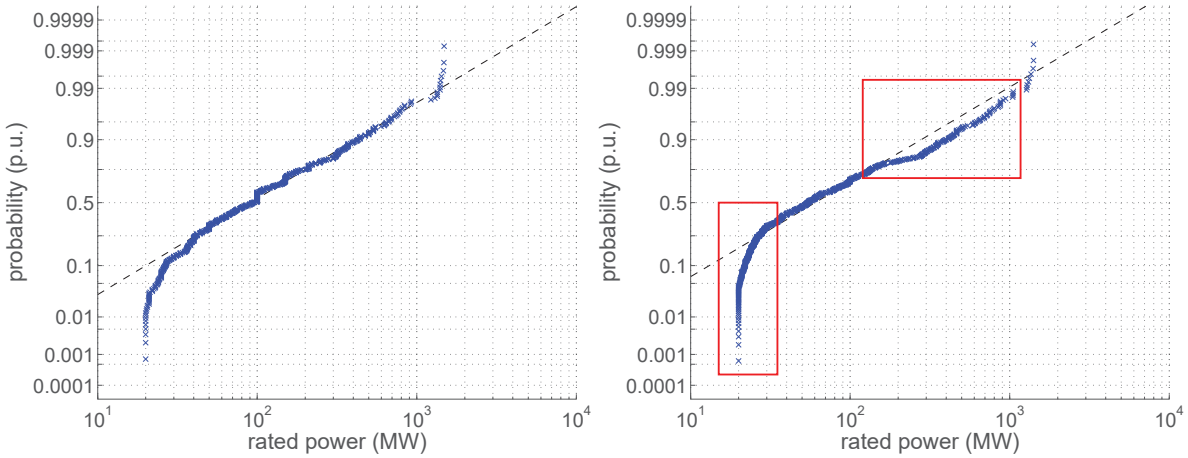

(a) power plant portfolio 1990, N=690 (b) power plant portfolio 2014, N=827

Fig. 2.2.: Probability density functions of power plant capacities in Germany for (a) 1990 and (b) 2014 with more than 20 MW rated power.

In terms of power plants between 20 MW and 50 MW rated capacity, the proportionate share of 31 % in 1990 shifted to 42 % in 2014. The number of power plants with the energy sources nuclear, lignite and hard coal has decreased by more than 50 % in the last decades. This is also a matter of fact of the German government's nuclear phase-out decision [24], ongoing changes in energy policy and regulations, supporting the integration of renewable energy sources. The changing characteristic of the power plant portfolio in Germany with renewable energy sources is illustrated

by means of Fig. 2.3. The majority of photovoltaic power plants are allocated in the low voltage (LV) and medium voltage (MV) level, whereas wind power plants are typically connected to medium and high voltage (HV) power systems. With increasing capacity and longer distances in alternating current systems, most offshore wind farms are integrated with high-voltage direct current technology [25]. Irrespective of the geographical distances of the site locations, those capacities are transferred on extra high voltage transmission systems (EHV) to high demand areas.

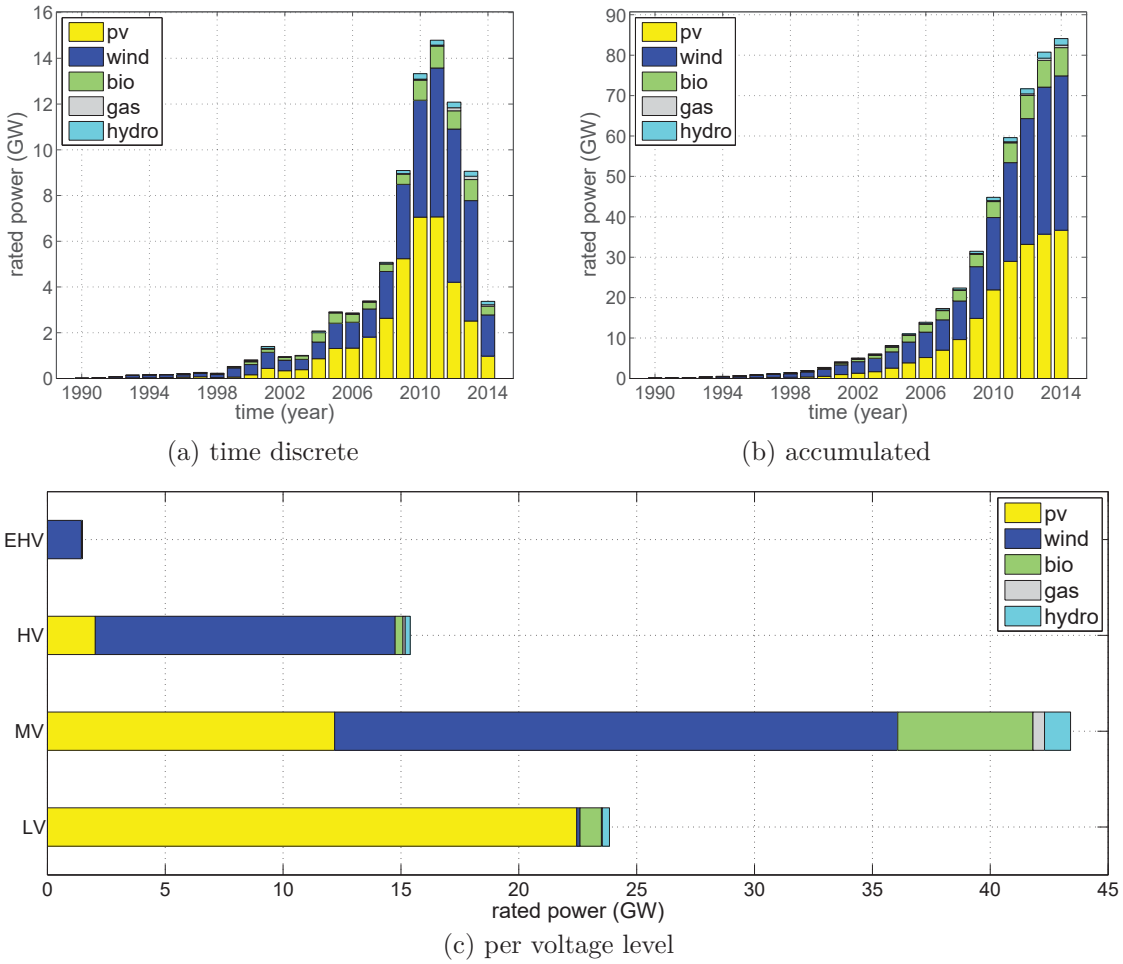

(a) time discrete

(b) accumulated

(c) per voltage level

Fig. 2.3.: Annual (a) time discrete and (b) accumulated installed capacity of renewable energy sources (1990-2014) in Germany, and (c) sorted by voltage level (2014).

In 2014, the large number of photovoltaic power plants represents almost 97 % of the total number of power plants with N=1,557,494 and 84.499 GW installed capacity. In comparison to wind power plants, which have almost the same share of installed capacity, the total number just accounts for 2 %. Table 2.1 provides an overview of the installed capacities grouped by voltage levels. With more than 80 % installed capacity in mainly lower voltage levels, the ongoing transformation process of the power plant portfolio is emphasized. In order to handle the operational problems related to the increased share of intermittent power generation of renewable energy sources, more and more redispatch and feed-in management measures are neces-

sary [26]. Without compromising the overall reliability of power systems, adequate coordination and active management approaches are required.

TABLE 2.1.: Installed capacity of renewable energy sources in Germany (2014) sorted by voltage levels, installed capacity 84.499 GW, N=1,557,494.

voltage level		voltage ranges	share of renewables*)	
			(GW)	(%)
Extra High Voltage	EHV	220 kV - 380 kV	1.53	1.8
High Voltage	HV	50 kV - 150 kV	15.57	18.4
Medium Voltage	MV	6 kV - 30 kV	43.43	51.4
Low Voltage	LV	230 V - 400 V	23.97	28.4

*) data refer to power plants promoted by the legal framework of the Renewable Energy Act.

2.2.2. Governmental Goals and Future Energy Supply

Influenced by the transformation process in the energy sector, the current framework of European liberalized energy markets also becomes subject to major changes [27–29]. Further progress towards this objective also raises important issues regarding the operating hours of the power plant technologies to maintain profitability and reach at the same time distinct governmental goals. To estimate the required amount of renewable energy sources to cover a desired share in the overall energy mix, further analyses are carried out using the full load hours FLH as an indicative criteria. The full load hours are calculated by (2.2), as a function of the power plant utilization at a constant level of power generation over a given time period T.

$$FLH = \frac{\sum_{t=1}^{T} P_{\mathrm{g},t} \cdot \Delta t}{P_{\mathrm{r}}} = \frac{E_{\mathrm{g}}}{P_{\mathrm{r}}} \quad \forall t \in T \tag{2.2}$$

The power generation P_{g} is multiplied with a variable time increment Δt and divided by the rated power P_{r}. The sum of the power generation gives the total energy E_{g} provided over the defined time period. Alternatively, the capacity factor may be used for the calculation, which is defined by the ratio of full load hours over a defined time period. Since the share of renewable energy supply in the gross energy demand depends on the installed capacity and provided energy within a defined period of time, the full load hours vary significantly in time and location, as detailed in Appendix B for wind and photovoltaic power plants. Table 2.2 indicates possible full load hours for the introduced power plant technologies.

TABLE 2.2.: Classification of conventional, renewable and storage technologies by unit types and respective sources of energy and assigned annual full load hours FLH.

conventional technologies		renewable technologies		storage technologies	
unit type	$FLH^{*)}$ (10^3h/a)	unit type	$FLH^{*)}$ (10^3h/a)	unit type	$FLH^{*)}$ (10^3h/a)
nuclear	6.20/<u>7.64</u>/8.30	wind	0.80/<u>1.65</u>/4.00	ps	0.10/<u>0.98</u>/2.00
lignite	5.00/<u>6.85</u>/8.00	pv	0.65/<u>0.97</u>/1.10	bat	- / - / -
hard coal	3.60/<u>3.79</u>/4.50	bio	5.00/<u>6.05</u>/7.00	ev	- / - / -
gas	0.50/<u>3.21</u>/3.80	hydro	0.90/<u>3.16</u>/6.20		
chp	2.70/<u>4.00</u>/6.50				
dg	1.00/<u>4.50</u>/6.00				

*) calculations and assumption based on [30–32] indicating low / <u>average</u> / high utilization.

Next, a power plant portfolio for a whole country *cnt* is constituted and installed capacities of conventional $P^{\mathrm{ces},cnt}_{\mathrm{r},year}$ and renewable energy sources $P^{\mathrm{res},cnt}_{\mathrm{r},year}$ aggregated. Then, considering the gross energy demand $E^{cnt}_{\mathrm{d},year}$, the energy balance calculated in (2.3), can be formulated with the sum of the corresponding energy equivalents.

$$\begin{aligned} E^{cnt}_{\mathrm{d},year} &= E^{\mathrm{ces},cnt}_{\mathrm{g},year} + E^{\mathrm{res},cnt}_{\mathrm{g},year} \\ &= P^{\mathrm{ces},cnt}_{\mathrm{r},year} \cdot FLH^{\mathrm{ces},cnt}_{year} + P^{\mathrm{res},cnt}_{\mathrm{r},year} \cdot FLH^{\mathrm{res},cnt}_{year} \end{aligned} \tag{2.3}$$

Finally, expressing the share of renewable energy sources in the annual cumulated gross energy demand by $\Gamma^{\mathrm{res}} = \frac{E^{\mathrm{res},cnt}_{\mathrm{g},year}}{E^{cnt}_{\mathrm{d},year}}$, (2.3) can be rewritten as (2.4).

$$E^{cnt}_{\mathrm{d},year} = \frac{P^{\mathrm{ces},cnt}_{\mathrm{r},year} \cdot FLH^{\mathrm{ces},cnt}_{year}}{1-\Gamma^{\mathrm{res}}} = \frac{P^{\mathrm{res},cnt}_{\mathrm{r},year} \cdot FLH^{\mathrm{res},cnt}_{year}}{\Gamma^{\mathrm{res}}} \tag{2.4}$$

For example, the average full load hours of the power plant technologies in Germany are calculated by (2.5) based on historical data. The energy equivalents are normalized to the base of the rated capacity.

$$\begin{aligned} FLH^{\mathrm{res,ger}}_{2011} &= \frac{E^{\mathrm{res,ger}}_{\mathrm{g},2011}}{P^{\mathrm{res,ger}}_{\mathrm{r},2011}} \approx \frac{120\ \mathrm{TWh}}{70\ \mathrm{GW}} \approx 1.7\ (10^3\mathrm{h/a}) \\ FLH^{\mathrm{ces,ger}}_{2011} &= \frac{E^{\mathrm{ces,ger}}_{\mathrm{g},2011}}{P^{\mathrm{ces,ger}}_{\mathrm{r},2011}} \approx \frac{470\ \mathrm{TWh}}{98\ \mathrm{GW}} \approx 4.8\ (10^3\mathrm{h/a}) \end{aligned} \tag{2.5}$$

Figure 2.4 shows the power plant capacity between 1991 and 2011. The red line indicates the overall decrease in the average full load hours.

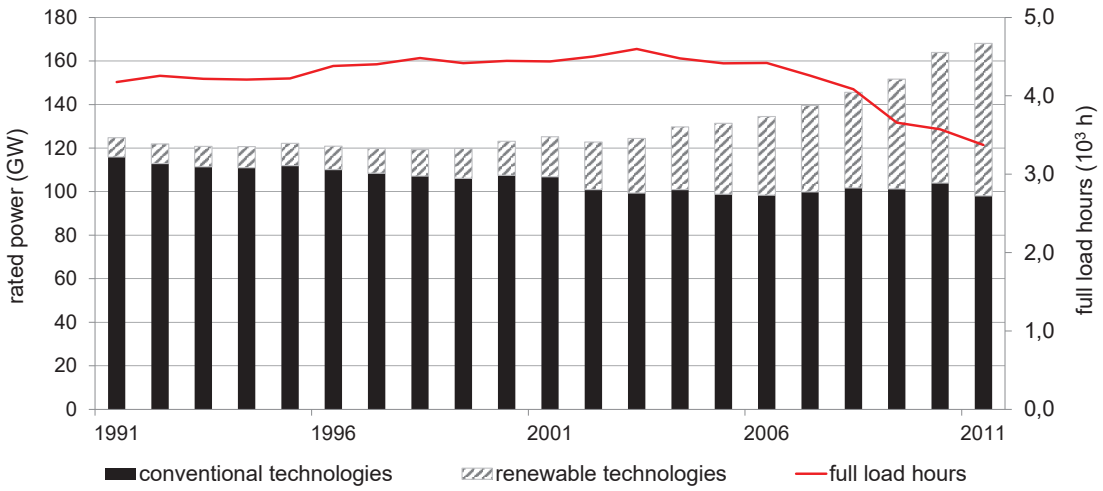

Fig. 2.4.: Calculated average full load hours of the power plant portfolio (1991-2011) in Germany as a function of installed capacities of conventional and renewable technologies.

For the estimation of the required capacities of renewable energy sources to cover defined shares in the gross energy demand, the derived values are applied within the following scenarios. Taking the governmental goals in Germany as an example, Table 2.3 lists the scenarios for 2030, 2040 and 2050. The cumulated annual gross energy demand is assumed with $E^{\mathrm{ger}}_{\mathrm{d},2011} = 588$ TWh. Scenario 1 [33] denotes the proposed goals of the German Federal Government. Scenario 2 and 3 show addition estimates according to Frauenhofer IWES and the German Institute for Aerospace and Aeronautics [31].

TABLE 2.3.: Share of renewable energy sources in the gross energy demand of Germany in 2030, 2040 and 2050 for defined scenarios.

share of renewables in	scenario 1	scenario 2	scenario 3
2030	50 %	59.5 %	59.9 %
2040	65 %	67.6 %	70.5 %
2050	80 %	74.3 %	78.8 %

The introduced (2.4) is reformulated to obtain (2.6) and determine the required cumulated installed capacity $P^{\mathrm{res,ced}}_{\mathrm{r},year}$ of renewable energy sources with a desired share in the overall energy mix. The initialized data is assigned in accordance with (2.5), where the cumulated annual gross energy demand is assumed to be constant over the next decades.

$$P^{\mathrm{res},cnt}_{\mathrm{r},year} = \frac{\Gamma^{\mathrm{res}} \cdot E^{cnt}_{\mathrm{d},year}}{FLH^{\mathrm{res},cnt}_{year}} \quad \Leftrightarrow \quad P^{\mathrm{ces},cnt}_{\mathrm{r},year} = \frac{(1-\Gamma^{\mathrm{res}}) \cdot E^{cnt}_{\mathrm{d},year}}{FLH^{\mathrm{ces},cnt}_{year}} \tag{2.6}$$

Within the framework assumptions and introduced scenarios, Fig. 2.5 shows the share of renewable energy sources in the power plant portfolio and the overall calculated average full load hours. The estimating calculation can be extended by further influencing factors such as the annual increase of energy demand or adjustment of the respective average full load hours for defined power plant technologies.

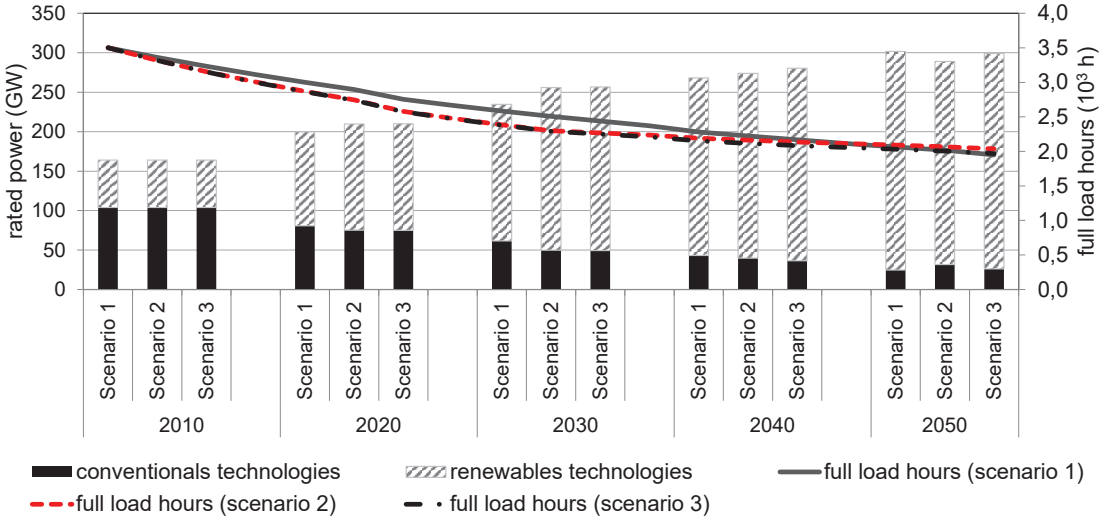

Fig. 2.5.: Scenarios with estimations of required power plant capacities (2010-2050) to cover defined shares in the gross energy demand with renewable energy sources.

The scenarios lead to similar results, with noticeable increase of the total installed capacity even though the gross energy demand is assumed to be constant. Compared with the base scenario with approximately 174 GW installed capacity of the power plant portfolio, almost twice as much capacity is needed to cover the future amount of gross energy demand in 2050 due to the lower average full load hours of renewable energy sources. Thus, the overall average full load hours of the entire power plant portfolio is $2.0 \cdot 10^3$h/a in 2050.

2.3. Application of Virtual Power Plant Concepts

As the power generation of renewable energy sources depends on the weather conditions, the before mentioned calculations also imply power generation surplus during solar and wind peak hours in time periods of extreme weather conditions. Therefore, adjustments in the power system and energy market design are required [34]. Here, the development of smart grid solutions can contribute to overcome some of the challenges associated with the transformation process in the energy sector. The Institute for Energy and Transport of the European Commission has implemented

a platform of reported smart grid projects in Europe since 2002 [1]. With regard to the development and implementation of the Virtual Power Plant concept, research projects, such as the EU-DEEP, FENIX, MERGE, SUSTAINABLE, or SUNSEED are carried out for demonstration and research purposes. The projects illustrate the variety of research questions associated with the Virtual Power Plant concept. However, there are some key objectives and efforts which include the following aspects:

- aggregation of multiple generation, load and storage systems
- consideration of variable power generation of renewable energy sources
- application of forecast processes and predictive analysis
- preparation of bidding strategies and scheduling profiles
- access and cost-effective participation in energy markets
- extension of information and communication infrastructures
- development of enhanced energy management systems and control schemes
- provision of ancillary services and support in power system operation

However, the proposed solutions differ considerably with respect to the integrated power plant technologies, system devices and rated capacities of the aggregated units and unit clusters. The listed projects indicate that few Virtual Power Plants exploit the potential of demand side management by the utilization of storage technologies and shiftable loads. Further, electric vehicles as mobile storage units are considered in demonstration projects, but not yet physically integrated.

2.3.1. Categorization, Characteristics and Functionalities

Considering generation, load and storage systems as single units or unit clusters, Fig. 2.6 illustrates possible allocations in partial feeders of the power system, adjacent places or regions. Either connected with (i) neighboring and/or higher-level power systems or (ii) autonomously, if disconnected from the power system [35, 36], these partial feeders can be considered as Microgrids. However, the single units or unit clusters or the entire Microgrid can be also considered as part of the Virtual Power Plant [35,37]. Hence, the Virtual Power Plants may profit from the geographical differences, technical differences and temporal availabilities.

[1] available on http : //ses.jrc.ec.europa.eu

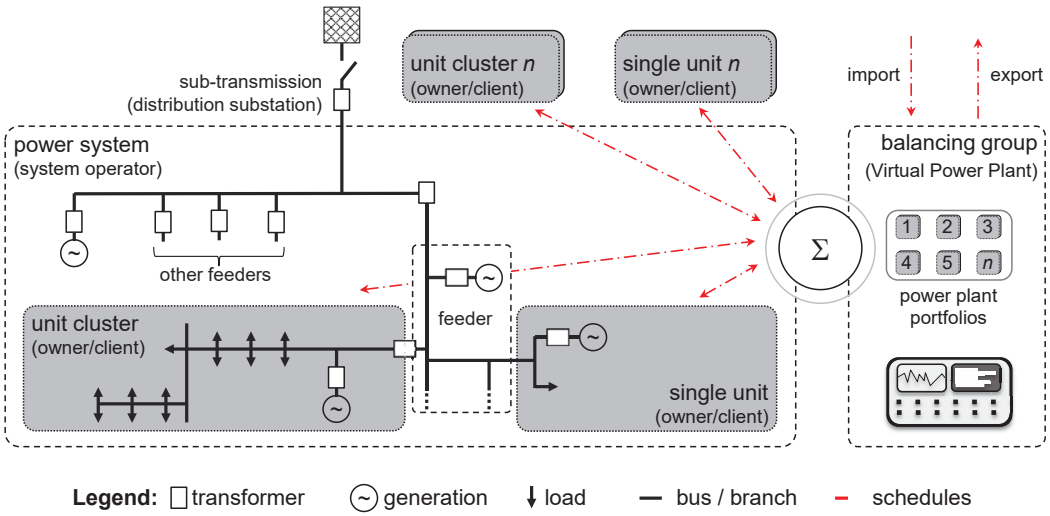

Fig. 2.6.: Schematical allocation of distributed and renewable energy sources in power systems and assignment to the balancing group of the Virtual Power Plant.

The aggregation concept further allows to reduce the complexity for market participants [38], while providing providing firm capacity and technical features for market participation and power system operation. Thus, the listed synergies and advantages as listed in Table 2.4 can be achieved.

TABLE 2.4.: Synergies and advantages of unit and unit cluster operators (owner/client) and Virtual Power Plant operator (aggregator/supplier).

wishes of unit and unit cluster operator (owner/client)	**offerings of virtual power plant operator (supplier/aggregator)**
• overcome substantial barriers to energy market entry	• achieve greater efficiency through economies of scale and scope
• gain access and visibility across the energy markets	• optimize the energy market position and maximize the revenue opportunities
• increase value of assets through market participation	• improve of efficiency and value of power plant portfolio
• simplify and reduce individual transaction cost	• mitigation of financial risk through aggregation and flexibility
	• improve ability to negotiate commercial conditions

One possible integration of the Virtual Power Plant concept in liberalized energy markets is illustrated by means of Fig. 2.7. The use case diagram schematizes the relationship between the main market entities and architectural elements. The arrows show the direction of the exchanged functionalities.

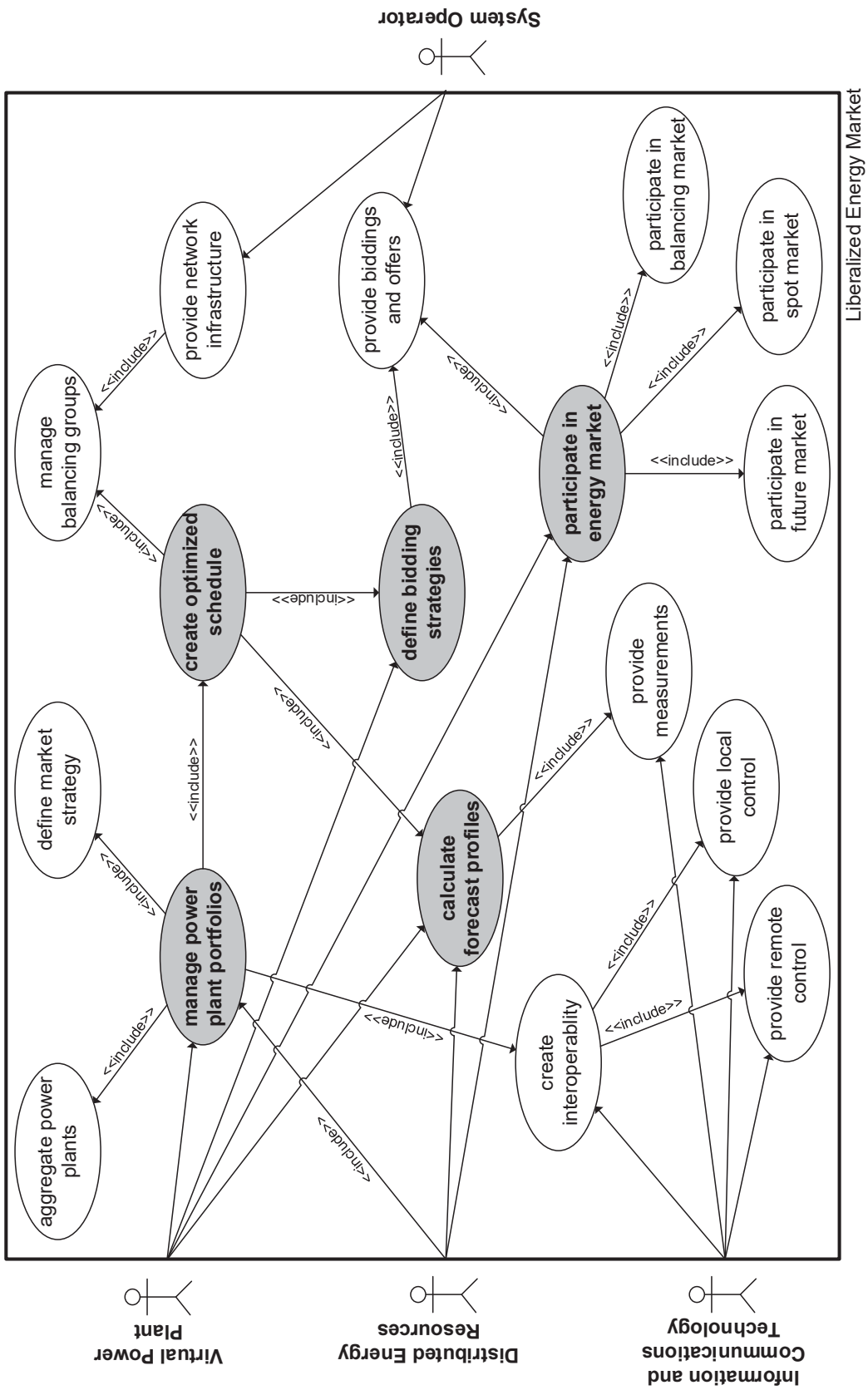

Fig. 2.7.: Use case diagram of main market entities and architectural elements of the Virtual Power Plant operator for the coordination of distributed and renewable energy sources in liberalized energy markets.

The functionalities covers main use cases, including (i) aggregation and monitoring, (ii) optimization and energy scheduling, (iii) representation and participation opportunity in energy markets and (iv) accounting of coordinated units and unit clusters. System operators can benefit from the optimal use of available capacity and may therefore be able to increase the efficiency of power system operation with improved coordination actions. In addition to the maximization of cost effective values in energy markets, the optimized market and service position can provide further revenue opportunities for the individual market participants.

2.3.2. Interoperability Layers and Communication Interfaces

Intelligent monitoring, control and communication enables the Virtual Power Plant to efficiently coordinate and manage distributed and renewable energy sources. Based on high data transfer bandwidth and low-cost access [39], the coordinative interaction can be automated and realized with supervisory control and data acquisition (SCADA) and energy management systems (EMS). The emergence and availability of the following information and communication technologies (ICT) can be used for such interconnected systems:

- smart meters
- intelligent electronic devices
- wireless and cable connections
- central control computer
- software applications

Necessary data are exchanged bi-directionally, processed and adjustment of the power generation or demand realized. This enables the Virtual Power Plant operator to meet optimized schedules in energy market tradings, respond to requested system services and improve the use of energy within the power plant portfolio. Bi-directional communication with distributed and renewable energy sources is already realized to ensure feed-in management measures or reduce the injected power of generation units to solve network congestions. However, the variety of systems and components provided by different manufacturers complicates the interoperability of the system as a whole. The implementation of advanced control and planning methods requires appropriate processing of information flows in interoperability layers, defined as the capability of two or more networks, systems, devices, applications, or components to externally exchange and handle information securely and effectively [40]. Protocols, canonical models and languages connect the interfaces and ensure interoperable information exchange between power system devices and components throughout the communication structure. In smart grid applications, several standardized protocols exist to cover certain information related interfaces [41] and can be distinguished in (i) open and (ii) closed protocols. While open protocols

allow standardized information and communication exchange, closed protocols represent proprietary solutions. Standardized communication protocols for information related interfaces create interoperable information flows from process to operation zones, as schematically structured by means of Fig. 2.8. The structure allows the assignment of communication and security protocols in smart grid architectures and provides on overview of possible solutions to standardize information related interfaces.

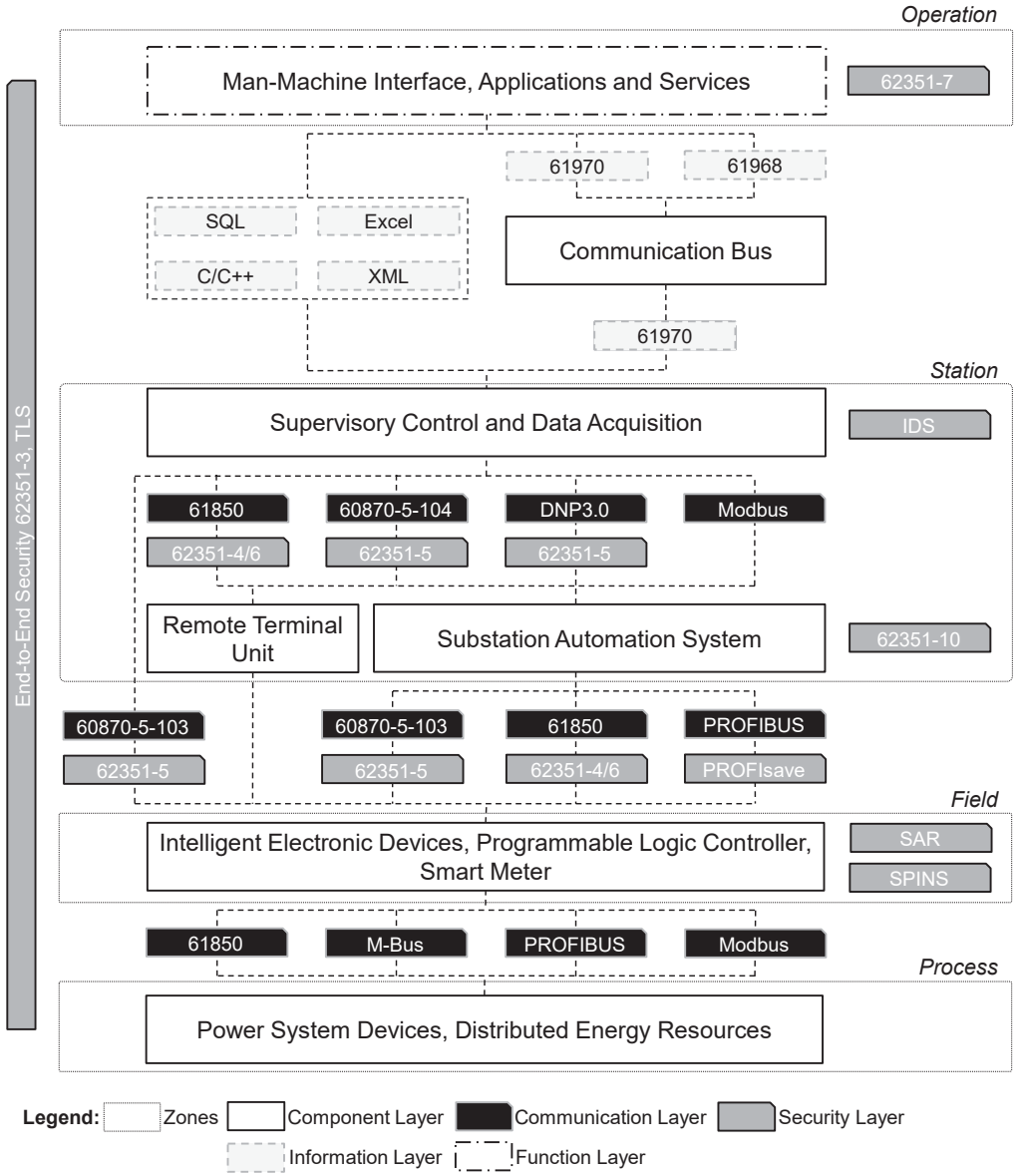

Fig. 2.8.: Layers and zones of communication structures that advance interoperability and address cybersecurity concerns applicable for smart grid architectures.

In compliance to the Smart Grid Architecture Model [42], the interoperability layers are categorized into hierarchically structured levels of power system management zones. The layers correspond to components, communication, information, and func-

tions while the zones reflect processes, fields, stations and operations. The information flows from process to operation zones are illustrated with dashed lines. In general, local control of power system devices and components requires low latency, e.g. IEC 61850 with less than 4 ms, and highly reliable communication of measurement and actuator to guarantee secure operation. Through intelligent electronic devices and programmable logic controllers, distributed control is also possible. Therefore, programmable logic controllers and smart meters communicate amongst each other and use protocols to distribute applications, reuse components and provide platform independency [43]. Additionally, security protocols and mechanisms have to be considered for the provision of secure data exchanges and protection against outages and cyberattacks [44, 45]. These security measures can be categorized into mandatory and recommended requirements:

- **mandatory:** confidentiality, integrity, availability, authenticity
- **recommended:** authentication and access control, communication efficiency and security, self-healing and resilience operations

Beside interoperable integration of information and communication technology, reliable and secured online measurements as well as current market and forecast data are necessary for the optimized management and control of the coordinated distributed and renewable energy sources. Therefore, a high level of standardization for interfaces and protocols is necessary in order to provide feasibility and flexibility for the integration process.

2.3.3. Realized Microgrid Architectures and Interconnections

The systemic complexity for the implementation of interconnected systems is captured in the physical realization of a Virtual Power Plant with Microgrid architectures, while [46] discusses further details. The interconnected systems are located at the European Energy Forum (EUREF-Campus) in Berlin-Schöneberg and at Technische Universität Berlin (TU-Berlin), Germany. Both test sites are operated as Microgrid architectures within local area networks. In the following elaborations, descriptive analysis of the relevant system components and evidence regarding the applicability of communication interfaces are detailed. The considered power system at EUREF-Campus is realized as low voltage smart distribution feeder connected to a 630 kVA transformer [47–49]. The local area network is realized as point-to-point and point-to-multipoint communication via Modbus TCP as standard industrial automation and part of the IEC 61158 for real-time distributed control. The low voltage distribution feeder at TU-Berlin is connected to a programmable in-

verter and can be operated up to 90 kVA. The power system is constructed as ring network with real-time Ethernet for Control Automation Technology (EtherCAT) interconnections between the integrated power system devices. Figure 2.9 shows the schematic interconnection of the Microgrids architectures including the supervisory and data acquisition structures. The system architecture is modular structured and scalable.

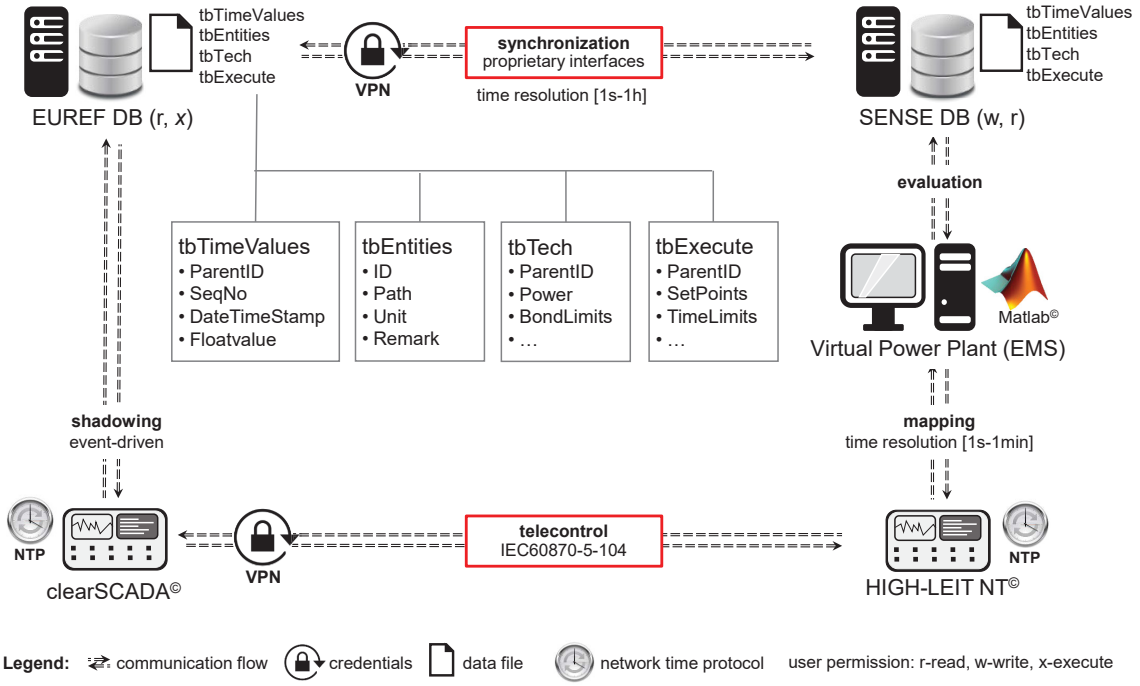

Fig. 2.9.: Interconnection and data exchanges of physically realized Microgrids architectures through (i) synchronization of databases and (ii) telecontrol equipment and systems.

The execution of application programs and software-interapplication can be realized through canonical data models, information systems, machine and program languages. Wide area networks [50, 51] and common network time protocol (NTP) for the clock synchronization of the integrated control centers are applied. Under consideration of secured information exchange, the interconnection can be realized through (i) synchronization of databases and (ii) telecontrol equipment and systems. The synchronization of databases allows data reconciliation and archiving without continuous operation, while telecontrol protocols provide reliable and safe transmission of recorded information during operation. In the next stage of development, the following bi-directional data exchange between the control centers is foreseen:

$$\text{VPP} \longleftrightarrow \text{HIGH-LEIT NT}$$
$$\longleftrightarrow \text{IEC 60870-5-104} \longleftrightarrow \text{clearSCADA}$$
$$\longleftrightarrow \text{Remote Terminal Unit} \longleftrightarrow \text{ModBus} \longleftrightarrow \text{Power System Devices}$$

Currently, the interconnection is realized through bi-directional database synchronization for selected data and execution of defined set-points. Datasets or time series are transmitted to the control center clearSCADA for telemetry and telecontrol applications. The measured process data at EUREF-Campus have a time resolution of 1-minute and are archived in 3-minute historical data bases. This enables upstream processing and graphical visualization of system states. Downstream data processing allows the control of power system components, units and unit cluster in reverse order. The smart grid laboratory environment at TU-Berlin is equipped with the control center HIGH-LEIT NT and realized as a mixture of real and emulated power system devices and distributed energy resources through the application of hardware and real-time simulators. The control center includes server units and virtual machines, a workstation as a man-machine interface and control panels. The additional terminal server allows internal and external access to the control center at the same time. The local area network consists of proprietary interfaces for EtherCAT buses. The processed data are stored and transformed in normed IEC information objects. Thus, the standard processing functions of the control center are also available for the real-time EtherCAT buses. The interconnected system provides a unique opportunity for the developed of Virtual Power Plants and validation of control algorithms in a secured testing environment.

2.4. Implications on Liberalized Energy Markets

To handle both emerging technical and economic conditions for the integration of Virtual Power Plants in the context of energy markets, efficient scheduling and operation strategies are required [52,53]. Typically, the participation opportunities are categorized in several time frames and in combination with different ownership relationships, preferences and tariff models. Short-term scheduling and operation, for example, allows secure and cost-effective representation of power plant portfolios, whereas mid-term and long-term planning processes influence the overall utilization and cost-effective energy management [54]. In order to overcome substantial barriers for the energy market participation, electricity trading transactions are either (i) standardized and concluded on the electricity exchange market or (ii) individually executed between two participants in off-exchange tradings in over-the-counter markets (OTC). However, depending on regulations and legal requirements in geographical areas of operation, the market participation opportunities can be limited and may vary from one electricity market to another. In general, the businesses of market tradings and financial equalization of mutual commitments between two or more parties is organized by forward transactions and clearing contracts.

2.4.1. Market Structures and Characteristics

There are numerous marketing possibilities of decentralized and renewable energy sources. Whether for aggregated pools, compensation of balancing group deviations, trading in the wholesale market, feed-in-tariffs, direct marketing or incentive systems for self-consumption [55, 56]. Through the breakdown of generation and load schedules in forward products higher flexibilities in market tradings can be achieved [57], under consideration of (i) delivery periods, (ii) time of contracting, (iii) counter-parties and (iv) disposition of quantities. Taking Germany as an example, Fig. 2.10 provides an overview of possible contracts and clearing sequences for standardized tradings. More details on the energy market characteristics can be found in Appendix A.

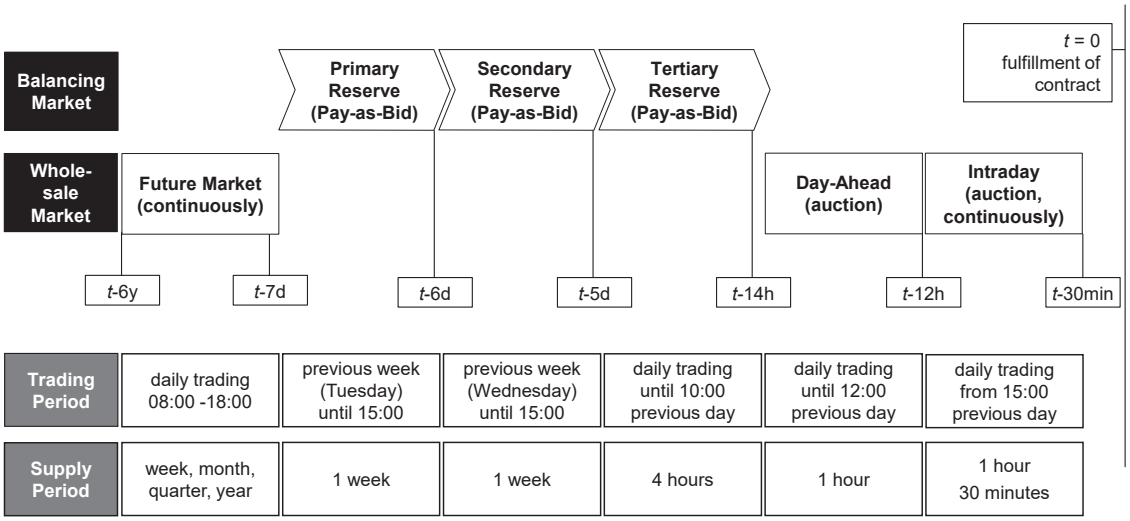

Fig. 2.10.: Overview of products and clearing sequences in the wholesale and balancing markets traded in the German-Austrian bidding zone.

For the participation of controllable generation, trading in the future market is appropriate with a variety of hedging and risk management strategies due to less volatile price characteristics [11]. Because of variable power generation of renewable energy sources and low predictability, participation opportunities in the future market is limited [58]. Hence, market participation opportunities are mainly realized in short-term tradings of spot markets. As a common feature of competitive wholesale markets, the auctions in spot markets underlie volatile price characteristics [59]. Spot market tradings are usually cleared on hourly or sub-hourly basis under consideration of staircase energy balance between supply and demand [60]. In order to compensate remaining imbalances, restore balance supply and demand, as well as ensure synchronous power system operation, the transmission system operator (TSO) provides additional control reserve (regulating power, balancing power, ancillary

power). With respect to balancing markets in Germany, the transmission system operators are obliged to apply transparent and competitive tendering proceedings. The tendered control reserve (CR) is divided into primary control (PCR), secondary control (SCR) and tertiary control reserve (TCR). Control power suppliers, also called Balancing Service Providers, have to fulfill distinct pre-qualification criteria [2] for the provision of control reserve. An example is given in Table 2.5.

TABLE 2.5.: Pre-qualification criteria for provision and activation of primary control (PCR), secondary control (SCR) and tertiary control reserve (TCR).

	primary control reserve	secondary control reserve	tertiary control reserve
tendering period	weekly	weekly	daily
product	pos. and neg. (symmetric)	pos. and/or neg. in two time slices	pos. and/or neg. in 6 times slices 4h each
minimum bid range	1 MW with 1 MW increment	5 MW with 1 MW increment	5 MW with 1 MW increment
pricing rule and award criterion	pay-as-bid auction (capacity price)	pay-as-bid auction (capacity and energy price)	pay-as-bid auction (capacity and energy price)
response time and activation	$<$ 30 sec to 15 min fully automated (P/f-control)	$<$ 5 min to 4 h automated (P/f-control)	$<$ 15 min by telephone or automated
measurement cycle	$<$ 1 sec	$<$ 1sec	$<$ 1min

Each control reserve capacity is in turn backed up by pre-qualified technical units located in the same control area. Cross-pooling is allowed to achieve the required minimum bid ranges, while bid pooling is restricted to one control area. In contrast to primary control reserve, secondary control reserve and tertiary control reserve (minute reserve) is tendered separately as positive (upward-regulating, incremental) indicated by ($^+$) and negative (downward-regulating, decremental) control power indicated by ($^-$). The procurement of control reserve takes place almost entirely by means of tendering procedures. Primary control reserve is tendered in single parts, based on the price for the amount of capacity reserved ϖ_{cp} in EUR/MW. Secondary and tertiary control power is tendered in multiple parts, consisting of capacity and energy prices ϖ_{ep} in EUR/MWh. The tradings are based on pay-as-bid auctions in contrast to spot market auctions, which apply uniform (marginal) pricing [61]. In order to facilitate the participation opportunities of decentralized and

[2] In case of Germany, further information are provided on https : //www.regelleistung.net.

renewable energy sources in balancing markets, the elimination of market framework barriers is essential. This may be achieved by shorter dispatch intervals in analogy to spot markets and additional incentives for the participation of dispatchable, flexible capacities [62].

2.4.2. Market Participation and Interactions

The contractual services and tradings on energy exchange markets are organized in accounting areas consisting of balancing groups (BG). According to the Electricity Grid Access Ordinance, market entities, such as power plant operators, electricity traders and suppliers using power system infrastructures, have to operate individual balancing groups or join third balancing groups. Balancing responsible parties, often called Balancing Group Responsible or Balancing Group Manager [63], are market entities that have the responsibility of balancing portfolios of generators and/or loads [13] and are financially responsible for residual imbalances. Consequently, the Virtual Power Plant operator as Supplier/Aggregator is required to handle all processes related to the balancing group management. The transmission system operator supports the allocation of cost accounting across the involved balancing responsible parties, incorporates balancing, reserve and congestion management restrictions. The time interval of accounting balancing groups and balancing energy for the European imbalance price system and regulations of the Association of European Transmission System Operators is defined with $\Delta t = 15$ minutes. For a distinct number of balancing groups within a control area, the required balancing reserve energy $E^{\mathrm{CR}\pm}$ is determined as sum of balancing group deviations $\Delta E_{\mathrm{BG}}^{\mathrm{CR}\pm}$ as follows:

$$\begin{aligned} E^{\mathrm{CR}\pm} &= \sum_{i=1}^{n} \Delta E_{\mathrm{BG}_i}^{\mathrm{CR}\pm} \text{ , with} \\ \Delta E_{\mathrm{BG}_i}^{\mathrm{CR}\pm} &= \Big((P_{\mathrm{g,BG}_i} + P_{\mathrm{IM,BG}_i}) - (P_{\mathrm{d,BG}_i} + P_{\mathrm{EX,BG}_i}) \Big) \cdot \Delta t. \end{aligned} \tag{2.7}$$

In case of negative values of balancing reserve energy, indicating a surplus of power demand P_{d} and/or exports P_{EX} in the control area, the transmission system operator activates positive control power provided by respective number of control power suppliers m. In case of positive values, indicating excess of power generation P_{g} and/or import P_{IM}, the transmission system operator activates negative control power. Figure 2.11 illustrates the logical relation (solid arrows) between involved market entities for the provision of control power, where physical power exchanges (dashed arrows) denote balance deviations within the control area of the transmission system operator.

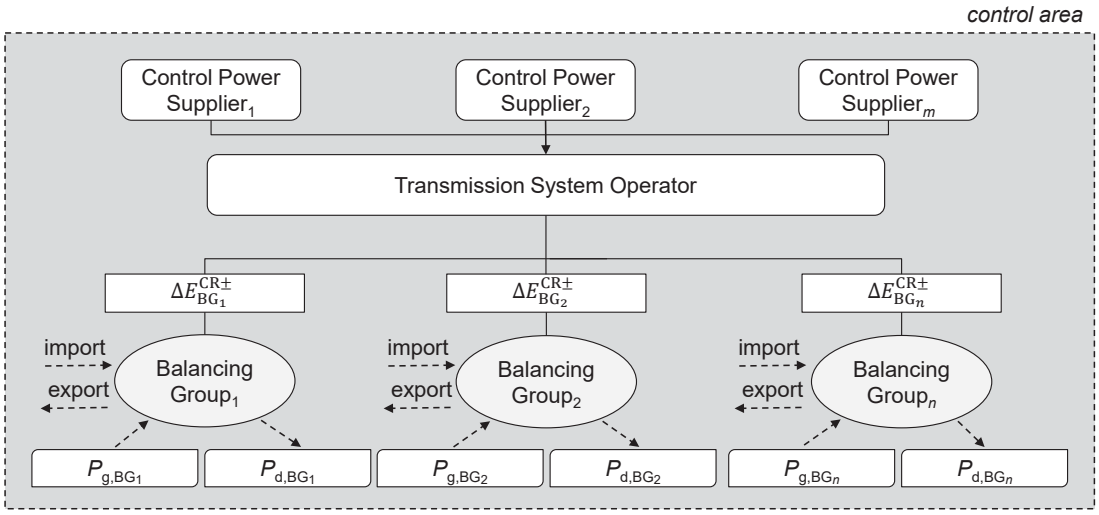

Fig. 2.11.: Schematic representation for the dimensioning of balancing energy and interaction schemes for the tendering of control power in the control area of the transmission system operator.

The required control reserve can be determined either for longer time periods (static dimensioning) or more frequently depending on the stochastic and deterministic of the weather conditions (dynamic dimensioning). Specifically, there are the following obligations for the determination: (i) ex ante determination, (ii) real time activation, (iii) ex ante acquisition, and (iv) ex post financial clearing. In any case transmission system operators charge balancing responsible parties according to the imbalances and/or recover disbursements via grid fees ex post for the compensation of the incurred expenditures. The payments for the balancing responsible parties are netted over the monthly accounting period and the clearing balance invoiced accordingly. As balancing responsible parties have several options to compensate unbalances with ex ante market trades or ex post payments, balancing markets and spot markets are not independent from each other [58]. The following commercial and technical specific characteristics of single units and unit clusters should be considered for the optimal utilization within the power plant portfolios:

- **commercially specific:** market framework and characteristics, risk assessment and portfolio management, tarification and congestion management, type of contracts and regulations
- **technically specific:** generation, load and storage capacities, level of controllability and limitations, temporal and spatial availability, response time and characteristics

Because of the limited storage capability of electricity and the characteristics of the energy system, more frequent auction and shorter dispatch intervals can contribute to increase the utilization of renewable energy sources [64]. Under those

preconditions and taking into account the market frameworks, Table 2.6 indicates the potential revenues for participation opportunities. The prices refer to average weighted energy and capacity prices in 2014 of selected wholesale and balancing markets.

TABLE 2.6.: Average weighted energy prices and capacity prices (2014) of selected wholesale and balancing markets in the German-Austrian bidding zone.

2014	**spot market**		**balancing market**				
	day-ahead	intraday	$PCR^{\pm}$	SCR^{+}	SCR^{-}	TCR^{+}	TCR^{-}
energy price (EUR/MWh)	1) 32.76	1) 33.01	-	3) 4) 78.16	3) 4) 9.73	2) 5) 203.25	2) 5) 49.02
capacity price (EUR/MW)	-	-	3) 3,513.17	3) 4) 468.08	3) 4) 348.09	2) 5) 3.33	2) 5) 12.90
tendering period	-	-	$7 \cdot 24$ h	$7 \cdot 12$ h	$7 \cdot 12$ h	$1 \cdot 4$ h	$1 \cdot 4$ h
normalized capacity price (EUR/MW $\cdot$ h)	-	-	20.91	5.57	4.97	0.83	3.23

1) 1-hour based average weighted prices 2) 4-hour based average weighted prices 3) 1-week based average weighted prices 4) time slice (8-20) 5) time slice (8-12).

Wholesale prices in the intraday and day-ahead market are remunerated for the contracted energy provided in EUR/MWh, whereas suppliers of control power receive additional payments for the reservation of capacity in EUR/MW. As the energy markets are characterized by different clearing sequences, the average weighted prices refer to the corresponding tendering period. The capacity prices are normalized by dividing the derived values in accordance to the tendering period and thus represents the theoretical remuneration of control reserve capacity per hour. These market characteristics are subject to changes and price movements as further detailed in the statistical assessments in Appendix A. For the pricing and reimbursement possibilities of the Virtual Power Plant operator, these are crucial factors when developing appropriate and affordable bidding strategies.

2.5. Concluding Remarks

The transformation process from a polycentric energy system featuring large-scale conventional and controllable generation units to a distributed energy system, primarily based on small-scale distributed and renewable energy sources is investigated.

The transformation process is assessed and quantified by comparison of the power plant portfolio in Germany in the years 1990 and 2014. Based on defined ranges for the share of renewable energy sources in the gross energy demand in 2030, 2040 and 2050, further changes in the power plant portfolio are estimated in scenarios. The results point to the increase of coordination efforts and requirements for efficient bidding and operational strategies of decentralized and renewable energy sources. In this context, driving forces for the adaptation of the Virtual Power Plant concept with feasible participation opportunities in liberalized energy markets are presented. The main characteristics and functionalities are introduced. Further, the interoperability and operating scheme of a physically realized Virtual Power Plant with Microgrid architectures is detailed as extension of the status quo. Current participation opportunities in liberalized energy markets are discussed according to the price characteristics and developments of the wholesale and balancing markets. Here, further research is necessary to evaluate alternative business developments and revenue opportunities in accordance to the bidding and operational strategy of the Virtual Power Plant operator and identify long-term effects of the outlined transformation process in the energy markets and designs.

3. VIRTUAL POWER PLANT IMPLEMENTATION AND OPTIMIZATION MODELS FOR JOINT MARKET OPERATIONS

Abstract – The chapter presents a Virtual Power Plant model for the participation in liberalized energy markets with large sets of power plant portfolios and enhancement of optimized energy procurements. First, the architecture and nodal-based aggregation methodology is introduced, including distinct unit models for the representation of a variety of generation, load and storage units. Then, the operational exchange with different market entities is structured and specified in communication sequences for joint market operations in day-ahead and intraday markets. The defined unit type specific characteristics serve as boundary and constraint conditions for the determination of the operating points obtained from multi-period optimization processes. An internal imbalance mechanism is developed as part of the optimization problem formulation to mitigate forecast uncertainties related to the intermittent power generation of renewable energy sources. Finally, the performance of the optimization model is evaluated and verified through various simulation and computational studies, investigating the sensitivity in cost and greenhouse gas emissions of distinct power plant portfolios.

Keywords – bidding strategy, cluster algorithm, mixed-integer linear programming, dispatch optimization, forecast accuracy, short-term scheduling, joint market operations, power balancing

3.1. Introduction

With the presence of the time-varying behavior of renewable energy sources and flexible loads, the unit commitment and dispatch problem can change significantly [65–67]. In that regard, there is a need for methodologies that leverage supplementary power plant capacities and provide additional flexibilities to compensate real-time imbalances [68]. To cope with unforeseen increases in demand, losses of power plants and transmission lines, and other contingencies [69], enhanced feed-

in management, redispatch measures, planning and forecasting methods, and efficient energy management strategies with appropriate optimization techniques are required [70–72]. With a similar rationale, the same applies to Virtual Power Plants that use the flexibilities provided by generation, demand and storage units to meet certain objectives [73,74]. For the determination of optimized control decisions, various planning and operation methods are dealt with in [75–78] and combinatorial dispatch solutions presented by [79–81]. Even though, optimization models for joint market participation of Virtual Power Plants have rarely been discussed in the scientific literature. For example, [82–84] design bidding strategies for the participation in the energy and balancing market. The deterministic price-based unit commitment considers the supply-demand balancing and security constraints of managed distributed and renewable energy sources to maximize the profit. The unit commitment and dispatch problem for a mid-term scheduling is discussed in [54] that maximizes the profit through day-ahead market participation and bilateral contracts. The optimization problem is subjected to long-term bilateral contracts and technical constraints. Interactive dispatch modes and bidding strategies are introduced in [81] for day-ahead scheduling, hours-ahead scheduling, and real-time dispatch. The chapter extends the previous methodologies in two important aspects. First, the developed unified model architecture and energy management algorithm shows possible realizations to deal with intermittent power generation of renewable energy source with arbitrary power plant portfolios under consideration of forecast errors. This is achieved thanks to a novel three-stage imbalance algorithm that utilizes multi-period optimization in joint market operations. Second, for the purpose of short-term scheduling and mitigation of balancing group deviations, an enhanced balancing algorithm is presented that integrates demand-side management services and functionalities for the provision of internal control reserve in combination with day-ahead and intraday market operations. The design of the model architectures is specified and the value of the developed balancing algorithm substantiated in numerical simulations.

3.2. Model Architecture and Functionalities

The unified model architecture of the Virtual Power Plant, as schematically shown by means of Fig. 3.1, allows the creation of arbitrary power plant portfolios. These are formed by different sets of generation (gen), load (load) and storage units (stor), which are not necessarily located in adjacent places or the same control area of a single system operator. Different services and functions are considered as part of energy management algorithm, including trading in the wholesale energy market,

power balancing and provision of internal control reserve. With increasing number of variables used for the mathematical formulation of the power plant portfolio characteristics, the computational efforts and complexity for solving the optimization problem related to the scheduling process increases. Therefore, different control concepts and cluster algorithms are developed to reduce the amount of variables while aiming to achieve comparable results to single optimization approaches.

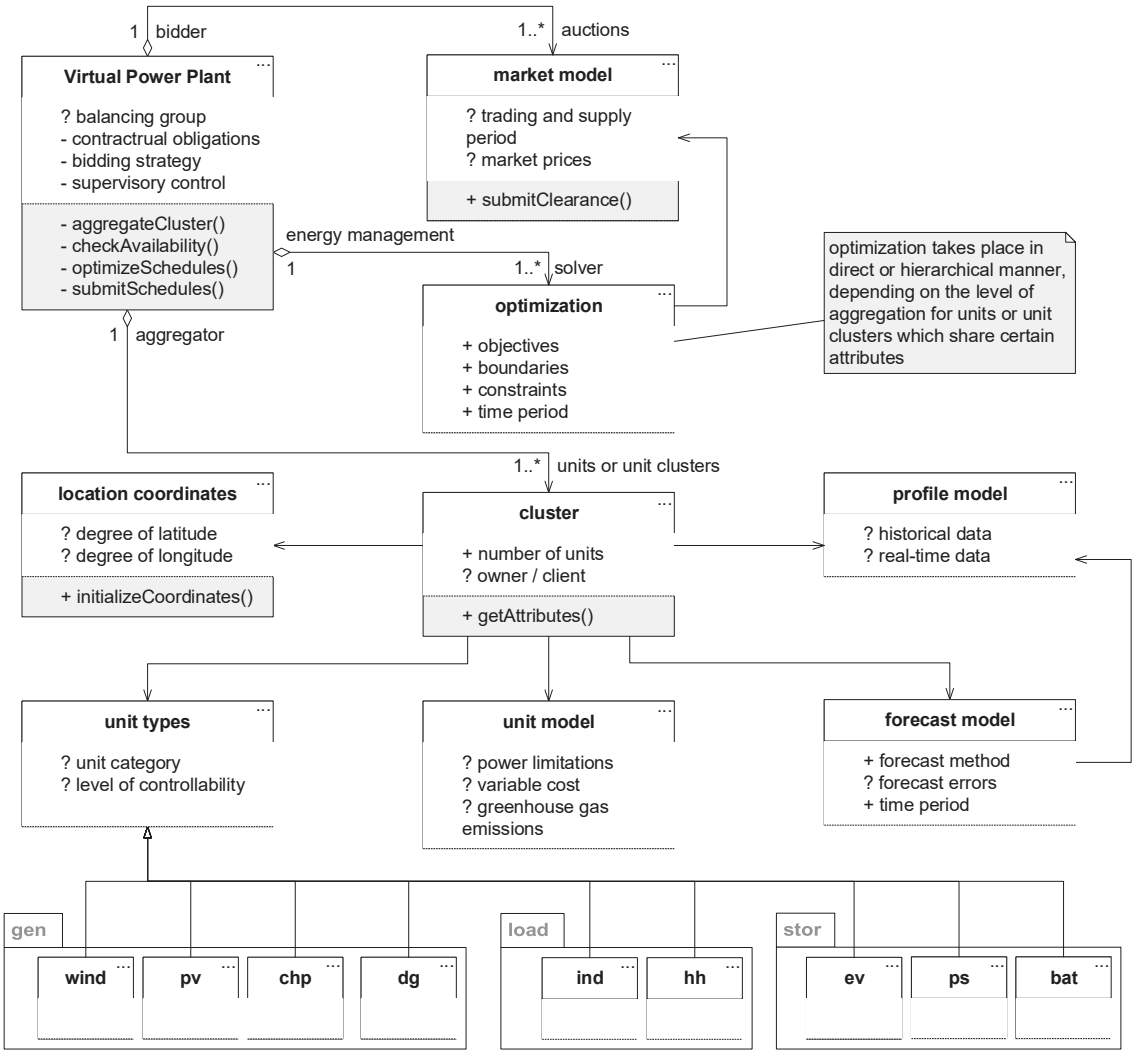

Fig. 3.1.: Unified model architecture of the Virtual Power Plant represented by generalized elements using unified modeling language class and package diagrams.

Based on the operational strategy and aggregation approach, Fig. 3.2 shows the considered solutions according to [85, 86]. Central control denotes direct interactions by sending set-points whereas hierarchical control implies aggregation on different hierarchical levels and decision-making, shared between hierarchical layers. Decentralized control refers to autonomous control, where power sources receive incentives in the form of price signals instead of set-points or auction processes. In the following elaborations, a distinction is made between local and remote control. Power sources are typically equipped with local controls to ensure security of operation,

whereas remote control allows online adjustments of the set-points for the operation. For example, local control is used by means of droop control of inverter based generators [87], maximum power point tracking of photovoltaic power plants [88], pitch control of wind power plants [89] or on-board charging of electrical vehicles [90].

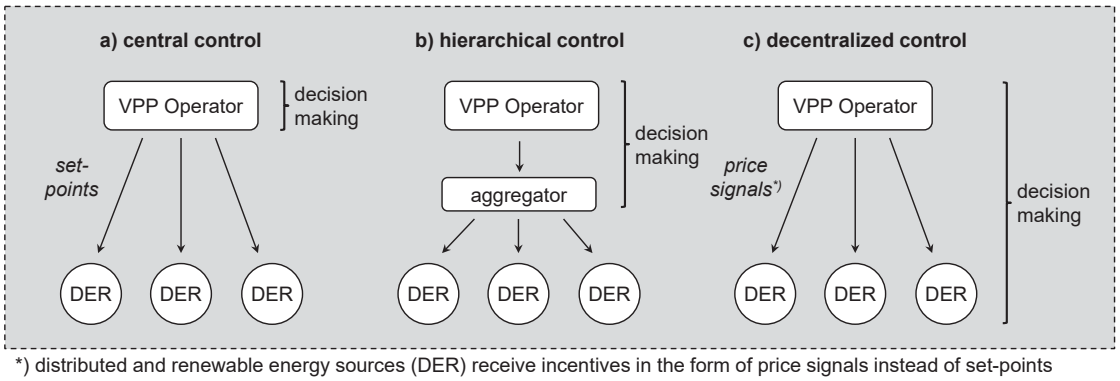

Fig. 3.2.: Operational strategy for Virtual Power Plants to coordinate distributed and renewable energy sources by central, hierarchical and decentralized control approaches.

Within the proposed unified model architecture as illustrated in 3.1, each single unit is primarily considered to be operated with central control. To realize also hierarchical control concepts, a nodal-based aggregation methodology is developed. For the developed control concepts, the following characteristics are taken into account:

- geographical location
- degree of efficiency
- power loading capability
- power curve characteristics
- installed capacity
- generation ranges
- stand-by capacity
- operating cost characteristics

For certain optimization processes, however, further characteristics may be crucial, such as ramp rates, fault ride through characteristics, frequency response characteristics, and voltage regulating capability. Additional characteristics for the optimization processes may be also given by economic influencing factors [91] as introduced in Chapter 2, e.g. contractual obligations with owners/clients.

3.2.1. Unit Categorization and Controllability

Through the combination of a variety of units and unit clusters, denoting the considered set of unit types $H_{\text{typ}} = \{typ \mid typ \in H_{\text{ces}} \vee typ \in H_{\text{res}} \vee typ \in H_{\text{stor}}\}$, distinct power plant portfolio are composed. Table 3.1 provides an overview of the unit types and assumed categories. Uncontrolled power generation or demand refer to units and unit clusters with limited external control options which are summarized as non-controlled (nc) unit types. Controlled power generation or demand with

external control options in time or unit specific limits is modeled by means of partly-controlled (pc) unit types. Fully-controlled (fc) unit types allow controlled power generation or demand within the minimum and maximum limits and allows stepless external control. Possible operating schedules are illustrated in Fig. 3.3 where the red arrow indicates the degree of freedom. For example, Fig. 3.3a schematically shows the intermittent power generation of wind and photovoltaic power plants that is considered to be uncontrolled. The unit type specific power generation can only be reduced through curtailments as part of redispatch measures.

TABLE 3.1.: Set of unit types H_{typ} and unit categories with associated levels of controllability used in the unified model architecture of the Virtual Power Plant.

unit type (ID)			unit category and level of controllability	
wind power plant	wind	10	gen	nc
photovoltaic power plant	pv	11	gen	nc
combined heat and power	chp	12	gen	fc
distributed generator	dg	13	gen	fc
electric vehicles	ev	14	stor	nc, pc, fc
pumped-storage system	ps	15	stor	fc
stationary battery system	bat	16	stor	fc
industrial load	ind	17	load	pc, fc
household load	hh	18	load	nc

Partly-controlled generators can increase or reduce the power generation within the boundaries of the lower and upper limits. Figure 3.3b shows the generation ranges, which can vary in time and operational condition. The gray shaded areas specify the flexibility ranges for the provision of positive P^{CR^+} and negative P^{CR^-} control reserve through the application of power adjustment or shifting mechanism. Power adjustment defines the temporal reduction or increase of the power generation or demand of fully-controlled unit types without later compensation. Power shifting means that part of the power generation or demand $\Delta P_k^{typ,\text{pc}}$ of partly-controlled unit types is brought forward or is postponed. The power adjustment and power shifting mechanism is modeled through the introduction of a virtual storage capacity where the corresponding amount of energy is calculated by

$$E_{k+1}^{typ,\text{pc}} = \begin{cases} E_k^{typ,\text{pc}} - \Delta P_{\text{g},k}^{typ,\text{pc}} \cdot \Delta t, & \text{generator units} \\ E_k^{typ,\text{pc}} + \Delta P_{\text{d},k}^{typ,\text{pc}} \cdot \Delta t, & \text{load units.} \end{cases} \tag{3.1}$$

Thus, a temporary load reduction or increase can be simulated by subsequent dis-

charging or charging processes of the virtual storage capacity, under the premise that the corresponding energy quantities must be compensated in following time steps. In Fig. 3.3c an example is given for an operation schedule of a fully-controlled generator. As schematically illustrated fully-controlled generators are assumed to allow stepless control of the power generation between $P^{typ,\mathrm{fc}}_{\mathrm{g,min}}$ and $P^{typ,\mathrm{fc}}_{\mathrm{g,max}}$, denoting the minimum and maximum operational limits.

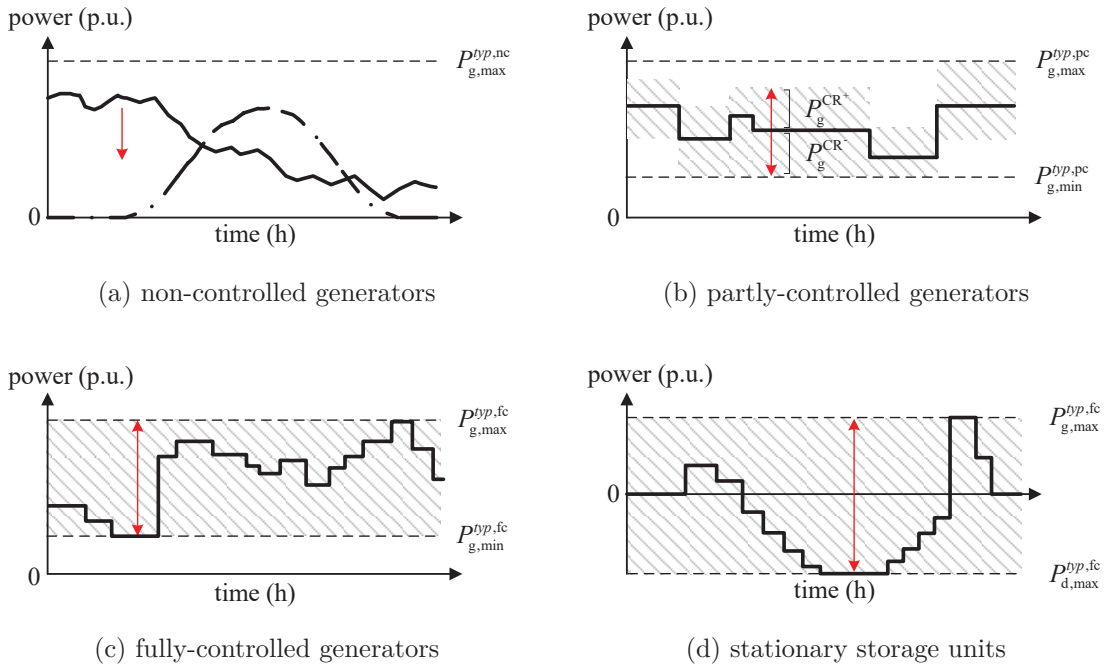

(a) non-controlled generators

(b) partly-controlled generators

(c) fully-controlled generators

(d) stationary storage units

Fig. 3.3.: Schematic illustration of possible operation schedules and controllability limitations for non-controlled, partly-controlled and fully-controlled generator and storage unit types.

Contrary to generation units, storage units can also be considered as a controllable load unit. As indicated in Fig. 3.3d, fully-controlled storage units can be operated in stepless charging/discharging processes between $P^{typ,\mathrm{fc}}_{\mathrm{d,max}}$ and $P^{typ,\mathrm{fc}}_{\mathrm{g,max}}$, denoting the maximum charging/discharging power. For identification purposes, each unit model is specified by a combination of various machine-readable sequences (ID). An example of which is shown in Fig. 3.4. The first two digits specify the unit type and the third digit is assigned to the unit model. The fourth digit specifies the operation schedule that is currently represented by a set of time series of historical data. The fifth digit indicates the level of aggregation, where "‘0"’ refers to a single unit and "‘1"’ to a unit cluster. The remaining digits represent a counter index for unit or unit clusters that share certain attributes. 10-2-5-0-070189 is a possible number generated by this approach and is interpreted as follows:

- 10: unit type for wind power plant
- 2: unit model for 1 MW rated capacity
- 5: profile of measured data

- 0: single unit
- 070189: is the 70,189th number generated within the unit type 10 with unit model 2.

In total 999,999 units or unit clusters of the same type and unit model can be simulated. The identification numbers are also used for the geographical assignment and refer to geographical regions, control areas or buses with location coordinates and different energy markets, e.g. spot market or balancing market.

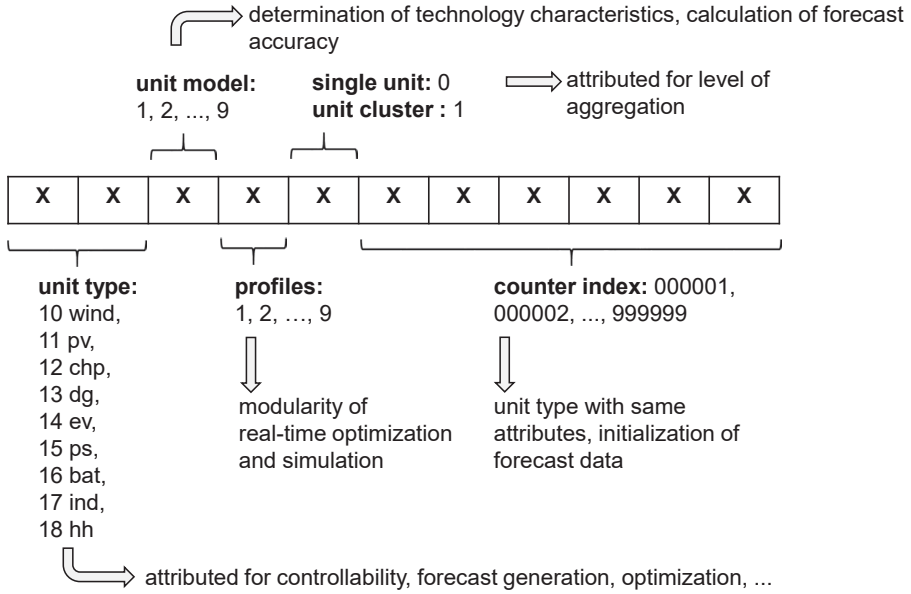

Fig. 3.4.: Structure of the developed machine-readable identification number (ID) used, specifying the embedded unit type models and attributes.

Appendix C details the integrated unit models and specifies the assigned attributes. These are used within the proposed energy management algorithm and specify the boundary and constraint conditions in the scheduling process of the unit commitment and optimization problem while achieving the operational objectives of the Virtual Power Plant operator. Among the given attributes, the specific greenhouse gas emissions ghg_{CO2}^{typ} in gCO2/kWh and variable cost $\varpi_{\mathrm{vc}}^{typ}$ in EUR/kWh serve as indicating parameters for the evaluation of economic and environmental operation strategies. Modifications can be made as necessary and according to the embedded model environment or development program.

3.2.2. Nodal-based Aggregation and Cluster Algorithm

In order to determine appropriate power system services but also participate in different energy markets, a nodal-based aggregation and cluster algorithm is introduced. Units and unit clusters that share certain attributes are aggregated and

the assigned unit model characteristics scaled linearly. The methodology makes it possible to reduce the amount of optimization variables and thus less computational effort is required to solve the optimization problem with the associated boundary and constraint conditions. Possible compositions and creation of unit type specific clusters are shown in Fig. 3.5. The dashed circles represent virtual nodes and the solid circles physical nodes. Virtual nodes refer to a specific geographical region/area or balancing group, while physical nodes indicate the physical buses of power systems. The units of three possible unit clusters, consisting of various unit combinations, are matched from their physical nodes of the network model to the virtual nodes of the portfolio. It is indicated that the unit clusters can be independently composed from the location of the units while the allocation of physical nodes is based on the respective geographic coordinates.

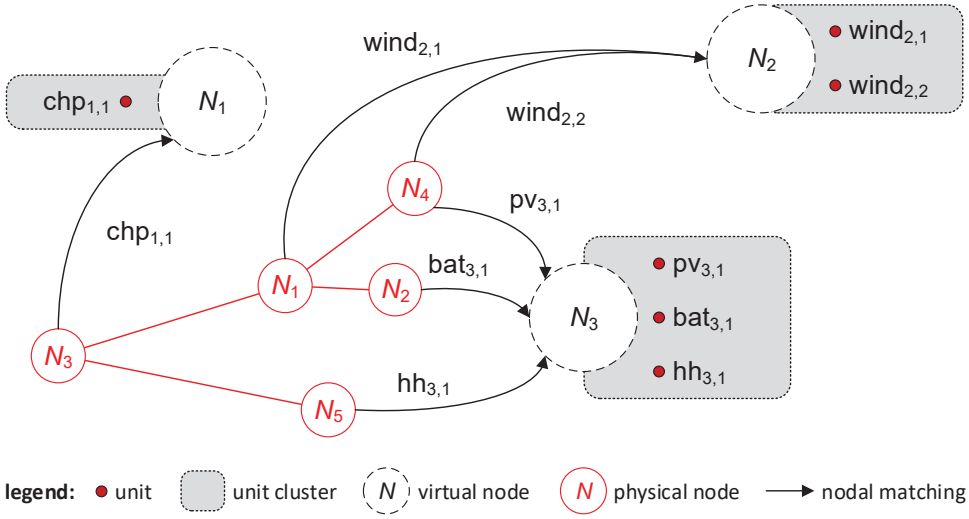

Fig. 3.5.: Nodal-based aggregation and geographical allocation of single units and unit clusters to virtual and physical nodes for the composition of distinct power plant portfolios.

For the purpose of nodal-based aggregation and geographical allocation, the latitude *lat* and longitude *lon* coordinates needs to be converted to cartesian coordinates, as these are usually given in different notations. For a distinct location L_i, (3.2) converts the spherical coordinates into the two-dimensional projections with cartesian coordinates.

$$L_i\left(lon_i^{\mathrm{sph}}, lat_i^{\mathrm{sph}}\right) \mapsto L_i\left(lon_i^{\mathrm{crt}}, lat_i^{\mathrm{crt}}\right) \tag{3.2}$$

By using the geodetic reference system WGS84, complex mathematical calculations for the geographical assignment can be eliminated as the meridians are subdivided into relative latitude sections and longitude sections through cylindrical projection. Therefore this method is used in the Virtual Power Plant for the geographical assignment. Possible examples are given in Fig. 3.6, showing sample-sets of existing distributed and renewable energy sources in Germany. Figure 3.6a shows a polygon

representation with triangles, where the verticals can be arbitrarily defined by latitude and longitude location coordinates. Figure 3.6b shows an example of sectoral representation, where distributed and renewable energy sources in the metropolitan region of Berlin are identified within a given radius.

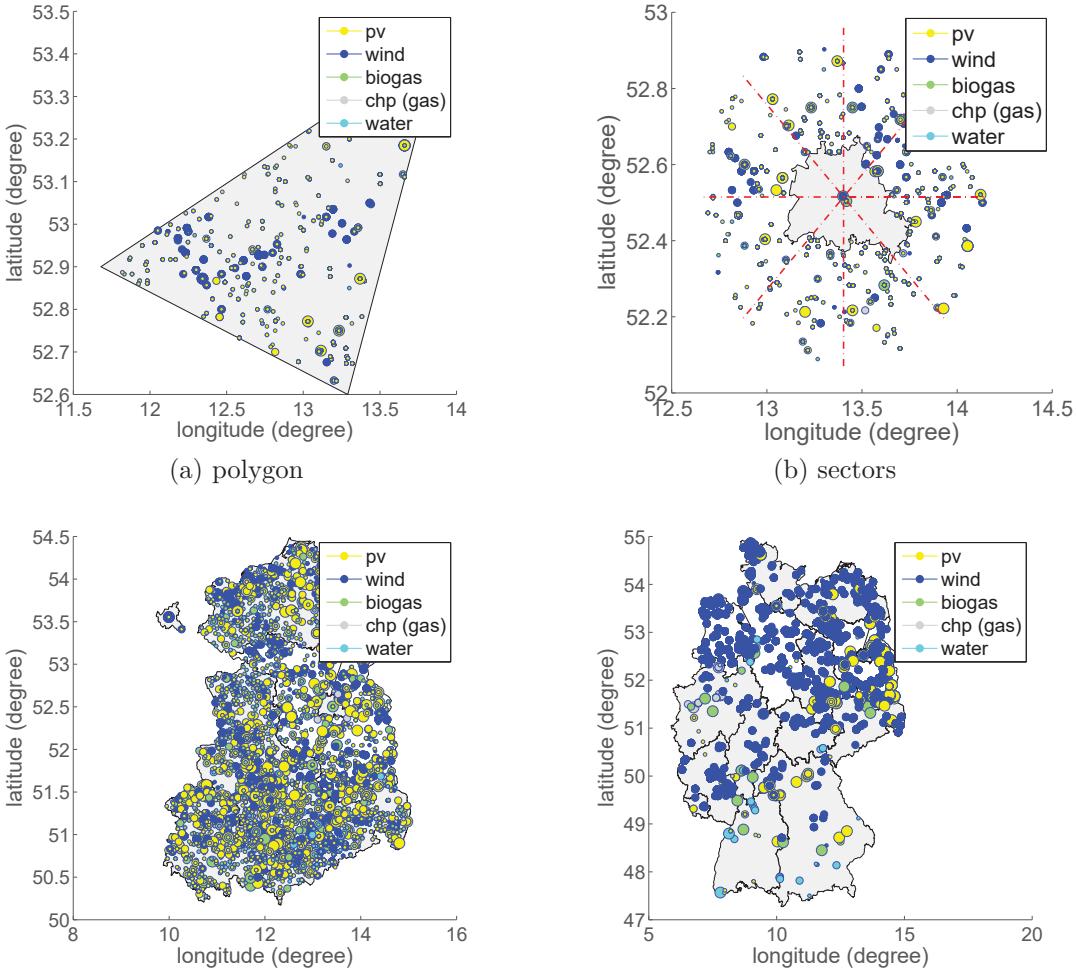

(a) polygon (b) sectors

(c) federal states (d) country

Fig. 3.6.: Schematic representation of power plant portfolios in geographical sample-sets consisting of (a) polygon, (b) sector, (c) federal states and (d) country allocation.

Considering power plant portfolios in federal states, Fig. 3.6c shows units or unit clusters in the high-voltage level. The illustration mainly corresponds to the control area of the German Transmission System Operator, 50Hertz Transmission GmbH. In the case of holistic analysis for an entire country, Fig. 3.6d highlights units or unit clusters connected to power systems in the medium-voltage level. All these units and unit clusters H_{cl} can be considered to be part of the Virtual Power Plant, which can be formulated as follows

$$\mathrm{VPP} = \coprod_{i=m}^{n} H_{\mathrm{cl},i} = \{H_{\mathrm{cl},i} \mid i \in \{m, m+1, \ldots, n\}\} \tag{3.3}$$

where m denotes the first and n the last set of aggregated units or unit clusters. Once the required model attributes, as specified in Appendix C are assigned, the power plant portfolio can be integrated in the energy management algorithm of the Virtual Power Plant.

3.3. Solution Method for Multi-period Optimization Processes

The implementation of an efficient energy management strategy for power plant portfolios requires the consideration of several uncertainties in the development of appropriate bidding algorithm [92]. This relates, for example, to the uncertainties regarding the expected generation of renewable energy sources [93], which becomes an important aspect for energy market participation and power system operation. Here, a three-stage imbalance compensation algorithm is proposed that takes into consideration the uncertainty related to the power scheduling problem with renewable energy sources for corresponding forecast horizons $fh \in \{24\text{h}, 1\text{h}, 0.25\text{h}\}$. Table 3.2 specifies the considered online-control and redispatch measures for each stage. Online-control and redispatch measures imply remote access that allows to send set-points for the operation and apply power adjustment and power shifting. The classification of the stages is derived from the trading period and clearing sequence of market operations as reviewed in Chapter 2 and summarized in Fig. 2.10. In order to eliminate market framework barriers for the participation of renewable energy sources, the energy management algorithm of the Virtual Power Plant operator integrates shorter dispatch intervals and determines the operation schedules within a multi-period optimization process in joint market operations.

TABLE 3.2.: Forecast horizons, online-control and redispatch measures considered in the three-stage imbalance compensation algorithm.

stage	forecast horizon		redispatch and online-control measures
1	day-ahead	24 hours up to several days	day-ahead optimization process
2	intraday	15 minutes up to several hours	intraday optimization process
3	real-time	several minutes	imbalance compensation process

The proposed methodology aims to mitigate power imbalances and meet the contracted power exchanges in the energy market operations while considering power system security constraints in advance. The sequence of communicative actions that

are needed to be exchanged with the main actors for joint market operation are detailed in Fig. 3.7.

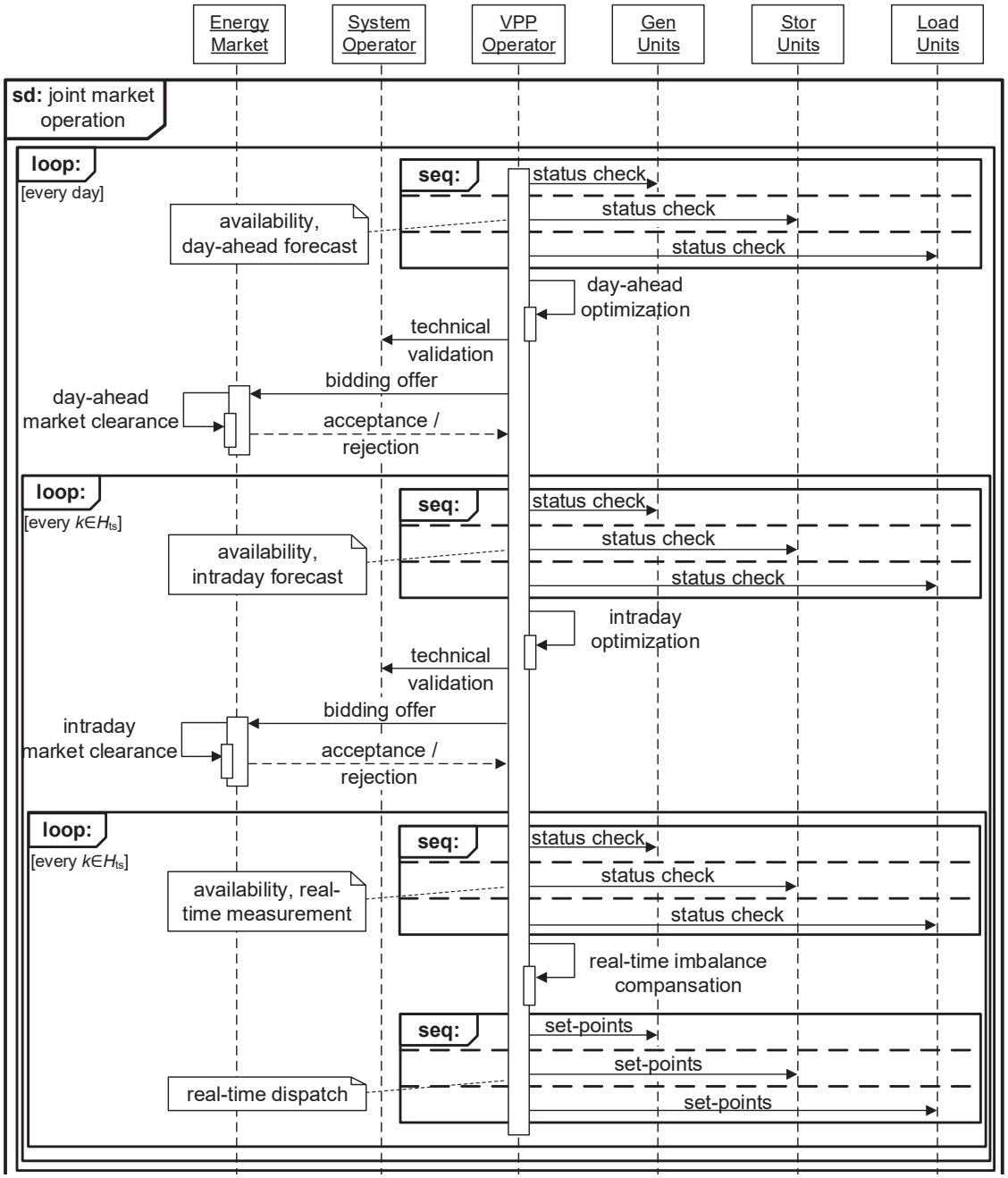

Fig. 3.7.: Sequence diagram of proposed three-stage imbalance compensation algorithm and interactions of the main actors in joint market operations.

Let H_{ts} be the set of time steps k, e.g. $H_{\mathrm{ts}} = \{1, 2, \ldots, 96\}$, for $\Delta t = 0.25\mathrm{h}$ reflecting the trading period and market sequence of the day-ahead and intraday market operation. The time increment Δt denotes the anticipated dispatch interval. Then, in each stage the total power generation $P_{\mathrm{g},k}^{\mathrm{VPP}}$ and demand $P_{\mathrm{d},k}^{\mathrm{VPP}}$ of the power plant portfolio is determined by

$$\begin{aligned} P_{\mathrm{g},k}^{\mathrm{VPP}} &= P_{\mathrm{g},k}^{\mathrm{pv}} + P_{\mathrm{g},k}^{\mathrm{wind}} + P_{\mathrm{g},k}^{\mathrm{chp}} + P_{\mathrm{g},k}^{\mathrm{dg}} + P_{\mathrm{g},k}^{\mathrm{bat}} + P_{\mathrm{g},k}^{\mathrm{ps}} + P_{\mathrm{IM},k}^{em} \\ P_{\mathrm{d},k}^{\mathrm{VPP}} &= P_{\mathrm{d},k}^{\mathrm{hh}} + P_{\mathrm{d},k}^{\mathrm{ind}} + P_{\mathrm{d},k}^{\mathrm{bat}} + P_{\mathrm{d},k}^{\mathrm{ps}} + P_{\mathrm{EX},k}^{em} \end{aligned} \tag{3.4}$$

where $P_{\mathrm{IM},k}^{em}$ and $P_{\mathrm{EX},k}^{em}$ denote the market imports and market exports. Generally, the power generation P_{g}^{typ} is defined as positive quantity and the demand P_{g}^{typ} as negative. The first and second stage utilizes multi-period optimization processes to yield minimum power imbalances during day-ahead and intraday market operations following a distinct bidding strategy. In each stage, the bidding schedules are optimized while considering the unit type specific boundary and constraint conditions including updated information and operational states. The sequences of the day-ahead market operation are as follows:

- forecasting of generation profiles, load profiles and flexibilities of aggregated units and unit clusters for each hour of the next day
- forwarding optimized day-ahead bidding schedules to the system operator for technical validation and adjustment processes in case of power system constraints violation
- forwarding optimized and adjusted bidding schedules for day-ahead market participation for each hour of the next day and receiving accepted biddings and offers after market clearance

In intraday market operations, the sequences are similarly structured under consideration of the contracted bidding schedules of the day-ahead operation for every hour of the respective day. To mitigate minute-to-minute power deviations within the balancing group of the Virtual Power Plant operator, a subsequent real-time imbalance compensation process takes place. As a consequence, balancing group deviations may be reduced and the overall power balance in the control area of the system operator maintained. In case of remaining real-time imbalances and with regard to power system operations, automatic-control solutions such as frequency response and automatic-generation-control are still required. However, as the physical power balancing is the responsibility of the system operator, these measures are not further considered in the following elaborations.

3.3.1. Power Balancing with Internal Imbalance Mechanism

In the day-ahead and intraday optimization process, the uncertainties of renewable power generation are modeled by different scenarios of renewable power forecasts as detailed in Appendix D. Depending on the forecast horizon as given in Table 3.2, (3.4) can be used to determine the power deviation of the predicted power generation

$\tilde{P}^{\mathrm{VPP}}_{\mathrm{g},k,fh}$ and demand $\tilde{P}^{\mathrm{VPP}}_{\mathrm{g},k,fh}$ in the first two stages. The obtained result is used for the determination of required market exchange, which is calculated as follows:

$$\Delta\tilde{P}^{em}_{k,fh} = -(\tilde{P}^{\mathrm{VPP}}_{\mathrm{g},k,fh} + \tilde{P}^{\mathrm{VPP}}_{\mathrm{d},k,fh}). \tag{3.5}$$

Next, the power deviation $\Delta P^{\mathrm{CR}^{\pm}}_{k}$ that defines the amount of required internal control reserve is determined

$$\Delta P^{\mathrm{CR}^{\pm}}_{k} = P^{typ,\mathrm{fc}}_{\mathrm{g},k} + P^{typ,\mathrm{fc}}_{\mathrm{d},k} + \Delta P^{typ,\mathrm{pc}}_{\mathrm{g},k} + \Delta P^{typ,\mathrm{pc}}_{\mathrm{d},k}. \tag{3.6}$$

where $P^{typ,\mathrm{fc}}_{\mathrm{g},k}$ and $P^{typ,\mathrm{fc}}_{\mathrm{d},k}$ denote the power generation and demand of fully controllable unit types, $\Delta P^{typ,\mathrm{pc}}_{\mathrm{g},k}$ and $\Delta P^{typ,\mathrm{pc}}_{\mathrm{g},k}$ the dispatchable power adjustments or shiftings of partly-controlled units, respectively. Figure 3.8 details the single steps taken into account when specifying the required quantities. The red shaded bars denote the forecast error $\Delta\tilde{P}^{\mathrm{err},typ}_{k,fh}$ related to the intermittent power generation of renewable energy sources. The white bars express the optimized bidding schedules for market exchanges in day-ahead and intraday optimization process, respectively. The residual market exchanges denote the sum of the cleared day-ahead and intraday market exchanges and indicated by the black bars.

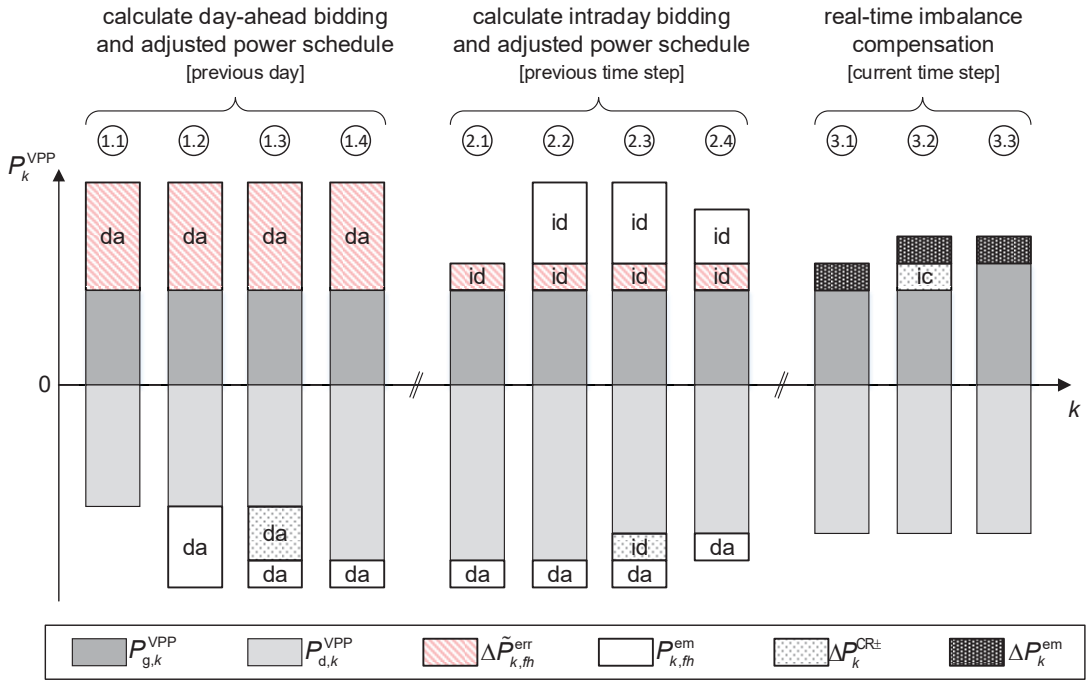

Fig. 3.8.: Schematic representation of the scheduling processes and preparation of market bidding schedules during day-ahead (da) and intraday (id) optimization process with subsequent real-time imbalance compensation (ic).

The steps 1.1-1.4 define the day-ahead optimization results of the previous day. In step 1.1 the initial power schedules are forecasted, while step 1.2 identifies the initial

day-ahead market exchange. The optimization process takes place in step 1.3 and the dispatch schedules are forwarded to the system operator for technical validation. The accepted power schedules after the day-ahead market clearing are given in step 1.4. For each time step of the following day, the continuous intraday optimization takes place using updated forecast information. This is summarized by means of steps 2.1-2.4. The steps of the intraday optimization process are equally structured while the results of the day-ahead optimization process serve as additional constraint conditions. The forecast errors related with the contracted day-ahead bidding schedules are partly compensated. In steps 3.1-3.3 the residual market exchange is calculated by (3.7) and the remaining real-time imbalances are determined in (3.8).

$$\Delta P_k^{em} = P_{\mathrm{IM},k,fh}^{\mathrm{id}} + P_{\mathrm{IM},k,fh}^{\mathrm{da}} + P_{\mathrm{EX},k,fh}^{\mathrm{id}} + P_{\mathrm{EX},k,fh}^{\mathrm{da}} \tag{3.7}$$

$$\Delta P_{\mathrm{imb},k}^{\mathrm{VPP}} = P_{\mathrm{g},k}^{\mathrm{VPP}} + P_{\mathrm{d},k}^{\mathrm{VPP}} + \Delta P_k^{em} \tag{3.8}$$

The market imports of the day-ahead and intraday operations are specified by $P_{\mathrm{IM},k}^{\mathrm{da}}$ and $P_{\mathrm{IM},k}^{\mathrm{id}}$ and the exports are given by $P_{\mathrm{EX},k}^{\mathrm{da}}$ and $P_{\mathrm{EX},k}^{\mathrm{id}}$, respectively. Through the activation of internal control reserve part of the power unbalances are mitigated. The real-time power generation and demand of the power plant portfolio are given by $P_{\mathrm{g},k}^{\mathrm{VPP}}$ and $P_{\mathrm{d},k}^{\mathrm{VPP}}$, respectively. For the real-time imbalance compensation, numerous contracted units and unit clusters of the power plant portfolio are utilized and activated following the merit order as listed in Table 3.3.

TABLE 3.3.: Merit order and segmented participant categories for the provision of internal control reserve as part of real-time power adjustments.

	I	**II**	**III**	**IV**
power surplus	$P_{\mathrm{d}}^{\mathrm{bat}} \uparrow$, $P_{\mathrm{g}}^{\mathrm{bat}} \downarrow$ $P_{\mathrm{d}}^{\mathrm{ps}} \uparrow$, $P_{\mathrm{g}}^{\mathrm{ps}} \downarrow$	$P_{\mathrm{g}}^{\mathrm{chp}} \downarrow$, $P_{\mathrm{g}}^{\mathrm{dg}} \downarrow$	$P_{\mathrm{d}}^{\mathrm{ind}} \uparrow$	$P_{\mathrm{g}}^{\mathrm{pv}} \downarrow$, $P_{\mathrm{g}}^{\mathrm{wind}} \downarrow$
power deficit	$P_{\mathrm{d}}^{\mathrm{bat}} \downarrow$, $P_{\mathrm{g}}^{\mathrm{bat}} \uparrow$ $P_{\mathrm{d}}^{\mathrm{ps}} \downarrow$, $P_{\mathrm{g}}^{\mathrm{ps}} \uparrow$	$P_{\mathrm{g}}^{\mathrm{chp}} \uparrow$, $P_{\mathrm{g}}^{\mathrm{dg}} \uparrow$	$P_{\mathrm{d}}^{\mathrm{ind}} \downarrow$	$\diagdown$

The order of activation is from fast **I** to slow reacting **IV** participant categories. The first-order **I** consists of contracted stationary battery and pump-storage systems, enabling fast power adjustments. For example, in case of power surplus the charging power $P_{\mathrm{d}}^{\mathrm{bat}}$ of stationary battery systems increases. The second-order units **II**, represented by controlled combined heat and power plant and distributed generation units, reduce the power generation $P_{\mathrm{g}}^{\mathrm{chp}}$ and $P_{\mathrm{g}}^{\mathrm{dg}}$. The third-order units **III**, are defined by controlled industrial load units that are capable to increase or reduce the power demand $P_{\mathrm{d}}^{\mathrm{ind}}$. Redispatch measures with wind and photovoltaic power plants,

which represent the forth-order units **IV**, are considered as the last option. As an alternative strategy for the provision of internal control reserve, single back-up power plants and storage capacities can be considered to reduce the coordination efforts. However, also in this stage the considered redispatch measures are subjected to the contractual obligations and controllability limitations given by the characteristic of the power plant portfolio.

3.3.2. Optimization Problem and Mathematical Formulation

The dimensionality of the unit commitment and dispatch problem requires a optimization method, capable to solve the whole problem for any real-size system [94,95]. This includes updated information of the coordinated units and unit clusters as well as the market status and deviation between the forecasted and contracted power schedules. The proposed optimization problem is formulated as a constrained mixed-integer linear programming problem subjected to boundary conditions and linear constraint functions, specified by the unit model characteristics. This can be achieved by taking into account constants as model attributes which allows to circumvent nonlinearities in the optimization problem [96]. The optimization problem $\mathcal{LP}$ is generally formulated as follows:

$$
\begin{aligned}
& \min_{x,y} && \boldsymbol{c}^{\mathrm{T}}\boldsymbol{x} + \boldsymbol{d}^{\mathrm{T}}\boldsymbol{y} \\
(\mathcal{LP}) \qquad & \text{s.t} && \boldsymbol{A}\boldsymbol{x} + \boldsymbol{B}\boldsymbol{y} \leq \boldsymbol{b} \\
& && \boldsymbol{A} \in \mathbb{Z}^{m\mathrm{x}n}, \boldsymbol{B} \in \mathbb{Z}^{m\mathrm{x}d}, \boldsymbol{b} \in \mathbb{Z}^{m}, \quad \boldsymbol{x} \in \mathbb{R}^{n}, \quad \boldsymbol{y} \in \mathbb{Z}^{d}_{\geq 0}
\end{aligned}
\tag{3.9}
$$

The continuous variables $\boldsymbol{x} \in [\boldsymbol{x}_{\min}, \boldsymbol{x}_{\max}]$ reflect the power schedules of controllable generation, load and storage units. The lower $\boldsymbol{x}_{\min}$ and upper $\boldsymbol{x}_{\max}$ bounds are specified by the unit model attributes. The integer variables $\boldsymbol{y} \in \{0, 1\}$ define the operation modes of the unit types with assigned storage capacities, where 1 indicates charging and 0 discharging processes. The coefficient matrices $\boldsymbol{A}$ and $\boldsymbol{B}$ in combination with the right hand side vector $\boldsymbol{b}$, define the constraints of the optimization problem. Let $\boldsymbol{c}^{\mathrm{T}}\boldsymbol{x} + \boldsymbol{d}^{\mathrm{T}}\boldsymbol{y} \in \mathbb{R}^{m}$ be the bidding strategy of the Virtual Power Plant, specified by (3.10)-(3.14). The mathematical formulation of the optimization problem covers the following economic and environmental objectives:

- **OB.1**: minimize variable cost $\min \left\{ \sum_{k \in H_{\mathrm{ts}}} OB^{\mathrm{VPP}}_{\mathrm{vc},k} \right\}$
- **OB.2**: minimize CO2 emission $\min \left\{ \sum_{k \in H_{\mathrm{ts}}} OB^{\mathrm{VPP}}_{\mathrm{CO2},k} \right\}$
- **OB.3**: minimize market exchange $\min \left\{ \sum_{k \in H_{\mathrm{ts}}} OB^{\mathrm{VPP}}_{\mathrm{em},k} \right\}$

In (3.10), the revenue opportunities are maximized through the minimization of the variable cost $OB^{\mathrm{VPP}}_{\mathrm{vc},k}$. The lowest cost solution considers the total variable cost for power adjustment and load shifting as well as the expected income or expenses of joint market operations.

$$\begin{aligned} OB^{\mathrm{VPP}}_{\mathrm{vc},k,j} = -\Big(& (-P^{typ,\mathrm{fc}}_{\mathrm{d},k,j} \cdot \varepsilon_{\mathrm{vc}} \cdot \varpi^{typ,\mathrm{fc}}_{\mathrm{vc}} - P^{typ,\mathrm{fc}}_{\mathrm{g},k,j} \cdot \varpi^{typ,\mathrm{fc}}_{\mathrm{vc}}) \\ & + (\Delta P^{typ,\mathrm{pc}}_{\mathrm{d},k,j} \cdot \varpi^{typ,\mathrm{pc}}_{\mathrm{vc,ctrl}} - \Delta P^{typ,\mathrm{pc}}_{\mathrm{g},k,j} \cdot \varpi^{typ,\mathrm{pc}}_{\mathrm{vc,ctrl}}) \\ & - (\tilde{P}^{em}_{k,fh,j} \cdot \varpi^{em}_{k,fh}) \Big) \cdot \Delta t \end{aligned} \tag{3.10}$$

The assigned market prices ϖ^{em}, detailed in Appendix A, refer to historical data of spot market auctions. The variable cost $\varpi^{typ,\mathrm{pc}}_{\mathrm{vc,ctrl}}$ for partly-controlled power generation and demand units are differentiated by the price for the provision of internal control reserve $\varpi^{\mathrm{CR}^{\pm}}$ and is calculated by

$$\varpi^{typ,\mathrm{pc}}_{\mathrm{vc,ctrl}} = \begin{cases} \varepsilon_{\mathrm{vc}} \cdot \varpi^{typ,\mathrm{pc}}_{\mathrm{vc}} - \varpi^{\mathrm{CR}^{\pm}} & \text{generation or demand increase} \\ \varepsilon_{\mathrm{vc}} \cdot \varpi^{typ,\mathrm{pc}}_{\mathrm{vc}} + \varpi^{\mathrm{CR}^{\pm}} & \text{generation or demand reduction.} \end{cases} \tag{3.11}$$

The variable cost $\varpi^{typ,\mathrm{pc}}_{\mathrm{vc}}$ for each unit type is multiplied by the scaling factor $\varepsilon_{\mathrm{vc}}$, used in later scenarios for cost sensitivity analysis. The default value of $\varepsilon_{\mathrm{vc}}$ is set to 1, leaving the original cost structure unchanged. Within the optimization processes, the initial market bidding schedules calculated in (3.5) are sequentially adjusted by (3.12) to determine the final market exchanges.

$$\Delta\tilde{P}^{em}_{k,fh,j} = \Delta\tilde{P}^{em}_{k,fh,j} - (P^{typ,\mathrm{fc}}_{\mathrm{g},k,j} + P^{typ,\mathrm{fc}}_{\mathrm{d},k,j} + \Delta P^{typ,\mathrm{pc}}_{\mathrm{g},k,j} + \Delta P^{typ,\mathrm{pc}}_{\mathrm{d},k,j}) \tag{3.12}$$

Similarly, (3.13) calculates the total emissions of the power plant portfolio. While the specific greenhouse gas emissions of generator units are fully taken into account, purchases from the spot market $\tilde{P}^{em}_{k,fh} > 0$ are assumed with $ghg^{em}_{\mathrm{CO2}} = 550$ gCO2/kWh, $ghg^{em}_{\mathrm{CO2}} = 0$ for $\tilde{P}^{em}_{k,fh} \leq 0$, respectively. The specific greenhouse gas emissions for purchases reflect the current average carbon dioxide emissions of the electricity mix in Germany.

$$\begin{aligned} OB^{\mathrm{VPP}}_{\mathrm{CO2},k,j} = & \Big((P^{typ,\mathrm{fc}}_{\mathrm{g},k,j} \cdot ghg^{typ,\mathrm{fc}}_{\mathrm{CO2}}) \\ & + (\Delta P^{typ,\mathrm{pc}}_{\mathrm{g},k,j} \cdot ghg^{typ,\mathrm{pc}}_{\mathrm{CO2}}) \\ & + (\tilde{P}^{em}_{k,fh,j} \cdot ghg^{em}_{\mathrm{CO2}}) \Big) \cdot \Delta t \end{aligned} \tag{3.13}$$

Additional bidding strategies, such as the mitigation of day-ahead and intraday mar-

ket exchanges, are realized through the application of (3.14). The objective function may be relevant for energy management algorithms within Microgrids simulations, e.g. to optimize the power balance associated within islanding operations.

$$OB^{\mathrm{VPP}}_{\mathrm{em},k,j} = (P^{em}_{\mathrm{IM}k,fh,j} - P^{em}_{\mathrm{EX}k,fh,j}) \cdot \Delta t \tag{3.14}$$

The optimization processes are restricted by the model attributes and operational states of the units and unit clusters. These are specified by the following series of boundary and constraint conditions.

Boundary Conditions – The lower and upper bounds of fully-controlled units are defined by the assigned operating ranges for the power generation or demand as follows:

$$0 \leq P^{typ,\mathrm{fc}}_{\mathrm{g},k,j} \leq P^{typ,\mathrm{fc}}_{\mathrm{g,max}} \tag{3.15}$$

$$P^{typ,\mathrm{fc}}_{\mathrm{d,max}} \leq P^{typ,\mathrm{fc}}_{\mathrm{d},k,j} \leq 0 \tag{3.16}$$

$$y^{stor,\mathrm{fc}}_{k,j} \cdot P^{stor,\mathrm{fc}}_{\mathrm{d,max}} \leq P^{stor,\mathrm{fc}}_{k,j} \leq (1 - y^{stor,\mathrm{fc}}_{k,j}) \cdot P^{stor,\mathrm{fc}}_{\mathrm{g,max}}. \tag{3.17}$$

The integer variables $y^{stor,\mathrm{fc}}_{k}$ of the fully controlled storage units indicate the operation mode. In case of $y^{stor,\mathrm{fc}}_{k} = 1$ charging processes, otherwise for $y^{stor,\mathrm{fc}}_{k} = 0$ discharging processes take place. The boundary conditions of partly-controlled generation and load units are given by (3.18) and (3.19). The equations represent the minimum and maximum power values for the possible provision of internal control reserve.

$$P^{typ,\mathrm{pc}}_{\mathrm{g,min}} \leq \Delta P^{typ,\mathrm{pc}}_{\mathrm{g},k,j} \leq P^{typ,\mathrm{pc}}_{\mathrm{g,max}} \tag{3.18}$$

$$P^{typ,\mathrm{pc}}_{\mathrm{d,min}} \leq \Delta P^{typ,\mathrm{pc}}_{\mathrm{d},k,j} \leq P^{typ,\mathrm{pc}}_{\mathrm{d,max}} \tag{3.19}$$

The lower and upper bounds for partly controlled generation units and load units are specified in (3.20) and (3.21), respectively.

$$P^{typ,\mathrm{pc}}_{\mathrm{g,min}} = y^{typ,\mathrm{pc}}_{k,j} \cdot \max\{-P^{typ,\mathrm{CR}^-}_{\mathrm{g,max}}, -\tilde{P}^{typ,\mathrm{pc}}_{\mathrm{g},k,fh}\} \tag{3.20}$$

$$P^{typ,\mathrm{pc}}_{\mathrm{g,max}} = (1 - y^{typ,\mathrm{pc}}_{k,j}) \cdot \min\{P^{typ,\mathrm{CR}^+}_{\mathrm{g,max}}, P^{typ,\mathrm{pc}}_{\mathrm{g,max}} - \tilde{P}^{typ,\mathrm{pc}}_{\mathrm{g},k,fh}\}$$

$$P_{\mathrm{d,min}}^{typ,\mathrm{pc}} = y_{k,j}^{typ,\mathrm{pc}} \cdot \max\{-P_{\mathrm{d,max}}^{typ,\mathrm{CR}^-}, -P_{\mathrm{d,max}}^{typ,\mathrm{pc}} - \tilde{P}_{\mathrm{d},k,fh}^{typ,\mathrm{pc}}\} \tag{3.21}$$

$$P_{\mathrm{d,max}}^{typ,\mathrm{pc}} = (1 - y_{k,j}^{typ,\mathrm{pc}}) \cdot \min\{P_{\mathrm{d,max}}^{typ,\mathrm{CR}^+}, -\tilde{P}_{\mathrm{d},k,fh}^{typ,\mathrm{pc}}\}$$

For partly controlled generator and load units, the activation of internal control reserve is determined by integer variables. Negative values of $\Delta P^{typ,\mathrm{pc}}$ indicate either a generation decrease or a load increase. In case of power adjustment and load shifting with partly controlled load units, the integer variable $y_k^{typ,\mathrm{pc}} = 1$ initiates a load increase while $y_k^{typ,\mathrm{pc}} = 0$ leads to a load reduction. In each time step of the optimization process, the operational conditions of the partly controlled generator and load units are taken into account and the maximum possible flexibilities are determined. Taking $P_{\mathrm{d,max}}^{typ,\mathrm{pc}}$ as an example, the maximum possible load decrease is either given by the limit value of the positive control reserve $P_{\mathrm{d,max}}^{typ,\mathrm{CR}^+}$ or the predicted demand value $\tilde{P}_{\mathrm{d},k,fh}^{typ,\mathrm{pc}}$.

Linear Inequality Constraints – In accordance with the assigned virtual storage capacity $E_{\mathrm{r}}^{typ,\mathrm{pc}}$ of partly-controlled units as specified in Appendix C, the available energy capacity is formulated as function of the state of energy and given by

$$SoE_{\mathrm{min}}^{typ,\mathrm{pc}} \leq SoE_{k+1,j}^{typ,\mathrm{pc}} \leq SoE_{\mathrm{max}}^{typ,\mathrm{pc}} \quad \text{with} \quad SoE_{k+1}^{typ,\mathrm{pc}} = \frac{100\% \cdot E_{k+1}^{typ,\mathrm{pc}}}{E_{\mathrm{r}}^{typ,\mathrm{pc}}}. \tag{3.22}$$

In case of storage units, E_{r}^{stor} denotes the unit type specific rated energy capacity and the constraint formulation is expressed as follows:

$$SoE_{\mathrm{min}}^{stor,\mathrm{fc}} \leq SoE_{k+1,j}^{stor,\mathrm{fc}} \leq SoE_{\mathrm{max}}^{stor,\mathrm{fc}} \quad \text{with} \quad SoE_{k+1}^{stor,\mathrm{fc}} = \frac{100\% \cdot E_{k+1}^{stor,\mathrm{fc}}}{E_{\mathrm{r}}^{stor,\mathrm{fc}}}. \tag{3.23}$$

While the energy values for the calculations for partly-controlled units are derived from (3.1), for storage units these energy values are given by

$$E_{k+1}^{stor,\mathrm{fc}} = \begin{cases} E_k^{stor,\mathrm{fc}} - P_{\mathrm{d},k}^{stor,\mathrm{fc}} \cdot \eta^{\mathrm{mod}} \cdot \Delta t, & \text{charging mode} \\ E_k^{stor,\mathrm{fc}} - P_{\mathrm{g},k}^{stor,\mathrm{fc}} \cdot \frac{1}{\eta^{\mathrm{mod}}} \cdot \Delta t, & \text{discharging mode.} \end{cases} \tag{3.24}$$

Problem Solving – The mixed-integer linear programming problem is solved by using a branch-and-cut method with simplex algorithm, offered by the Matlab extension of ILOG CPLEX Optimization solver. The optimization variables are updated at each iteration during the optimization processes until a defined tolerance on the change of the objective function value is satisfied, or the maximum number

of iterations is reached. Depending on the selected optimization solver, the optimization processes can be further accelerated, e.g. through the adjustments of the function tolerances, constraint and step tolerances, respectively. However, the computational effort to solve the multi-period optimization problem can still be limited, e.g. due to the speed of data measurement, data exchange or data processing.

3.4. Simulation and Computational Study

The energy management algorithm and optimization model is validated using time-series analysis with variations of the power plant portfolio characteristics and optimization parameters. For comparison purposes, the power plant portfolios are similarly constituted, as can be seen in Table 3.4. The share of the stationary battery systems $\Gamma^{\text{bat}} \in \{5\%, 10\%, 15\%, 20\%, 50\%\}$ in case 2-6 is a multiple of the total installed capacity of case 1.

First, the effectiveness of the three-stage imbalance compensation algorithm is tested in the base scenario. Hereby, the dynamic effects of the forecast accuracies on the power scheduling processes and coordinated redispatch measures are investigated. Second, the economic efficiency of cost-optimized and CO2-optimized joint market operations are assessed in case 1 and 2. Third, the specific utilization and dispatch of stationary battery systems with different unit models are analyzed. Forth, the revenue perspective of the Virtual Power Plant operator is specified in cost sensitivity analysis.

TABLE 3.4.: Power plant portfolio parametrization for case studies with different shares of stationary battery systems.

scenario	wind	pv	chp	dg	bat*)	ind	hh	total
	(MW)							
case 1: base	140	130	20	20	\	60	30	400
case 2: base + 5% battery capacity	140	130	20	20	$(1+\Gamma^{\text{bat}}) \cdot 20$	60	30	$400 + (1+\Gamma^{\text{bat}}) \cdot 20$

*) minimum and maximum state of energy are assumed with $SoE^{\text{bat}}_{\text{min}} := 10\ \%$ and $SoE^{\text{bat}}_{\text{max}} := 90\ \%$, respectively.

The simulation results are quantified according to specific and absolute evaluation parameters. For each time step, the total variable cost $\varpi^{\text{VPP}}_{\text{vc},k}$, greenhouse gas emissions $ghg^{\text{VPP}}_{\text{CO2},k}$, and the market energy exchange $E^{\text{VPP}}_{\text{em},k}$ are determined and normalized as follows:

$$\lambda_{\mathrm{vc}}^{\mathrm{VPP}} = \sum_k \frac{\varpi_{\mathrm{vc},k}^{\mathrm{VPP}}}{P_{\mathrm{g},k}^{\mathrm{VPP}} \cdot \Delta t}, \quad \lambda_{\mathrm{CO2}}^{\mathrm{VPP}} = \sum_k \frac{ghg_{\mathrm{CO2},k}^{\mathrm{VPP}}}{P_{\mathrm{g},k}^{\mathrm{VPP}} \cdot \Delta t}, \text{ and } \quad \lambda_{\mathrm{em}}^{\mathrm{VPP}} = \sum_k \frac{E_{\mathrm{em},k}^{\mathrm{VPP}}}{P_{\mathrm{g},k}^{\mathrm{VPP}} \cdot \Delta t}$$

with

$$\begin{aligned}
\varpi_{\mathrm{vc},k}^{\mathrm{VPP}} =& \Big((|P_{\mathrm{d},k}^{typ,\mathrm{nc}} \cdot \varepsilon_{\mathrm{vc}} \cdot \varpi_{\mathrm{vc}}^{typ,\mathrm{nc}}| - P_{\mathrm{g},k}^{typ,\mathrm{nc}} \cdot \varpi_{\mathrm{vc}}^{typ,\mathrm{nc}}) \\
&+ (|P_{\mathrm{d},k}^{typ,\mathrm{fc}} \cdot \varepsilon_{\mathrm{vc}} \cdot \varpi_{\mathrm{vc}}^{typ,\mathrm{fc}}| - P_{\mathrm{g},k}^{typ,\mathrm{fc}} \cdot \varpi_{\mathrm{vc}}^{typ,\mathrm{fc}}) \\
&+ (|P_{\mathrm{d},k}^{typ,\mathrm{pc,ref}} \cdot \varepsilon_{\mathrm{vc}} \cdot \varpi_{\mathrm{vc}}^{typ,\mathrm{pc}}| - P_{\mathrm{g},k}^{typ,\mathrm{pc,ref}} \cdot \varpi_{\mathrm{vc}}^{typ,\mathrm{pc}}) \\
&+ (-\Delta P_{\mathrm{d},k}^{typ,\mathrm{pc}} \cdot \varpi_{\mathrm{vc,ctrl}}^{typ,\mathrm{pc}} - \Delta P_{\mathrm{g},k}^{typ,\mathrm{pc}} \cdot \varpi_{\mathrm{vc,ctrl}}^{typ,\mathrm{pc}}) \\
&+ (|P_{\mathrm{EX},k}^{\mathrm{da}} \cdot \varpi_k^{\mathrm{da}}| - P_{\mathrm{IM},k}^{\mathrm{da}} \cdot \varpi_k^{\mathrm{da}}) \\
&+ (|P_{\mathrm{EX},k}^{\mathrm{id}} \cdot \varpi_k^{\mathrm{id}}| - P_{\mathrm{IM},k}^{\mathrm{id}} \cdot \varpi_k^{\mathrm{id}}) \Big) \cdot \Delta t \\
ghg_{\mathrm{CO2},k}^{\mathrm{VPP}} =& \Big((P_{\mathrm{g},k}^{typ,\mathrm{nc}} \cdot ghg_{\mathrm{CO2}}^{typ,\mathrm{nc}}) + (P_{\mathrm{g},k}^{typ,\mathrm{fc}} \cdot ghg_{\mathrm{CO2}}^{typ,\mathrm{fc}}) \\
&+ (P_{\mathrm{g},k}^{typ,\mathrm{pc,ref}} \cdot ghg_{\mathrm{CO2}}^{typ,\mathrm{pc}}) + (\Delta P_{\mathrm{g},k}^{typ,\mathrm{pc}} \cdot ghg_{\mathrm{CO2}}^{typ,\mathrm{pc}}) \\
&+ (P_{\mathrm{IM},k}^{\mathrm{da}} \cdot ghg_{\mathrm{CO2}}^{em}) + (P_{\mathrm{IM},k}^{\mathrm{id}} \cdot ghg_{\mathrm{CO2}}^{em}) \Big) \cdot \Delta t \\
E_{\mathrm{em},k}^{\mathrm{VPP}} =& \Big((P_{\mathrm{IM},k}^{\mathrm{da}} - P_{\mathrm{EX},k}^{\mathrm{da}}) + (P_{\mathrm{IM},k}^{\mathrm{id}} - P_{\mathrm{EX},k}^{\mathrm{id}}) \Big) \cdot \Delta t
\end{aligned} \tag{3.25}$$

Further, the energy equivalents $E_{\mathrm{g}} = \sum_k P_{\mathrm{g},k}^{\mathrm{VPP}} \cdot \Delta t$ and $E^{\mathrm{CR}^{\pm}} = \sum_k |\Delta P_k^{\mathrm{CR}^{\pm}}| \cdot \Delta t$ are calculated, denoting the total generated and purchased energy and the provided internal power adjustments and power shifting, respectively. As a simplification for the provision of internal control reserve, the price $\varpi^{\mathrm{CR}^{\pm}}$ is assumed to be the same for all unit types with 10 EUR/MWh. Each scenario covers 10 days, whereby the first 3 days refer as initialization period and are therefore not considered in the evaluation results.

3.4.1. Impacts of Forecast Accuracy in Joint Market Operations

To participate in the joint market operation, the Virtual Power Plant operator predicts the expected power generation of renewable energy sources. However, the forecasts have particular forecast accuracies which differ regionally and over time. As an approximation of different forecast scenarios, Appendix D introduces a forecast model that uses normal and uniform distribution functions to synthetically generate forecast profiles with defined forecast errors. The average normalized root mean square error $err_{fh}^{\mathrm{NRMSE}}$ is used as an indicator for the forecast accuracy. Depending on the forecast horizon, Table 3.5 lists the obtained values as a result of the applied forecast model. The tabulated values have similar forecast accuracies in comparison with analogous values found in the literature [97–106]. A selection of

the generation forecast of wind and photovoltaic power plants is given in Fig. 3.9. The grey area denotes the real-time schedules. The synthetic forecast profiles with forecast horizons of 24h, 1h and 0.25h are highlighted as solid red, dotted black and solid blue lines, respectively.

TABLE 3.5.: Evaluated forecast accuracies of time-varying forecast profiles of wind and photovoltaic power plants given for distinct forecast horizons of 24h, 1h and 0.25h.

wind			pv		
err_{24h}^{NRMSE}	err_{1h}^{NRMSE}	$err_{0.25h}^{NRMSE}$	err_{24h}^{NRMSE}	err_{1h}^{NRMSE}	$err_{0.25h}^{NRMSE}$
(p.u.)					
0.064	0.028	0.016	0.065	0.030	0.012

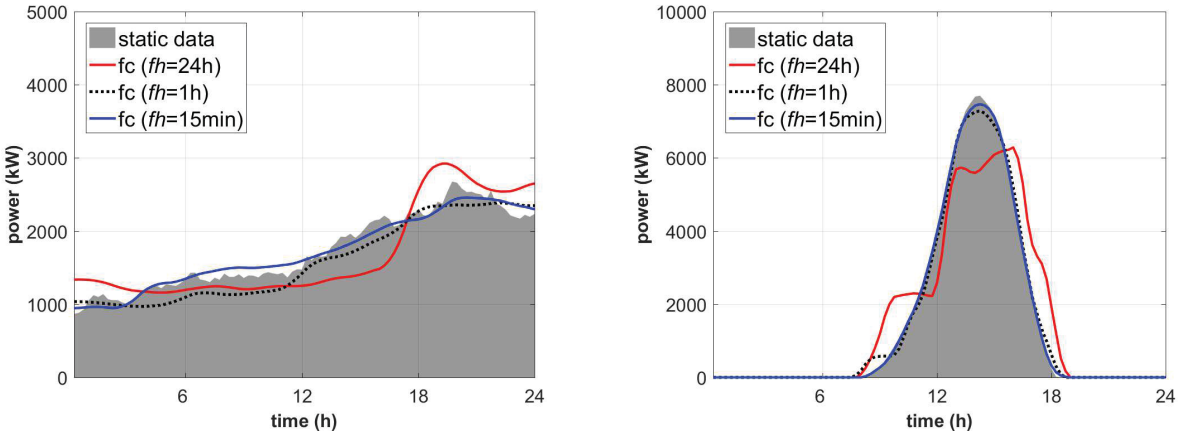

(a) wind power plant

(b) photovoltaic power plant

Fig. 3.9.: Day-ahead and intraday renewable power generation forecasts for wind and photovoltaic power plants.

Considering the power plant portfolio configuration of case 1, as defined in Table 3.4, the forecast uncertainties of the renewable energy sources are modeled similarly and used as inputs for the multi-period optimization processes. Selected results of the obtained bidding schedules are provided in Fig. 3.10a and shows the power imbalances for the day-ahead optimization with an forecast horizon of 24h and the intraday optimization with a forecast horizon of 1h.

In comparison of the cost-optimized scenario, Fig. 3.10b shows the results obtained in shorter dispatch intervals and use of 0.25h generation forecasts. The power imbalances for each time step of the day-ahead and intraday optimization processes are indicated by the red solid trend line and blue solid trend line, respectively. Due to higher forecast accuracies available in the intraday operation and shorter dispatch intervals, the power imbalances can be reduced from almost 6 MW down to 4 MW. In addition, Figure 3.10c and Fig. 3.10d provide a selection of the obtained real-time schedules of both scenarios, segmented by unit types. The red solid line illustrates

the remaining real-time power imbalances, which are fully mitigated after the three-stage imbalance compensation algorithm has been executed.

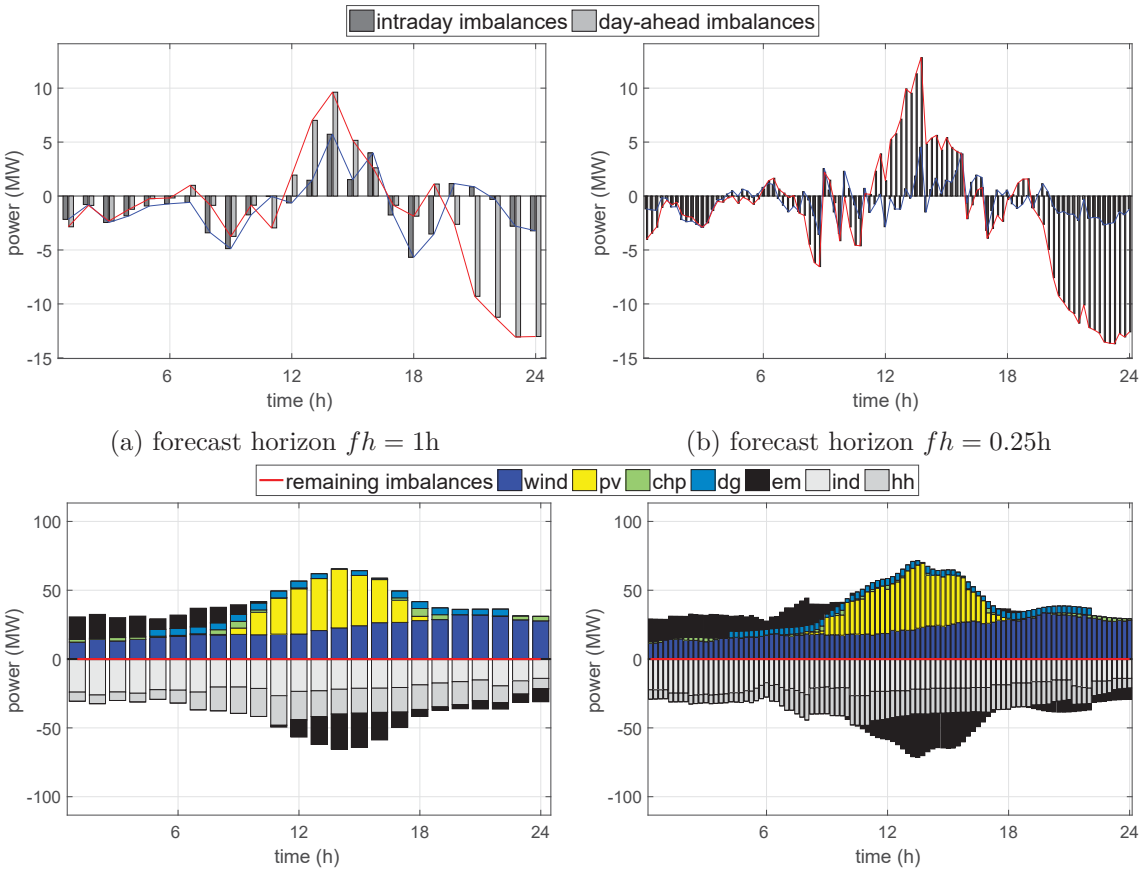

(a) forecast horizon $fh = 1\text{h}$ (b) forecast horizon $fh = 0.25\text{h}$

(c) forecast horizon $fh = 1\text{h}$ (d) forecast horizon $fh = 0.25\text{h}$

Fig. 3.10.: Comparison of power imbalances after cost-optimized day-ahead and intraday optimization process considering $fh = 1\text{h}$ and $fh = 0.25\text{h}$ forecast horizons in the energy management algorithm and corresponding real-time schedules after activation of internal control reserve.

Disregarding the forecast horizon, the contracted power exchanges in day-ahead and intraday markets stay almost unchanged but differentiate in the use of internal control reserve, as summarized in Table 3.6. Additionally, the variable cost and greenhouse gas emissions of the dispatch results are provided.

TABLE 3.6.: Comparison of the traded energy in cost-optimized scenarios over 168 hours indicating the effect of shorter dispatch intervals and use of internal control reserve.

forecast horizon	E_g	$E^{\text{CR}\pm}$		$\lambda_\text{vc}^\text{VPP}$	$\lambda_\text{CO2}^\text{VPP}$
	(MWh)	(MWh)	($\%E_\text{g}$)	(EUR/MWh)	(gCO2/kWh)
$fh = 1\text{h}$	6,975.52	1,029.69	14.76	-18.18	90.57
$fh = 0.25\text{h}$	7,024.96	900.89	12.82	-16.88	97.38

Through the utilization of shorter dispatch intervals, the provision of internal control reserve can be significantly reduced, by almost 2 % of the generated energy in the power plant portfolio. This in turn leads to decreasing operational cost for

the Virtual Power Plant operator. Particularly, the absolute values when using 1h and 0.25h generation forecasts in the scheduling process are given by the tabulated values. In summary, the simulation results confirm the feasibility of the developed three-stage imbalance compensation algorithm to mitigate balancing group deviations. This improves the reliability of the delivered power schedules while scaling down the overall power imbalances. This is also accomplished by considering shorter dispatch intervals and clearing sequences.

3.4.2. Comparative Assessment of Bidding Strategies

In this case study, comparatives assessments are carried out for economic and environmental bidding strategies in joint market operations. Table 3.7 summarizes the obtained results for the investigated power plant portfolios, which uses the same forecast profiles in cost-optimized and CO2-optimized scenarios.

TABLE 3.7.: Results obtained from cost-optimized (OB.1) and CO2-optimized (OB.2) base scenario and base +5% battery capacity scenario over 168 hours.

scenario		E_{g}	$E^{\mathrm{CR}\pm}$		$\lambda_{\mathrm{vc}}^{\mathrm{VPP}}$	$\lambda_{\mathrm{CO2}}^{\mathrm{VPP}}$
		(MWh)	(MWh)	(%E_{g})	(EUR/MWh)	(gCO2/MWh)
case 1	OB.1	7,024.96	900.89	12.82	-16.88	97.38
	OB.2	6,764.31	1,772.07	26.20	-44.73	20.17
case 2	OB.1	7,203.97	1,201.28	16.68	-14.51	96.23
	OB.2	6,735.53	1,872.40	27.80	-42.34	15.08

*) negative specific variable cost $\lambda_{\mathrm{vc}}^{\mathrm{VPP}}$ refer to expenses, positive values refer to incomes.

The total amount of energy traded, increases from 7,025 MWh to 7,204 MWh in cost-optimized scenarios and decreases from 6,764 MWh to 6,736 MWh in CO2-optimized scenarios. In the latter scenario, the specific variable costs are more than doubled due to the activation of the additional internal control reserve to substitute the market exchanges. For case 1, Fig. 3.11a and Fig. 3.11b provide the obtained results in the cost-optimized and CO2-optimized scenario. The gray lines indicate the day-ahead and intraday market exchanges while the red line shows the activation of the internal control reserve. Additionally, the day-ahead and intraday market prices are given in the black lines. The differences of the evaluated economic and environmental bidding strategy can be observed especially in moments of low markets prices. Here, the extracted cost-optimized power schedules in day-ahead operation are mostly compensated through activation of the internal control reserve. The import of the energy market is primarily compensated by controllable generation units to maintain the power balance of the power plant portfolio.

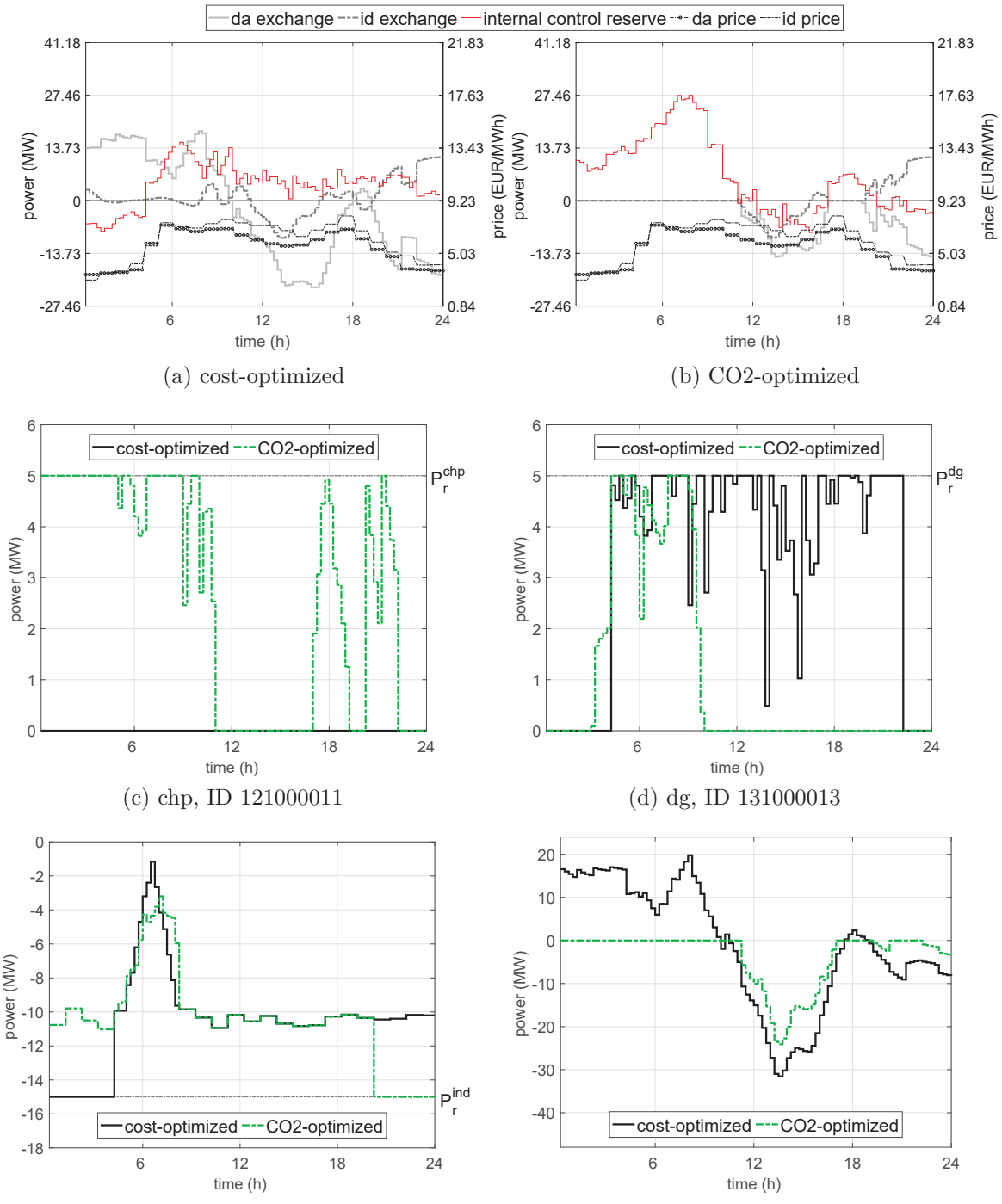

(a) cost-optimized

(b) CO2-optimized

(c) chp, ID 121000011

(d) dg, ID 131000013

(e) ind, ID 170000001

(f) em, ID 300000001+300000002

Fig. 3.11.: Activated internal reserve capacity in (a) cost-optimized and (b) CO2-optimized base scenario (case 1) with selected real-time schedules (c)-(e) of unit and unit clusters and the residual (f) energy market exchanges.

Insight into the obtained dispatch results is given in Fig. 3.11c-Fig. 3.11e for selected unit types, while Fig. 3.11f shows the residual market exchange. Thereby, the black line indicate the dispatched power in cost-optimized and the green line in CO2-optimized scenarios. For example, Fig. 3.11c shows that the combined heat and power unit is not committed in the cost-optimized scenario, as the assigned generation cost $\varpi_{\text{vc}}^{typ} = 141$ EUR/MWh are significantly above the market prices.

However, within the CO2-optimized scenario the combined heat and power unit is committed and dispatched for the aforementioned market import compensation. In comparison to the cost-optimized scenario, the residual market exchanges for the CO2-optimized scenario are significantly reduced as shown in Fig. 3.11f and thus also the total emissions of the power plant portfolio.

3.4.3. Objective Specific Stationary Battery System Utilization

The charging/discharging process of the integrated stationary battery systems can differ in accordance to the bidding strategy and assigned unit models, which are detailed in Appendix C. As an extension of the previous assessment, Table 3.8 summarizes the results of the analyzed scenarios with increasing share of stationary battery systems in the power plant portfolio for a total of 168 evaluated hours.

TABLE 3.8.: Dispatch results using forecast horizon of 0.25 hours for cost-optimized (OB.1) and CO2-optimized (OB.2) scenarios with different share of stationary battery systems.

scenario		E_g	$E^{CR\pm}$		λ_{vc}^{VPP}	λ_{CO2}^{VPP}
		(MWh)	(MWh)	(%E_g)	(EUR/MWh)	(gCO2/MWh)
case 2	OB.1	7,203.97	1,201.28	16.68	-14.51	96.23
	OB.2	6,735.53	1,872.40	27.80	-42.34	15.08
case 3	OB.1	7,458.44	1,611.19	21.60	-13.37	99.61
	OB.2	6,736.69	1,922.89	28.54	-42.42	15.30
case 4	OB.1	7,760.40	2,037.59	26.26	-12.19	105.58
	OB.2	6,746.17	1,995.06	29.57	-41.54	15.25
case 5	OB.1	8,071.64	2,389.48	29.60	-11.14	111.91
	OB.2	6,744.11	2,003.43	29.71	-42.12	14.55
case 6	OB.1	10,106.85	4,577.98	45.30	-6.34	147.56
	OB.2	6,754.62	2,224.05	32.93	-41.44	14.28

*) negative specific variable cost λ_{vc}^{VPP} refer to expenses, positive values refer to incomes.

In CO2-optimized optimized scenarios, the stationary battery systems are mostly charged at time periods of energy surplus, e.g. at noon hours to store power surplus provided by photovoltaic power plants instead of selling in the energy market. The stored energy is used during time periods with power deficit. In cost-optimized scenarios, the stationary battery systems are primarily charged in periods of low market prices and discharged in periods with higher market prices. Since those values are likely to drive results in scenarios with very high penetration rates of stationary battery systems, an extreme test is performed by means of case 6. Here the specific greenhouse gas emissions also remain almost unchanged in CO2-optimized scenar-

ios and confirm the saturation area of the previous simulations. Small variations are still possible due to the increasing battery capacity and resulting dispatch of the optimization processes. The specific variable costs decrease continuously in the cost-optimized scenarios, but are still at a negative level.

Specifying the utilization of the different battery technologies within the energy management system of the Virtual Power Plant operator, the assigned unit models as given in Appendix C, are further investigated. For example, taking the power plant portfolio configuration of case 2, Fig. 3.12 compares the dispatch schedules in cost-optimized and CO2-optimized scenarios.

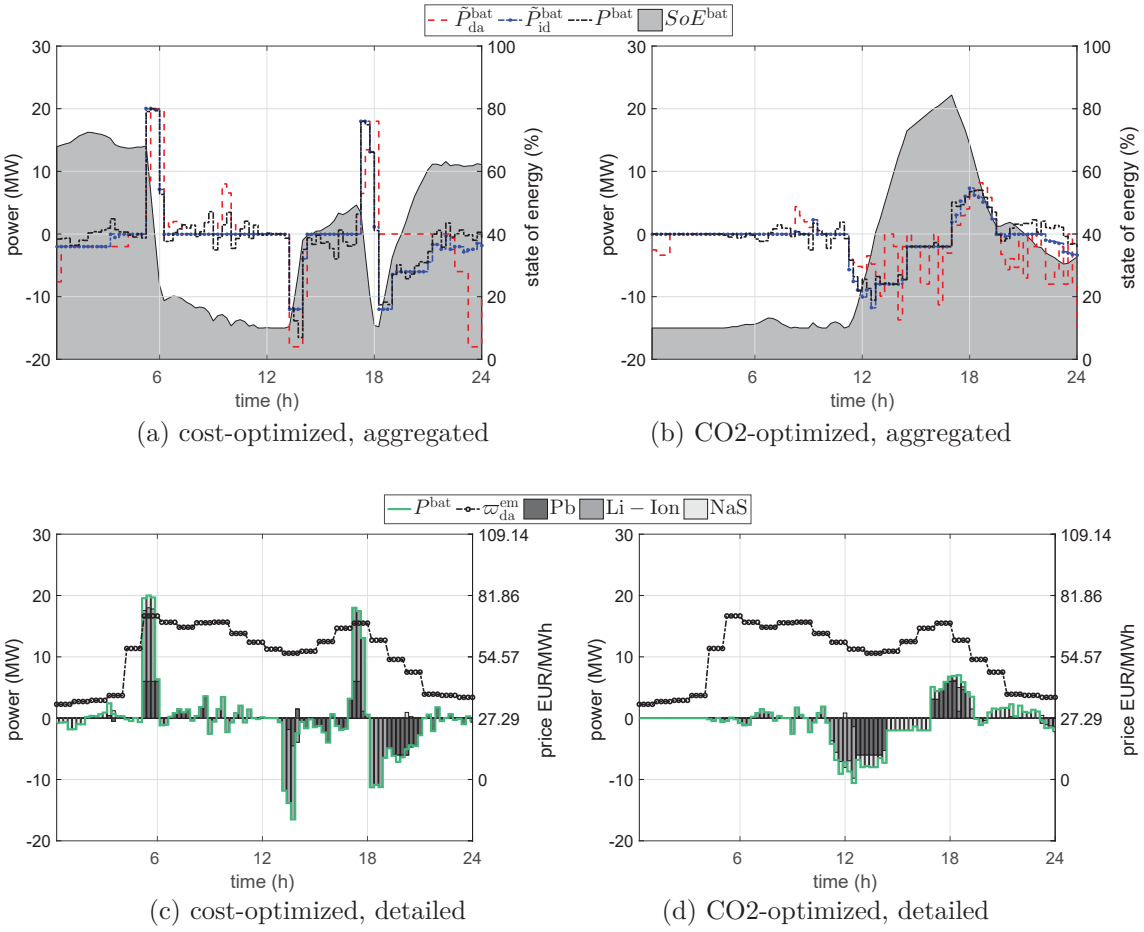

(a) cost-optimized, aggregated (b) CO2-optimized, aggregated

(c) cost-optimized, detailed (d) CO2-optimized, detailed

Fig. 3.12.: Cumulated (a),(b) day-ahead, intraday and real-time schedules of stationary battery systems with (c),(d) detailed unit model specific real-time schedules.

In Fig. 3.12a and Fig. 3.12b the aggregated dispatch schedules of the stationary battery systems are shown, whereby the red line represent the day-ahead, the blue line the intraday, the black line the real-time schedule and the gray area the state of energy of the battery systems. The real-time dispatch results are further detailed by means of Fig. 3.12c and Fig. 3.12d for cost- and CO2-optimized scenario, respectively. Additionally, the day-ahead market price signal is given by the black dashed line marked with circular markers. It can be observed that for the charg-

ing/discharging process first lithium-ion (Li-Ion) batteries are applied, followed by lead-acid (Pb) and sodium-sulphur (NaS) at last. The dispatched time interval for the charging/discharging increases from the lithium-ion to the sodium-sulphur technology from 1 hour up to 3 hours. The result complies the attributed linear inequality constraints of the unit models which are specified in Table C.3 and calculated in (3.23)-(3.24). The real-time schedule follows mainly the optimized intraday bidding schedule in correlation with the market price. Minor deviations are caused by the real-time imbalance compensation process to mitigate remaining power imbalances.

3.4.4. Cost Sensitivity Analysis and Revenue Perspective

Although the price structures, as given by the unit model attributes in Appendix C, are modeled on realistic assumptions, the Virtual Power Plan operator has more expenses than income opportunities as indicated in the previous assessments. This is because the price structures are explicitly modeled without any consideration of additional subsidies. As a possible solution to gain profit when participating in the energy market, the negative profit margin could be counterbalanced as it is the current practice, e.g. in Germany given by the feed-in tariff, subsidies or direct marketing of renewable energy sources [56].

Alternatively, different pricing methods and price strategies can be examined for the Virtual Power Plant operator. This is achieved by changing the cost structure as calculated by (3.11), through the variation of $\varepsilon_{\mathrm{vc}}$. The remaining variable cost and expenses for power adjustment and power shifting remain unchanged. In case of $\varepsilon_{\mathrm{vc}} = 1$, the variable cost for purchases are given in Table 3.9, referring to standard values provided by the European statistical data support Eurostat.

TABLE 3.9.: Overview of defined variable cost factors $\varepsilon_{\mathrm{vc}}$ and ranges of the adjusted demand oriented variable cost $\varpi_{\mathrm{vc}}^{typ,\mathrm{pc}}$ for energy supplies to industry, commercial and household load units.

unit type	variable cost $\varpi_{\mathrm{vc}}^{typ,\mathrm{pc}}$ in EUR/kWh, with $\varepsilon_{\mathrm{vc}}$:							
	1.00*)	1.05	1.10	1.15	1.20	1.25	1.30	1.35
ind	[0.0445, 0.0610]	[0.0467, 0.0641]	[0.0490, 0.0671]	[0.0512, 0.0702]	[0.0534, 0.0732]	[0.0556, 0.0763]	[0.0579, 0.0793]	[0.0601, 0.0824]
hh	[0.0741, 0.0772]	[0.0778, 0.0811]	[0.0815, 0.0849]	[0.0852, 0.0888]	[0.0889, 0.0926]	[0.0926, 0.0965]	[0.0963, 0.1004]	[0.1000, 0.1042]

*) derived from statistics provided by the European statistical data support Eurostat.

For example, the lower value of the interval $\varpi_{\mathrm{vc}}^{typ,\mathrm{pc}} = 0.0445$ EUR/kWh denotes the variable cost for industry load units with an annual energy demand between

70,000 MWh and 150,000 MWh. For commercial and household loads, the lower value $\varpi_{\mathrm{vc}}^{typ,\mathrm{pc}} = 0.0741$ EUR/kWh specifies the purchase cost with less than 15 MWh annual energy demand.

The results obtained in the cost sensitivity analysis are summarized in Fig. 3.13. There are noticeable differences with or without consideration of stationary battery systems. For example, with the regular cost structure $\varepsilon_{\mathrm{vc}} = 1$, as a result of applying (3.25) the ranges of the calculated specific variable cost $\lambda_{\mathrm{vc}}^{\mathrm{VPP}} = [-16.88, -6.11]$ in EUR/MWh are obtained with increasing penetration of battery systems from 0% up to 50%. Income opportunities can be already achieved in scenarios with $\varepsilon_{\mathrm{vc}} = 1.3$ times the variable cost for purchases and with 5% share of stationary battery systems. The range of the specific CO2 emissions of the power plant portfolio is $\lambda_{\mathrm{CO2}}^{\mathrm{VPP}} = [96.23, 147.56]$ in gCO2/kWh and remain approximately the same for an increasing variable cost factor. This is due to the formulated objective function that minimizes the variable operating cost of the power plant portfolio.

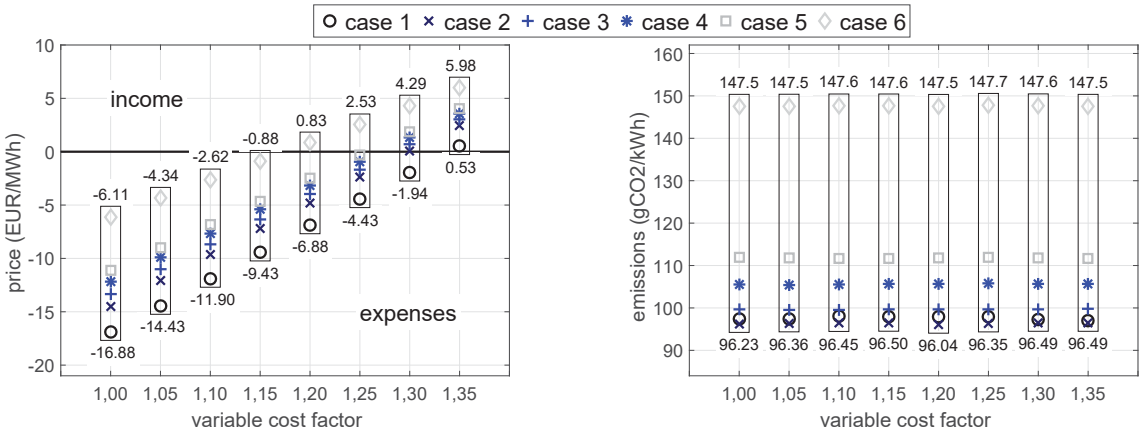

Fig. 3.13.: Cost sensitivity results for each power plant portfolio configuration, specified by the obtained specific variable cost $\lambda_{\mathrm{vc}}^{\mathrm{VPP}}$ and greenhouse gas emissions $\lambda_{\mathrm{CO2}}^{\mathrm{VPP}}$.

In summary, this simplified cost-sensitivity analysis shows the complexity of the effects on possible price structures under given conditions and identifies the deficit or surplus of the profit margins. The results can be used of the Virtual Power Plant operator within the decision-making process related to identify the most cost-effective values and pricing strategy for the use of different power plant technologies. Alternatively, the calculations can be adapted to identify the required subsidies to reach grid parity especially with renewable energy sources and storage systems.

3.5. Concluding Remarks

A Virtual Power Plant model is developed for the operational planning of power plant portfolios and solving multi-period optimization processes in joint market

operation. Nodal-based aggregation and cluster algorithm is presented and combined with different control concepts. The unified model architecture allows creating various power plant portfolios with unique unit models and simulate time-varying characteristics of renewable energy sources under consideration of distinct forecast accuracies. The mathematical formulation of the optimization problem is specified and validated for a variety of power plant portfolio configurations. The results indicate the potential to solve the multi-period optimization problem with different time resolution and forecast horizons and fully compensate power imbalances through the proposed three-stage imbalance compensation algorithm. The presented methodology can contribute to improve the compliance of the Virtual Power Plant operator in joint market operations. The optimization problem is formulated as a mixed integer linear programming and embedded in modular structured energy management algorithm. Extensions to include multilateral transactions and hierarchical optimization techniques are a straightforward process. For further research, the physical limitations defined by the speed of data measurement and data processing have to be appropriately determined to enhance operation and obtain desired dispatch results.

4. OPTIMIZED ENERGY PROCUREMENT FOR ELECTRIC VEHICLE FLEETS MANAGED IN VIRTUAL POWER PLANTS

Abstract – With the share of electric vehicles within the transportation sector rising, solutions for the market and system integration are of increasing importance. With regards to the operational management of charging processes and optimized energy procurement and supply, the chapter details the extension of the Virtual Power Plant concept for promoting an effective integration of electric vehicles. A hierarchically structured optimization approach is established to achieve optimal charging power schedules considering multilateral transactions in joint market operations. A profound understanding of the multilateral transactions between the market entities involved in the charging process is given and substantiated through comprehensive simulation studies. For distinct electric vehicle fleets, consisting of private and commercial electric vehicles, a methodology for prediction of the required energy demand is presented. The main characteristics are investigated and used as inputs for the energy management algorithm. The proposed optimization model is verified in numerical analysis and the applicability of using the energy capacity of the electric vehicle fleets in the power plant portfolio demonstrated.

Keywords – aggregation algorithm, average modeling, charging infrastructure, hierarchical optimization, driving profiles, electric vehicles, multilateral transactions, power scheduling, redispatch measures

4.1. Introduction

Developments in the energy and transport sectors present complex challenges for operators and suppliers involved in the charging process of small- and large-scale electric vehicles. The rollout of mobility solutions and its integration in a fleet and charging management is accompanied by substantial challenges, e.g. the reduction of the total cost of ownership [107, 108], provision of sufficient charging infrastructures [109, 110], and standardization of regulatory requirements [111]. With predictable improvements of the batteries technologies and performances, electric

vehicles might not be regarded just as loads but also as mobile energy resources. Hence, electric vehicles can be either consumer, when in charging mode, or injectors of power to the grid, in so called vehicle-to-grid (V2G) mode [112, 113]. This requires extended network functionalities and standards to avoid bulky grid reinforcements and facilitate the market integration. Specifically, enhanced planning and operation methods need to be considered to offer suitable charging strategies, market and business models [114, 115]. In that regard, optimization techniques for smart charging strategies are proposed [116–118] to lower the overall energy cost, avoid grid congestion and peak loads caused by charging processes [46]. A critical aspect hereby is the determination of the energy demand for charging processes at a range of spatial and temporal scales. This requires to obtain additional information, e.g. through transportation network simulations [63], traffic generators [119, 120] or field-recorded driving cycles stamped with dwell times and locations [121]. Here, the offered planning methods of the existing research anticipate full information of the user behaviors, driving profiles, charging times. This can be complicated and in practical cases can be realized efficiently only by means of smart or optimal charging schemes that uses direct load controls and state information of the electric vehicles [122, 123]. Compared to the existing research, the chapter proposes a solution to integrate electric vehicles in the Virtual Power Plant to obtain optimal charging schedules and make use of those additional mobile energy sources for energy market participation and provision of power system services. This is achieved thanks to novel Virtual Power Plant functions proposed here that predicts the required energy demand for charging processes through the integration of activity-based and timetable-based driving schedules of electric vehicles fleets instead of using extensive methods for the determination of the user behaviors or trip-based management solutions. The second important contribution lies in the formulation of a hierarchically structured optimization model allowing multilateral transactions with the main market entities involved in the charging processes. Different scenarios are studied in simulations to evaluate the cost-effective and environment-friendly features of the proposed optimization model.

4.2. Implementation Schemes for Electric Mobility

The integration process of electric vehicles in the energy and transport sector poses serious challenges for market entities involved in the charging process. Therefore well coordinated interactions are required to lower the complexity for market participation and power system operation purposes. Aggregation entities, including the Virtual Power Plant operator, represent an option to bid and participate in energy

markets under the same market entity [38, 124–126]. This offers the possibility to provide several services, including trading in the energy market, balancing of trading portfolios and provision of services for system operators [127]. Charging points for electric vehicles can be equipped with various conductive and inductive charging technologies [128], whereby some charging points can be used for bidirectional operations. For this purpose, smart meter infrastructures and sufficient information and communication technologies (ICT) are a prerequisite. According to established standards [1], the electric vehicles already communicates control and usage data with the charging point. Depending on the established connection requirements, the system operators may also communicate directly with the charging point to turn the charging point off/on in order to relieve problems of congestion in the power system.

4.2.1. Joint Market Operations and Transactions

Subjected to the level of aggregation and according to the total load and energy demand of the electric vehicles, a distinction can be made between intermediate and higher-level aggregation entities [85]. Intermediate aggregation entities are responsible to communicate with higher-level aggregation entities. This allows an efficient system management without full information availability [129–131]. The market entities will have contracts with the owner of the electric vehicles for selling charging services, offering access and metering services with transparent and unbundled charges as required by directives, e.g. 2009/72/EC concerning common rules for the internal market in electricity and repealing. Depending on the charging point locations (CPs), either in (i) private areas with private access, (ii) private areas with public access, or (iii) public areas with public access, charging point managers (CPMs) are responsible for developing and operating charging infrastructure. The classification for charging point locations is based on the ownership and access permission. For single electric vehicles in private areas with private access also local distributors may exist that take over the tasks of a charging point managers. The responsibilities may include the energy procurement, managing payment for charging processes, and dealing with Electric Vehicle Supplier/Aggregator (EVS/A) and system operators. The EV Supplier/Aggregator is the market entity which collates the energy demand of a number of electric vehicles and is responsible for the maintenance planning, operating data acquisition and management. Depending on the number of electric vehicles, the EV Supplier/Aggregator negotiates the commercial conditions with the Virtual Power Plant operator and buys the electric-

[1] e.g. SAE2836-1 use cases for communication between plug-in vehicles and the utility grid, SAEJ2847-1 communication between plug-in vehicles and the utility grid.

ity for charging services or directly participates in the energy market. Figure 4.1 shows a possible solution for the integration of these market entities in the Virtual Power Plant. Each EV Supplier/Aggregator combines the functions of managing and retailing the energy demand for the operation of distinct electric vehicles, e.g. passenger or commercial electric vehicles. The segments of the pie diagram indicate the number of electric vehicles assigned to possible charging point locations. The Virtual Power Plant operator offers differentiated charging tariffs in accordance to the control and charging strategy of the EV Suppliers/Aggregators and receives the corresponding information to determine possible operation schedules.

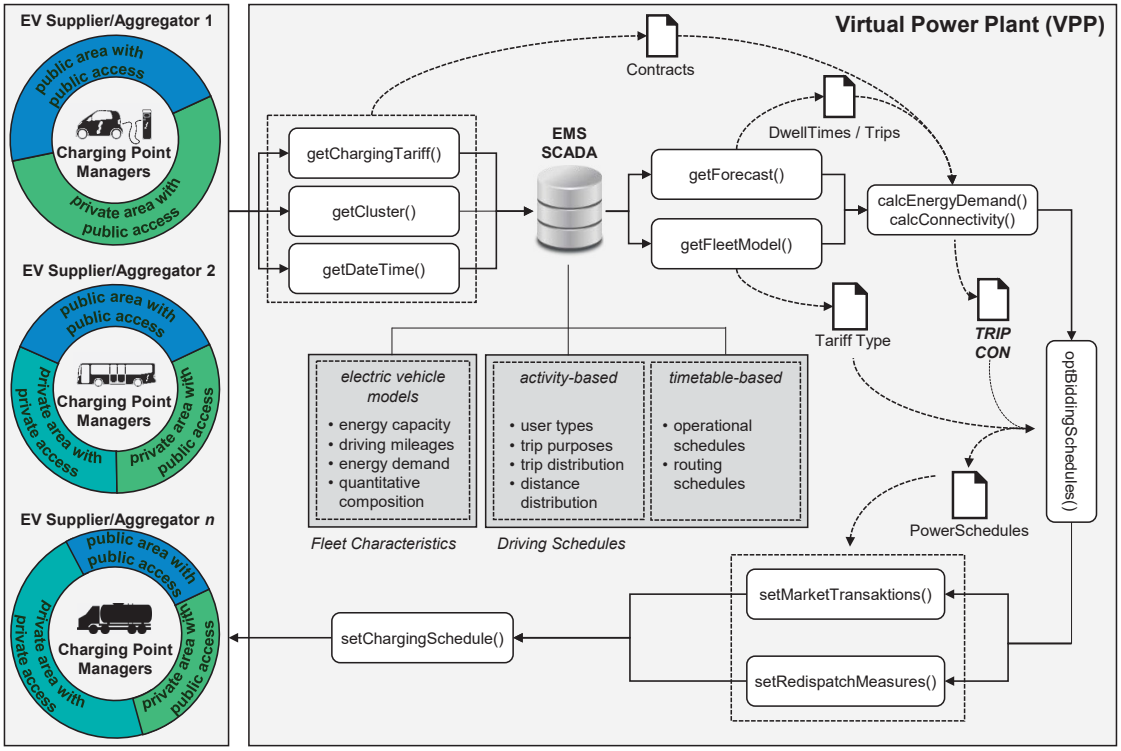

Fig. 4.1.: Solution approach for the integration of electric vehicles in joint market operations through the coordinated interaction between the Virtual Power Plant operator and different EV Suppliers/Aggregators.

Depending on the assigned contract, the Virtual Power Plant operator functions as trading and energy supplier and includes the set of electric vehicles fleets H_{fleet} in its supervisory control and data acquisition (SCADA) and energy management systems (EMS). This allows to directly link the aggregated energy demand of the electric vehicles to the optimization problem for the operational planning of the power plant portfolio and solving multi-period optimization processes in joint market operation, as discussed in Chapter 3. Therefore, appropriate electric vehicle models needs to be defined that capture the main characteristics of the electric vehicle fleets. The total number of electric vehicles $H_{\text{ev}} \in \{1, 2, \ldots, i, \ldots n^{\text{ev}}\}$ in the power plant portfolio can be specified by (4.1). Let $H_{\text{mstor}} = H_{\text{pev}} \cup H_{\text{cev}}$ be the set of electric vehicle

models, composed by the subsets of passenger and commercial electric vehicles.

$$H_{\text{ev}} \supseteq H_{\text{fleet}} \quad \text{, with} \quad \bigsqcup H_{\text{fleet}} = \{(mstor, i) \mid mstor \in H_{\text{mstor}} \;\; i \in H_{\text{fleet}} \} \quad (4.1)$$

Each of the electric vehicle models is specified with model attributes and matched with activity-based and timetable-based driving schedules (grey rectangle) so that the fleet characteristic can be integrated in the energy management algorithm. The Virtual Power Plant operator determines the optimized energy procurement and evaluates opportunities for the provision of services offered to the energy market or system operators, which is detailed in the following elaborations. Finally, the proposed charging schedules are forwarded to the EV Suppliers/Aggregators that takes care of the ongoing operations.

4.2.2. Charging Strategies and Tariffing

For the development of business related applications, Table 4.1 provides an overview of possible charging concepts and strategies at specific charging point locations [132], to conceive charging attractive for different EV Supplier/Aggregators and electric vehicle users.

TABLE 4.1.: Charging concepts and strategies for private and commercial electric vehicles related to charging point locations.

	private areas with private access	**private areas with public access**	**public areas with public access**
locations	home parking	public parking	
		parking garage	terminal station
		underground parking	intermediate station
		business buildings	motorway
		retail location	railway station
charging concept	1st-base charging	1st- and 2nd-base charging	2nd-base charging
	overnight charging	opportunity charging	

A distinction is made between 1st- and 2nd-base charging that allows the application of different charging tariffs. While 1st-base charging offers opportunities to

charge at a specific location, e.g. home, depot, workplace, office, 2nd-base-charging on the other hand, provides additional opportunities to charge at recharge stations, e.g. shopping district, supermarket, on-street. With particular focus on electric vehicle fleets different charging concepts are proposed. This includes opportunity charging at terminal or intermediate stations [133], up to automated exchange stations through battery swapping [134]. Depending on the charging infrastructure and on-board electronics of the electric vehicle, different charging schemes as schematically depicted in Fig. 4.2 can theoretically be realized for inductive and conductive charging technologies.

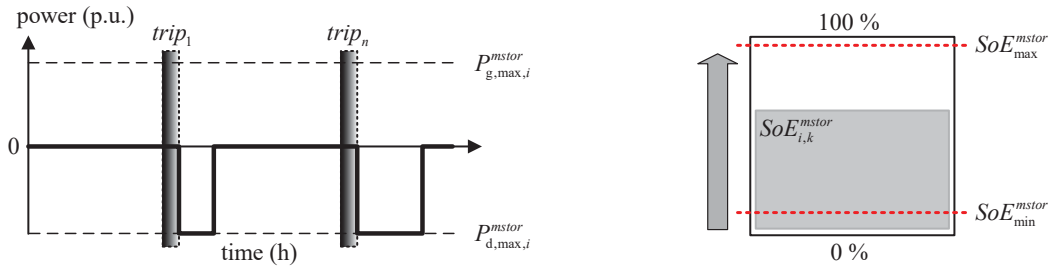

(a) non-controlled charging

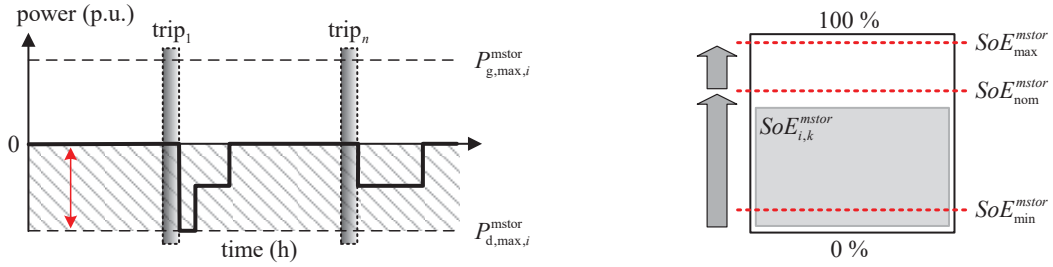

(b) partly-controlled charging

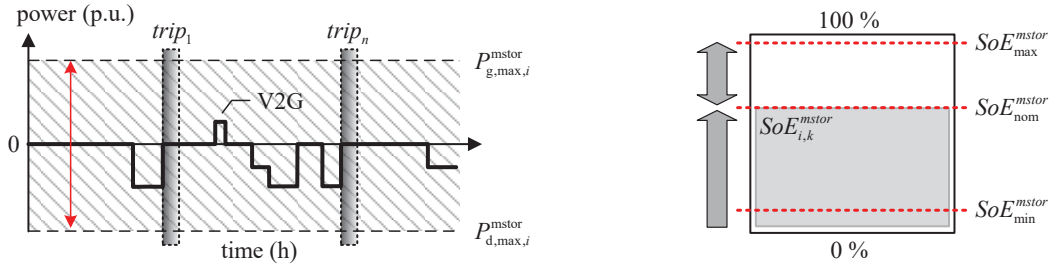

(c) fully-controlled charging

Fig. 4.2.: Charging schemes for electric vehicles and operation ranges for (a) non-controlled, (b) partly-controlled, and (c) fully-controlled charging strategies.

The charging schemes are derived from considerations on different charging strategies

[86, 135, 136] and combines SoE-based and price-based charging. Possible operation ranges are indicated by the red arrow and highlighted by the gray shaded areas. In order to counteract the aging of the energy storage [137, 138], the useable energy capacity is limited. The ranges are indicated by the minimum SoE_{min} and maximum SoE_{max} state of energy in relation to the rated energy capacity E_{r} of the energy storage. An example of which is given on the right hand side in Fig. 4.2. In accordance to the flexibilities that can be provided by the electric vehicle fleets within the operational planning of the power plant portfolio, the charging schemes are translated into power boundary and constraint conditions in the optimization model and summarized as possible set of charging tariffs H_{tariff} . Table 4.2 specifies the constraint variable for the charging power P_{r} and nominal state of energy SoE_{nom}, as well as the considered charging prices and remuneration for the provision of vehice-to-grid services.

TABLE 4.2.: Set of charging tariffs H_{tariff} for electric vehicles distinguished by the rated charging/discharging power P_{r}, nominal state of energy SoE_{nom}, charging price and V2G remuneration.

tariff ID	tariff type	P_{r}	SoE_{nom}	charging price	V2G remuneration
		(kW)	(%)	(EUR/kWh)	(EUR/kWh)
1	base	3.7	(-)	0.14	(-)
2	flex	11.4	70	0.12	(-)
3	V2G	44	80	0.10	0.17
4	base	450	(-)	0.14	(-)
5	flex	150	70	0.10	(-)
6	V2G	100	80	0.10	0.17

The charging tariffs are differentiated according to available charging infrastructures, charging systems, and applicable standards [139], e.g. IEC 61851 standard series and plug types according to IEC 62196-2. While the charging tariffs (ID1-ID3) are used in combination with passenger electric vehicles, the charging tariffs (ID4-ID6) refer to operations related with commercial electric vehicle. Here, the rated charging power indicates the state of the art, e.g. charging infrastructures used for the operation of electrified buses. However, extensions by individualized tariffs and changes of the tabulated values are possible. The charging tariffs are summarized in the following.

Base-tariff – Includes all the necessary functionalities to cope with less demanding requirements and defines non-controlled charging. Figure 4.2a provides a possible

charging process for 1st-base and 2nd-base charging. The charging power is assumed to be constant. Therefore, no economic incentives are given to electric vehicle users for the provision of flexibilities as the charging process cannot be optimized. As can be seen, once the electric vehicle user plugs-in after the first trip ends, the charging process immediately starts and lasts until the electric vehicle gets disconnected or the energy storage is fully charged. The second charging process indicates second-base charging after the n-th trip ends.

Flex-tariff – A possible charging process when using the flex-tariff is illustrated by means of Fig. 4.2b. This charging tariff provides a more efficient usage of the available resources and enables the application of optimized power scheduling. This envisages an active management of electric vehicles where the Virtual Power Plant operator serves as a link between the EV Supplier/Aggregator and the electric vehicle user. Partly-controlled charging assumes that the charging process can be actively managed, by adjusting the charging power instead of using an on-off solution. This charging strategy allows variable charging rates between SoE_{nom} and SoE_{max} as indicated by the stepwise charging process. The imperative charging up to a defined nominal state of energy SoE_{nom} is supposed to guarantee a desired level at the next departure time.

V2G-tariff – As an extension of the previous charging tariff, the V2G-tariff aims to exploit the most advanced usage of electric vehicles in the power plant portfolio. Under certain circumstances, e.g. provision of system services, the electric vehicles can behave as generator unit when the state of energy ranges between SoE_{nom} and SoE_{max}. The activation, as shown in Fig. 4.2c, can be combined with approval and permission signals from the market entities involved in the charging process. In order to foster electric vehicles users adherence to the V2G services, an additional incentive is provided in form of V2G remuneration.

The electric vehicles are regarded in the energy management algorithm for day-ahead and intraday optimization as well as for the real-time imbalance compensation as introduced in Chapter 3. Thus, the introduced SoE-based charging can be linked to price-based charging in an economic operation that explicitly considers the energy market prices. In that regard, the variation of electricity prices can be also taken into account for the determination of optimized charging processes which contribute to eliminating concerns regarding the single use of price-based charging. Considering a large number of electric vehicles, price-based charging can lead to peak loads in the power system when starting charging simultaneously [134].

4.3. Modeling Electric Vehicle Fleet Characteristics

With the presence of electric vehicles as additional loads, the currently used standard load profiles, as detailed in Appendix C, might not be appropriate anymore [140] and needs to be updated. For energy purchases in the wholesale and retail market, the energy demand of customers is usually estimated by registered power measurements or predicted with standard load profiles, e.g. based on regulatory requirements or guidelines for the management of balancing groups, e.g BK6-07-002, VDI 4655. For the prediction of the required energy demand and application of appropriate charging concepts, a variety of limiting factors has to be considered [109,141], such as distance traveled, road topology (elevation), driving behavior (desired speed, acceleration, prevailing traffic conditions, ambient temperature). A simplified representation of these event-oriented operation schedules is given by means of Fig. 4.3. For an individual trip $trip_n^{\mathrm{ev},m}$ of an electric vehicle, $t^{\mathrm{D},O}$ denotes the specific departure time at origin, $t^{\mathrm{A},D}$ the arrival time at destination, and m^{OD} the mileages of driving.

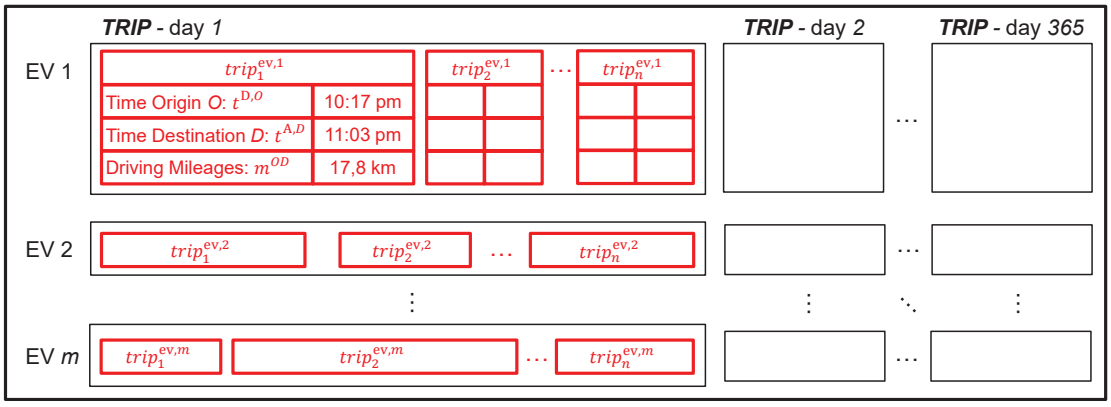

Fig. 4.3.: Event-oriented operation schedules of electric vehicles, specified by the departure time $t^{\mathrm{D},O}$ at origin, arrival time $t^{\mathrm{A},D}$ at destination and the mileages of driving m^{OD}.

To model the driving behavior of an entire electric vehicle fleet and determine the required energy demand, activity-based and timetable-based driving profiles are developed that completely avoid the usage of user-related data. Under consideration of different user types, statistical data from a nationwide travel survey [142] are used for modeling the activity-based driving profiles while timetable-based driving profiles are obtained from operation schedules of specific bus routes.

4.3.1. Trip Prediction and Methodology

The electric vehicles are clustered in electric vehicle fleets which share certain attributes and characteristics. Then, the estimates of the activity-based and timetable-based driving profiles are aggregated on hourly or sub-hourly bases, to determine

the contractual obligations and cope with the uncertainty associated with the evaluation of appropriate charging schedules and service procurements. Therefore, the event-oriented trips are converted to time-oriented data with k discrete time steps for a given time period, so that event-oriented information can be used in the energy management algorithm with variable time increments, e.g. $\Delta t = 0.25$ h. The $\boldsymbol{TRIP}$ matrix contains the vectors $\boldsymbol{trip}$ which is defined as follows:

$$\boldsymbol{TRIP} : H_{\text{ts}} \times H_{\text{fleet}} \rightarrow \mathbb{R}^3 \text{ with } \boldsymbol{trip}_{k,i} \mapsto \begin{pmatrix} k_{k,i}^{\text{D},O} \\ k_{k,i}^{\text{A},D} \\ m_{k,i}^{OD} \end{pmatrix}. \tag{4.2}$$

The discrete variables $k_{k,i}^{\text{D},O}$ and $k_{k,i}^{\text{A},D}$ denote the time-discrete departure and arrival time while m^{OD} specifies the mileages of driving. These are equally distributed among the corresponding time steps, using the stepwise approximation. The trip information in the k-th time step from the i-th electric vehicle in kilometers are summarized as follows:

$$\boldsymbol{TRIP} = \begin{array}{c} \begin{array}{cccccc} \text{EV 1} & \text{EV 2} & \cdots & \text{EV } i & \cdots & \text{EV } m \end{array} \\ \begin{bmatrix} \begin{pmatrix} k_{k_{\text{ini}},1}^{\text{D},O} \\ k_{k_{\text{ini}},1}^{\text{A},D} \\ m_{k_{\text{ini}},1}^{OD} \end{pmatrix} & \begin{pmatrix} k_{k_{\text{ini}},2}^{\text{D},O} \\ k_{k_{\text{ini}},2}^{\text{A},D} \\ m_{k_{\text{ini}},2}^{OD} \end{pmatrix} & \cdots & \begin{pmatrix} k_{k_{\text{ini}},i}^{\text{D},O} \\ k_{k_{\text{ini}},i}^{\text{A},D} \\ m_{k_{\text{ini}},i}^{OD} \end{pmatrix} & \cdots & \begin{pmatrix} k_{k_{\text{ini}},m}^{\text{D},O} \\ k_{k_{\text{ini}},m}^{\text{A},D} \\ m_{k_{\text{ini}},m}^{OD} \end{pmatrix} \\ \vdots & \vdots & \ddots & \vdots & \iddots & \vdots \\ \begin{pmatrix} k_{k,1}^{\text{D},O} \\ k_{k,1}^{\text{A},D} \\ m_{k,1}^{OD} \end{pmatrix} & \begin{pmatrix} k_{k,2}^{\text{D},O} \\ k_{k,2}^{\text{A},D} \\ m_{k,2}^{OD} \end{pmatrix} & \cdots & \begin{pmatrix} k_{k,i}^{\text{D},O} \\ k_{k,i}^{\text{A},D} \\ m_{k,i}^{OD} \end{pmatrix} & \cdots & \begin{pmatrix} k_{k,m}^{\text{D},O} \\ k_{k,m}^{\text{A},D} \\ m_{k,m}^{OD} \end{pmatrix} \\ \vdots & \vdots & \iddots & \vdots & \ddots & \vdots \\ \begin{pmatrix} k_{k_{\text{fin}},1}^{\text{D},O} \\ k_{k_{\text{fin}},1}^{\text{A},D} \\ m_{k_{\text{fin}},1}^{OD} \end{pmatrix} & \begin{pmatrix} k_{k_{\text{fin}},2}^{\text{D},O} \\ k_{k_{\text{fin}},2}^{\text{A},D} \\ m_{k_{\text{fin}},2}^{OD} \end{pmatrix} & \cdots & \begin{pmatrix} k_{k_{\text{fin}},i}^{\text{D},O} \\ k_{k_{\text{fin}},i}^{\text{A},D} \\ m_{k_{\text{fin}},i}^{OD} \end{pmatrix} & \cdots & \begin{pmatrix} k_{k_{\text{fin}},m}^{\text{D},O} \\ k_{k_{\text{fin}},m}^{\text{A},D} \\ m_{k_{\text{fin}},m}^{OD} \end{pmatrix} \end{bmatrix} \begin{array}{c} k_{\text{ini}} \\ \vdots \\ k \\ \vdots \\ k_{\text{fin}} \end{array} \end{array} \tag{4.3}$$

The matrix has the format $|H_{\text{ts}}| \times |H_{\text{fleet}}| \times 3$ defined by the cardinality of the set of time steps $H_{\text{ts}} = \{k_{\text{ini}}, \ldots, k_{\text{fin}}\}$ and the set of electric vehicle fleets. For a single electric vehicle, the 3rd element of an arbitrary $\boldsymbol{trip}_{k,i}$ in (4.3) gives the mileages of driving. As the electric vehicles are individually connected to charging infrastructures, charging strategies need to be processed differently. An example for single electric vehicle charging is provided in [143]. This is expressed by the connection matrix $\boldsymbol{CON}$, which has the format $|H_{\text{ts}}| \times |H_{\text{fleet}}|$, denoting the binary

relation of spatial movement of electric vehicles and temporal availability at the charging infrastructure for an entire electric vehicle fleet. The logical relation is

$$\{con_{k,i} = 1\} \oplus \{\boldsymbol{trip}_{k,i}(3) > 0\} \qquad \forall k \in H_{\text{ts}} \ , \ i \in H_{\text{fleet}} \ . \tag{4.4}$$

The disjunct and separable matrices $\boldsymbol{CON}$ and $\boldsymbol{TRIP}$ identify the time steps for charging and driving. The element $con_{k,i}$ is equal to 1 if the i-th electric vehicle is connected to the charging infrastructure in the k-th time step and 0 otherwise. Subsequently, the energy demand for an electric vehicle fleet can be calculated by (4.5), through the assignment of a specific energy demand for driving $E_{\text{d},k}^{mstor,\text{km}}$, e.g. 0.2 kWh/km. The specific energy demand is a representative value for the entire cluster. The resulting profile is normalized based on the aggregated energy capacity of the assigned electric vehicle models. The rated energy capacity of the energy storages serves as scaling factor to simulate different cluster sizes.

$$E_{\text{d},k}^{\text{fleet}} = E_{\text{d},k}^{mstor,\text{km}} \cdot \sum \boldsymbol{trip}_{k,i}(3) \qquad \forall mstor \in H_{\text{mstor}} \ , \ \forall k \in H_{\text{ts}} \ , \ \forall i \in H_{\text{fleet}} \tag{4.5}$$

For simplicity, the specific energy demand for driving is assumed to cover the required energy for the traction and energy conversion units, such as heating, cooling, air conditioning, lighting, pump, presses. Additional factors, such as the driving behavior, weight loading, rolling resistance and ambient temperature are not explicitly considered in the following elaboration.

4.3.2. Passenger Electric Vehicles Models

The solution of driver scheduling problems must satisfy specific driving purposes in order to cover the planned trips [144]. For the purpose of modeling such activity-based driving profiles, statistical data from a nationwide travel survey [142] is used. The travel survey covers the data of 25,922 households, 60,713 persons, 193,290 distances, 34,601 vehicles and 36,182 trips. A classification is carried out by neglecting the allocation of trips between the origin and destination. The proportion of daily and weekly mileages of driving, driving distance and corresponding trip duration times are analyzed. Based on different driving purposes p1-p7 as summarized by (4.6), distinct user types are defined.

$$H_{\text{prp}} = \{\text{work}, \text{official}, \text{educational}, \text{shopping}, \text{execution}, \text{leisure}, \text{company}\} \tag{4.6}$$

Table 4.3 provides an overview of the classified user types and gives the average distance per trip and purpose that varies between 7.2 and 36.9 kilometers.

TABLE 4.3.: Classification of passenger electric vehicle user types by different driving purposes.

profile (ID)	user type	driving purposes						
		p_1	p_2	p_3	p_4	p_5	p_6	p_7
1	private				x		x	
2	education private			x	x		x	x
3	commuter	x						
4	official commuter	x	x			x		
5	commercial		x					
6	semi commercial		x				x	
average distance per trip and purpose (km)		20.0	36.9	12.0	7.2	11.4	20.5	9.1

In total, 10.000 randomized trips for each user type are simulated and concatenated to form the driving profiles. This results in an approximation of the trip distributions which are similarly compared to the reported values of the nationwide travel survey [142]. Table 4.4 summarizes the results for each user types.

TABLE 4.4.: Transportation statistics of assigned activity-based driving profiles for passenger electric vehicle user types.

profile (ID)	user type	annual mileage *) (km)	average connectivity (p.u.)
1	private	1,669/6,893/16,840	0.9485
2	education private	2,682/7,317/15,501	0.9344
3	commuter	10,135/15,429/24,377	0.9153
4	official commuter	9,135/16,859/28,311	0.8977
5	commercial	23,774/32,421/45,578	0.8448
6	semi commercial	9,031/17,358/33,13	0.9014

*) values refer to lower 25th, median 50th and upper 75th percentile, outliers are excluded.

For example, the annual mileage of driving is between 1,669 and 16,840 for the analyzed activity-based driving profiles of the private user type. Next, these driving profiles are assigned to distinct passenger electric vehicle models, as introduced in Table 4.5, by comparing the daily energy demands and required energy capacity. The given energy capacities and specific energy demands are derived from data provided by [114, 143] and specify the model attributes of the subcompact (SC), compact (CO), and premium (PR) unit model.

TABLE 4.5.: Classification parameters for the assignment of passenger electric vehicles unit models, specified by the energy capacity, annual mileage of driving, and specific energy demand.

unit model		energy capacity	annual mileage *)	specific energy demand **)	daily energy demand
		(kWh)	(km)	(kWh/km)	(kWh)
subcompact	SC	17.6	8,882/13,344/17,784	0.10/<u>0.17</u>/0.20	0-30
compact	CO	24.4	17,456/23,317/31,479	0.15/<u>0.20</u>/0.25	30-60
premium	PR	60	23,292/31,356/41,714	0.15/<u>0.25</u>/0.35	>60

*) values refer to lower 25th, median 50th and upper 75th percentile, outliers are excluded while **) indicates low / <u>average</u> / high values of the calculated energy demands.

The aggregated demand profiles are shown in Fig. 4.4, which represent the average hourly-based power demand of connected electric vehicles for each cluster.

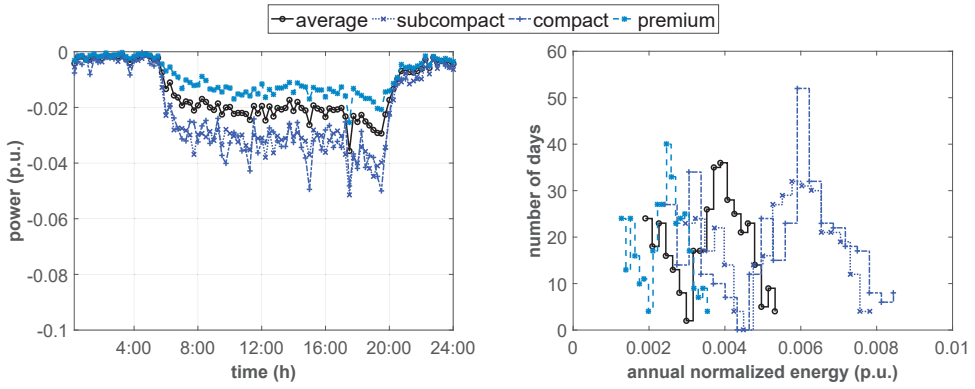

(a) hourly-based average profiles

(b) probability distribution

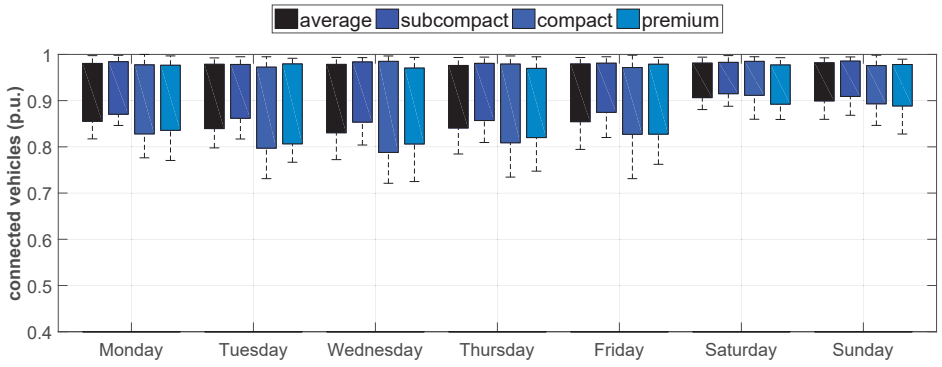

(c) weekly connected vehicles

Fig. 4.4.: Clusters characteristics of passenger electric vehicles, specified by the (a) hourly-based power demand, (b) probability distribution, and (c) boxplot of connected vehicles.

As can be seen in Fig. 4.4a the power demand of the hourly-based average profiles is slightly different. This is a result of assigning the driving profiles to distinct passenger electric vehicle models. As given in Table 4.5, the driving profiles assigned to the subcompact unit model, for example, have 8,882 to 17,784 kilometers driven annually. Compared to the assigned driving profiles that are used within

the premium class, the annual mileages are between 23,292 and 41,714 kilometers. Expressing the relationship between the energy demand for driving and auxiliary devices, field-recorded measurement data [114, 145] is taken into account. Here, a linear regression model is initialized as a hypothesis concerning the relationship among the specific energy demand and ambient temperature. This is indicated by the results provided in Fig. 4.4b which shows the probability distribution of the annual normalized energy for each unit model. The calculations are derived from applying (C.1) given in Appendix C. Although the energy demand of the user types that uses the premium model is higher compared to the remaining vehicle models, the normalized values (light blue dashed line) are lower due to the assigned rated energy capacity as listed in Table 4.5. The boxplot given in Fig. 4.4c shows the 25th lower and 75th upper percentile of the weekly connected passenger electric vehicles. The values are derived from the $\boldsymbol{CON}$ matrix and indicates the sum of simultaneous available electric vehicles Γ_k^{CON} for charging/discharging processes at a time step, which is normalized by the total number of electric vehicle considered in the fleet. The general calculation is as follows:

$$\Gamma_k^{\mathrm{CON}} = \frac{\sum_{i \in H_{\mathrm{fleet}}} con_{k,i}}{|H_{\mathrm{fleet}}|} \qquad \forall k \in H_{\mathrm{ts}} \ , \ \forall i \in H_{\mathrm{fleet}} \ . \tag{4.7}$$

From the results obtained in Fig. 4.4c, it can be observed that the connectivity within the cluster of subcompact unit models is higher compared to the remaining clusters of unit models. Regardless of the classified unit models and assigned driving profiles, all aggregated profiles are characterized by high connectivity levels that allows the Virtual Power Plant operator to make use of available energy capacities.

4.3.3. Commercial Electric Vehicle Models

To model the utilization of commercial electric vehicles, timetable-based driving schedules are investigated. The vehicle scheduling problem, e.g. public transport, waste disposal or transport of goods, addresses the task of serving company-specific services under consideration of a given set of timetabled trips to fulfill specific requirements [146, 147], such as to satisfy demand patterns, maximize the number of well-timed passenger transfers, minimize waiting times [144]. Taking public transport as an example for the representation of commercial electric vehicles, field-recorded operation and routing schedules are analyzed. As a derivation of the operation schedules of specific bus routes of the Berlin metropolitan area, a set of timetabled trips, driving and dwell times as well as trip distances is established. In total 1,229 buses that serve 197 bus lines are taken into account. The weekly mileages

of driving are more than 1,500,000 kilometers with a total number of 8,300 trips. For the approximation of the required driving energy, field-recorded diesel demands of standard buses (SB), articulated buses (AB), and double decker buses (DD) are analyzed and the energy equivalents determined using the efficiency method. A schematic representation is given by Fig. 4.5.

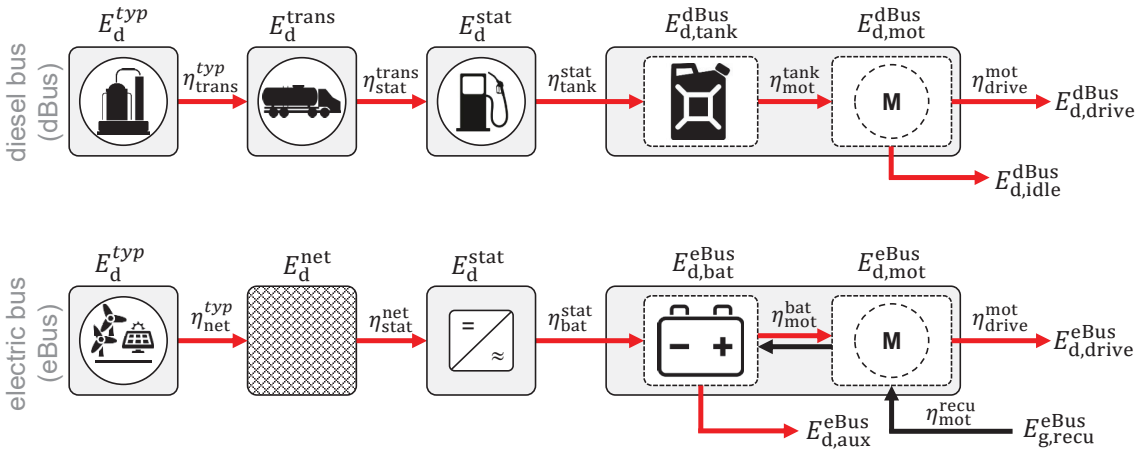

Fig. 4.5.: Efficiency chain and energy flow from secondary, final and effective energy utilized for the operation of diesel and electric vehicles.

The energy flow from secondary, final and effective energy utilized for combustion (dBus) and electric vehicles (eBus) is calculated by (4.8)-(4.10). The efficiency values, summarized in Table 4.6, are taken from the literature.

TABLE 4.6.: Specification of applicable chemical, mechanical and electrical efficiencies for calculating the energy flows related to the mobility and transport with diesel and electric buses.

	input	output	transformation processes	efficiency*) (%)	source
η_{tank}^{mot}	chemical	mechanical	combustion	22/<u>27</u>/32	[148, 149]
η_{mot}^{drive}	mechanical	mechanical	gearing transmission	90/<u>94</u>/95	[150, 151]
η_{stat}^{bat}	electric	chemical	charging	90/<u>95</u>/98	[152, 153]
η_{bat}^{mot}	chemical	mechanical	(dis)charging el.-mech. conversion	80/<u>86</u>/90	[154, 155]

*) values are intended to indicate low / <u>medium</u> / high efficiencies and needs to be confirmed by thermodynamic analysis, field test or measurements.

For simplification, similar operational conditions of diesel and electric buses are assumed while neglecting the additional weight from the battery. However, the

number of passengers and the traffic flow need to be considered as these factors have a significant influence on the driving resistance and therefore required driving energy. First, the average diesel demand $E^{\text{dBus}}_{\text{tank}}$ per kilometer is calculated by (4.8), as a function of the diesel demand of an entire fleet $V^{\text{fleet}}_{\text{d,diesel}}$, the lower calorific value of diesel LCV and the total mileage of driving.

$$E^{\text{dBus}}_{\text{tank}} = \frac{V^{\text{fleet}}_{\text{d,diesel}} \cdot LCV}{\sum\sum \boldsymbol{trip}_{k,i}(3)} \qquad \forall k \in H_{\text{ts}} \, , \forall i \in H_{\text{fleet}} \tag{4.8}$$

For example, assuming an annual mileage of driving $\sum\sum \boldsymbol{trip}_{k,i}(3) = 100 \cdot 10^6$ km and a total amount of $V^{\text{fleet}}_{\text{d,diesel}} = 50 \cdot 10^6$ l diesel with $LCV = 9.94$ kWh/l, the average diesel demand is $E^{\text{dBus}}_{\text{tank}} = 4.97$ kWh/km. Then, the energy demand for driving $E^{\text{eBus}}_{\text{d,drive}}$ is approximated by (4.9), under the assumption that the energy demand for driving of diesel and electric buses is equal.

$$E^{\text{eBus}}_{\text{d,drive}} = E^{\text{dBus}}_{\text{d,drive}} = E^{\text{dBus}}_{\text{tank}} \cdot \eta^{\text{tank}}_{\text{mot}} \cdot \eta^{\text{mot}}_{\text{drive}} - E^{\text{dBus}}_{\text{d,idle}} \tag{4.9}$$

The diesel equivalent is multiplied with the tank-motor $\eta^{\text{tank}}_{\text{mot}}$ and motor-drive $\eta^{\text{mot}}_{\text{drive}}$ efficiency. Further, the idling losses $E^{\text{dBus}}_{\text{d,idle}}$ are considered within the approximation. Finally, the energy demand served by the battery $E^{\text{eBus}}_{\text{d,bat}}$ for the traction process is estimated with (4.10), where $\eta^{\text{bat}}_{\text{mot}}$ and $\eta^{\text{recu}}_{\text{mot}}$ denote the battery-motor and recuperation-motor efficiency, respectively. The offset values correspond to the energy demand for driving, auxiliary components $E^{\text{eBus}}_{\text{d,aux}}$ and the energy $E^{\text{eBus}}_{\text{g,recu}}$ of the recuperation process.

$$E^{\text{eBus}}_{\text{d,bat}} = \frac{E^{\text{eBus}}_{\text{d,drive}}}{\eta^{\text{bat}}_{\text{mot}} \cdot \eta^{\text{mot}}_{\text{drive}}} + E^{\text{eBus}}_{\text{d,aux}} - E^{\text{eBus}}_{\text{g,recu}} \cdot \eta^{\text{bat}}_{\text{mot}} \cdot \eta^{\text{recu}}_{\text{mot}} \tag{4.10}$$

Possible numbers for auxiliary components are $E^{\text{eBus}}_{\text{d,aux}} \in \{0.6, 0.9, 1.3\}$ kWh/km [156] and for the energy of the recuperation process $E^{\text{eBus}}_{\text{g,recu}} = [20, 40]$ kWh/100km [157]. A linear regression model is initialized as a hypothesis concerning the relationship among the specific energy demand, use of auxiliary devices and the ambient temperature. In order to consider the effects of the ambient temperature on the energy demand, field-recorded demand curves as shown in Fig. 4.6a are used, substituting $V^{\text{fleet}}_{\text{d,diesel}}$ in (4.8). For simplification, four distinct operating periods according to [156] are considered. The different operation scenarios are indicated by the changing conditions of the ambient temperature, peak and off-peak hours. Table 4.7 specifies the corresponding values. The peak and off-peak hours are derived from the time sequences of the timetabled operation and routing schedules. Figure 4.6b shows the lower, upper and total values (red line) of the specific energy demand as a result

of (4.10). In peak hours, for example, there is a higher energy demand required indicating higher passenger loads and traffic volumes.

TABLE 4.7.: Interim, cooling, and heating operating scenarios for electric buses specified by a classification of ambient temperature, peak and off-peak hours.

heating mode	transition mode	cooling mode	off-peak hours	peak hours
			(h)	
≤ 7 °C	8...29 °C	≥ 30 °C	20:00 to 06:00 10:30 to 14:30	06:00 to 10:30 14:30 to 20:00

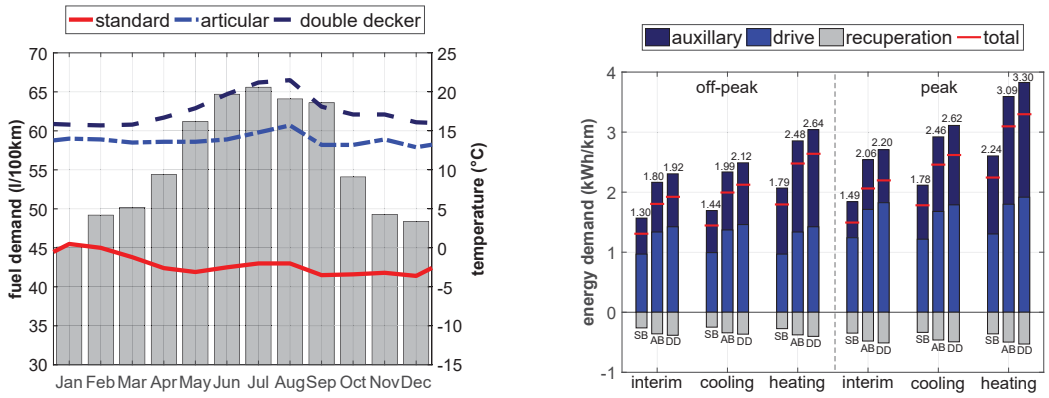

(a) dBus energy demand

(b) eBus energy demand

Fig. 4.6.: Fuel demand of (a) diesel buses in accordance to the ambient temperature and (b) approximated energy demands of electrified buses for defined operating scenarios.

In heating and cooling mode, the energy demand rises due to the additional operation of auxiliary devices. This includes the operation of cooling and heating units, auxiliary pumps, air compressor and battery cooling. Table 4.8 provides a summary of the obtained parametrization values of each unit model. The assigned energy capacities of 175, 225, 250 kWh refer to the usable battery capacity of electrified buses used in pilot projects [158].

TABLE 4.8.: Classification parameters for the assignment of commercial electric vehicles (eBus) unit models, specified by the energy capacity, weekly mileage of driving, and specific energy demand.

unit model		energy capacity	weekly mileage of driving *)	specific energy demand **)	daily energy demand
		(kWh)	(km)	(kWh/km)	(kWh)
standard	SB	175	1,045/1,147/1,469	1.30/<u>1.80</u>/2.30	245-345
articular	AB	225	1,135/1,231/1,566	1.80/<u>2.50</u>/3.10	368-508
double decker	DD	250	1,118/1,231/1,500	1.90/<u>2.60</u>/3.30	385-517

*) values refer to lower 25th, median 50th and upper 75th percentile, outliers are excluded

**) indicates low / <u>average</u> / high values of the calculated energy demands.

The introduced operation and routing schedules define the timetable-based driving profiles for each unit model. As indicated by the hourly-based average profiles in Fig. 4.7a the energy demand is equally distributed during the day as the electrified buses are in service. Also the results given in Fig. 4.7b show that a large portion of the energy demand is required for the operation of the electric vehicle fleet during the whole year compared to passenger electric vehicles as illustrated in Fig. 4.4b. Therefore appropriate charging strategies are required to serve the energy demand, e.g. through opportunity charging at terminal or intermediate stations, as introduced in Table 4.1. The results provided in Fig. 4.7b gives the propability distribution of the annual normalized energy for each unit model which is derived from (C.1) in Appendix C. The values of the annual normalized energy of all analyzed driving demand profiles are more equally distributed

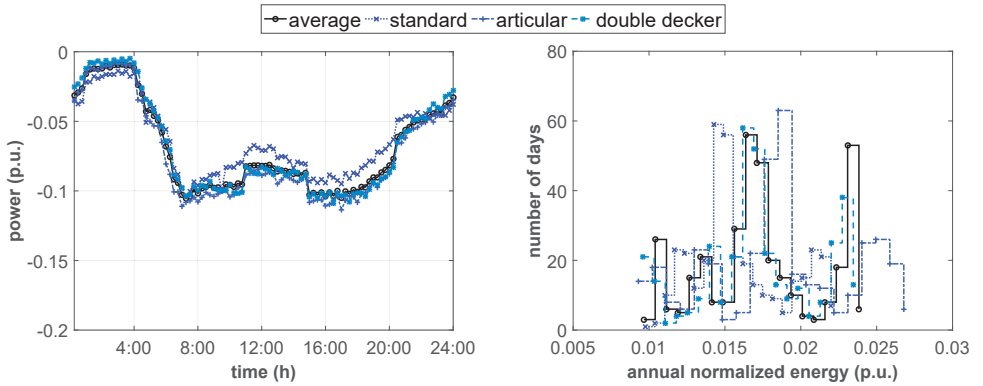

(a) hourly-based average profiles (b) propability distribution

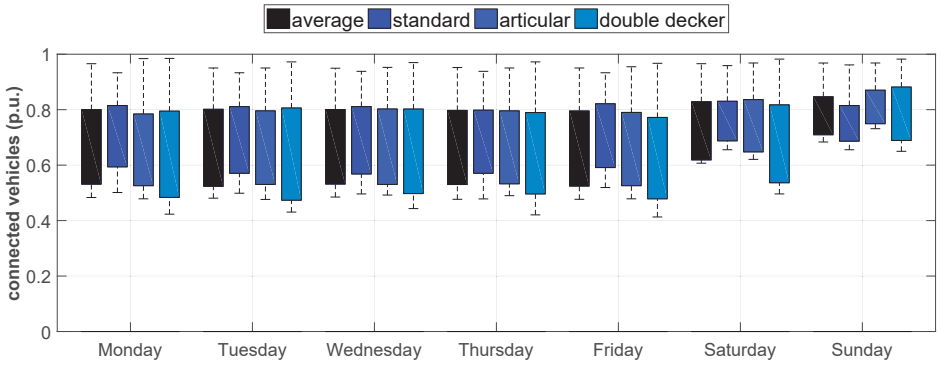

(c) weekly connected vehicles

Fig. 4.7.: Clusters characteristics of commercial electric vehicles (eBus), specified by the (a) hourly-based power demand, (b) probability distribution, and (c) boxplot of connected vehicles.

The boxplot given in Fig. 4.7c shows the 25th lower and 75th upper percentile of the weekly connected commercial electric vehicles as a result of (4.7). It can be seen that the timetabled driving schedules have a wide range of the connectivity levels $\Gamma^{\mathrm{CON}} =]0.41, 0.99)$. This is due to the operation and routing schedules which leads to a limitation in use of the energy capacity in the energy management algorithm of the Virtual Power Plant. Thus, the findings reveal significant boundary and con-

straint conditions for the optimization problem to determine appropriate charging strategies. However, optimized charging/discharging strategies can be developed during off-peak hours especially in the night and noon period, or at the weekend as a large proportion of the electric vehicle fleet is not in service.

4.4. Optimization of Energy Procurements

For optimized energy procurement, a suitable market structure within which effective interaction between the involved market entities can be fostered is required. To cope with the unbundled nature of liberalized energy markets and separate the activities of the market entities at a competitive level, a hierarchically structured optimization algorithm is proposed. The solution approach aims to gain access and visibility across the energy market for the EV Supplier/Aggregator, correspond to redispatch requests of the system operator, while determine optimized charging power schedules for the operation of electric vehicles. Therefore, the introduced optimization model in Chapter 3 for joint market operation is enhanced in two aspects:

1. Extension of hierarchically structured optimization by means of upper and lower level considering the fleet characteristics of electric vehicles.
2. Introduction of additional constraints representing redispatch measures and multilateral transactions with the EV Supplier/Aggregator and power system operator.

The optimization model reflects a hierarchical game of decision makers [159, 160] and may contribute to improve individual optimization results of each market entity while performing optimized balancing group management.

4.4.1. Implementation of Energy Demand Profiles

In order to integrate the developed activity-based and timetable-based driving schedules in the energy management algorithm of the Virtual Power Plant operator and consider the availability of renewable energy sources for charging processes, the introduced charging tariffs in Table 4.1 require further investigations. Both the predictive driving profiles as well as the charging tariffs in combination with the model attributes for passenger and commercial electric vehicles are translated into boundary and constraint conditions.

First, the charging opportunity for first-base and second-base charging are analyzed by separating the energy demand of an arbitrary electric vehicle fleet as follows:

$$E_{\mathrm{d},k}^{\mathrm{fleet}} = E_{\mathrm{d},k}^{\mathrm{fleet,1st}} + E_{\mathrm{d},k}^{\mathrm{fleet,2nd}} \tag{4.11}$$
$$= \underbrace{\sum_{i \in H_{\mathrm{fleet}}} con_{k,i}^{\mathrm{1st}} \cdot P_{\mathrm{r}}^{tariff} \cdot \eta^{mod} \cdot \Delta t^{mod,\mathrm{1st}}}_{\text{1st-base charging}} + \underbrace{\sum_{i \in H_{\mathrm{fleet}}} con_{k,i}^{\mathrm{2nd}} \cdot P_{\mathrm{r}}^{tariff} \cdot \eta^{mod} \cdot \Delta t^{mod,\mathrm{2nd}}}_{\text{2nd-base charging}}.$$

The energy demand $E_{\mathrm{d},k}^{\mathrm{fleet,1st}}$ for 1st-base charging considers the amount of electric vehicles available, e.g. at home, depot, workplace, office. The second part denotes the energy demand $E_{\mathrm{d},k}^{\mathrm{fleet,2nd}}$ supplied during second-base charging to serve the mobility needs of the electric vehicles. The corresponding amount of connected electric vehicles is given by $\boldsymbol{CON}^{\mathrm{1st}}$ for 1st-base charging and $\boldsymbol{CON}^{\mathrm{2nd}}$ for 2nd-base charging. The temporal availability for the charging/discharging processes is denoted by $\Delta t^{mod,\mathrm{1st}}$ and $\Delta t^{mod,\mathrm{2nd}}$, respectively. This allows the application of different charging tariffs as introduced by Table 4.2. Accordingly, the charging power can be different, e.g. $P_{\mathrm{r}}^{tariff} = P_{\mathrm{r}}^{\mathrm{V2G}}$ for 1st-base and $P_{\mathrm{r}}^{tariff} = P_{\mathrm{r}}^{\mathrm{base}}$ for 2nd-base charging, respectively. As an example, Fig. 4.8a shows the total energy demand of an arbitrary electrified bus fleet at an intra-urban depot and the separated energy demand profiles at 1st-base and 2nd-base charging locations in Fig. 4.8b and Fig. 4.8c, respectively.

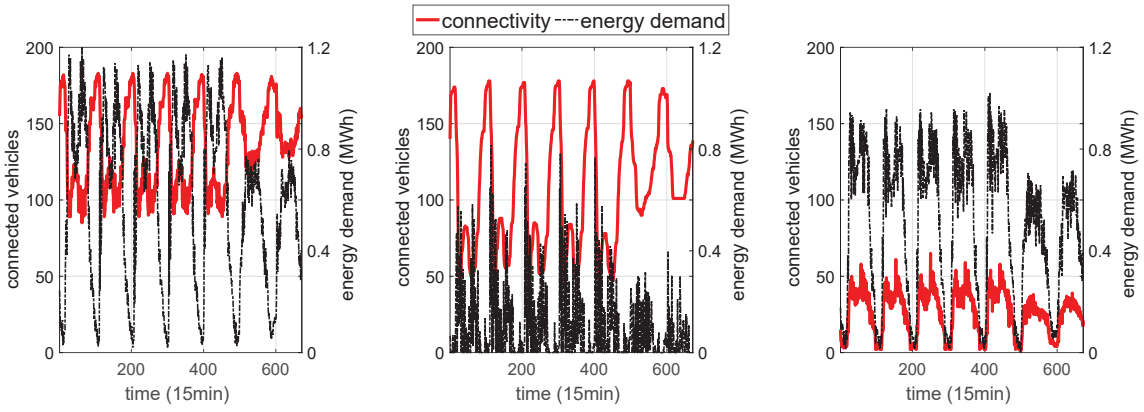

(a) total (b) 1st-base (c) 2nd-base

Fig. 4.8.: Energy demand of an (a) arbitrary electric fleet separated by energy demand occurring at (b) 1-st base charging at depot and (c) 2nd-base charging at termini.

The connectivity of the aggregated profiles are indicated by the red solid line while the black dashed line denotes the corresponding energy demand. In summary, the elaborations indicate that there are different charging concepts and strategies possible which is determined by the expected level of connected electric vehicles and the total energy demand. However, further research is necessary as the level of connectivity may change when considering uncertainties related to planned and unplanned

influencing events, e.g. traffic jams, construction sites on roads and the railway, maintenance and servicing, but also human factors. This in turn can influence the determination of appropriate charging/discharging processes which is part of future investigations and not addressed in the following elaborations.

4.4.2. Optimization Model and Problem Formulation

The hierarchically structured optimization is formulated as a mixed-integer linear programming problem. Fig. 4.9 provides the main sequences of the optimization problem and highlights the considered input and output variables.

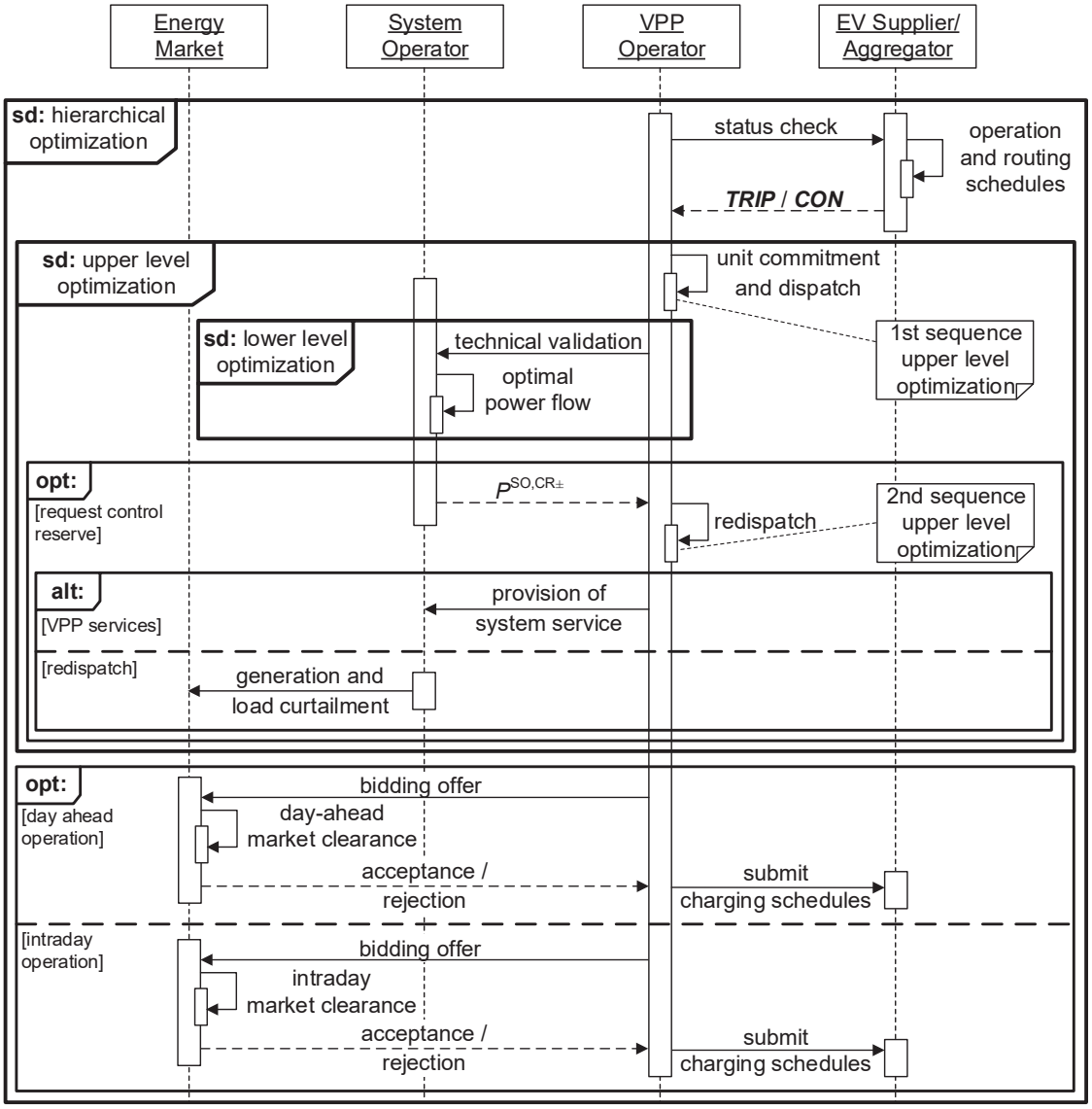

Fig. 4.9.: Optimization model for the integration of electric vehicle fleets in energy management algorithm of the Virtual Power Plant considering multilateral transactions with the EV Supplier/Aggregator and system operator.

The Virtual Power Plant operator determines the optimized bidding schedules for joint market operations in the upper level optimization. The contractual obligations with the EV Supplier/Aggregator are considered by the assignment of the introduced charging tariffs. The received information is integrated in the 1st sequence of the upper level optimization by means of ***TRIP*** and ***CON*** matrices, handed over from the EV Supplier/Aggregator. Then, the Virtual Power Plant operator forms its power balance

$$P_{\mathrm{g},k}^{\mathrm{VPP,1st}} = P_{\mathrm{d},k}^{\mathrm{VPP,1st}} \tag{4.12}$$

with

$$\begin{aligned} P_{\mathrm{g},k}^{\mathrm{VPP,1st}} =& P_{\mathrm{g},k}^{\mathrm{pv}} + P_{\mathrm{g},k}^{\mathrm{wind}} + P_{\mathrm{g},k}^{\mathrm{chp}} + P_{\mathrm{g},k}^{\mathrm{dg}} \\ &+ (1 - y_k^{\mathrm{bat}}) \cdot P_{\mathrm{g},k}^{\mathrm{bat}} + (1 - y_k^{\mathrm{ps}}) \cdot P_{\mathrm{g},k}^{\mathrm{ps}} + (1 - y_k^{\mathrm{fleet}}) \cdot P_{\mathrm{g},k}^{\mathrm{fleet}} + P_{\mathrm{IM},k}^{em} \\ P_{\mathrm{d},k}^{\mathrm{VPP,1st}} =& P_{\mathrm{d},k}^{\mathrm{hh}} + P_{\mathrm{d},k}^{\mathrm{ind}} + y_k^{\mathrm{bat}} \cdot P_{\mathrm{d},k}^{\mathrm{bat}} + y_k^{\mathrm{ps}} \cdot P_{\mathrm{d},k}^{\mathrm{ps}} + y_k^{\mathrm{fleet}} \cdot P_{\mathrm{d},k}^{\mathrm{fleet}} + P_{\mathrm{EX},k}^{em} \end{aligned}$$

where the charging power $P_{\mathrm{d},k}^{\mathrm{fleet}}$ and discharging power $P_{\mathrm{g},k}^{\mathrm{fleet}}$ of electric vehicle fleets are added. The sum of the individual summands denote the total power generation $P_{\mathrm{g},k}^{\mathrm{VPP,1st}}$ and demand $P_{\mathrm{d},k}^{\mathrm{VPP,1st}}$ of the power plant portfolio. The results of the 1st sequence provide the contracted energy market exchanges, consisting of imports $P_{\mathrm{IM},k}^{em}$ and exports $P_{\mathrm{EX},k}^{em}$, and are considered hereafter as constants. The forwarded contracted power schedules $P^{\mathrm{VPP,1st}}$ are used by the system operator to direct the decision making in the lower level optimization, which is assumed to be solved by the system operator. For example to find solutions that fulfill the physical network conditions, e.g. to handle the power flows with acceptable reliability and cost effectiveness [68]. Here, the optimal power flow problem is simplified and possible adjustment processes represented in terms of positive and negative $P^{\mathrm{SO,CR}\pm}$ control reserve requests. The control reserve requests are supposed to reflect feasible redispatch solutions for dispatchable units and unit clusters represented by the Virtual Power Plant operator. Otherwise, further redispatch measures of the system operator have to be taken into account, e.g. curtailment, load shedding, or disconnections. In case of $P^{\mathrm{SO,CR}\pm} \neq 0$, a redispatch optimization is performed where the flexibilities provided by distinct electric vehicle fleets are considered. The optimization problem is solved as part of the 2nd sequence of the upper level optimization. The updated power balance is given by

$$P_{\mathrm{g},k}^{\mathrm{VPP,2nd}} + P_k^{\mathrm{SO,CR}^-} = P_{\mathrm{d},k}^{\mathrm{VPP,2nd}} + P_k^{\mathrm{SO,CR}^+}. \tag{4.13}$$

The positive $P_k^{\mathrm{SO,CR}^+}$ and negative $P_k^{\mathrm{SO,CR}^-}$ requests for control reserve power are assumed to represent necessary adjustments as a result of the optimum power flow problem solved by the system operator. These control reserve requests are considered in the 2nd sequence of the upper level optimization. This simplification allows the Virtual Power Plant operator the allocation of power system services at a particular time and location. After the 2nd sequence, the system operator validates the received power schedules $P^{\mathrm{VPP,2nd}}$ that include the offered control reserve. Finally, the determined charging power schedules P^{fleet} are submitted to the EV Supplier/Aggregator as set points for the charging processes. In that regard, the result represents an ideal situation where electric vehicle fleets contribute to solve congestion in the power system. In each time step $k+1$, the energy capacity E_{k+1}^{fleet} of the electric vehicle fleet is calculated by (4.14) as a function of the predicted energy demand $E_{\mathrm{d},k}^{\mathrm{fleet}}$, which is given by the use of the developed activity-based and timetable-based driving schedules.

$$E_{k+1}^{\mathrm{fleet}} = E_k^{\mathrm{fleet}} + E_{\mathrm{d},k}^{\mathrm{fleet}} - P_{\mathrm{d},k}^{\mathrm{fleet}} \cdot \Delta t \cdot \eta^{mod} - P_{\mathrm{g},k}^{\mathrm{fleet}} \cdot \Delta t \cdot \frac{1}{\eta^{mod}}. \tag{4.14}$$

Charging processes are calculated by $P_{\mathrm{d},k}^{\mathrm{fleet}} \cdot \Delta t \cdot \eta^{mod}$, reflecting the boundary conditions given in (4.15). The charging power and the energy demand are defined as negative values. Discharging processes are expressed by the calculation of $P_{\mathrm{g},k}^{\mathrm{fleet}} \cdot \Delta t \cdot \frac{1}{\eta^{mod}}$. The boundary conditions for discharging processes are formulated by (4.16). The values state the linear inequality constraint and can vary according to the selected charging tariff as defined in Table 4.2.

$$-y_k^{\mathrm{fleet}} \cdot P_{\mathrm{r}}^{tariff} \cdot \sum_{\forall i \in H_{\mathrm{fleet}}} \boldsymbol{con}_{k,i} \leq P_{\mathrm{d},k}^{\mathrm{fleet}} \leq 0 \tag{4.15}$$

$$0 \leq P_{\mathrm{g},k}^{\mathrm{fleet}} \leq (1 - y_k^{\mathrm{fleet}}) \cdot P_{\mathrm{r}}^{tariff} \cdot \sum_{\forall i \in H_{\mathrm{fleet}}} \boldsymbol{con}_{k,i} \tag{4.16}$$

The integer variables y_k^{fleet} indicate the operation mode. In case of $y_k^{\mathrm{fleet}} = 1$ charging processes, otherwise for $y_k^{\mathrm{fleet}} = 0$ discharging processes, take place. Accordingly, the available state of energy $SoE_{k+1}^{\mathrm{fleet}}$ is calculated under consideration of the assigned energy capacity E_{r}^{mstor}, defined by the unit models attributes

$$SoE_{\mathrm{nom}}^{tariff} \leq SoE_{k+1}^{\mathrm{fleet}} \leq SoE_{\mathrm{max}}^{tariff} \quad \text{with} \quad SoE_{k+1}^{\mathrm{fleet}} = \frac{E_{k+1}^{\mathrm{fleet}}}{E_{\mathrm{r}}^{mstor} \cdot |H_{\mathrm{fleet}}|}. \tag{4.17}$$

The nominal state of energy $SoE_{\mathrm{nom}}^{tariff}$ defines the lower boundary and is derived from the specifications of the selected charging tariff. The upper boundary is defined by

$SoE_{\max}^{tariff}$ which is the maximum possible state of energy, e.g. $SoE_{\max}^{tariff} = 0.95$p.u. in order to preserve a backup for the provision of negative control reserve. Disregarding the results achieved through the optimization process of the Virtual Power Plant operator as a service for the EV Supplier/Aggregator, extended charging flexibilities for electric vehicles should be still possible when required. This can be realized, for example, with approval or permission signals from the EV Supplier/Aggregator in combination with dynamic tariffs as an extension of the contractual obligations.

4.4.3. Performance Validation and Method Comparison

The performance of the developed optimization model is assessed for a given power plant portfolio, whereby the energy capacity serves as a comparative parameter and is assumed to be the same for all electric vehicle fleets with $E_{\mathrm{r}}^{\mathrm{fleet}} = 10$ MWh. Based on this capacity the number of distinct vehicles of each unit type as listed in Tab. 4.5 and Tab. 4.8 are determined. For example, passenger vehicles of the subcompact type have an assigned energy capacity of 17.6kWh, therefore 570 vehicles are required for a total fleet capacity of 10MWh. Table 4.9 provides an overview of the resulting electric vehicle fleet composition. Additionally, the daily energy demand and average connectivity of the electric vehicle fleets is given which vary depending on the selected unit model.

TABLE 4.9.: Quantitative composition of passenger and commercial electric vehicle fleets specified by the number of vehicles, average connectivity and daily energy demand for 1st-base charging assessments.

unit model		number of vehicles	daily energy demand	average connectivity
		(-)	(MWh)	(p.u.)
passenger	subcompact	570	3.59	0.9469
	compact	408	2.85	0.9482
	premium	168	1.66	0.9343
commercial	standard	57	1.67	0.5058
	articular	44	1.64	0.5085
	double decker	40	1.93	0.4516

The daily energy demand is separated by (4.11). For passenger vehicles only 1st-base charging is assumed while commercial vehicles have the additional possibility of 2nd-base charging during the trips. As a result, the daily energy demand of commercial vehicles for 1st-base charging is relatively small and approximately 10-20%

of the total energy demand listed in Table 4.8. The upper level optimization is solved under consideration of the predicted energy demands and connected vehicles. The convergence characteristic of the optimization model is shown in Fig. 4.10. For each iteration, the intermediate objective values of the cost-optimized day-ahead operation are given in Fig. 4.10a and Fig. 4.10c for passenger and commercial vehicle types, respectively. Thereby, the black line with circle markers refers to the subcompact or standard model, the blue line with diamond markers to compact or articular model and the red line with square markers to premium or double decker model. For each vehicle model, the related connectivity is indicated through dashed lines and the energy demand through solid lines as depicted in Fig. 4.10b and Fig. 4.10d for passenger and commercial vehicle models, respectively.

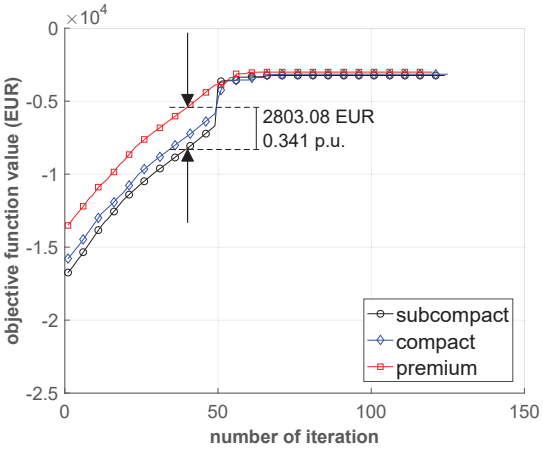

(a) objective function values, passenger vehicles

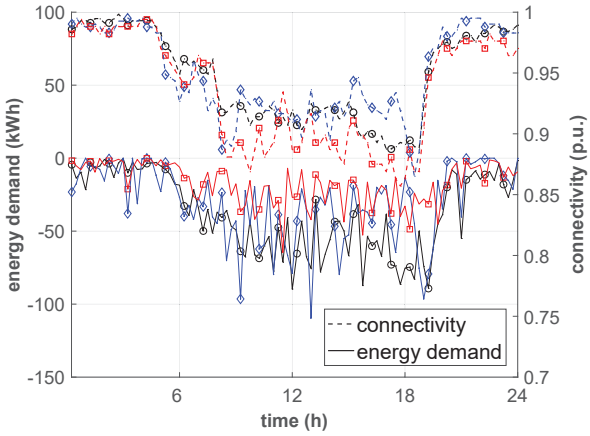

(b) demand and connectivity, passenger vehicles

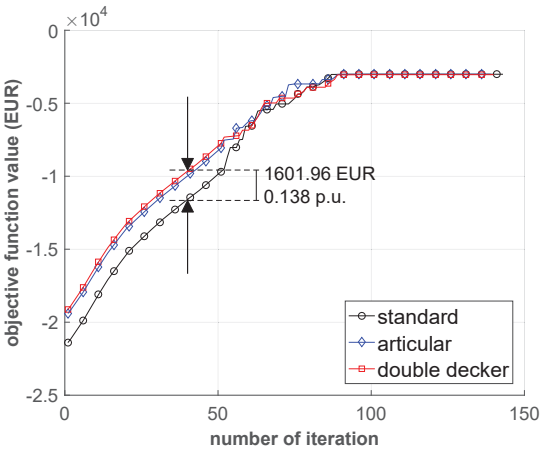

(c) objective function values, commercial vehicles

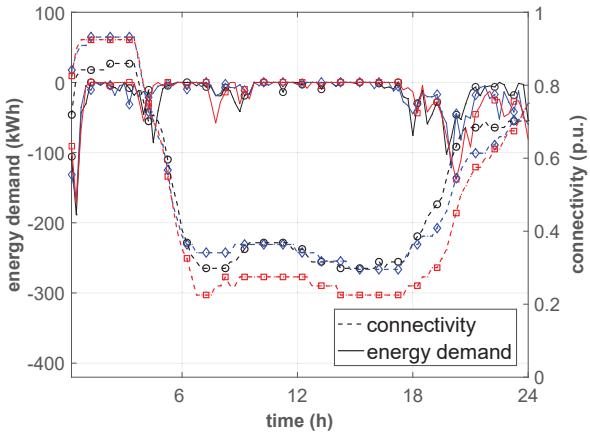

(d) demand and connectivity, commercial vehicles

Fig. 4.10.: Convergence characteristic of the optimization model testing different unit models of passenger and commercial electric vehicle fleets in cost-optimized day-ahead operation.

The optimized parameter refers to the charging/discharging power for the electric vehicle fleet used to determine the absolute values of the energy capacity defined in

(4.14). The intraday optimization results are not explicitly shown since the number of iterations to reach optimality decreases with smaller time periods. The mixed-integer linear programming problem is solved, and the number of complied constraints and boundaries increase in each iteration. The stochastic variation of the connectivity and energy demand of passenger vehicles in Fig. 4.10b is spread over the whole day. For commercial vehicles in Fig. 4.10d several peaks during work time can be observed, especially in the morning and evening hours. The higher the energy demand in a defined time step, the more capacity has to be optimized at any time step of the day-ahead optimization. This is stated through the investigation of the converging lines of the objective function values. For example in Fig. 4.10a, as the daily energy demand is smaller for the premium vehicles than for the other two passenger vehicle models, less capacity or power can be optimized and the objective function value is larger from the beginning of the day-ahead optimization. The spread between the solutions found for premium and subcompact vehicles at 40 iterations is 2,803.08 EUR and 0.341 p.u. in relative numbers of the objective function value.

Analogously, the investigations is applied for the commercial vehicles and the results summarized in Fig. 4.10c. The total spread at 40 iterations is 1,601.96 EUR and 0.138 p.u. between articular and standard buses, respectively. The final objective function values are reached for all assessed activity-based and timetable-based driving schedules after around 70 iterations for passenger and 100 iterations for commercial vehicles. This is due to the higher average connectivity of the passenger vehicles. However, the optimization problem using electric vehicle fleets with higher levels of connectivity and energy demands converges faster to the respective final optimal objective function value. As a result, the additional constraints given by the temporal availability and energy demand profiles of electric vehicle fleets are fully reflected in the hierarchically structured optimization model. Optimality conditions are reached for the identification of optimal charging solutions for passenger and commercial electric vehicle fleets on the basis of the examined driving profiles, which can be confirmed by the results of the convergence analysis.

4.5. Numerical Analysis and Application

The value of the proposed Virtual Power Plant model is substantiated in the numerical analysis and applications of the developed activity-based and timetable-based driving schedules. For distinct use cases, Table 4.10 summarizes the composition of the power plant portfolios considered in the optimization problem for the participation in joint market operation with electric vehicles. The distributed and renewable

energy sources are modeled as described in Chapter 3. In order to respond to concerns for energy efficiency, [2] charging/discharging efficiencies $\eta^{mod} \in \{\eta^{\text{char}}, \eta^{\text{dis}}\}$, are considered. For simplification these are assumed to be equal. The nominal state of energy, as given by the selected charging tariffs in Table 4.2, varies to examine electric vehicle charging under different operating strategies. The range from the nominal up to the maximum state of energy denotes the energy capacity which can be utilized as flexibilities within the power plant portfolio, e.g. to store the surplus energy of renewable energy sources, provide internal control reserve, contribute to power balancing and provide services for system operators.

TABLE 4.10.: Power plant portfolio parametrization for case studies analyzing optimized energy procurements for electric vehicles fleets operated in metropolitan regions (case 1) and at an intra-urban depot (case 2).

scenario	wind	pv	chp	dg	bat*)	ind	hh	total
	(MW)							
case 1	130	20	10	540	10	30	30	700
case 2	\	0.5	0.3	\	0.5	0.5	\	2.8

*) minimum and maximum state of energy state of energy are assumed with $SoE^{\text{bat}}_{\text{min}} = 10$ % and $SoE^{\text{bat}}_{\text{max}} = 90$ %, respectively.

In the first case, the optimized energy procurement for two exemplary electric vehicle fleets is studied, in which the introduced tariff types in Table 4.2 are investigated. The proposed hierarchically structured optimization with upper and lower level is adopted and the charging strategies compared. The second case addresses the provision of internal control reserve at an intra-urban depot. The available capacity of an electrified bus fleet is used and potential redispatch measures derived from experiments.

4.5.1. Verification of Energy Management Solutions for Private and Commercial Electric Vehicle Fleets

Assessing the proposed charging power strategies as a solution of joint market operation, two electric vehicle fleets as listed in Table 4.11 are considered. The electric vehicle fleets are assumed to be managed by distinct EV Suppliers/Aggregators that define either cost- or CO2-optimized charging strategies in combination with different charging tariffs. For comparison reason, both electric vehicle fleets have the same rated energy capacity of 56 MWh. The first electric vehicle fleet consists of 2,023 passenger vehicles with a daily energy demand of 14.86 MWh and is modeled with

[2] e.g. power losses for the operation of the charging infrastructure, power electronics and cooling equipment.

compact and premium unit models as introduced in Table 4.5. The second electric vehicle fleet represents an electrified bus fleet requiring a daily energy demand of 10.33 MWh. In total, 80 standard, 20 articular, and 150 double decker buses are considered and assigned with the unit models attributes as listed in Table 4.8.

TABLE 4.11.: Composition of passenger and commercial electric vehicles fleets with assigned unit models used for optimized energy procurements in joint market operation.

	EVS/A 1 passenger		EVS/A 2 commercial		
unit model*)	CO	PR	SB	AB	DD
vehicle numbers	1,836	187	80	20	150
daily energy demand (MWh)	14.68		10.33		

*) CO - compact, PR - premium, SB - standard, AB - articular, DD - double decker

First, the driving behavior is approximated with the assigned activity-based and timetable-based driving schedules as shown in Fig. 4.11a for passenger and in Fig. 4.11b for commercial vehicles, respectively.

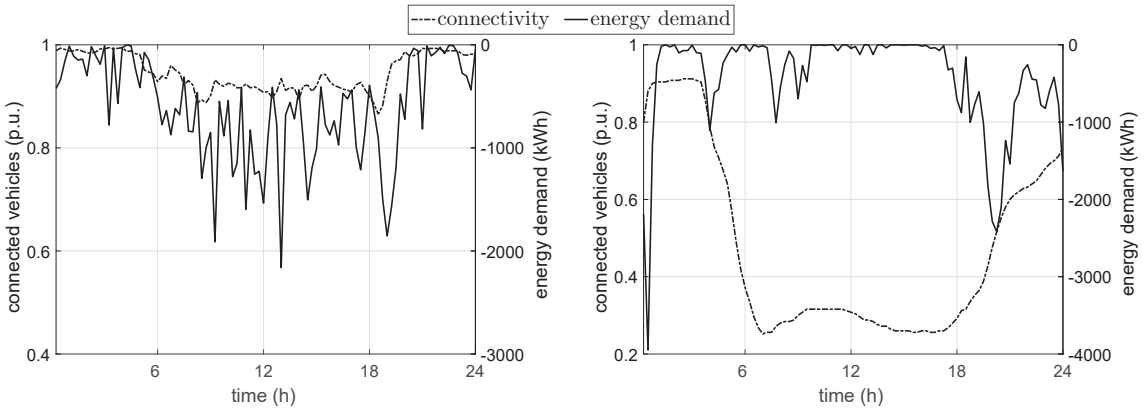

(a) driving pattern, passenger vehicles

(b) driving pattern, commercial vehicles

Fig. 4.11.: Driving pattern for (a) passenger and (b) commercial electric vehicle fleets specified by the energy demand and connectivty.

The predictive driving profiles are used in the energy management algorithm of the Virtual Power Plant to obtain the charging/discharging profiles as shown in Fig. 4.12a and Fig. 4.12b in the cost-optimized scenarios, Fig. 4.12c and Fig. 4.12d for the CO2-optimized scenarios, respectively. In the base-tariff (solid black line), the maximum possible charging power is applied for both, passenger and commercial electric vehicle fleets independent of the objective function. Here, the optimized power schedules fit the trend of the respective energy demand as no flexibilities are foreseen within the selected charging tariff. The charging power in the flex-tariff is primarily dispatched in periods of low market prices as long as the nominal state of energy is exceeded. In comparison, the charging period is shifted to time periods with a power surplus of renewable energy resources in the CO2-optimized scenarios

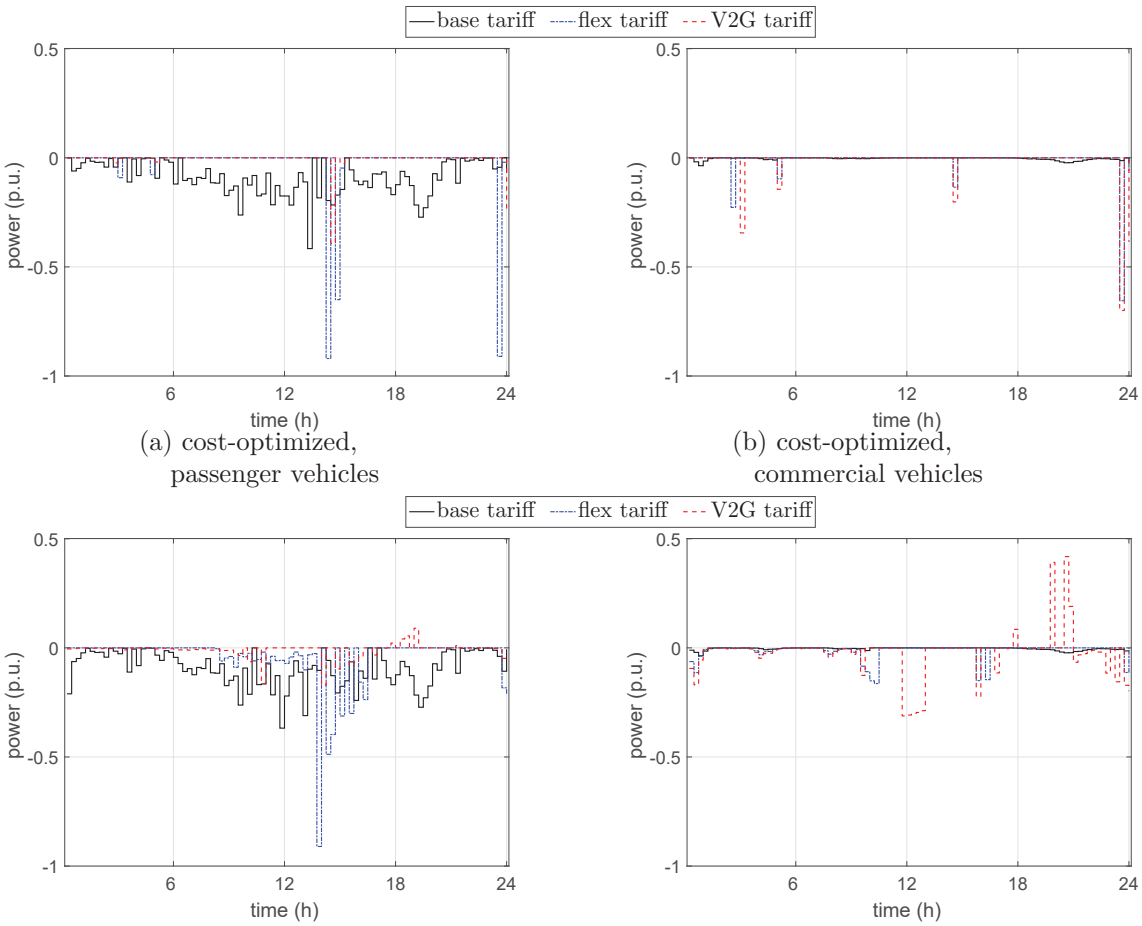

(a) cost-optimized, passenger vehicles

(b) cost-optimized, commercial vehicles

(c) CO2-optimized, passenger vehicles

(d) CO2-optimized, commercial vehicles

Fig. 4.12.: Obtained dispatch schedules for (a) and (c) passenger as well as (b) and (d) commercial electric vehicle fleets cost-optimized (OB.1) and CO2-optimized (OB.2) scenarios, respectively.

as can be seen in Fig. 4.12c and Fig. 4.12d in the noon hours. When applying the V2G-tariff, the stored energy is even reused in the evening and allows to serve additional demand within the power plant portfolio. The charging process can be shifted to later time steps as long as the nominal state of energy constraints are fulfilled, which is further investigated in Fig. 4.13. Figure 4.13a and Fig 4.13b show the obtained results for the cost-optimized scenarios, and Fig 4.13c and Fig 4.13d for the CO2-optimized scenarios, respectively. The parameters are used to indicate the overall performance of the energy management algorithm as introduced in Chapter 3 and refer to calculations defined in (3.25). Additionally, the daily energy supply E^{ev} for charging processes, the resulting charging time $t_{\mathrm{ch}}^{\mathrm{ev}}$ as well as the average state of energy of the electric vehicle fleet are depicted. Based on the assessments of the dispatch schedules, the following aspects are further investigated:

- scheduled power fits trend of respective energy demand in base-tariff for cost- and CO2-optimized scenarios

- power primarily scheduled in times of lower market prices with flex- and V2G-tariff for cost-optimized scenarios
- increasing utilization of renewable energy resources through V2G operation for CO2-optimized scenarios

When applying the flex- or V2G-tariff in cost-optimized scenarios, the charging time is significantly reduced compared to the base-tariff as seen in Fig 4.13a and Fig 4.13b. Taking the charging process of the commercial electric vehicle fleet as an example, from 22 hours per day to less than 2 hours. Even more energy provided by renewable energy sources can be utilized for the charging process in the V2G-tariff. This is due to the assigned rated charging/discharging power, with $P_{\mathrm{r}}^{\mathrm{V2G}} = 100$ kW in V2G-tariff compared to $P_{\mathrm{r}}^{\mathrm{base}} = 450$ kW in base-tariff, since the charging process is conducted over a longer time interval with smaller charging power.

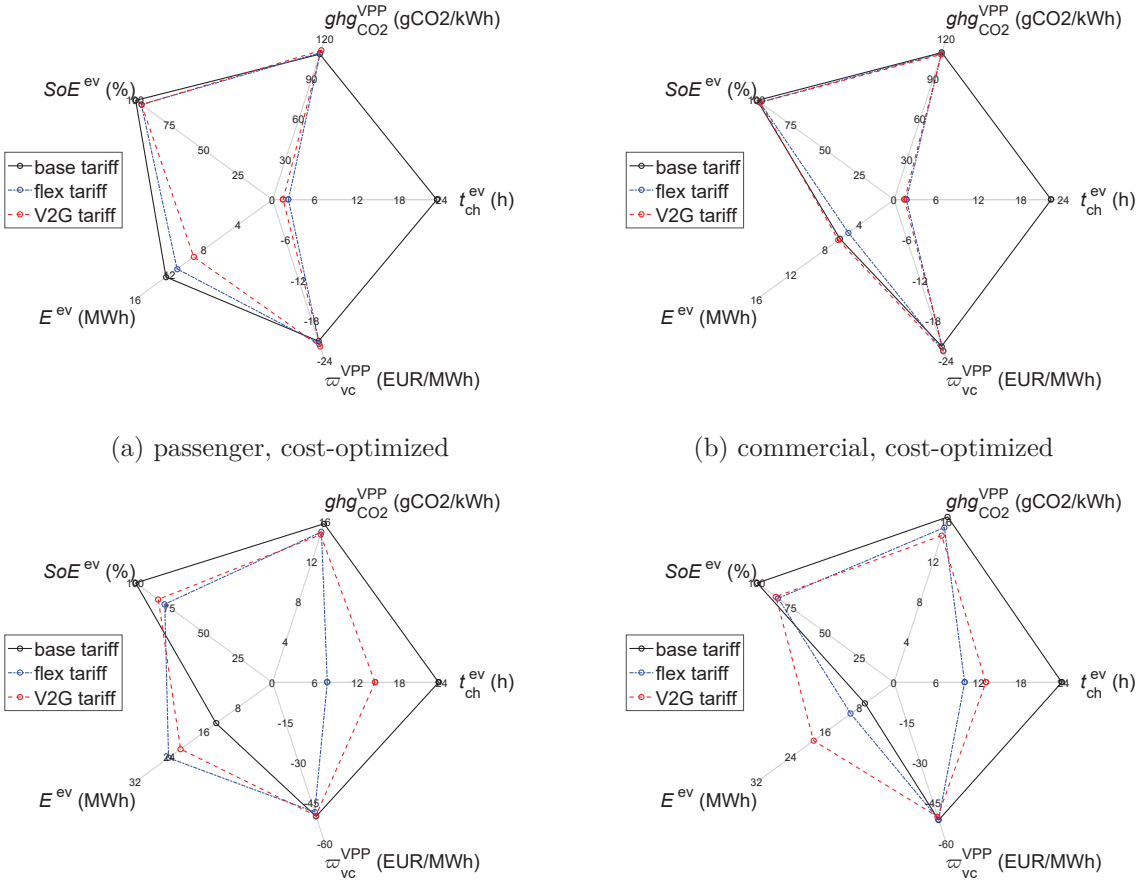

(a) passenger, cost-optimized

(b) commercial, cost-optimized

(c) passenger, CO2-optimized

(d) commercial, CO2-optimized

Fig. 4.13.: Simulation results and evaluation parameter of cost- and CO2-optimized energy procurements for the EV Supplier/Aggregator managing (a) passenger and (b) commercial electric vehicle fleets.

The same applies to passenger electric vehicles but is case vice versa as can be seen in Fig 4.13a, since the assigned rated charging/discharging power is defined in reversed sequence with $P_{\mathrm{r}}^{\mathrm{V2G}} = 44$ kW down to $P_{\mathrm{r}}^{\mathrm{base}} = 3.7$ kW. However, the

nominal values of the state of energy as introduced in Tab. 4.2 are still met as stated by the evaluation parameter SoE^{ev}. In case of applying CO2-optimized charging strategies, Fig 4.13c and Fig 4.13d show similar results. Additionally, the specific CO2-emissions are significantly reduced but coupled with higher expenses. This is indicated by the evaluation parameter of the specific variable operating cost $\varpi_{\mathrm{vc}}^{\mathrm{VPP}}$ and greenhouse gas emissions $ghg_{\mathrm{CO2}}^{\mathrm{VPP}}$. Further, the hours of the charging processes increase for the flex- and V2G-tariff since the energy supply is split up in time periods with renewable energy surplus to reduce the CO2-emissions. In V2G-tariff, the shiftable energy and capacity of the electric vehicle fleets is recovered during later time periods when additional energy is provided to serve the load demand in the power plant portfolio. Hence, an improvement of the greenhouse gas emissions for the entire power plant portfolio can be observed. In total, the simulation results show the benefits arising when considering the flexibilities provided by the electric vehicle fleets in the power plant portfolio operation.

4.5.2. Assessing Nodal Redispatch Measures with Electrified Bus Fleets at Intra-Urban Depots

The following elaborations combine the merits of the optimization model considering multilateral transactions with the EV Supplier/Aggregator and system operator. After the 1st sequence of the upper level optimization has been executed, the optimization problem is solved with relaxed network constraints, handed over from the system operator. It is assumed that the EV Supplier/Aggregator applies first-base and 2nd-base charging opportunity with base- and V2G-tariff, respectively. Taking into account the flexibility that can be provided by the defined electrified bus fleet in Table 4.11, three different cases of positive and negative control reserve requests from the system operator are tested on the scenario case 2 described in 4.10. The simulation cases are performed in order to observe the temporal capabilities that can be provided under extreme operation condition and specified as follows:

- case 2.1: positive/negative control reserve request of 0.5 MWh over 1 hour
- case 2.2: positive/negative control reserve request of 1.0 MWh over 1 hour
- case 2.3: positive/negative control reserve request of 2.0 MWh over 1 hour

The tested electrified bus fleet is located at an intra-urban depot which is assigned to a single node of the power system. As part of the hierarchically structured optimization with upper and lower level extended optimization model, the requests of the system operator are reflected as additional constraints in 2nd sequence of the upper level optimization as calculated in (4.13). Hence, the upper level result is

conversely influenced by the objection of the lower level optimization performed by the system operator. The resulting charging power schedules for the operation of the electrified bus fleet are shown in Fig. 4.14, with and without considering of the power adjustments for the provision of redispatch measures. Thereby, the control reserve request is modeled as an additional and non-controlled power demand in case of positive control reserve and power generation in case of negative control reserve.

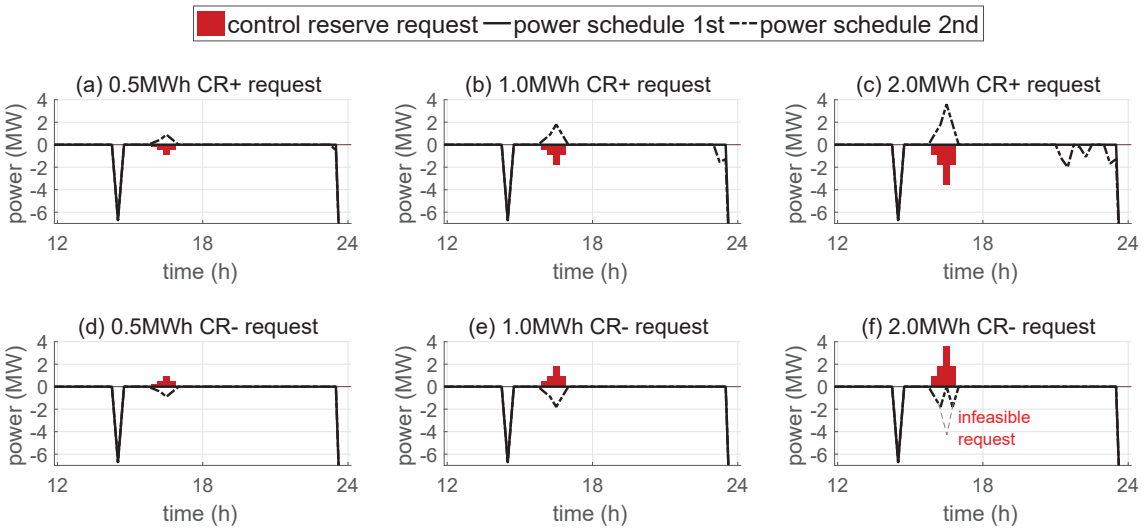

Fig. 4.14.: Quantification of (a)-(c) positive and (d)-(f) negative reserve power requests of the system operator and feasibility solutions for the provision of nodal redisptach measures with an electrified bus fleets at an intra-Urban depots.

Figure 4.14a-Fig. 4.14c show the reserve power requests from the system operator for the provision of positive capacity reserve with a total of 0.5MWh, 1.0MWh and 2.0MWh. Analogously, Fig. 4.14d-Fig. 4.14f show the negative reserve requests. The results given in Fig. 4.15 indicate that every positive control reserve request can be fulfilled through utilization of available reserve capacity provided by the electrified bus fleet. While this also applies for the first scenarios of negative control reserve requests, the peak request within the 2 MWh scenarios in Fig. 4.14f cannot be fulfilled due to insufficient available reserve capacity at the intra-urban bus depot. Thus, the request in this time step is denied. The available reserve capacity in the remaining periods is shown in Fig. 4.15a and Fig. 4.15c for positive and Fig. 4.15b and Fig. 4.15d for negative control reserve. Additionally, the response on the reserve power requests of the system operator are illustrated. As shown in the results obtained by case 2.3, the available capacity is reduced to zero after the first time step of activation as shown in Fig. 4.14d. Subsequent, the available negative reserve capacity is restored through internal compensation processes, which is specified by the upcoming energy demand in the subsequent time steps. When assessing the potential provision of positive control reserve requests the same effect can be observed within the last hours of the power schedule in Fig. 4.14c.

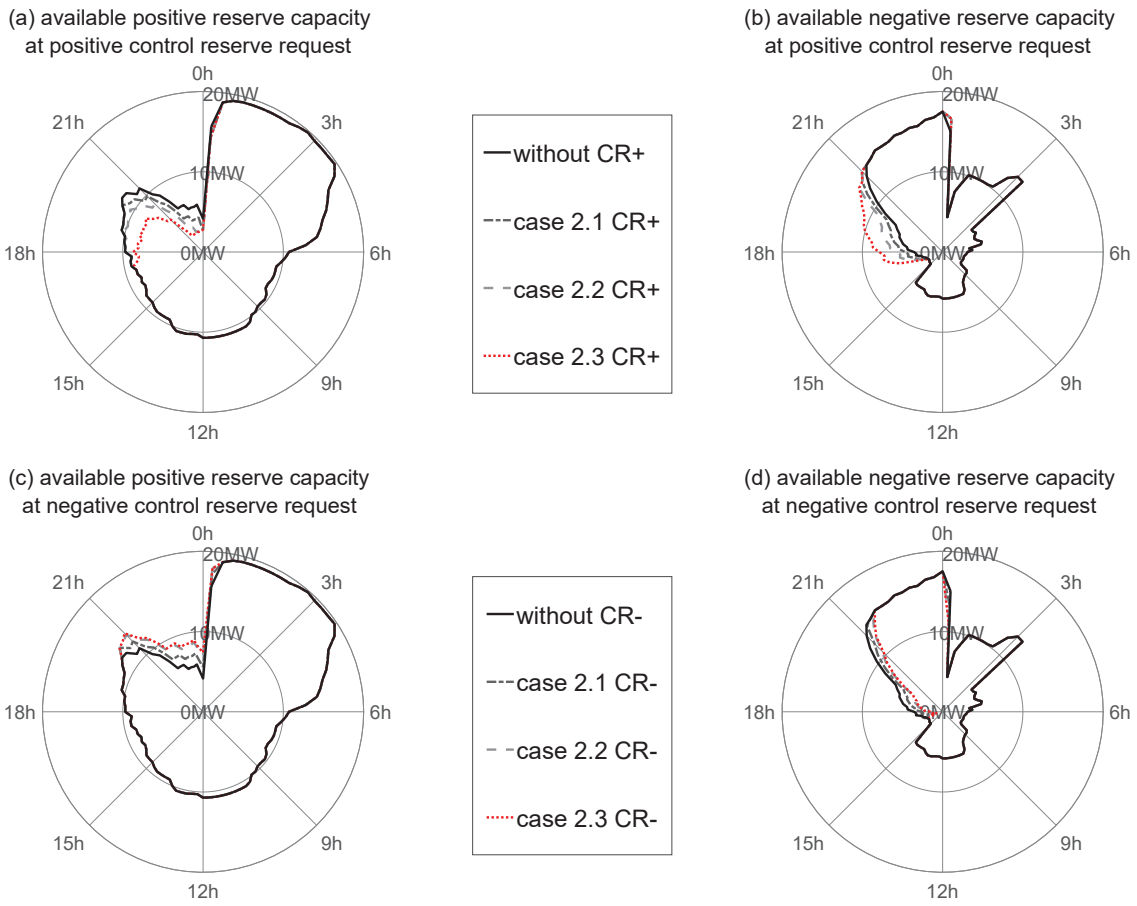

Fig. 4.15.: Available (a), (c) positive and (b), (d) negative reserve capacity of the electrified bus fleet at an intra-urban depot over one day including the response on (a)-(b) positive and (c)-(d) negative reserve power requests of the system operator.

The simulation results prove that the proposed optimization model can properly follow the requests of the power system operator and provide a possible solution for coordinated redispatch measures while fulfilling the contract position with the EV Supplier/Aggregator and the energy market. The provided flexibility of the electrified bus fleet at the intra-urban depot allows the Virtual Power Plant operator to make a better use of mobile energy resources while contributing to increase the overall power system efficiency. Moreover, the simulation results proof the optimality of the proposed charging strategies and demonstrate the balancing mechanism between desired reserve capacities and acquired charging/discharging profiles by providing the nodal redispatch measures.

4.6. Concluding Remarks

The chapter describes the extension of the Virtual Power Plant concept considering electric vehicles as additional energy sources in joint market operations. As part of an efficient service oriented operations with electric vehicle fleets, intermediate and

higher-level aggregation entities are introduced. The multilateral transactions with the Virtual Power Plant operator are specified and transferred into a hierarchically structured optimization model. Activity-based and timetable-based driving profiles are established for the prediction of the required energy demand of passenger and commercial electric vehicle fleets. Relevant parameters are identified to model the characteristics of distinct electric vehicle fleets and to provide a compact format that can be used in the optimization model of the Virtual Power Plant operator. Comparative assessments for the optimized charging strategies are performed and analysis presented to illustrate the efficiency and robustness of the extended functionalities included in the Virtual Power Plant operation schemes.

Taking into account the characteristics and operational limitation of different power plant portfolios, it is shown that electric vehicles can be efficiently used for the mitigation of power imbalances and coordinated redispatch measures. The presented charging strategies incorporate 1st-base and 2nd-base charging opportunities and allow further assessments to identify upfront investment costs, avoiding technological obsolescence and lowering the costs of charging infrastructure development. However, research is still needed in order to assess the costs/benefits and potential added value of the distinct market entities. As the presented methodology assumes that the driving profiles for each electric vehicle represents a feasible sequence of trips that can be executed, adjustments or enrichment with field recorded data may be necessary to provide further insights.

5. COORDINATED VOLTAGE REGULATION WITH VIRTUAL POWER PLANTS IN DISTRIBUTION SYSTEMS

Abstract – The characteristics of energy supply in smart distribution networks change with the presence of distributed, renewable and mobile energy sources. Reverse power flows and unpredictable generation profiles can cause voltage overshoots and fast voltage changes. As a result, the power system integration is limited by technical and operational constraints regarding bus voltage limits and capacity ratings of power system devices. In order to overcome these difficulties and to provide alternative solutions for reinforcement and expansion of power systems infrastructures, enhanced coordinated voltage regulation and management approaches are investigated. First, the chapter provides a suitable schedule of interactions and communications between the Virtual Power Plant operator and system operator regarding the application of advanced voltage control and management approaches as part of active network management solutions. Then, enhanced voltage control solutions are presented for the mitigation of time-varying voltage variations. Finally, the proposed algorithm is verified through multi-period AC power flow analysis and simulation with a benchmark distribution system.

Keywords – active network management, droop control, remote control, power system operation, voltage support, network losses

5.1. Introduction

In conventional power systems, stable and reliable power supply is guaranteed by the system operators with limited control of connected generators and loads [63]. This is achieved through compulsory and enhanced services to maintain and regulate the most important organizational processes [161, 162]. Compulsory services are defined in (i) legal conditions and ordinances, (ii) regulatory frameworks, (iii) grid codes, (iv) technical connection requirements and numerous (v) guidelines [163–165]. On top of the basic requirements, enhanced and non-compulsory services can be provided

as a result of deregulated energy markets [166]. Although distributed flexibility potentially supports power system operations, system operators tend to rely mostly on conventional voltage control solutions, e.g. topology adjustments, network reinforcements, compensating devices and stand-alone generators. This is because of the limited system monitoring and control of flexible resources currently available to system operators. Under consideration of time-varying power generation and demand in future distribution systems, active network management and control algorithms are required [68, 167, 168]. Here, limitations in power system operations can be mitigated through the application of several voltage control strategies supported by distributed and renewable energy sources [169]. For those applications, an overview including on-load tap-changer (OLTC), distributed generator, and compensator devices is presented in [170]. The potential application of coordinated on-load tap-changing transformer with different distributed voltage control devices, such as shunt capacitor and step voltage regulator, is discussed in [171–173]. To reduce the operating cost of those regulating devices, rule-based and optimizing algorithm for coordinated voltage control can be applied [174, 175]. Alternatively, [176] presents a coordinated voltage control scheme that uses dynamically changing master slave definitions. The elaborations aim to reduce the amount of tap-changes and at the same time increasing the capacity margin of additional control devices, while improving the voltage quality and service reliability. The existing research assumes full information on the power system architecture, integrated system devices and corresponding operating states. Moreover, the suggested control schemes mostly rely on the direct controllability of coordinated control devices. However, in liberalized energy markets the power system operator is restricted in the operation of such distributed generators or even loads, and therefore has to interact with numerous market participants. Here, the Virtual Power Plant provides advanced voltage control and management approaches and combines the advantages of local droop and remote control for coordinated voltage regulation. Compared with existing voltage control solutions, the chapter provides a simulation framework for the verification of the proposed coordinated voltage regulation and discusses the effectiveness on the mitigation of time-varying voltage variations.

5.2. Voltage Control Solutions and Emerging Interactions

In future distribution systems characterized by time-varying power generation and demand, it is assumed that normal voltage conditions are required to guarantee security of supply and operation of power electronic equipment. The European standard EN 50160, for example, defines an allowable median voltage deviation of

maximum ±10% of the nominal voltage to keep the service voltage to customers within acceptable voltage ranges [163]. The same applies to abnormal conditions which can be caused by unpredicted changes in demand or generation, failure of system devices or the inability to compensate the reactive power demand [67, 177]. In order to keep the power system voltages at all buses in acceptable ranges in both normal and abnormal conditions, voltage control solutions are used in distribution systems, an example of which is shown in Fig. 5.1.

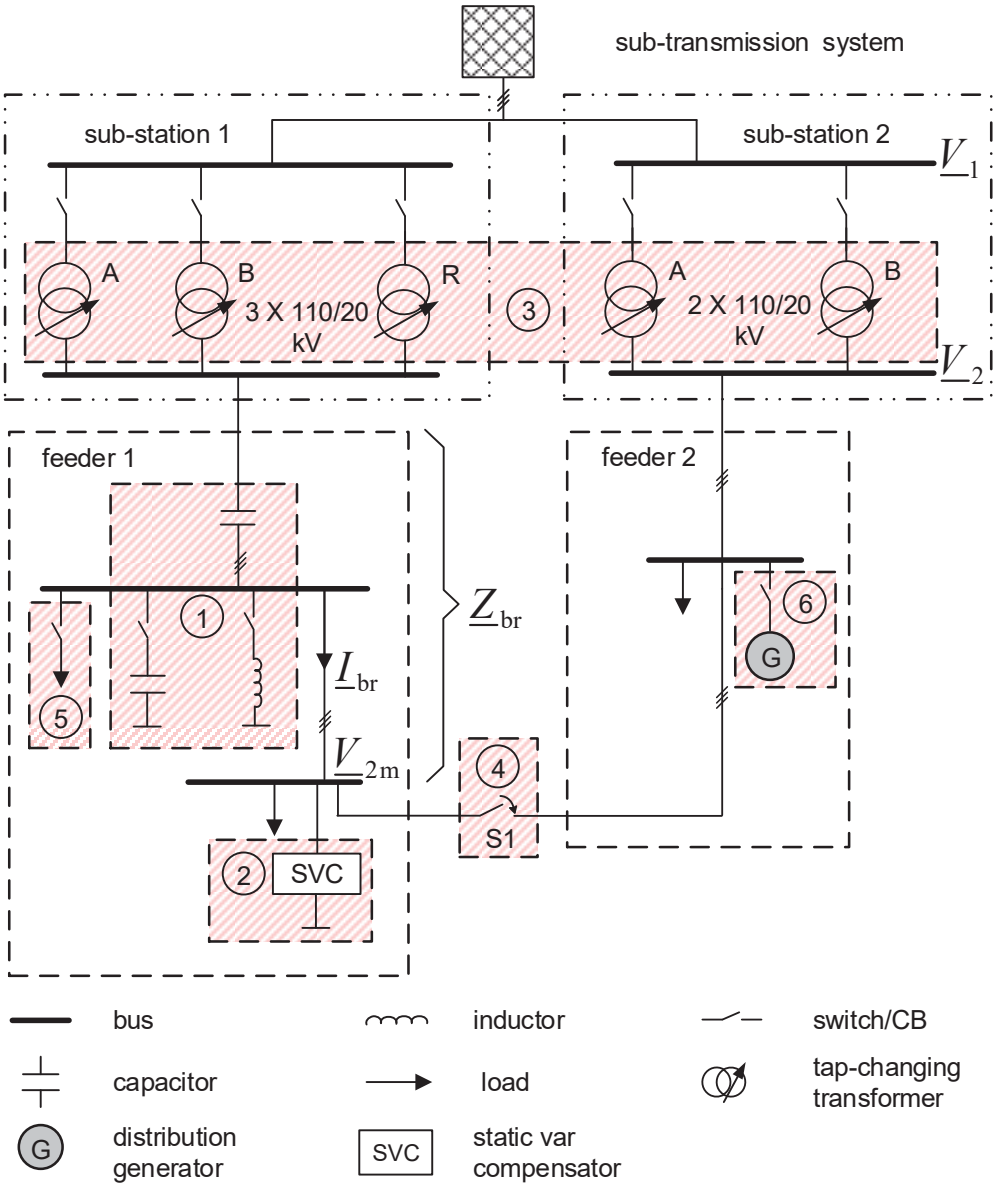

Fig. 5.1.: Voltage control solutions in distribution systems with (1) passive sources, (2) active sources, (3) tap-changing transformer, (4) topology adjustments, (5) load scheduling and demand side management, and (6) controllable generators.

One important distinction for the provision of voltage support is based on the different locations and the associated power system voltages. The primary voltage denotes

the voltage magnitude at the point of the primary side of the transformer V_1. The voltage magnitude V_2 refers to the transformer secondary side of the sub-station. The service voltage means the voltage magnitude at the meter installed on every load bus $V_{2\mathrm{m}}$ or is equal to the feeder voltage magnitude $V_{2\mathrm{m}}$ minus the voltage drop across the transformer and the secondary circuit connection. The utilization voltage is defined by the voltage magnitude at the point of use where the outlet equipment is plugged in. Either permanently connected to the power system or switched, voltage regulating devices contribute to voltage control by the modification of the network characteristic. Through the provision of enhanced and non-compulsory services of Virtual Power Plants, these voltage control solutions may be extended [173, 178], as proposed by the following elaborations.

5.2.1. Voltage Stability and Measurements

The classification of voltages ranges in distribution systems can be defined in accordance to [179] and serve as guidelines for system operators. However, the voltage limits are individually specified by the system operators depending on the network characteristics and existing voltage control devices. Here, the ratio of the resistance R and reactance X, defined as R/X-ratio of the power system, influences the voltage variation in the power system indirectly. With respect to distribution systems, reactive and active power can have equivalent influence for voltage support [180]. In case of uni-directional power flow with connected loads in the power system, Fig. 5.2 schematically shows the voltage drop along the feeder.

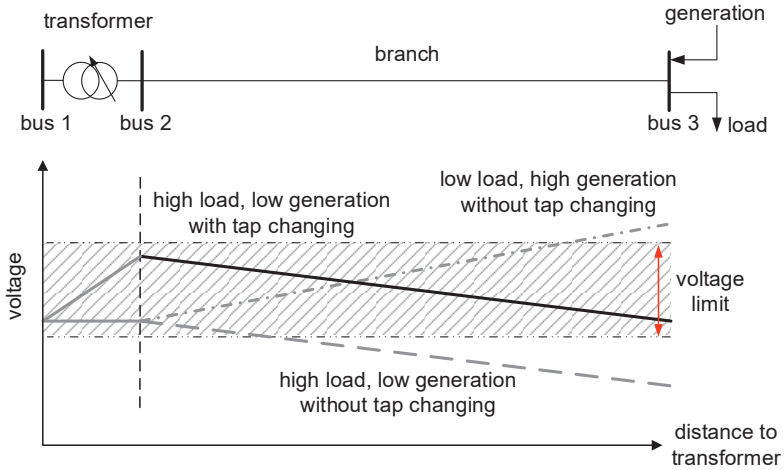

Fig. 5.2.: Voltage profile and deviation along the feeder with time-varying power generation and demand with and without tap changing operation.

The power system voltage can also rise above 1 per unit due to time-varying power generation and demand as a results of high reverse power flow and low power demand [181]. For analytic simplicity, the voltage difference between bus 1 and 3 can be

generally expressed as the voltage difference between bus 1 and 2, and the voltage difference between bus 2 and 3

$$\underline{V}_1 - \underline{V}_3 = (\underline{V}_1 - \underline{V}_2) + (\underline{V}_2 - \underline{V}_3)\,. \tag{5.1}$$

Then, the voltage profile along the feeder is determined as the relationship between the bus voltages

$$\underline{V}_2 = \underline{V}_3 + (R_{\mathrm{br}} + \mathrm{j}X_{\mathrm{br}}) \cdot \underline{I} \qquad \text{with} \qquad \underline{I} = \left(\frac{P + \mathrm{j}Q}{\underline{V}_3}\right)^* . \tag{5.2}$$

The active power P and reactive power Q expresses the generation or load at bus 3, and $\underline{I}$ the corresponding current. As a result of (5.2), the voltage difference $\underline{V}_2 - \underline{V}_3$ can be described as

$$\underline{V}_2 - \underline{V}_3 = \frac{P\,R_{\mathrm{br}} - Q\,X_{\mathrm{br}}}{\underline{V}_3} + \mathrm{j}\frac{P\,X_{\mathrm{br}} + Q\,R_{\mathrm{br}}}{\underline{V}_3}. \tag{5.3}$$

It is shown that the power system voltage can be controlled through active or reactive power adjustments at bus 3. However, with more reactive power circulation in the power system, the thermal capacity of the overhead lines or underground cables is limited. Therefore conventional voltage control solutions such as reactive power compensation, topology adjustment and load shedding are not further discussed. Alternatively, tap-changing transformers can be applied to minimize voltage variations [172]. The voltage difference between bus 1 and 2, referring to the primary and secondary bus of the tap-changing transformer, is calculated by

$$\underline{V}_1 - \underline{V}_2 = \bar{n} \cdot \mathrm{j}X_{\mathrm{tr}} \cdot \underline{I}_{\mathrm{Z}_1} = \bar{n} \cdot \mathrm{j}X_{\mathrm{tr}} \cdot (\underline{I}_{\mathrm{Z}_3} - \underline{I}_2) \tag{5.4}$$

with $\underline{I}_{\mathrm{Z}_3} = \left(1 - \frac{1}{\bar{n}}\right) \cdot \frac{\underline{V}_2}{\mathrm{j}X_{\mathrm{tr}}}$, where X_{tr} defines the reactance and $\bar{n}$ the turns ratio of the tap-changing transformer. By assuming $\underline{I} = -\underline{I}_2$, (5.4) is reformulated to obtain the voltage difference

$$\underline{V}_1 - \underline{V}_2 = (\bar{n} - 1) \cdot \underline{V}_2 + \bar{n} \cdot \mathrm{j}X_{\mathrm{tr}} \frac{P + \mathrm{j}Q}{\underline{V}_3}. \tag{5.5}$$

In case that the tap-changer remains at tap position of the rated turns ratio $\bar{n} = 1$, the voltage difference is $(\underline{V}_1 - \underline{V}_2)\,|_{\bar{\mathrm{n}}=1} = \mathrm{j}X_{\mathrm{tr}} \frac{P + \mathrm{j}Q}{\underline{V}_3}$, otherwise the voltage on the secondary side of the transformer changes. As $\underline{V}_2 \gg \mathrm{j}X_{\mathrm{tr}} \frac{P + \mathrm{j}Q}{\underline{V}_3}$, the impact of the tap-changing transformer can be described as follows:

- when the turns ratio $\bar{n} > 1$, the tap-changer position is higher than the nominal tap position, the voltage difference $(\underline{V}_1 - \underline{V}_2)\,|_{\bar{n}\neq 1}$ increases and the power system voltage decreases.
- when the turns ratio $\bar{n} < 1$, the tap-changer position is lower than the nominal tap position, the voltage difference $(\underline{V}_1 - \underline{V}_2)\,|_{\bar{n}\neq 1}$ decreases and the power system voltage increases.

In the latter case, the tap-changing transformer impedance Z_3 can be characterized as capacitor for the provision of capacitive reactive power and can therefore be interpreted as a compensation source. Considering additional voltage control measures by means of distributed and renewable energy sources, voltage control solutions with on-load tap-changer may need to be updated [169]. When the reactive power capabilities are insufficient for maintaining the power system voltage within the statutory limits, coordinated voltage regulation with tap-changing transformers can be limited [182]. Here, the objective of the proposed coordinated voltage regulation covers the following requirements to a feasible extent:

- assignment of location-dependent voltage control methods for voltage support in power system operations
- provision of coordinated voltage regulation to maintain steady acceptable voltages at all buses within defined ranges
- prioritization of unit type specific voltage control methods under consideration of controllability levels and physical limitations

The proposed voltage control solution combines the advantages of local droop [183] and remote control [184] and may contribute to the development of active network management solutions. Local droop control reacts within seconds and is defined as a decentralized and automatic control that can use remote sensors and concentrators at MV/LV sub-stations as well data from the low voltage network. A local voltage control algorithm installed in the sub-station of the tap-changing transformer may process the aggregated information received. The implemented local droop control reacts instantaneously and is governed by the operational constraints of the bus voltage magnitudes, active and reactive power injection. The remote control is centralized and allows coordinated control within minutes by sending switching commands, activation signals or set-points. The coordination is assumed to be automated with control systems, e.g. supervisory control and data acquisition, energy management systems, or distribution management sytems [174, 184, 185]. Alternatively, the local controller at the primary sub-station level can perform real-time analysis and send set-points to the contracted Virtual Power Plant units and unit clusters depending on local measurements and power system conditions.

5.2.2. Proposed Rule-Based Algorithm

Distributed, renewable and mobile energy sources are assumed to be dispatchable and meet the requirements for grid interconnection, such as grid codes, standards and upcoming recommendation [1]. The interconnection with the power system is assumed to be realized with programmable four-quadrant inverter technology. Based on the technical specifications and network requirements, pooling agreements and service provisions are negotiated that allows the system operator to assure the amount of sufficient voltage regulation capacity. Rule-based techniques are applied for the activation and provision of the voltage control support. The coordinated voltage regulation is realized with multiple distributed, renewable and mobile energy sources and control devices and incorporated in an active network management. The following voltage control methods are investigated:

- T-control: mitigation of mid-term and long-term voltage variation through tap-changing transformer operation
- Q-control: reduction of short-time voltage variations through distributed, renewable and mobile energy sources
- P-control: adjustment of active power and provision of additional control reserve to restore power system voltages between acceptable limits during large disturbance events

The activation follows a temporal sequence as illustrated by means of Figure 5.3. According to [186–188], variable delay times T_{d} for the reduction of short-time voltage variations and avoidance of unnecessary tap-position changes are considered. After the activation of a specific voltage control method, move times T_{m} define the response time for set-point adjustments. Depending on the spatial available capacities, the system states and therefore the operational strategy of the system operator can change. In normal operation, all customers are supplied without overloads, and the $n-1$ criterion is ensured. In abnormal operation, there are overloads of some power system devices and supply failures. As a fundamental prerequisite for the proposed coordinated voltage regulation, relevant system information are reported and exchanged in advance regardless the power system conditions. The data include the spatial and temporal flexibilities that the Virtual Power Plant operator can provide. An example of which is given in Chapter 3, that presents a solution for a nodal-based aggregation and energy management algorithm to determine these flexibilities. At this stage, the power system operator normally applies conventional voltage control solutions, including the operation of tap-changing transformer.

[1] e.g. requirements for the interconnection IEEE Std 1547-2003, operation of electrical installations EN 50110, voltage disturbances standard EN 50160, and BDEW roadmap.

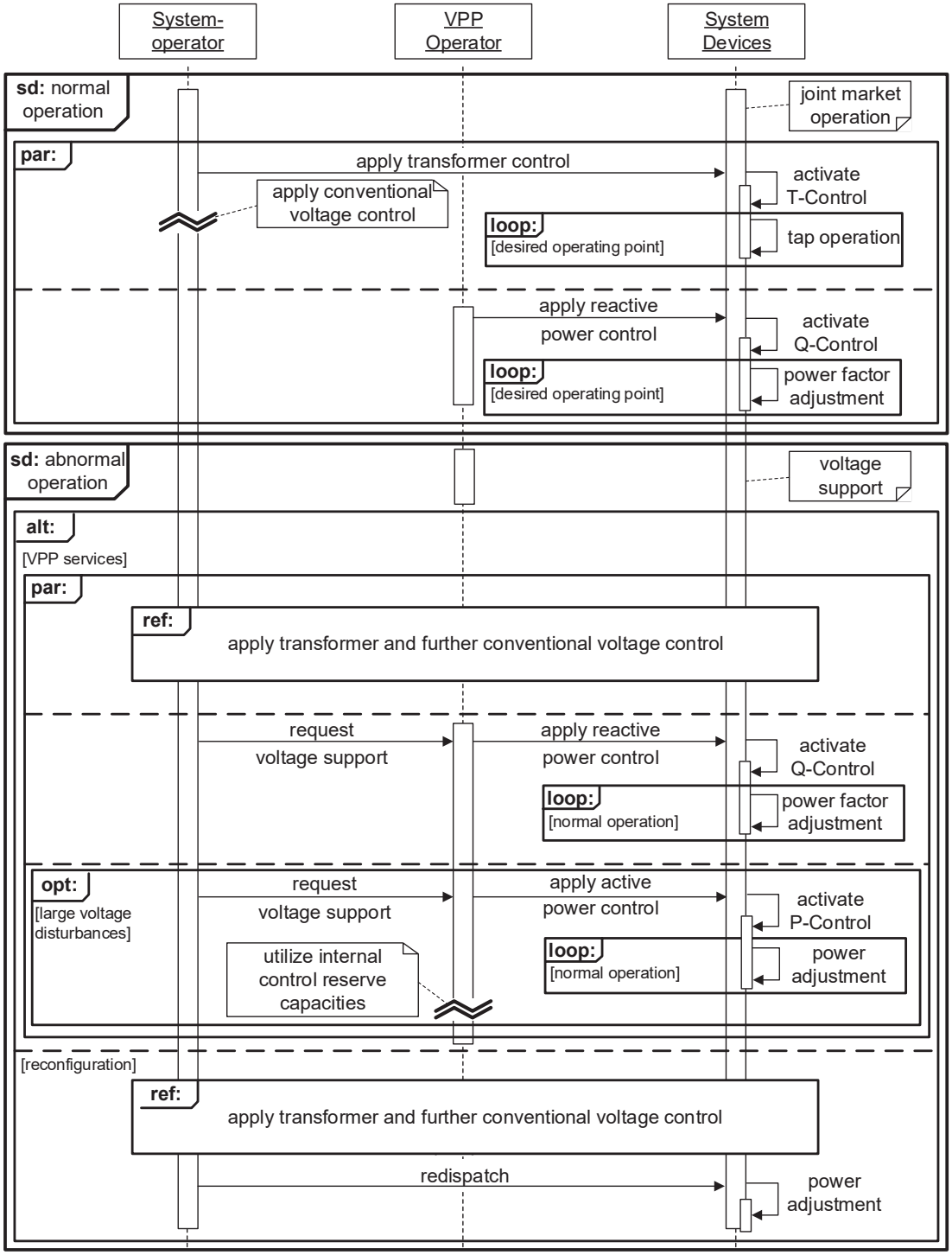

Fig. 5.3.: Sequences of coordinated voltage regulation in power systems separated into voltage support services of the Virtual Power Plant operator in normal and abnormal operation conditions.

Once the system voltages exceed defined voltage limits, support of voltage control is performed through the provision of reactive power control. Here, the Virtual Power Plant operator provides additional local reserve capacity while still achieving compliance with the contracted active power schedules in the energy market. In case

of large voltage disturbances, the system operator requests voltage support services including active power control or directly sends set-points to adjust the generation and load schedules. The activation of the proposed P-control follows the merit order as listed in Table 5.1 from fast **I** to low **IV** reacting participant categories.

TABLE 5.1.: Merit-order and segmented participant categories for the provision and adjustment of active power as part of the proposed P-control.

	I	**II**	**III**	**IV**	**V**
under-voltage	$P_{\mathrm{d}}^{\mathrm{ev}} \downarrow$, $P_{\mathrm{d}}^{\mathrm{bat}} \downarrow$	$P_{\mathrm{d}}^{\mathrm{ind}} \downarrow$	$P_{\mathrm{g}}^{\mathrm{chp}} \uparrow$, $P_{\mathrm{g}}^{\mathrm{dg}} \uparrow$	$P_{\mathrm{g}}^{\mathrm{bat}} \uparrow$	$P_{\mathrm{g}}^{\mathrm{ev}} \uparrow$
over-voltage	$P_{\mathrm{d}}^{\mathrm{ev}} \uparrow$	$P_{\mathrm{d}}^{\mathrm{bat}} \uparrow$	$P_{\mathrm{d}}^{\mathrm{ind}} \uparrow$	$P_{\mathrm{g}}^{\mathrm{chp}} \downarrow$, $P_{\mathrm{g}}^{\mathrm{dg}} \downarrow$	$P_{\mathrm{g}}^{\mathrm{wind}} \downarrow$, $P_{\mathrm{g}}^{\mathrm{pv}} \downarrow$

In case of under-voltage conditions, first-order units **I**, represented by stationary battery systems and electric vehicles, provide active power up to the maximum contracted value without delay times. The second-order units **II**, represented by controlled industry and flexible loads, reduce the power demand within short time periods. The third-order units **III** representing combined heat and power and distributed generators with combustion engines and are activated for further P-control reserve. The contracted flexibilities of the forth-order units **IV** and fifth-order units **V** are provided by stationary battery systems and electric vehicles which are capable to re-inject power to the power system in case of under-voltage power conditions. In case of over-voltage conditions, electric vehicles are activated first and increase the charging power as well as stationary battery systems as second order units. Additional power surplus is used by increasing the demand of industry units. In the last two participant categories, the amount of curtailed power is successively increased. The provision and adjustment of active and reactive power is restricted by the power capacity, inverter limitations, adjustable phase shift angles, and corresponding controllability levels of the corresponding unit or unit cluster. The activation of the P-control is modeled in sequential order and ensures that further control sequences are obliged if necessary. As a result, the ratio of active and reactive power changes and thus also the power factor

$$pf = |\cos\phi| = \frac{P}{\sqrt{P^2 + Q^2}} \qquad \Rightarrow \qquad Q = \pm P \cdot \sqrt{\left(\frac{1}{pf}\right)^2 - 1}. \tag{5.6}$$

The power factor is equal to the absolute value of the cosine of the apparent power phase angle ϕ. If necessary, power curtailment is possible when the apparent power limits of the inverters are reached due to reactive power provision. In some cases, the adjustment of active power schedules can result in deviations of the total power available and contracted for energy market participation. Here, the Virtual Power

Plant operator compensates these power deviations through redispatch measures and utilization of internal control reserve capacities provided by fully-controlled and partly-controlled generation, loads and storage units.

5.3. Validation Model and Mathematical Formulation

With focus on electric vehicles, different voltage control methods are investigated according to the introduced levels of controllability. Most electric vehicles currently available and offered by the automobile manufacturers can be interpreted as non-controlled units. Reflecting future developments, electric vehicles are considered as partly-controlled units, when the charging power can be decreased. The use of electric vehicles as fully-controlled units allows Vehicle-to-Grid services and thus serves as additional generation units in abnormal operation. For the evaluation of different operation strategies in active network management, a validation model as schematically shown in Fig. 5.4, is developed and incorporated in a Matlab/Matpower [189] environment.

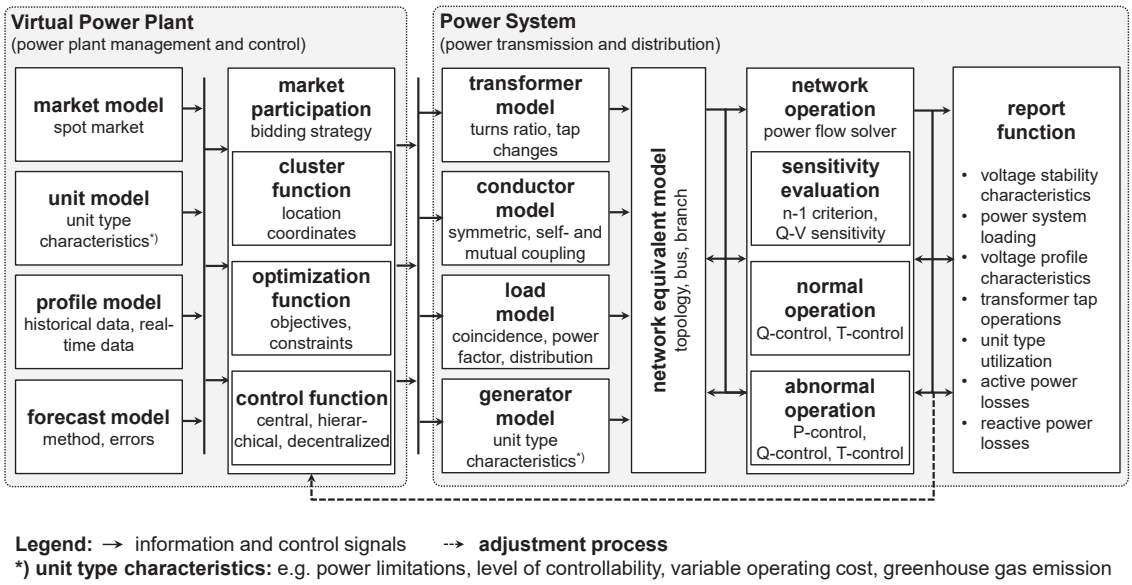

Fig. 5.4.: Validation model for steady-state analysis including schematic representation of generalized functions and models for Virtual Power Plants and system operators.

The power system is defined by a set of buses $H_{\text{bus}} = \{1, 2, \ldots, i, \ldots n^{\text{bus}}\}$, with n^{bus} as the total number of buses. Further, additional models of power system devices are included. For evaluation purposes, the line flows, bus voltages, and stability criteria are observed. The main models and sequences related to the physical power system data are detailed by means of Fig. 5.5. Subsequently, for each hour the system variables such as voltage magnitudes, transformer tap operation and network

losses are obtained and evaluated in multi-period AC power flow analysis. The integrated functions of the rule-based algorithmic is specified in Fig. 5.6. Here, the optimized scheduled profiles as result of the joint market operation are added to the power system generation and load profiles. In case of small voltage disturbances the proposed Q-control, highlighted with light gray area, is activated. In abnormal operation, the time increment of the AC power flow calculations changes to $\Delta t = 1$ seconds in order to investigate short-term voltage variations. In this case, the contracted unit and unit cluster provide additional local reserve capacity through the activation of the proposed P-control, as denoted with the dark gray area in Fig. 5.6.

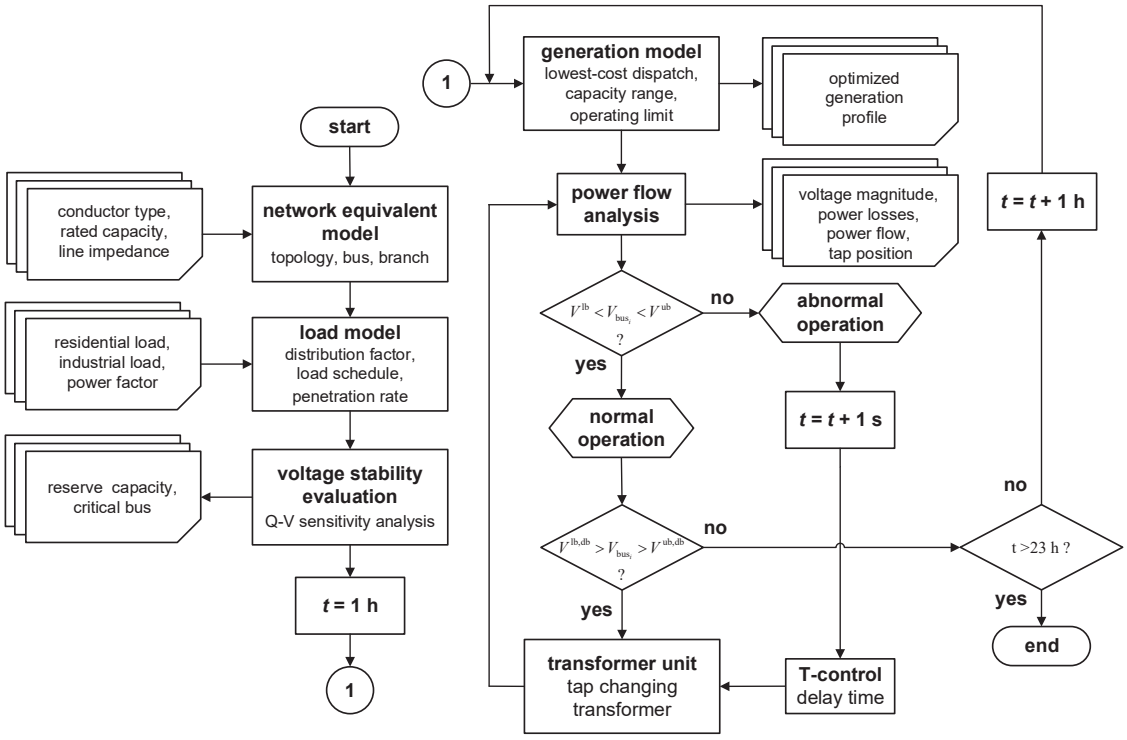

Fig. 5.5.: Realized model architecture and sequences for active network management for modeling distribution systems with tap-changing transformer and conventional generators in multi-period AC power flow analysis.

In each time step, the bus voltage magnitudes $V_{\mathrm{bus},i}$ are compared to the permissible voltage ranges for the identification of small and large voltage disturbances. The power system is in normal operation when every bus voltage magnitude $V_{\mathrm{bus},i}$ is within the defined lower and upper voltage boundary $V_{\mathrm{bus},i} \in [V^{\mathrm{lb}}, V^{\mathrm{ub}}]$. Here, the activated Q-control provides local ancillary services and supports the power system operation. In case of large voltage disturbances, the activated P-control supports to restore the active power balance through the provision of additional control reserve. In order to reduce the delay times or avoid additional information exchange between the system operator and the Virtual Power Plant operator, the P-control can be initialized in advance before unpredictable failures occur.

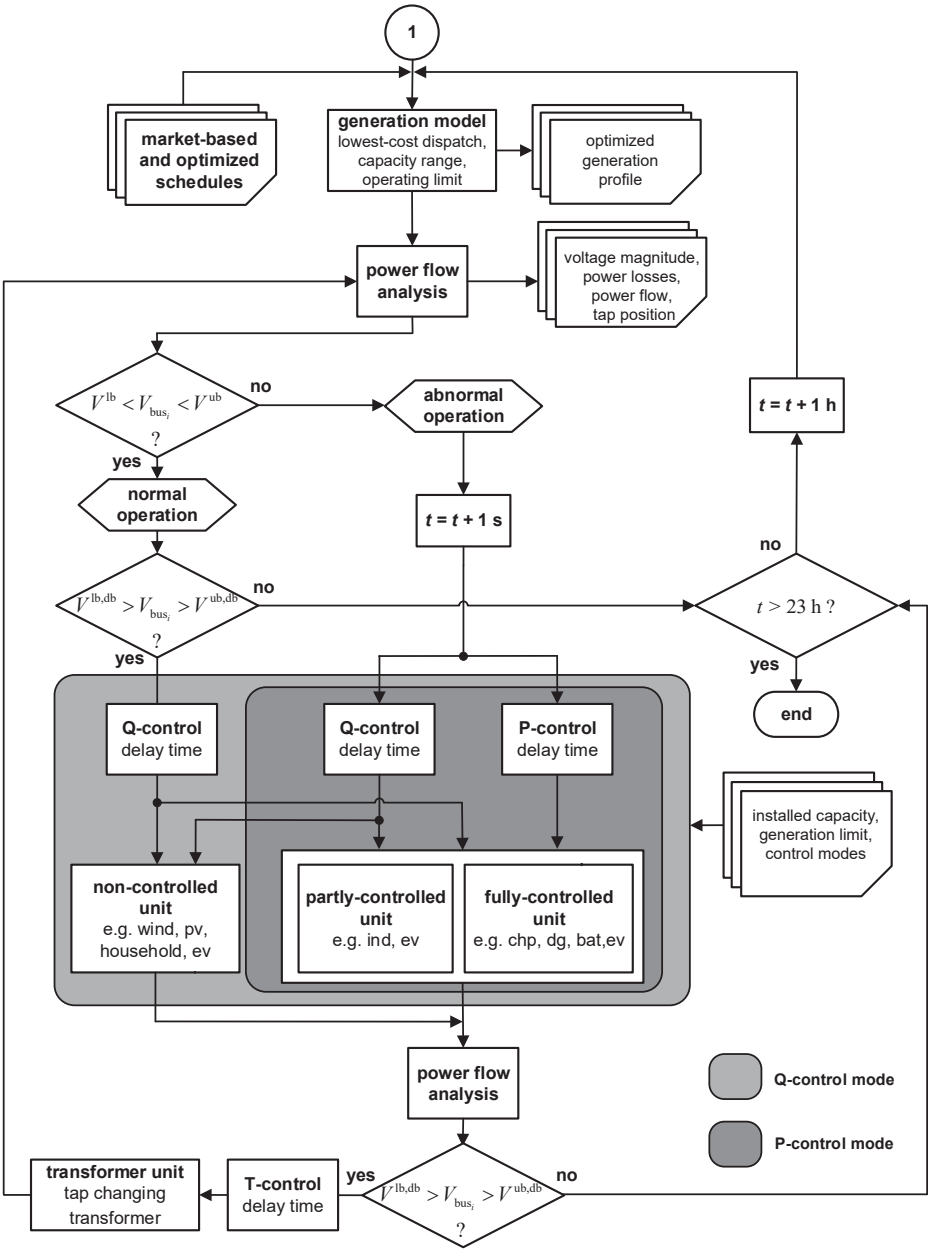

Fig. 5.6.: Control sequences of the proposed rule-based algorithmic for coordinated voltage regulation in distribution networks in normal and abnormal operation conditions.

5.3.1. Characteristics of Proposed Voltage Control Methods

The operation of the on-load tap-changing transformers is realized with standard control schemes according to [186, 190] with subsequent extensions for local and remote controls. Details of the tap-changing transformer model are provided in Appendix E. The following set of voltage signals at defined reference buses V_{ref} is used as input for the control schemes:

$$H_{\mathrm{T^{ctr}}} = \{V_2, V_{2\mathrm{m}}^{\mathrm{sen}}, V_{2\mathrm{m}}^{\mathrm{cr}}\}. \tag{5.7}$$

The voltage signal V_2 refers to the local bus on the secondary side of the transformer, $V_{2\mathrm{m}}^{\mathrm{sen}}$ to the sensitive bus, and $V_{2\mathrm{m}}^{\mathrm{cr}}$ to the critical bus of the power system. Based on voltage stability evaluation with Q-V sensitivity analysis, the sensitive voltage signals $V_{2\mathrm{m}}^{\mathrm{sen}}$ are received from bus 7 of feeder 1 and bus 15 of feeder 2. In comparison, the reference voltage of the critical bus $V_{2\mathrm{m}}^{\mathrm{cr}}$ can change in dependence of the location of measured minimum and maximum power system voltages. The T-control integrates a dead band that prevents short-term responding of the tap-changing transformer during small voltage variations [187, 191]. The specific default values of the control parameters are listed in Table 5.2.

TABLE 5.2.: Default control parameters of the integrated T-control for tap-changing transformer specified for the delay time $T_{\mathrm{d}}^{\mathrm{Tctr}}$, move time $T_{\mathrm{m}}^{\mathrm{Tctr}}$, dead band and tap limits.

delay time $T_{\mathrm{d}}^{\mathrm{Tctr}}$ (s)	move time $T_{\mathrm{m}}^{\mathrm{Tctr}}$ (s)	dead band $V^{\mathrm{lb,db}}$ - $V^{\mathrm{ub,db}}$ (p.u.)	tap limit $n_{\mathrm{min}}^{\mathrm{tap}}$ - $n_{\mathrm{max}}^{\mathrm{tap}}$
30	6	[0.95,1.03]	[-16,+16]

The Q-control is realized with a piecewise linear droop design and can be configured individually. An example of which is shown in Fig. 5.7. The programmable four-quadrant inverter share the active and reactive power according to the indicated slope λ^{Qctr} characteristic.

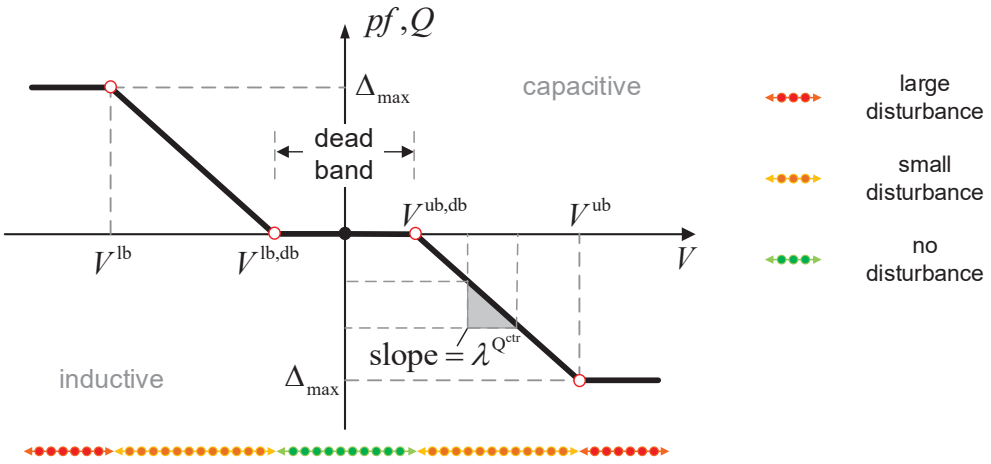

Fig. 5.7.: Schematic representation of the piecewise linear droop design used for modeling the Q-control modes and characteristics.

Typically, the slope defines the gradient of reactive power provision and adjustments of the power factor to maintain a constant steady-state level [191]. The linear droop design is used in existing and enhanced reactive power methods. These are summarized by (5.8) and define the set of Q-control modes.

$$H_{\mathrm{Qctr}} = \{\mathrm{PF}^{\mathrm{fix}}, \mathrm{Q}^{\mathrm{fix}}, \mathrm{Q}\ (V), \mathrm{PF}^{\mathrm{lim}}(V), \mathrm{PF}^{\mathrm{nor}}(V), \mathrm{PF}^{\mathrm{ext}}(V)\} \tag{5.8}$$

The first three Q-control modes, $\mathrm{Q}^{\mathrm{fix}}$, $\mathrm{PF}^{\mathrm{fix}}$, Q (V), represent standard reactive power methods [192]. Additionally, Q-control modes with a higher degree of flexibility in power system operations are developed. The extended reactive power methods are based on local voltage measurements and adjustable power factors, hereafter summarized as PF(V) modes. The default values for the considered Q-control modes are summarized in Table 5.3 and can be defined by either constant values and/or piecewise linear equations. The enhanced PF(V) modes are highlighted in light gray. Considering fixed set-points or standard cos$\phi(P)$ mode [193], the voltage control method may be independent of the power system conditions or adjustments according to the current active power output. As a result, network losses may increase [182] even though the bus voltage magnitudes are between defined lower V^{lb} and upper voltage V^{ub} boundary limits.

TABLE 5.3.: Q-control modes characteristics and specifications of implemented droop control modes, specified by the width of voltage limits, slopes, nominal and maximum values.

Q-mode	dead band ($V^{\mathrm{lb,db}}$, $V^{\mathrm{ub,db}}$)	width of limit (V^{lb}, V^{ub})	slope ($\lambda^{\mathrm{Q^{ctr}}}$)	maximum value (Δ_{max})	nominal value (pf, Q)
$\mathrm{PF}^{\mathrm{fix}}$	\	\	\	pf_{set}	pf_{set}
$\mathrm{Q}^{\mathrm{fix}}$	\	\	\	Q_{set}	Q_{set}
Q (V)	0.97-1.01	0.94-1.04	\	Q_{max}	0
$\mathrm{PF}^{\mathrm{lim}}(V)$	0.95-1.03	0.94-1.04	0.05/0.01	0.95	1
$\mathrm{PF}^{\mathrm{nor}}(V)$	0.97-1.01	0.94-1.04	0.05/0.03	0.95	1
$\mathrm{PF}^{\mathrm{ext}}(V)$	0.95-1.03	0.94-1.04	0.20/0.01	0.8	1

In comparison, the use of Q-control modes with adjustable power factors are less disruptive for network voltage control devices such as tap-changing transformers and result in lower field currents [194]. Here, the set-points are determined by local measurements where the reactive power provision increases with higher local voltage variations. A distinction is made between the following Q-control modes:

1) limited $\mathrm{PF}^{\mathrm{lim}}(V)$ 2) normal $\mathrm{PF}^{\mathrm{nor}}(V)$ 3) extended $\mathrm{PF}^{\mathrm{ext}}(V)$

The $\mathrm{PF}^{\mathrm{lim}}(V)$ mode reaches the maximum power factor directly after the lower voltage boundary of the dead band $V^{\mathrm{lb,db}}$ is exceeded. In contrast, the determination of the power factor with the other PF(V) modes depends mainly on the voltage magnitudes outside the defined dead band. The $\mathrm{PF}^{\mathrm{lim}}(V)$ and $\mathrm{PF}^{\mathrm{ext}}(V)$ modes are characterized by higher ranges of dead band limitations, denoted by the upper $V^{\mathrm{ub,db}}$ and lower voltage boundary $V^{\mathrm{lb,db}}$ set-points. The extended $\mathrm{PF}^{\mathrm{ext}}(V)$ mode is specified by a maximum value of the power factor $pf_{\mathrm{max}} = 0.8$ and allows higher

flexibilities for the provision of voltage support. Similar to the transformer control scheme, the Q-control modes are modeled with a (i) dead band element, (ii) delay time element, and (iii) power factor control elements as shown in Fig. 5.8.

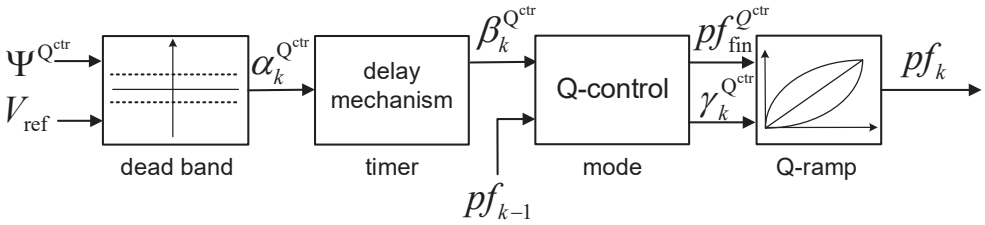

Fig. 5.8.: Q-control flow chart of for units and unit clusters integrated through grid coupling inverters modeled with dead band element, delay time element, and power factor control elements.

First, the Q-control is activated with the activation signal $\Psi^{\mathrm{Q^{ctr}}}$. Then, the reference voltages is sent to the dead band element. Here, the voltage error is determined by comparing the reference voltage with the defined defined lower $V^{\mathrm{lb,db}}$ and upper $V^{\mathrm{ub,db}}$ voltage ranges of the dead band

$$\alpha_k^{\mathrm{Q^{ctr}}} = \begin{cases} +1, & \text{if } V_{\mathrm{ref}} < V^{\mathrm{lb,db}} \quad \text{capacitive} \\ -1, & \text{if } V_{\mathrm{ref}} > V^{\mathrm{ub,db}} \quad \text{inductive} \\ 0, & \text{otherwise.} \end{cases} \tag{5.9}$$

Then, the output signal $\alpha_k^{\mathrm{Q^{ctr}}}$ is sent to the delay time element and used in (5.10) to determine the output signal $\beta_k^{\mathrm{Q^{ctr}}}$. The time parameter $c_k^{\mathrm{Q^{ctr}}}$ changes in case of higher or lower time values compared to the defined delay time $T_{\mathrm{d}}^{\mathrm{Q^{ctr}}}$.

$$\beta_k^{\mathrm{Q^{ctr}}} = \begin{cases} +1, & \text{if } c_k^{\mathrm{Q^{ctr}}} \geq T_{\mathrm{d}}^{\mathrm{Q^{ctr}}} \\ -1, & \text{if } c_k^{\mathrm{Q^{ctr}}} \leq -T_{\mathrm{d}}^{\mathrm{Q^{ctr}}} \\ 0, & \text{otherwise} \end{cases} \tag{5.10}$$

with

$$c_k^{\mathrm{Q^{ctr}}} = \begin{cases} c_{k-1}^{\mathrm{Q^{ctr}}} + 1\mathrm{s}, & \text{if } \alpha_k^{\mathrm{Q^{ctr}}} = +1 \text{ and } c_{k-1}^{\mathrm{Q^{ctr}}} \geq 0\mathrm{s} \\ c_{k-1}^{\mathrm{Q^{ctr}}} - 1\mathrm{s}, & \text{if } \alpha_k^{\mathrm{Q^{ctr}}} = -1 \text{ and } c_{k-1}^{\mathrm{Q^{ctr}}} \leq 0\mathrm{s} \\ 0, & \text{otherwise} \end{cases}$$

Hereafter, the set-point for the power factor pf_k is determined within the control elements. The delay mechanism is reset in the case that the voltage limit excitation changes at the bus. The output signal of the delay time element and the value of

the power factor are forwarded to the Q-control element. Depending on the selected Q-control mode, the incremental change of the power factor $\gamma_k^{\mathrm{Q^{ctr}}}$ is calculated as the spread of the last pf_{k-1} to the final value $pf_{\mathrm{fin}}^{Q^{\mathrm{ctr}}}$ of the power factor as follows

$$\gamma_k^{\mathrm{Q^{ctr}}} = \begin{cases} \mid pf_{k-1} - pf_{\mathrm{fin}}^{Q^{\mathrm{ctr}}} \mid, & \text{if } pf_{k-1} \cdot pf_{\mathrm{fin}}^{Q^{\mathrm{ctr}}} > 0 \\ 2 - \Big(\mid pf_{k-1} \mid + \mid pf_{\mathrm{fin}}^{Q^{\mathrm{ctr}}} \mid \Big), & \text{if } pf_{k-1} \cdot pf_{\mathrm{fin}}^{Q^{\mathrm{ctr}}} < 0 \\ 0, & \text{otherwise.} \end{cases} \tag{5.11}$$

with

$$pf_{\mathrm{fin}}^{Q^{\mathrm{ctr}}} = \begin{cases} pf_{\max}, & \text{if } V_{\mathrm{ref}} < V^{\mathrm{lb}} \text{ or } V_{\mathrm{ref}} > V^{\mathrm{ub}} \\ \beta_k^{\mathrm{Q^{ctr}}} \cdot \Big(1 - \Big((1 - pf_{\max}) \cdot \dfrac{V_{\mathrm{ref}} - V^{\mathrm{ub,db}}}{V^{\mathrm{ub}} - V^{\mathrm{ub,db}}}\Big)\Big), & \text{if } V^{\mathrm{lb}} \leq V_{\mathrm{ref}} < V^{\mathrm{lb,db}} \\ \beta_k^{\mathrm{Q^{ctr}}} \cdot \Big(1 - \Big((1 - pf_{\max}) \cdot \dfrac{V^{\mathrm{lb,db}} - V_{\mathrm{ref}}}{V^{\mathrm{lb,db}} - V^{\mathrm{lb}}}\Big)\Big), & \text{if } V^{\mathrm{ub}} \geq V_{\mathrm{ref}} > V^{\mathrm{ub,db}}. \end{cases}$$

The final value is modeled through the combination of Q(U)- and cos$\phi(P)$-control formulas [182, 192]. In the last step, the inverter changes the power factor to the set-point

$$pf_k = pf_{k-1} + \beta_k^{\mathrm{Q^{ctr}}} \cdot \gamma_k^{\mathrm{Q^{ctr}}} \cdot \kappa_k^{\mathrm{Q^{ctr}}} \tag{5.12}$$

with

$$\kappa_k^{\mathrm{Q^{ctr}}} = \begin{cases} 1, & \mathrm{Q}_{\mathrm{ramp}}^{\mathrm{ctr}} = 1 \\ \dfrac{1}{\mid H_{\mathrm{ts}}^{T_{\mathrm{m}}^{\mathrm{Q^{ctr}}}} \mid}, & \mathrm{Q}_{\mathrm{ramp}}^{\mathrm{ctr}} = 2 \\ \sin\Big(k \cdot \dfrac{\pi}{2 \cdot \mid H_{\mathrm{ts}}^{T_{\mathrm{m}}^{\mathrm{Q^{ctr}}}} \mid}\Big) - \sin\Big((k-1) \cdot \dfrac{\pi}{2 \cdot \mid H_{\mathrm{ts}}^{T_{\mathrm{m}}^{\mathrm{Q^{ctr}}}} \mid}\Big), & \mathrm{Q}_{\mathrm{ramp}}^{\mathrm{ctr}} = 3 \\ \Big|\cos\Big(k \cdot \dfrac{\pi}{2 \cdot \mid H_{\mathrm{ts}}^{T_{\mathrm{m}}^{\mathrm{Q^{ctr}}}} \mid}\Big) - \cos\Big((k-1) \cdot \dfrac{\pi}{2 \cdot \mid H_{\mathrm{ts}}^{T_{\mathrm{m}}^{\mathrm{Q^{ctr}}}} \mid}\Big)\Big|, & \mathrm{Q}_{\mathrm{ramp}}^{\mathrm{ctr}} = 4 \end{cases}$$

where $\kappa_k^{\mathrm{Q^{ctr}}}$ denotes the incremental output adjustment per time step. For example, let the variable time increment $\Delta t = 1\mathrm{s}$ and move time $T_{\mathrm{m}}^{\mathrm{Q^{ctr}}} = 10\mathrm{s}$ be given, then the set of time steps is $H_{\mathrm{ts}}^{T_{\mathrm{m}}^{\mathrm{Q^{ctr}}}} = \{1s,\ ..., 10s\}$. The piecewise linear droop design as introduced in Fig. 5.7 can be changed through the adjustment of the above mentioned droop parameters with respect to the temporal changes of the voltage. For evaluation purposes, the following characteristics of the Q-ramp function $\mathrm{Q}_{\mathrm{ramp}}^{\mathrm{ctr}}$ are implemented, namely:

1) block 2) stepwise 3) degressive 4) progressive.

The first slope applies block functions to adjust the set-point within one time step. The second slope adjusts the reactive power output stepwise with constant power factor adjustments for each time step. The third slope, starts with a high slope and decreases in subsequent time steps while getting closer to the specified set-point. In contrast, the forth slope is characterized by low slopes in the first time steps and increases the slope before the maximum value is reached. Compared to the progressive and stepwise Q-ramp functions, the degressive slope increases the reactive power output faster than the other slopes, as illustrated in Fig. 5.9. Therefore, stepwise slope characteristics are used as the default Q-ramp function that additionally assure constant response behaviors.

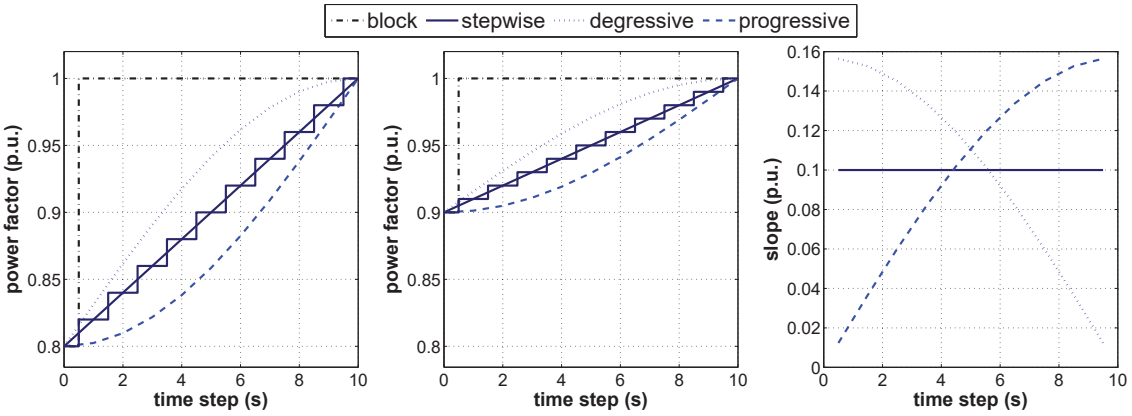

(a) $pf_{k=1} = 0.8$ p.u. (b) $pf_{k=1} = 0.9$ p.u. (c) adjustments $\kappa^{\mathrm{Q_k^{ctr}}}$

Fig. 5.9.: Slope characteristics for power factor adjustments within a defined move time $T_{\mathrm{m}}^{\mathrm{Q^{ctr}}} = 10s$ in case of (a) $pf_{k=1} = 0.8$ p.u. and (b) $pf_{k=1} = 0.9$ p.u. where (c) compares the corresponding output adjustments $\kappa^{\mathrm{Q_k^{ctr}}}$.

In contrast to active power curtailment, which may contribute to mitigate over-voltage conditions [182,195], the proposed P-control uses the potential of controllable units and unit clusters to compensate under-voltage conditions by increasing the active power output [180, 196]. The P-control is also realized with a (i) dead band element, (ii) delay time element, and (iii) active power control elements, as shown in Fig. 5.10. First, the P-control is activated by the activation signal $\Psi^{\mathrm{P^{ctr}}}$ from the system operator or the Virtual Power Plant operator. The power system condition is evaluated through the comparison of reference voltage V_{ref}, which refers to the local bus voltage magnitude. The control element determines the voltage error of the defined voltage ranges, specified by the lower $V^{\mathrm{lb,P^{ctr}}}$ and upper voltage boundary $V^{\mathrm{ub,P^{ctr}}}$ as calculated in (5.13).

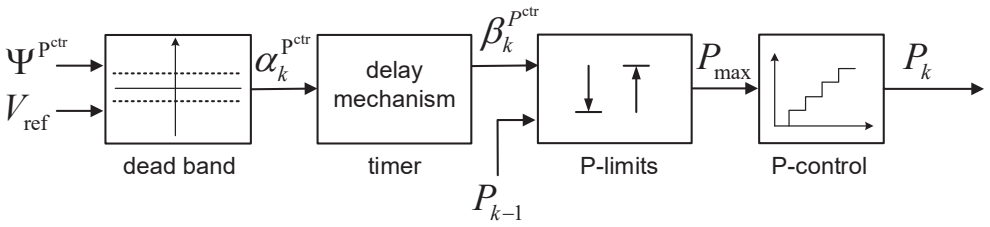

Fig. 5.10.: P-control flow chart for units and unit clusters integrated through grid coupling inverters modeled with dead band element, delay time element, and active power control elements.

In case that the output value $\alpha_k^{\mathrm{Pctr}} \neq 0$, the contracted unit or unit cluster is activated for the provision of control reserve. Normal operation is indicated by $\alpha_k^{\mathrm{Pctr}} = 0$.

$$\alpha_k^{\mathrm{Pctr}} = \begin{cases} +1, & \text{if } V_{\mathrm{ref}} < V^{\mathrm{lb,Pctr}} \\ -1, & \text{if } V_{\mathrm{ref}} > V^{\mathrm{ub,Pctr}} \\ 0, & \text{otherwise} \end{cases} \tag{5.13}$$

Although the function of the delay element is the same as introduced for the Q-control, the delay time $T_{\mathrm{d}}^{\mathrm{Pctr}}$ differs for each unit type. The calculation is as follows

$$\beta_k^{\mathrm{Pctr}} = \begin{cases} +1, & \text{if } c_k^{\mathrm{Pctr}} \geq T_{\mathrm{d}}^{\mathrm{Pctr}} \\ -1, & \text{if } c_k^{\mathrm{Pctr}} \leq -T_{\mathrm{d}}^{\mathrm{Pctr}} \\ 0, & \text{otherwise} \end{cases} \tag{5.14}$$

with

$$c_k^{\mathrm{Pctr}} = \begin{cases} c_{k-1}^{\mathrm{Pctr}} + 1\mathrm{s}, & \text{if } \alpha_k^{\mathrm{Pctr}} = +1 \text{ and } c_{k-1}^{\mathrm{Pctr}} \geq 0\mathrm{s} \\ c_{k-1}^{\mathrm{Pctr}} - 1\mathrm{s}, & \text{if } \alpha_k^{\mathrm{Pctr}} = -1 \text{ and } c_{k-1}^{\mathrm{Pctr}} \leq 0\mathrm{s} \\ 0, & \text{otherwise.} \end{cases}$$

The power limitation element considers the minimum $P_{\min}$ and maximum $P_{\max}$ active power values of the corresponding unit or unit cluster. In the last step, the active power is changed stepwise, with variable percentage adjustments κ_k^{Pctr} as follows:

$$P_k = \begin{cases} P_{k-1} + \beta_k^{\mathrm{Pctr}} \cdot \kappa_k^{\mathrm{Pctr}} \cdot P_{\max}, & \text{if } \beta_k^{\mathrm{Pctr}} = +1 \\ P_{k-1} + \beta_k^{\mathrm{Pctr}} \cdot \kappa_k^{\mathrm{Pctr}} \cdot P_{\min}, & \text{if } \beta_k^{\mathrm{Pctr}} = -1 \\ P_{k-1}, & \text{otherwise.} \end{cases} \tag{5.15}$$

In order to allow fast response, the default adjustment factor is assumed with $\kappa_k^{\mathrm{P^{ctr}}} = 0.15$ in per unit. However, the activated P-control can be modified gradually but is still limited to rated power capacity of the unit or unit cluster and the actual power factor. Finally, the reactive power is proportionally adjusted.

5.3.2. Network Model and Implementation Environment

The presented operational principles and proposed voltage control methods are integrated in an exemplary distribution network. The power system under study is derived from the European medium voltage distribution network benchmark, established by the CIGRE Task Force C6.04.02 [197]. Appendix E provides further details of the 15-bus network model. The network topology is characterized by two feeder sections, directly connected with 25 MVA 110/20kV on-load tap-changing transformer to the primary sub-transmission system. The total line length of the conductors, consisting of overhead lines and underground cables, is 24.95 km. The network model is assumed to be operated as a three phase balanced system. The apparent power demand for each time step is calculated by (5.16) as product of the maximum apparent power demand for individual loads at each bus.

$$\begin{bmatrix} S_{\mathrm{d,max,bus}_1} \\ S_{\mathrm{d,max,bus}_2} \\ \vdots \\ S_{\mathrm{d,max,bus}_n} \end{bmatrix} \times \begin{bmatrix} \kappa_{\mathrm{d},1} & \kappa_{\mathrm{d},2} & \cdots & \kappa_{\mathrm{d},m} \end{bmatrix} = \begin{bmatrix} S_{\mathrm{d,bus}_1,1} & S_{\mathrm{d,bus}_1,2} & \cdots & S_{\mathrm{d,bus}_1,m} \\ S_{\mathrm{d,bus}_2,1} & S_{\mathrm{d,bus}_2,2} & \cdots & S_{\mathrm{d,bus}_2,m} \\ \vdots & \vdots & \ddots & \vdots \\ S_{\mathrm{d,bus}_n,1} & S_{\mathrm{d,bus}_n,2} & \cdots & S_{\mathrm{d,bus}_n,m} \end{bmatrix} \quad (5.16)$$

The coincidence factor $\boldsymbol{\kappa}_{\mathrm{d}}$ expresses the number of customers served [197]. Equation 5.16 can be summarized as $\boldsymbol{S}_{\mathrm{d,max}} \times \boldsymbol{\kappa}_{\mathrm{d}} = \boldsymbol{S}_{\mathrm{d}}$. The coincidence factor changes in accordance to the variable time increment Δt, e.g. 1 hour and corresponding set of time steps $H_{\mathrm{ts}} = \{1, 2, \ldots, 24\}$, as listed in Table E.5. A distinction is made between the power factors for individual residential and industrial loads. The maximum load of feeder section 1 is 25.98 MVA, and 20.23 MVA for feeder section 2. The daily power demand excluding power system losses, is 461.12 MWh and 290.27 MVarh, respectively. The loads at each bus are modeled as quantity of active and reactive power demand, following the load distribution detailed in Appendix E.3. Figure 5.11 shows the daily load distribution where the contour plots display the isolines of the apparent power demand $\boldsymbol{S}_{\mathrm{d}}$ per bus and hour. The star plot represents the hourly load demand at each bus, separated into 24-hour time segments. The load values for bus 2 and 13 are significantly shifted towards the center and the end of the feeder sections that result in time-varying load shifts in the feeder sections and voltage

variations and violations in the power system. Further, a multi-period AC optimal power flow is adapted to determine the generation schedules of additionally integrated conventional generation units at bus 12 and 14. Appendix E.5 provides further specifications of the generator model.

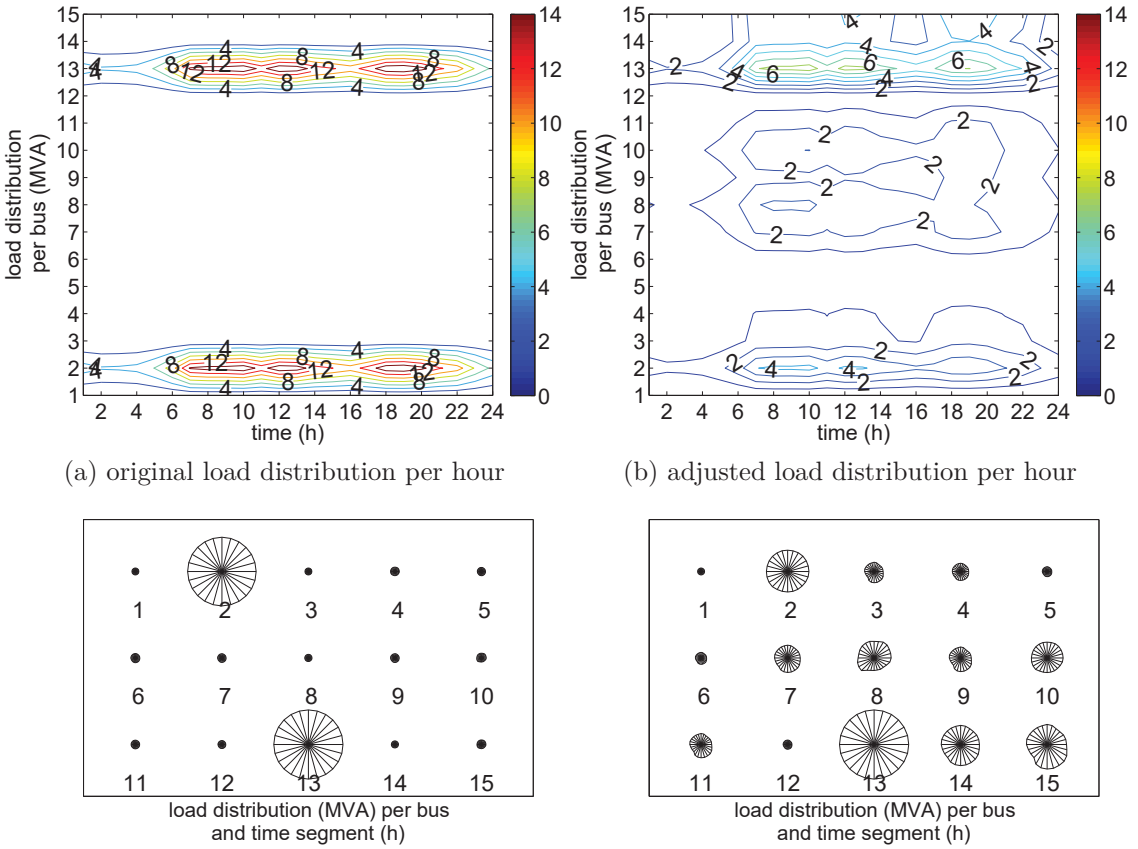

(a) original load distribution per hour

(b) adjusted load distribution per hour

(c) original load distribution per bus

(d) adjusted load distribution per bus

Fig. 5.11.: Load distribution and hourly loading conditions of the European 20 kV distribution network benchmark with (a),(c) original values and (b),(d) adjusted values.

The Virtual Power Plant coordinated units and unit clusters are assigned to specific buses in the network model under consideration of the (i) physical restriction of power system components and (ii) V-Q sensitivity of each bus. For the support of voltage control, buses characterized by higher sensitivity values are primary selected for the allocation of generation, load and storage units. The restrictions are as follows:

- minimum power generation covers the base system load in feeder 1 and feeder 2,
- maximum power generation is below the capacity ratings of conductors.

For different scenarios, Table 5.4 summarized the power capacities and penetration rates of the considered distributed, renewable and mobile energy sources. The penetration rate denotes the ratio of the installed capacity of wind and photovoltaic power plants to the maximum load of the power system. The base scenario (case 1)

considers the daily load distribution of the power system with additional industrial loads as part of the Virtual Power Plant. The remaining scenarios includes additional units and unit clusters as integral multiples of the installed capacities defined in the 25 % RES scenario (case 2).

TABLE 5.4.: Considered power capacities in use cases for the assessment of voltage support of Virtual Power Plant coordinated unit types.

scenario	wind	pv	chp	dg	ev	bat	ind	net
	(MW)							
case 1: base	\	\	\	\	\	\	3.20	26.95
case 2: base +25%-RES	6.00	7.50	1.50	2.00	8.45	1.21	3.20	26.95
case 3: base +50%-RES	12.00	14.50	1.50	2.00	8.45	2.42	3.20	26.95
case 4: base +75%-RES	18.00	21.70	1.50	2.00	8.45	2.42	3.20	26.95

The maximum load in the power system is defined as the sum of all inflows and outflows at each bus. This is expressed by (5.17) for the calculation of the residual ΔP_k active power. The same formula applies for the determination of the residual ΔQ_k reactive power.

$$\sum_{k=k_{\text{ini}}}^{k_{\text{fin}}} \Delta P_k = \sum_{k=k_{\text{ini}}}^{k_{\text{fin}}} (P_{\text{g},k}^{\text{gen}} + P_{\text{g},k}^{\text{VPP}} + P_{\text{d},k}^{\text{net}} + P_{\text{d},k}^{\text{VPP}} + P_{\text{d},k}^{\text{loss}}), \qquad \forall k \in H_{\text{ts}} \tag{5.17}$$

$P_{\text{g},k}^{\text{gen}}$ represents the power generation of the conventional generators, $P_{\text{d},k}^{\text{net}}$ the defined load demand and $P_{\text{d},k}^{\text{loss}}$ the network losses. The terms $P_{\text{g},k}^{\text{VPP}}$ and $P_{\text{d},k}^{\text{VPP}}$ denote the sum of power generation and demand of the Virtual Power Plant and can be decomposed by (5.18) and (5.19), respectively.

$$P_{\text{g},k}^{\text{VPP}} = P_{\text{g},k}^{\text{pv}} + P_{\text{g},k}^{\text{wind}} + P_{\text{g},k}^{\text{chp}} + P_{\text{g},k}^{\text{dg}} + P_{\text{g},k}^{\text{ev}} + P_{\text{g},k}^{\text{bat}} \tag{5.18}$$

$$P_{\text{d},k}^{\text{VPP}} = P_{\text{d},k}^{\text{hh}} + P_{\text{d},k}^{\text{ind}} + P_{\text{d},k}^{\text{ev}} + P_{\text{d},k}^{\text{bat}}. \tag{5.19}$$

The power generation and load demand of the extended European 20 kV distribution network benchmark and the Virtual Power Plant are matched to form the nodal power balance equations of the network model. The loads of the Virtual Power Plant includes industrial loads and the charging loads of electric vehicles and stationary batteries. The total number of electric vehicles is determined by (5.20)-(5.22) as a function of the total number of considered households n^{hh} in the power system.

$$n^{\mathrm{ev}} = \Gamma^{\mathrm{ev}} \cdot n^{\mathrm{hh}} \tag{5.20}$$

Let Γ^{ev} be the penetration rate of electric vehicles. For simplification, the household loads are approximated as follows

$$S^{\mathrm{hh}}_{\mathrm{d,max}} = \kappa^{\mathrm{hh}}_{\mathrm{d}} \cdot \sum_{\mathrm{i=1}}^{n^{\mathrm{hh}}} S^{\mathrm{hh}}_{\mathrm{d},i} \quad \text{, with} \quad \kappa^{\mathrm{hh}}_{\mathrm{d}} = 0.6 \cdot (1 + \frac{1}{n^{\mathrm{hh}}}) \tag{5.21}$$

where $S^{\mathrm{hh}}_{\mathrm{d},i}$ denotes the individual household loads. The coincident maximum loads $\boldsymbol{S}^{\mathrm{hh}}_{\mathrm{d,max}}$ are expressed as a function of the equivalent household loads and coincidence factors $\kappa^{\mathrm{hh}}_{\mathrm{d}}$, as reported in [197]. For example, by assuming a mean daily maximum demand $\tilde{S}^{\mathrm{hh}}_{\mathrm{d,max}}$= 2.5 kVA [198, 199], (5.21) can be rewritten as

$$\begin{aligned} \kappa^{\mathrm{hh}}_{\mathrm{d}} &= \frac{S^{\mathrm{hh}}_{\mathrm{d,max}}}{n^{\mathrm{hh}} \cdot \tilde{S}^{hh}_{\mathrm{d,max}}} = 0.6 \cdot \tilde{S}^{\mathrm{hh}}_{\mathrm{d,max}} \cdot (1 + n^{\mathrm{hh}}) \\ \Rightarrow n^{\mathrm{hh}} &= \frac{S^{\mathrm{hh}}_{\mathrm{d,max}} - \kappa^{\mathrm{hh}}_{\mathrm{d}} \cdot \tilde{S}^{hh}_{\mathrm{d}}}{\kappa^{\mathrm{hh}}_{\mathrm{d}} \cdot \tilde{S}^{\mathrm{hh}}_{\mathrm{d}}} \end{aligned} \tag{5.22}$$

For example, let $n^{\mathrm{ev}} = 22,843$ be the total number of households, $\Gamma^{\mathrm{ev}} = 0.10$ the penetration rate of electric vehicles, and $P^{\mathrm{ev}}_{r} = 3.7$ kW the rated charging/discharging power. Then, the theoretical maximum power capacity is 8.45 MW in case that all electric vehicles simultaneously charge.

5.4. Computational Study and Simulation Results

The coordinated voltage regulation and management approach is evaluated in normal and abnormal operation in simulations with different loading conditions as a result of the optimized energy procurements in joint market operations. Following state-of-the-art characteristics, Table 5.5 summarizes the considered default values. The values in parentheses indicate unit types that are capable of re-injecting power to the network in case of under-voltage power conditions. The default values are set to $T^{\mathrm{T^{ctr}}}_{\mathrm{m}} = 6$ seconds for one tap operation, $T^{\mathrm{Q^{ctr}}}_{\mathrm{m}} = 10$ seconds for Q-control, and $T^{\mathrm{P_{ctr}}}_{\mathrm{m}} = 4$ seconds for P-control. $T^{\mathrm{Q^{ctr}}}_{\mathrm{m}}$ and $T^{\mathrm{P_{ctr}}}_{\mathrm{m}}$ specify the total time to reach a desired final value of the respective control operation. The default values for the delay times are set to $T^{\mathrm{T^{ctr}}}_{\mathrm{d}} = 30$ seconds and $T^{\mathrm{Q^{ctr}}}_{\mathrm{d}} = 20$ seconds, respectively. For simplicity, the delay time $T^{\mathrm{P_{ctr}}}_{\mathrm{d}}$ is assumed to be the same for each unit type.

First, the integrated T-control is evaluated and the operational limits of the tap-changing transformer determined. Second, the mitigation of voltage variations in

TABLE 5.5.: Specification of delay times $T_{\mathrm{d}}^{\mathrm{Pctr}}$ for the activation of P-control in under-voltage and over-voltage conditions based on the defined level of controllability.

cluster of units	unit type	under-voltage		over-voltage	
		controllability*)	$T_{\mathrm{d}}^{\mathrm{Pctr}}$	controllability*)	$T_{\mathrm{d}}^{\mathrm{Pctr}}$
	[10-17]	[1-3]	(s)	[1-3]	(s)
wind, pv	10,11	1	\	2	40
chp, dg	12,13	3	8	3	32
ev	14	3	0(12)	2	0
bat	16	3	0(8)	3	8
ind	17	2	8	2	16

*) 1:= non-controlled, 2:= partly-controlled, 3:= fully-controlled

normal operation with the activated T-control and Q-control is examined. Third, the effectiveness of the proposed coordinated voltage regulation with focus on voltage support solutions with electric vehicles is further assessed in abnormal operation. Here, the proposed P-control is additionally activated in case that the power system voltage is not within the defined limits. In order to confirm the validity of the voltage control methods, the simulations are conducted with the introduced default values and remain unchanged.

5.4.1. Evaluation and Limitations of Modified Tap-Changing Transformer Control Modes

The performance of the T-control modes is validated, using the hourly load demand as defined in the base scenario (case 1) and use of different T-control modes. The observed minimum V_{min} and maximal voltage magnitudes V_{min} are summarized in Fig. 5.12. The remaining bus voltage magnitudes are between the depicted minimum and maximum values. The voltage ranges of the lower and upper voltage boundary limits are highlighted by the gray rectangle. In Fig. 5.13, the variation of tap positions of the tap-changing transformer in feeder 1 and the residual load served by the transformer sub-stations are detailed. The observed voltage variations in feeder 2 remain unchanged.

The results without transformer control are given in Fig 5.12a and for V_2 control in Fig. 5.12b, respectively. As can be seen, the results are similar when comparing the obtained voltage profiles. This is due to the fact that the tap-changer position keeps constant when applying V_2 as reference voltage signal as shown in Fig. 5.13. Partial

over-voltages are observed in Fig. 5.12c and Fig. 5.12d, when local voltages V_2 and sensitive voltages $V_{2\mathrm{m}}^{\mathrm{sen}}$ are applied as reference voltage signals for the tap-changing transformer control.

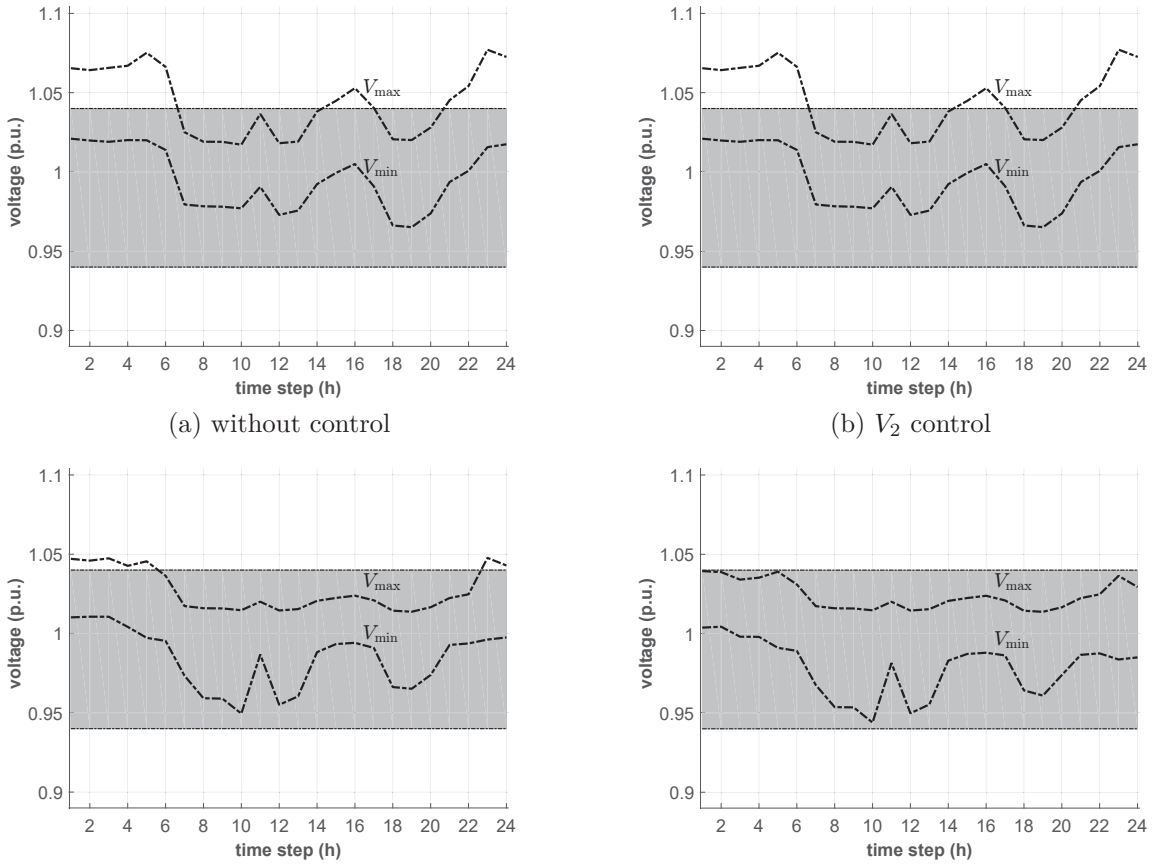

(a) without control (b) V_2 control

(c) $V_{2\mathrm{m}}^{\mathrm{sen}}$ control (d) $V_{2\mathrm{m}}^{\mathrm{cr}}$ control

Fig. 5.12.: Voltage profile with different T-control modes (case 1), specified by (a) without control, (b) V_2 control, (c) $V_{2\mathrm{m}}^{\mathrm{sen}}$ control, and (d) $V_{2\mathrm{m}}^{\mathrm{cr}}$ control.

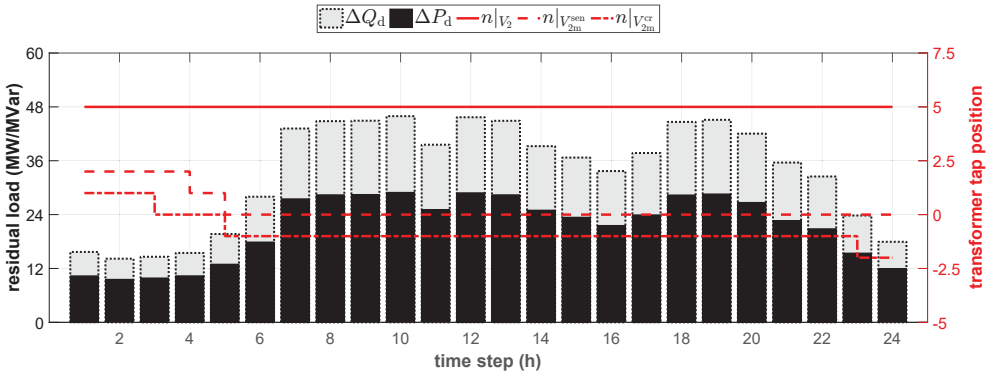

Fig. 5.13.: Impact of different T-control modes, specified by V_2 control, $V_{2\mathrm{m}}^{\mathrm{sen}}$ control, and $V_{2\mathrm{m}}^{\mathrm{cr}}$ control, on the operation of the tap-changing transformer in feeder 1 (case 1).

In case of over-voltages, however, it is possible that the maximum voltage is not measured at the local or sensitive bus and in case of under-voltages, for example, the minimum voltage can not be measured at the heavy loaded buses. In terms of number of tap operations, the results in Fig. 5.13 show that the power system

voltages remain only within the defined voltage ranges when V_{2m}^{cr} control is applied. In the remaining cases, the power system voltages exceed the defined upper voltage limit. Comparing the power flows in the distribution system, differences in the use of the transformer control modes can also be detected. For example, Table 5.6 provides the power flow deviations of selected buses. The results refer to hour 23, where the maximum differences of tap positions have been identified.

TABLE 5.6.: Comparison of power flow deviation with T-control modes in hour 23 on selected branches as result of different reference voltage signals for V_{2m}^{cr} and V_2, V_{2m}^{sen} and V_2.

from bus	to bus	ΔP_{2m}^{sen} (kW)	ΔP_{2m}^{cr} (kW)	ΔQ_{2m}^{sen} (kVar)	ΔQ_{2m}^{cr} (kVar)
2	3	13.42	19.11	37.48	52.78
3	4	9.52	13.56	28.51	40.11
4	5	2.46	3.50	9.13	12.83
4	9	1.16	1.66	5.58	7.81

The power flow deviation ΔP_{2m}^{sen} compares the active and reactive power values when applying V_{2m}^{sen} and V_2 control. ΔP_{2m}^{cr} denotes the power flow deviation when V_{2m}^{cr} and V_2 are used as reference voltage signals for the transformer control. The use of both T-control modes, V_{2m}^{sen} and V_{2m}^{cr}, shows that the network losses can be reduced in comparison to V_2 control. In summary, the results confirm the applicability of the control scheme for tap-changing transformer but also show the limitations to compensate voltage variations caused by time-varying generation or load profiles. Among the three analyzed T-control modes, V_{2m}^{cr} control is the most effective one for tap changing operations in order to reduce voltage variations during the power system operations. An additional advantage of the proposed remote control is given by the more efficient use and possibility of savings of network losses during operation.

5.4.2. Comparison of Proposed Voltage Control Methods with Multiple Voltage Regulating Devices

In the following, the integrated T-control modes are further investigated for smart grid applications in combination with voltage control methods provided by the Virtual Power Plant. For the mitigation of over-voltages in power system operation during low load periods, the proposed T-control and Q-control modes are activated. While the power system load remains the same, the residual load distribution changes in scenarios with different penetration rates $\Gamma^{res} \in \{0\%, 25\%, 50\%, 75\%\}$ of renewable energy sources. Table 5.7 summarizes the residual load served by the

transformer sub-stations of feeder 1 and 2. The configuration and location of the units and unit clusters in the power system is specified in Appendix E.1. Especially feeder 1 integrates most of the distributed, renewable and mobile energy sources.

TABLE 5.7.: Residual load served by the transformer sub-stations during 24 hours (case 1 - case 4) with increasing share of renewable energy sources.

	case 1, $\Gamma^{\text{res}} = 0\%$	case 2, $\Gamma^{\text{res}} = 25\%$	case 3, $\Gamma^{\text{res}} = 50\%$	case 4, $\Gamma^{\text{res}} = 75\%$
	(MWh)			
feeder 1	33.002	1.271	-33.123	-67.143
feeder 2	146.250	148.241	138.927	130.455

In order to test the effectiveness of the proposed Q-control modes, the voltage variations as a result of the AC power flow are examined. First, the T-control is disabled and the tap-positions are set to the initial tap positions. Then, the PF^{fix} mode is investigated as part of conventional voltage control methods [180]. Subsequently, the enhanced $\text{PF}(V)$ modes are activated and the results compared. For example, considering $\Gamma^{\text{res}} = 50\%$ penetration of renewable energy sources (case 3), Fig. 5.14 summarizes the results for all evaluated Q-control modes.

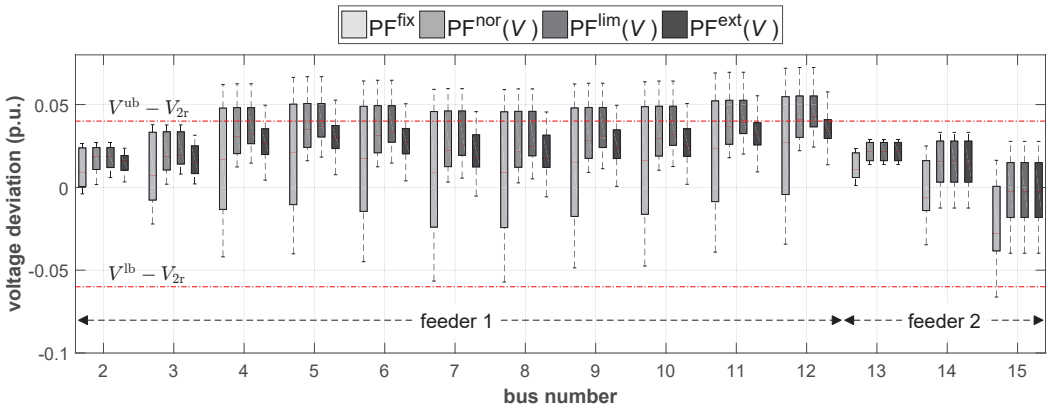

Fig. 5.14.: Boxplot of observed voltage deviations in the power system (case 3), considering $\text{PF}(V)$ modes compared with PF^{fix} for the provision of voltage support.

The boxplot shows the 25th lower and 75th upper percentile of the voltage deviations observed in the power system. The ends of the whiskers represent the minimum and maximum values. The general formula for the calculation of the voltage deviation values is given by $\Delta V = V_{\text{bus},i} - V_{2\text{r}} \quad \forall i \in H_{\text{bus}}$, where $V_{\text{bus},i}$ denotes the measured voltage magnitude at a specific bus i and $V_{2\text{r}}$ the rated voltage of the power system. The red lines indicate the lower V^{lb} and upper V^{ub} voltage boundary limits, also represented as difference values. When applying the PF^{fix} mode, the minimum and maximum differences of the bus voltage magnitudes are between $V_{\text{bus},i} \in [-0.0662, 0.0719]$ in per unit. In comparison, when $\text{PF}^{\text{lim}}(V)$ and $\text{PF}^{\text{nor}}(V)$ are activated, the voltage variations can be reduced as indicated by the

anthracite gray and dark gray bars in Fig. 5.14. Only the $\mathrm{PF}^{\mathrm{ext}}(V)$ mode offers greater voltage support and keeps the bus voltage magnitudes in defined ranges, $V_{\mathrm{bus},i} \in [-0.0398, 0.0578]$ in per unit. For a better insight into the developed voltage control method, the 24-hour time simulation is repeated and the best identified control strategies for T-control and Q-control modes are applied. The critical bus voltages $V_{2\mathrm{m}}^{\mathrm{cr}}$ are used as reference voltage for the tap-changing control and the voltage control combined with the $\mathrm{PF}^{\mathrm{ext}}(V)$ mode, using the stepwise Q-ramps. The results are given in Fig. 5.15.

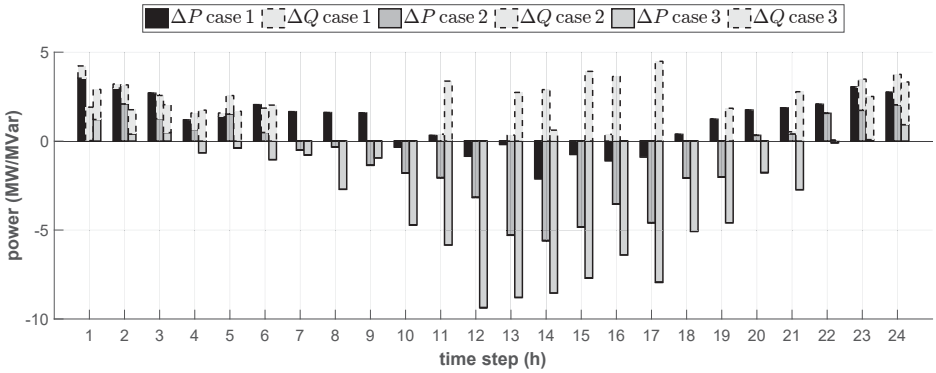

(a) residual power served served by the primary sub-transmission system (case 2 - case 4)

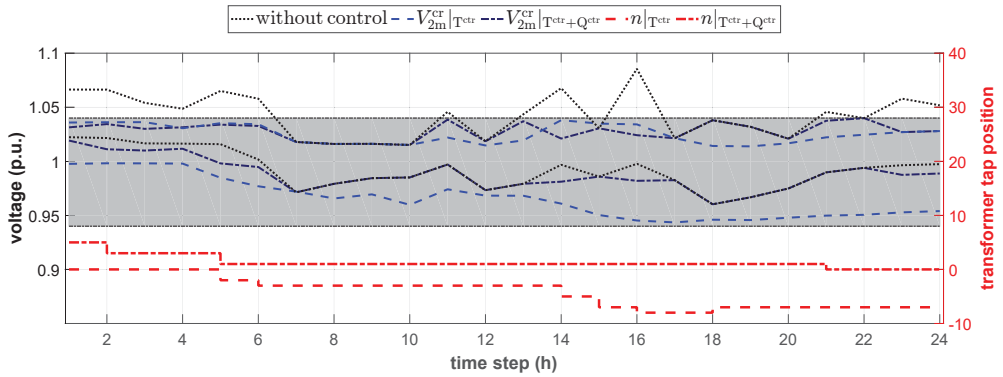

(b) voltage profiles in feeder 1 an number of tap operations (case 3)

Fig. 5.15.: Impact of activated $\mathrm{PF}^{\mathrm{ext}}(V)$ mode in power system operation with active network management.

As can be seen in Fig. 5.15a, the increasing share of renewable energy sources coordinated by the Virtual Power Plant successively reduces the residual power that needs to be served by the primary sub-station. Additionally, through the activated $\mathrm{PF}^{\mathrm{ext}}(V)$ mode, reactive power can also be efficiently provided. The results can be obtained from Fig. 5.15b, which shows selected voltage profiles (case 2) and provides an overview of the required number of tap operations. The gray rectangle defines the lower voltage V^{lb} and upper voltage V^{ub} boundary limits. As can be observed, the increasing power generation of renewable energy sources with time-varying characteristics, causes partial over-voltages in the power system without voltage control. In the case that only $V_{2\mathrm{m}}^{\mathrm{cr}}$ control is activated for tap-changing operations, over-

voltage conditions can be mitigated in the power system. However, more frequent tap operations are necessary, as highlighted with the red dashed line. Through the activation of Q-control, the range of minimum and maximum power system voltages as well as the total tap operations is reduced as summarized in Table 5.8.

TABLE 5.8.: Minimum and maximum voltage magnitudes observed during 24 hours (case 2 - case 4) without control, T-control, and combined T- and Q-control.

scenario	control method *)	$V_{\min}$ (p.u.)	$V_{\max}$ (p.u.)	tap operations	reactive power provision VPP (MVarh)
case 2, $I^{\text{res}} = 25\%$	without control	0.9620	1.0794	\	\
	T-control	0.9584	1.0396	1	\
	T- and Q-control	0.9620	1.0397	3	1.53
case 3, $I^{\text{res}} = 50\%$	without control	0.9603	1.1000	\	\
	T-control	0.9435	1.0380	9	\
	T- and Q-control	0.9603	1.0399	5	18.42
case 4, $I^{\text{res}} = 75\%$	without control	0.9589	1.1000	\	\
	T-control	0.9388	1.0399	11	\
	T- and Q-control	0.9555	1.0387	4	34.73

*) Q-control with $\text{PF}^{\text{ext}}(V)$ mode and T-control with $V_{2\text{m}}^{\text{cr}}$ mode.

The total tap operations are listed in comparison with the total reactive power provided. For example in case 4, the number of tap operations is 11 moves without Q-control which can be reduced to only 4 moves with activated Q-control. The maximum bus voltage magnitudes without control is $V_{\max} = 1.1000$ and $V_{\max} = 1.0387$ in per unit when applying T-control and Q-control. The results confirm the added value of the proposed coordinated voltage regulation in minimizing voltage variations. The proposed coordinated voltage regulation is capable to maintain the power system voltages within admissible voltages ranges, even in scenarios with high penetration of renewable energy sources. Additionally, compared with the standard reactive power method the superiority of the extended Q-Control mode is demonstrated with the results obtained.

5.4.3. Droop Controlled Power Adjustments and Balancing Under Generation Failure

In order to simulate under-voltage conditions, a generation block of the conventional generator located at bus 12 fails and results in 5 MW active power loss. A sudden increase of wind power generation is simulated and its impact assessed in over-voltage

conditions. The investigations are based on the loading conditions of the 75%-RES scenario (case 4). In both cases, the proposed P-control is activated to restore and maintain the power system voltage and compensate the power balance. The observed minimum voltage magnitudes during under-voltage conditions are shown in Fig. 5.16a for feeder section 1. The first time step k denotes the values in normal operation before the failure, the second $k+1$ after the failure, while the third $k+2$ provides the set-points for the subsequent time steps in abnormal operation.

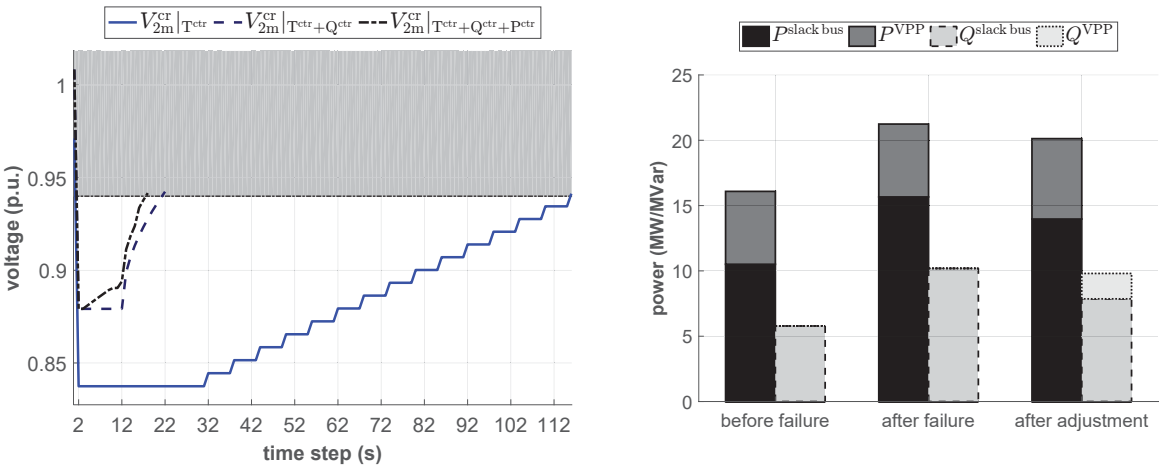

(a) voltage profile with different voltage controls

(b) active and reactive power adjustments

Fig. 5.16.: Mitigation of short-term voltage variations in critical under-voltage conditions (case 4) specified by (a) critical bus voltage magnitudes V_{2m}^{cr} and (b) served residual loads before and after activation of the coordinated voltage control.

As shown, the tap-changing transformer control (blue solid line) is capable of restoring the desired power system voltage within 116 seconds through 15 tap operations. However, the use of combined T-control, Q-control and P-control modes (black dash-dotted line) reaches a faster solution within 17 seconds and without any tap operations. The corresponding quantities of active and reactive power provision before and after the generation failure are given in Fig. 5.16b for the case that T-control, Q-control and P-control modes are activated. In total, the power provided by the primary sub-transmission system (slack bus) can be reduced through local reserve capacity provided by the Virtual Power Plant. The contribution of the integrated electric vehicles is shown in Fig. 5.17, which differently adjust the charging power according to investigated voltage control methods. In T-control mode, the charging power remains unchanged while the combined operation with Q-control mode results in additional reactive power adjustments for voltage support. In case of T- and Q-control and additional P-control, the charging power of the electric vehicles is gradually reduced. In this case, further reactive power adjustments are not necessary as illustrated by the electric vehicles located at bus 8.

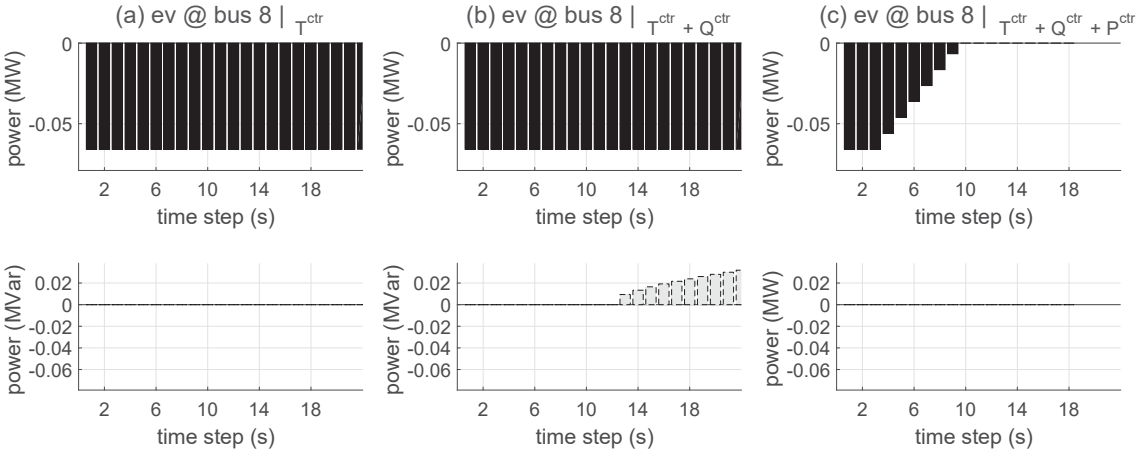

Fig. 5.17.: Contribution of electric vehicles (case 4) for the mitigation of under-voltage conditions with charging power adjustments at bus 8.

For the verification of the proposed coordinated voltage regulation in over-voltage condition, an alternative solution to active power curtailment is provided. As a result of a sudden increase of the wind speeds in the area of the power system, the integrated wind power plants inject more active power as shown in Fig. 5.18a.

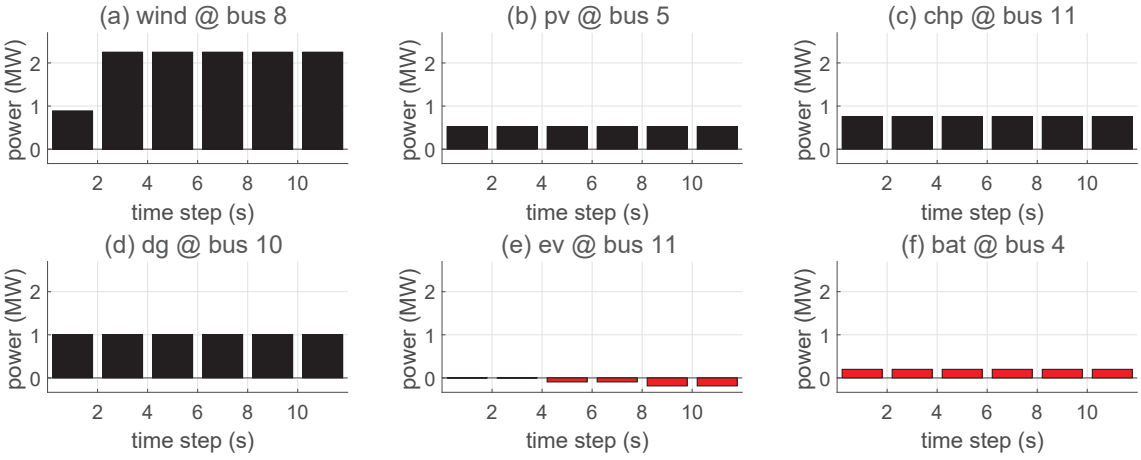

Fig. 5.18.: Active power adjustments during abnormal operation (case 4) with activated P-control mode for selected units, connected to different buses in the power system.

Based on the controllability levels of the contracted units and unit clusters, as specified in Table 5.5, and the merit-order for the activation of the proposed P-control as given in Table 5.1, the Virtual Power Plant coordinated units and unit cluster react in different manner. Due to the fast response of contracted and available electric vehicles and stationary batteries, the surplus of active power is efficiently used for charging processes and the power system voltages maintained in the desired voltage limits. An example of the power adjustment process with the activated P-control is given by Fig. 5.18e and Fig. 5.18f for electric vehicles and stationary battery systems, respectively. Further adjustments are not necessary, as can be seen in Fig. 5.18b-Fig. 5.18d, which provide some examples of remaining units. Thanks to the coor-

dinated voltage regulation with the Virtual Power Plant operator and the proposed rule-based algorithm, the dynamics in abnormal operation can be efficiently captured. It is shown that electric vehicles can contribute to mitigate under- and overvoltage conditions in power system operation through the adjustment of the charging power. However, the disconnection times for fault-ride-through operations [200] may need to be considered in order to avoid the temporary or full disconnection of units or unit cluster after a few seconds. Here, further analyses are required to examine the power system dynamics, short-circuit current capacity limitations, and inherent necessary modification in the protection systems.

5.5. Concluding Remarks

A coordinated voltage regulation and management approach for distribution networks including multiple power sources and system devices is proposed and studied. The voltage control solutions combine local and remote controls and enable the system operator to exploit the temporal and spatial flexibilities of a comprehensive set of additional power system services provided by the Virtual Power Plant operator. The proposed voltage control methods are modeled and examined in the extended European 20 kV distribution network benchmark. The elaborations include various case studies and address the possibilities to evaluate the novel voltage support services that are of value to diverse actors involved in the energy and power system, e.g. identifying appropriate remuneration mechanisms that ensure efficient operation with distributed, renewable, and mobile energy sources. The characteristics of the developed active network management account for the operational condition at each bus and considers the controllability levels of the corresponding units or unit clusters. However, the network effects of spatial and temporal mixed application of the presented voltage control methods need to be further investigated and the implementation in current liberalized energy markets addressed. The simulation results confirm the potential and effectiveness of proposed voltage control solution to provide greater voltage support and possible measures for active network management solutions in comparison with conventional control methods. Further solutions can include various distribution system functionalities, such as service restoration, consideration of changing network characteristics, adaptable Volt/VAR optimization, and state estimations.

6. CONCLUSIONS AND OUTLOOK

The results of the thesis and developed methodologies reveal several aspects concerning the integration of distributed, renewable and mobile energy sources in Virtual Power Plants. This chapter concludes the thesis by summarizing the work, drawing conclusions, and providing an outlook on potential, associated research.

6.1. Summary of the Thesis

A unified model architecture and energy management algorithm for the modeling of scalable Virtual Power Plants is developed. Joint market operations within the framework of liberalized energy markets are investigated based on the integrated optimization models. For this purpose, the thesis briefly reviews the structure of power plant portfolios for the operational planning in future energy supply. Then, in order to provide an overarching approach for the systemic integration of decentralized, renewable and mobile energy sources, a possible realization of interconnected and interoperable solutions as part of a research and laboratory environment is detailed. Driving forces for the adaptation of aggregation concepts in existing market structures and power systems with feasible participation opportunities are outlined.

The framework of liberalized energy markets is adopted to structure the optimization problems related to joint market operations. To create arbitrary power plant portfolios, the Virtual Power Plant is substantiated with distinct unit types and unit models, based on real-data sets. The unit models are used for the abstraction of power scheduling processes and coordinated redispatch measures. An energy management algorithm is formulated and integrates the services and functions in multi-period optimization processes. A stochastic simulation method is utilized to appropriately address forecast uncertainties related to the intermittent power generation of renewable energy sources. In the first and second stage of the proposed three-stage imbalance compensation algorithm, power imbalances are compensated in day-ahead and intraday market operation. In the third stage, remaining real-time imbalances are compensated through internal power adjustments and power shifting functionalities in time frames less than 15 minutes. A proof-of-concept for the

proposed framework is provided by selecting appropriate case scenarios that validate the optimization model and control algorithm in joint market operations. The dispatch results demonstrate the capability to handle different bidding strategies for economic and environmental objectives while considering the unit type specific boundaries and updated information and operational states of the power plant portfolio.

Additional aggregation entities are introduced, so called EV Suppliers/Aggregators that collate the energy demand of a number of electric vehicles and negotiate the commercial conditions with the Virtual Power Plant operator. Following the principles used for energy purchases in the wholesale and retail market, activity-based and timetable-based driving schedules are developed for the prediction of the required energy demand of passenger and commercial electric vehicle fleets. The contractual obligations with the EV Supplier/Aggregator and power system operator are integrated in the energy management algorithm and the optimization problem structured in an upper level and lower level optimization, respectively. Then, the hierarchically structured optimization problem is solved for achieving optimized energy procurements for electric vehicle fleets and taking into account different charging tariffs. To demonstrate the systemic complexity related to redispatch measures requested by the system operator, nodal-based optimization scenarios are presented for an electrified bus fleet at an intra-urban bus depot. The simulation cases show the reciprocal effects in the unit commitment and dispatch of the power plant portfolio and provision of additional system services through electric vehicles.

Enhanced coordinated voltage regulation and management approaches are developed and evaluated in a European 20 kV distribution network benchmark under normal and abnormal operation conditions. The validation model includes the schematic representation of generalized functions and models for the Virtual Power Plant and system operator. A rule-based algorithm for the coordinated voltage regulation of multiple power sources and system devices is presented. It is capable of dealing with voltage variations and maintains steady acceptable voltages at all buses in the network. Current reactive power control modes, including fixed power factor PF^{fix} control, fixed reactive power Q^{fix} control, and voltage-dependent reactive power Q(V) control are examined. Based on a combined local and remote control approach and with focus on electric vehicles, voltage support services are investigated in multi-period AC power flows. It is shown that the presented solution enables the system operator to exploit the temporal and spatial flexibilities of a comprehensive set of additional system services provided by the Virtual Power Plant.

6.2. Contribution to Research

Operational planning, modeling and control algorithms for Virtual Power Plants with electric vehicles were presented separately in each chapter. Concerning the applicability in joint market and power system operations, the major contribution of the thesis is provided in the following.

1. Unified model architecture and energy management algorithm for scalable Virtual Power Plants: The framework of liberalized energy markets is adopted to structure the optimization problems related to joint market operations. The operational planning, control and management of distributed, renewable and mobile energy sources is substantiated in distinct optimization models.

a) A nodal-based aggregation and cluster algorithm allows the collocation of units and unit clusters to virtual or physical buses. This allows to lower the number of optimization variables in the optimization processes and therefore helps to reduce the computational effort for solving the unit commitment and dispatch problem.

b) Controllable loads are integrated in the unified model architecture and assigned with virtual storage capacities. This modeling technique was specifically designed to investigate demand-side management services and the provision of an internal control reserve solution.

c) Power imbalances caused by forecast errors are efficiently compensated in a three-stage imbalance algorithm as part of the multi-period optimization processes. Here, the utilization of available flexibilities of fully-controlled and partly-controlled generation, loads and storage units was considered.

It can be concluded that the presented Virtual Power Plant model is capable of exploring efficient solutions of multi-period optimization problems in joint market operations and handle economic and environmental bidding strategies with a manageable set of power plant portfolios. Further, the simulation results show the potentials arising from shorter dispatch intervals that allow better balancing of power deviations and thus contribute to a more efficient way to handle balance group deviations.

2. Prediction-based power scheduling and optimized energy procurement for passenger and commercial electric vehicle fleets: A price-based charging and tarification model for the operation of electric vehicles is introduced and combined with SoE-based charging strategy. The extended model environment of the Virtual Power Plant features different charging tariffs, from non-controlled to fully-controlled charging processes including vehicle-to-grid services and demonstrates the utilization of electric vehicles in the energy management algorithm.

a) Standard driving profiles for the representation of the driving behavior of private and commercial electric vehicles are developed to serve as input for the prediction of the energy demand and determination of optimized energy procurements in joint market operations.

b) Multilateral transactions with EV Suppliers/Aggregators and power system operator are represented in the hierarchically structured optimization model. This allows to consider electric vehicle fleets in the optimization process of the Virtual Power Plant for the determination of feasible optimization solutions and nodal redispatch measures.

The flexibility provided by the proposed methodology is motivated by the fact that the developed standard driving profiles can be utilized by EV Suppliers/Aggregators and Virtual Power Plant operators to cope with the uncertainty associated with the prediction of charging scheduling and service procurement.

3. Enhancing power system operation through coordinated voltage regulation with combined local droop and remote control algorithm: Coordinated voltage regulation for multiple power sources and devices is developed for enhancing power system operations in normal and abnormal operation conditions. The validation model for steady-state analysis includes schematic representation of generalized functions and models for the Virtual Power Plant and system operator.

a) Combined local and remote controls exploit the temporal and spatial flexibilities of distributed, renewable and mobile energy sources through droop controlled power adjustments that efficiently mitigates time-varying voltage variations.

b) The validation model comprehensively integrates different piecewise linear and non-linear droop designs of voltage control methods and configurations of power plant portfolios.

The computational experiments are compared in multi-period AC power flow analysis. The results are systematically evaluated and show the technical and economic feasible solutions as a part of the already existing voltage control solutions.

6.3. Outlook

The proposed solutions outline the potential benefits when distributed, renewable and mobile energy source are regarded as active elements in energy market and power system operations. However, as the legal requirements, regulations and market framework change as well as the operational practices with the adaptation of developing interoperable communication and information technologies, modifications of the introduced Virtual Power Plant concepts are recommended. Additionally, the design of suitable trading and market platforms is of particular interest for the successful implementation of the presented framework. Further research is necessary to quantify the system integration benefits. For example, this includes the allocation of cost savings and efficiency improvements in the tendering process of control reserve of system operators.

The diversification in the power plant portfolio and potential risk reduction of power imbalance in the balancing group management should be considered for further research. The presented energy management algorithm could be further improved by incorporating additional characteristics of the introduced unit models and handle the multilateral transactions between the Virtual Power Plant, EV Supplier/Aggregator and system operator in embedded optimization models. So far, this is not fully implemented. It remains to be investigated how the integration of network models and characteristics can extend the optimization model through the capability of additionally solving a security constraint unit commitment and dispatch.

Moreover, the provision of additional system services may vary according to the specifications determined by the energy market and power system operations. The integration of the proposed coordinated voltage regulation may require adjustments of existing standards and regulatory requirements to fully exploit the flexibility of local and remote controlled power sources and system devices and avoid temporarily disconnections.

Bibliography

[1] United Nations, "Adoption of the Paris Agreement - Draft Decision -/CP.21," United Nations Framework Convention on Climate Change (UNFCCC), Tech. Rep., 2015.

[2] F. Birol, L. Cozzi, D. Dorner, T. Gül, B. Wanner, F. Kesicki, C. Hood, M. Baroni, S. Bennett, C. Besson, S. Bouckaert, A. Bromhead, O. Durand-Lasserve, T. El-Laboudy, T. Gould, M. Hashimoto, M. Klingbeil, A. Kurozumi, E. Levina, J. Liu, S. McCoy, P. Olejarnik, N. Selmet, D. Sinopoli, S. Suehiro, J. Trüby, C. Vailles, D. Wilkinson, G. Zazias, S. Zhang, S. Mooney, T. Coon, and R. Priddle, "Energy and Climate Change," International Energy Agency (IEA), Tech. Rep., 2015.

[3] F. deLlano Paz, A. Calvo-Silvosa, S. I. Antelo, and I. Soares, "The European Low-Carbon Mix for 2030: The Role of Renewable Energy Sources in an Environmentally and Socially Efficient Approach," *Journal on Renewable and Sustainable Energy Reviews*, vol. 48, pp. 49–61, 2015.

[4] M. Pollitt, "The Role of Policy in Energy Transitions: Lessons from the Energy Liberalisation Era," *Energy Policy*, vol. 50, pp. 128 – 137, 2012, special Section: Past and Prospective Energy Transitions - Insights from History.

[5] Ela, E. and Milligan, M. and Kirby, B., "Operating Reserves and Variable Generation," National Renewable Energy Laboratory (NREL), Tech. Rep. August, 2011.

[6] S. Trümper, S. Gerhard, S. Saatmann, and O. Weinmann, "Qualitative Analysis of Strategies for the Integration of Renewable Energies in the Electricity Grid," *Energy Procedia*, vol. 46, pp. 161 – 170, 2014, 8th International Renewable Energy Storage Conference and Exhibition (IRES 2013).

[7] DENA, "DENA Ancillary Services Study 2030." German Energy Agency - Deutsche Energie-Agentur GmbH (dena), Tech. Rep., 2014.

[8] B. Sudhakara Reddy, "Access to Modern Energy Services: An Economic and Policy Framework," *Renewable and Sustainable Energy Reviews*, vol. 47, pp. 198 – 212, 2015.

[9] C. Grimmond, M. Roth, T. Oke, Y. Au, M. Best, R. Betts, G. Carmichael, H. Cleugh, W. Dabberdt, R. Emmanuel, E. Freitas, K. Fortuniak, S. Hanna, P. Klein, L. Kalkstein, C. Liu, A. Nickson, D. Pearlmutter, D. Sailor, and J. Voogt, "Climate and More Sustainable Cities: Climate Information for Improved Planning and Management of Cities (Producers/Capabilities Perspective)," *Procedia Environmental Sciences*, vol. 1, pp. 247–274, 2010.

[10] M. C. Rodríguez, L. Dupont-Courtade, and W. Oueslati, "Air Pollution and Urban Structure Linkages: Evidence from European Cities," *Renewable and Sustainable Energy Reviews*, vol. 53, pp. 1–9, 2015.

[11] F. Sensfuß, M. Ragwitz, and M. Genoese, "The Merit-Order Effect: A Detailed Analysis of the Price Effect of Renewable Electricity Generation on Spot Market Prices in Germany," *Energy Policy*, vol. 36, no. 8, pp. 3086–3094, 2008.

[12] J. C. Ketterer, "The Impact of Wind Power Generation on the Electricity Price in Germany," *Energy Economics*, vol. 44, pp. 270–280, 2014.

[13] L. Hirth, "The Market Value of Variable Renewables," *Energy Economics*, vol. 38, pp. 218–236, 2013.

[14] J. Cludius, H. Hermann, F. C. Matthes, and V. Graichen, "The Merit Order Effect of Wind and Photovoltaic Electricity Generation in Germany 2008-2016: Estimation and Distributional Implications," *Energy Economics*, vol. 44, pp. 302–313, 2014.

[15] S. Wichmann, "Die Energiewende in Deutschland," Bundesministerium für Wirtschaft und Technologie (BMWi), Tech. Rep., 2012.

[16] S. You, "Developing Virtual Power Plant for Optimized Distributed Energy Resources Operation and Integration," PhD thesis, Technical University of Denmark, 2010.

[17] S. Sučić, T. Dragičević, T. Capuder, and M. Delimar, "Economic Dispatch of Virtual Power Plants in an Event-driven Service-oriented Framework using Standards-based Communications," *Electric Power Systems Research*, vol. 81, no. 12, pp. 2108–2119, 2011.

[18] S. Skarvelis-Kazakos, "Emissions of Aggregated Micro-Generators," PhD thesis, Cardiff University, 2011.

[19] D. Pudjianto, C. Ramsay, and G. Strbac, "Microgrids and Virtual Power Plants: Concepts to Support the Integration of Distributed Energy Resources," *Proceedings of the Institution of Mechanical Engineers, Part A: Jour-*

nal of Power and Energy, vol. 222, no. 7, pp. 731–741, 2008.

[20] Bundesministerium für Umwelt, Naturschutz und Reaktorsicherheit (BMUB), "Kraftwerksliste von 1990 (bundesweit; alle Netz- und Umspannebenen)," 2013.

[21] Bundesnetzagentur, "Kraftwerksliste der Bundesnetzagentur - 2014 (bundesweit; alle Netz- und Umspannebenen)," 2014.

[22] Deutsche Gesellschaft für Solarenergie e.V (DGS), "EEG Anlagenregister 2014," 2014. [Online]. Available: http://www.energymap.info/

[23] Bundesministerium für Wirtschaft und Energie (BMWi), "Stromerzeugungskapazitäten, Bruttostromerzeugung und Bruttostromverbrauch," 2014.

[24] Deutscher Bundestag (DBT), "Die Beschlüsse des Bundestages am 30. Juni und 1. Juli 2011, Bundesregierung," 2014.

[25] O-NEP, "Offshore-Netzentwicklungsplan 2013," 50Hertz Transmission GmbH; Amprion GmbH; TenneT TSO GmbH; TransnetBW GmbH, Tech. Rep., 2013.

[26] J. Homann and A. Mundt, "Monitoringbericht Elektrizitäts- und Gasmarkt 2014," Bundesnetzagentur and Bundeskartellamt, Tech. Rep., 2014.

[27] M. Prabavathi and R. Gnanadass, "Energy Bidding Strategies for Restructured Electricity Market ," *International Journal of Electrical Power & Energy Systems* , vol. 64, pp. 956 – 966, 2015.

[28] K. De Vos, "Negative Wholesale Electricity Prices in the German, French and Belgian Day-Ahead, Intra-Day and Real-time Markets," *The Electricity Journal*, vol. 28, no. 4, pp. 36 – 50, 2015.

[29] M. Alcázar-Ortega, C. Calpe, T. Theisen, and J. F. Carbonell-Carretero, "Methodology for the Identification, Evaluation and Prioritization of Market Handicaps which Prevent the Implementation of Demand Response: Application to European Electricity Markets ," *Energy Policy*, vol. 86, pp. 529 – 543, 2015.

[30] S. Wissel, S. Rath-Nagel, M. Blesl, U. Fahl, and A. Voß, "Stromerzeugungskosten im Vergleich," Universität Stuttgart - Institut für Energiewirtschaft und Rationelle Energieanwendung, Tech. Rep., 2008.

[31] J. Nitsch, T. Pregger, T. Naegler, D. Heide, D. L. de Tena, F. Trieb, Y. Scholz, K. Nienhaus, N. Gerhardt, M. Sterner, T. Trost, A. von Oehsen, R. Schwinn, C. Pape, H. Hahn, M. Wickert, and B. Wenzel, "Langfristszenarien und Strate-

gien für den Ausbau der erneuerbaren Energien in Deutschland bei Berücksichtigung der Entwicklung in Europa und Global," Deutsches Zentrum für Luft- und Raumfahrt (DLR),Fraunhofer Institut für Windenergie und Energiesystemtechnik (IWES), Ingenieurbüro für neue Energien (IFNE), Tech. Rep., 2012.

[32] C. Kunz, "Die Auslastung von Kraftwerken im Zuge der Energiewende," Agentur für Erneuerbare Energien, Tech. Rep., 2013.

[33] Bundesministerium für Wirtschaft und Technologie (BMWi), "The Energy of the Future," Federal Ministry for Economic Affairs and Energy (BMWi), Tech. Rep., 2014.

[34] A. Molderink and V. Bakker, "Management and Control of Domestic Smart Grid Technology," *IEEE Transactions on Smart Grid*, vol. 1, no. 2, pp. 109–119, 2010.

[35] N. Hatziargyriou, C. Schwaegerl, L. Tao, A. Dimeas, A. Tsikalakis, G. Kariniotakis, G. Korres, T. Degner, N. Soultanis, A. Engler, A. G. d. Muro, A. Oudalov, F. v. Overbeeke, J. M. Yarza, J. A. P. Lopes, A. Madureira, N. Gil, and F. Resende, *Microgrids - Architectures and Control*, 1st ed. John Wiley and Sons Ltd, 2014.

[36] K. Strunz, E. Abbasi, and D. N. Huu, "DC Microgrid for Wind and Solar Power Integration," *IEEE Journal of Emerging and Selected Topics in Power Electronics*, vol. 2, no. 1, pp. 115–126, 2014.

[37] T. G. Werner and R. Remberg, "Technical, Economical and Regulatory Aspects of Virtual Power Plants," in *IEEE Third International Conference on Electric Utility Deregulation and Restructuring and Power Technologies*, no. April, Nanjuing, China, 2008, pp. 2427–2433.

[38] L. Nikonowicz and J. Milewski, "Virtual Power Plants - General Review: Structure, Application and Optimization." *Journal of Power Technologies*, vol. 92, no. 3, pp. 135–149, 2012.

[39] M. Ferdowsi, I. G. Unda, E. Karfopoulos, P. Papadopoulos, S. Skarvelis-Kazakos, L. M. Cipcigan, A. F. Raab, A. Dimeas, E. Abbasi, and K. Strunz, "Controls and Electric Vehicle Aggregation for Virtual Power Plants," Mobile Energy Resources in Grids of Electricity (MERGE), Tech. Rep., 2010.

[40] IEEE Standards Coordinating Committee 21, "IEEE Guide for Smart Grid Interoperability of Energy Technology and Information Technology Operation

with the Electric Power System (EPS), End-Use Applications, and Loads," *IEEE Std 2030-2011*, pp. 1–126, 2011.

[41] S. Mohagheghi, J. Stoupis, and Z. Wang, "Communication Protocols and Networks for Power Systems-current Status and Future Trends," Tech. Rep., 2009.

[42] CEN-CENELEC-ETSI Smart Grid Coordination Group, "Smart Grid Coordination Group Smart Grid Reference Architecture," CEN-CENELEC-ETSI Smart Grid Coordination Group, Tech. Rep., 2012.

[43] M. Wenger, A. Zoitl, C. Sunder, and H. Steininger, "Transformation of IEC 61131-3 to IEC 61499 Based on a Model Driven Development Approach," in *7th IEEE International Conference on Industrial Informatics*, Cardiff, UK, 2009, pp. 715–720.

[44] X. Li, X. Liang, R. Lu, X. Shen, X. Lin, and H. Zhu, "Securing Smart Grid: Cyber Attacks, Countermeasures, and Challenges," *Communications Magazine, IEEE*, vol. 50, no. 8, pp. 38–45, 2012.

[45] D. Rawat and C. Bajracharya, "Cyber Security for Smart Grid Systems: Status, Challenges and Perspectives," in *SoutheastCon*, Ft. Lauderdale, USA, 2015, pp. 1–6.

[46] A. F. Raab, J. Keiser, R. Schmidt, P. Röger, J. Sigulla, N. El Sayed, J. Twele, C. Clemens, J. Sorge, N. Priess, P. Teske, M. Gronau, S. Albayrak, M. Lützenberger, F. Reetz, B. Wilfert, J. Krause, M. Werner, C. Wiezorek, A. Arancibia, F. Klein, and K. Strunz, *Smart Grid Architectures in Research and Laboratory Environments - Lessons Learned*, 1st ed. Berlin, Germany: Research Campus Mobility2Grid, author's edition, 2015.

[47] T. Küster, M. Lützenberger, and D. Freund, "An Evolutionary Optimisation for Electric Price Responsive Manufacturing," in *EUROSIS-ITI Proceedings of the 9th Industrial Simulation Conference*, S. Balsamo and A. Marin, Eds., Venice, Italy, 2011, pp. 97–104.

[48] T. Küster, M. Lützenberger, and D. Freund, "Distributed Optimization of Energy Costs in Manufacturing using Multi-Agent System Technology," in *IARIA Proceedings of the 2nd International Conference on Smart Grids, Green Communications and IT Energy-aware Technologies*, P. Lorenz and K. Nygard, Eds., Maho Beach, St. Maarten, 2012, pp. 53–59.

[49] D. Freund, A. F. Raab, T. Küster, S. Albayrak, and K. Strunz, "Agent-based Integration of an Electric Car Sharing Fleet into a Smart Distribution Feeder,"

in *IEEE PES Innovative Smart Grid Technologies Conference Europe*, Berlin, Germany, 2012, pp. 1–8.

[50] J. Blackman and T. Hissey, "Impact of Local and Wide Area Networks on SCADA and SCADA/EMS Systems," in *IEE Colloquium on Advanced SCADA and Energy Management Systems*, London, UK, 1990, pp. 8/1–8/15.

[51] T. Gönen, *Electric Power Distribution Engineering, Third Edition*, 3rd ed. CRC Press, 2014.

[52] S. You, C. Træholt, and B. Poulsen, "Generic Virtual Power Plants: Management of Distributed Energy Resources under Liberalized Electricity Market," in *IET 8th International Conference on Advances in Power System Control, Operation and Management (APSCOM)*, Hong Kong, China, 2009, pp. 63–63.

[53] L. M. de Menezes and M. A. Houllier, "Reassessing the Integration of European Electricity Markets: A Fractional Cointegration Analysis," *Energy Economics*, vol. 53, pp. 132 – 150, 2016, energy Markets.

[54] H. Pandžić, I. Kuzle, and T. Capuder, "Virtual Power Plant Mid-term Dispatch Optimization," *Applied Energy*, vol. 101, pp. 134–141, 2013.

[55] B. Fais, M. Blesl, U. Fahl, and A. Voß, "Comparing Different Support Schemes for Renewable Electricity in the Scope of an Energy Systems Analysis," *Journal on Applied Energy*, vol. 131, pp. 479–489, 2014.

[56] S. Wassermann, M. Reeg, and K. Nienhaus, "Current Challenges of Germany's Energy Transition Project and Competing Strategies of Challengers and Incumbents: The Case of Direct Marketing of Electricity from Renewable Energy Sources," *Journal on Energy Policy*, vol. 76, pp. 66–75, 2015.

[57] L. M. Ausubel and P. Cramton, "Virtual Power Plant Auctions," *Utilities Policy*, vol. 18, no. 4, pp. 201–208, 2010.

[58] L. Hirth and I. Ziegenhagen, "Control Power and Variable Renewables," Potsdam-Institute for Climate Impact Research, Vattenfall GmbH, Tech. Rep., 2013.

[59] M. P. Tooraj Jamasb, "Electricity Market Reform in the European Union: Review of Progress toward Liberalization and Integration," *The Energy Journal*, vol. 26, pp. 11–41, 2005.

[60] G. Morales-Espana, A. Ramos, and J. Garcia-Gonzalez, "An MIP Formulation for Joint Market-Clearing of Energy and Reserves Based on Ramp Scheduling,"

IEEE Transactions on Power Systems, vol. 29, no. 1, pp. 476–488, 2014.

[61] H. P. Chao and R. Wilson, "Multi-dimensional Procurement Auctions for Power Reserves: Robust Incentive-Compatible Scoring and Settlement Rules," pp. 161–183, 2002.

[62] J. Riesz, J. Gilmore, and M. Hindsberger, *Market Design for the Integration of Variable Generation*, 1st ed., F. P. Sioshansi, Ed. Boston, USA: Academic Press, 2013.

[63] M. D. Galus, "Agent-based Modeling and Simulation of Large Scale Electric Mobility in Power Systems," PhD thesis, ETH Zurich, Zürich, Switzerland, 2012.

[64] F. Ueckerdt, R. Brecha, G. Luderer, P. Sullivan, E. Schmid, N. Bauer, D. Böttger, and R. Pietzcker, "Representing power sector variability and the integration of variable renewables in long-term energy-economy models using residual load duration curves ," *Energy*, vol. 90, Part 2, pp. 1799 – 1814, 2015.

[65] M. Shahidehpour, H. Yamin, and Z. Li, "Security Constrained Unit Commitment," in *Market Operations in Electric Power Systems:Forecasting, Scheduling, and Risk Management*. Wiley-IEEE Press, 2002, pp. 275–310.

[66] H. Louie and K. Strunz, "Hierarchical Multiobjective Optimization for Independent System Operators (ISOS) in Electricity Markets," *IEEE Transactions on Power Systems*, vol. 21, no. 4, pp. 1583–1591, 2006.

[67] L. F. Ochoa, A. Padilha-Feltrin, and G. P. Harrison, "Evaluating Distributed Time-Varying Generation Through a Multiobjective Index," *IEEE Transactions on Power Delivery*, vol. 23, no. 2, pp. 1132–1138, 2008.

[68] L. Ochoa, C. Dent, and G. Harrison, "Distribution network capacity assessment: Variable dg and active networks," *IEEE Transactions on Power Systems*, vol. 25, no. 1, pp. 87–95, 2010.

[69] P. Denholm and M. Hand, "Grid Flexibility and Storage Required to Achieve Very High Penetration of Variable Renewable Electricity," *Energy Policy*, vol. 39, no. 3, pp. 1817 – 1830, 2011.

[70] S. You, C. Træholt, and B. Poulsen, "A Market-based Virtual Power Plant," in *IEEE International Conference on Clean Electrical Power*, Capri, Italy, 2009, pp. 460–465.

[71] P. Asmus, "Microgrids, Virtual Power Plants and our Distributed Energy Fu-

ture," *The Electricity Journal*, vol. 23, no. 10, pp. 72–82, 2010.

[72] B. Saravanan, S. Das, S. Sikri, and D. P. Kothari, "A Solution to the Unit Commitment Problem - A Review," *Frontiers in Energy*, vol. 7, no. 2, pp. 223–236, 2013.

[73] L. Grigsby, *Power System Stability and Control*, 3rd ed., ser. The Electric Power Engineering Handbook. CRC Press, 2012, no. Bd. 5.

[74] H. Kanchev, F. Colas, V. Lazarov, and B. Francois, "Emission Reduction and Economical Optimization of an Urban Microgrid Operation Including Dispatched PV-Based Active Generators," *IEEE Transactions on Sustainable Energy*, vol. 5, no. 4, pp. 1397–1405, 2014.

[75] A. L. Dimeas and N. D. Hatziargyriou, "Agent Based Control of Virtual Power Plants," in *IEEE International Conference on Intelligent Systems Applications*, Niigata, Japan, 2007, pp. 1–6.

[76] M. Shafie-khah, M. Parsa Moghaddam, M. K. Sheikh-El-Eslami, and M. Rahmani-Andebili, "Modeling of Interactions between Market Regulations and Behavior of Plug-in Electric Vehicle Aggregators in a Virtual Power Market Environment," *Energy*, vol. 40, no. 1, pp. 139–150, 2012.

[77] M. A. Abido, "Environmental/Economic Power Dispatch Using Multiobjective Evolutionary Algorithms," *IEEE Transactions on Power Systems*, vol. 18, no. 4, pp. 1529–1537, 2003.

[78] F. J. Heredia, M. J. Rider, and C. Corchero, "Optimal Bidding Strategies for Thermal and Generic Programming Units in the Day-Ahead Electricity Market," *IEEE Transactions on Power Systems*, vol. 25, no. 3, pp. 1504–1518, 2010.

[79] J. Sun, V. Palade, X.-J. Wu, W. Fang, and Z. Wang, "Solving the Power Economic Dispatch Problem with Generator Constraints by Random Drift Particle Swarm Optimization," *IEEE Transactions on Industrial Informatics*, vol. 10, no. 1, pp. 222–232, 2014.

[80] P. Srikantha and D. Kundur, "Distributed Optimization of Dispatch in Sustainable Generation Systems via Dual Decomposition," *IEEE Transactions on Smart Grid*, vol. 6, no. 5, pp. 2501–2509, 2015.

[81] Y. Wang, X. Ai, Z. Tan, L. Yan, and S. Liu, "Interactive Dispatch Modes and Bidding Strategy of Multiple Virtual Power Plants Based on Demand Response and Game Theory," *IEEE Transactions on Smart Grid*, vol. 7, no. 1,

pp. 510–519, 2016.

[82] E. Mashhour and S. M. Moghaddas-Tafreshi, "Bidding Strategy of Virtual Power Plant for Participating in Energy and Spinning Reserve Markets - Part I: Problem Formulation," *IEEE Transactions on Power Systems*, vol. 26, no. 2, pp. 949–956, 2011.

[83] E. Mashhour and S. M. Moghaddas-Tafreshi, "Bidding Strategy of Virtual Power Plant for Participating in Energy and Spinning Reserve Markets - Part II: Numerical Analysis," *IEEE Transactions on Power Systems*, vol. 26, no. 2, pp. 957–964, 2011.

[84] D. Koraki and K. Strunz, "Wind and Solar Power Integration in Electricity Markets and Distribution Networks Through Service-centric Virtual Power Plants," *IEEE Transactions on Power Systems*, vol. PP, no. 99, pp. 1–1, 2017.

[85] A. F. Raab, M. Ferdowsi, E. Karfopoulos, I. G. Unda, S. Skarvelis-Kazakos, P. Papadopoulos, E. Abbasi, L. M. Cipcigan, N. Jenkins, N. Hatziargyriou, and K. Strunz, "Virtual Power Plant Control Concepts with Electric Vehicles," in *IEEE 16th International Conference on Intelligent System Applications to Power Systems*, Hersonissos, Greece, 2011, pp. 1–6.

[86] D. S. Callaway and I. a. Hiskens, "Achieving Controllability of Electric Loads," *Proceedings of the IEEE*, vol. 99, no. 1, pp. 184–199, 2011.

[87] F. Guo, C. Wen, J. Mao, and Y.-D. Song, "Distributed Secondary Voltage and Frequency Restoration Control of Droop-Controlled Inverter-based Microgrids," *IEEE Transactions on Industrial Electronics*, vol. 62, no. 7, pp. 4355–4364, 2015.

[88] M. Hossain, H. Pota, M. Mahmud, and M. Aldeen, "Robust Control for Power Sharing in Microgrids with Low-Inertia Wind and PV Generators," *IEEE Transactions on Sustainable Energy*, vol. 6, no. 3, pp. 1067–1077, 2015.

[89] T. L. Van, T. H. Nguyen, and D.-C. Lee, "Advanced Pitch Angle Control Based on Fuzzy Logic for Variable-Speed Wind Turbine Systems," *IEEE Transactions on Energy Conversion*, vol. 30, no. 2, pp. 578–587, 2015.

[90] S. Kim and F.-S. Kang, "Multifunctional Onboard Battery Charger for Plug-in Electric Vehicles," *IEEE Transactions on Industrial Electronics*, vol. 62, no. 6, pp. 3460–3472, 2015.

[91] A. Wood, B. Wollenberg, and G. Sheblé, *Power Generation, Operation, and Control*, 3rd ed. Hoboken, USA: John Wiley and Sons, 2014.

[92] M. Peik-Herfeh, H. Seifi, and M. K. Sheikh-El-Eslami, "Decision Making of a Virtual Power Plant under Uncertainties for Bidding in a Day-ahead Market using Point Estimate Method," *International Journal of Electrical Power & Energy Systems*, vol. 44, no. 1, pp. 88–98, 2013.

[93] H. Pandžić, J. M. Morales, A. J. Conejo, and I. Kuzle, "Offering Model for a Virtual Power Plant Based on Stochastic Programming," *Applied Energy*, vol. 105, pp. 282–292, 2013.

[94] S. Salam, "Unit Commitment Solution Methods," *Engineering and Technology*, vol. 26, no. December, pp. 600–605, 2007.

[95] A. Wood, B. Wollenberg, and G. Sheblé, *Power Generation, Operation, and Control*, 3rd ed. Minnesota, USA: Wiley, 2013.

[96] M. Giuntoli and D. Poli, "Optimized Thermal and Electrical Scheduling of a Large Scale Virtual Power Plant in the Presence of Energy Storages," *IEEE Transactions on Smart Grid*, vol. 4, no. 2, pp. 942–955, 2013.

[97] H. Holttinen, P. Meibom, A. Orths, F. v. Hulle, B. Lange, M. O'Malley, J. Pierik, B. Ummels, J. O. Tande, A. Estanqueiro, M. Matos, E. Gomez, L. Söder, G. Strbac, A. Shakoor, J. Ricardo, J. C. Smith, M. Milligan, and E. Ela, "Design and Operation of Power Systems with Large Amounts of Wind Power," International Energy Agency (IEA), Tech. Rep., 2009.

[98] DENA, "DENA-Netzstudie II - Integration Erneuerbarer Energien in die Deutsche Stromversorgung im Zeitraum 2015-2020 mit Ausblick 2025," Deutsche Energie-Agentur (DENA), Tech. Rep., 2010.

[99] G. Giebel, R. Brownsword, G. Kariniotakis, M. Denhard, and C. Draxl, "The State-Of-The-Art in Short-Term Prediction of Wind Power," Technical University of Denmark, Tech. Rep., 2011.

[100] K. Rohrig, K. Janssen, S. Faulstich, B. Hahn, J. Hirsch, M. Neuschäfer, S. Pfaffel, A. Sack, L. Schuldt, E. Stark, and M. Zieße, "Windenergie Report 2014," Fraunhofer IWES, Tech. Rep., 2015.

[101] Ü. Cali, "Grid and Market Integration of Large-Scale Wind Farms using Advanced Wind Power Forecasting: Technical and Energy Economic Aspects," Ph.D. dissertation, Universität Kassel, 2011.

[102] B. Lange, K. Rohrig, J. Dobschinksi, A. Wessel, Y.-M. Saint-Drenan, and M. Felder, "Prognosen der zeitlich-räumlichen Variabilität von Erneuerbaren," pp. 93–101, 2011.

[103] A. Lau and P. McSharry, "Approaches for Multi-Step Density Forecasts With Application to Aggregated Wind Power," *The Annals of Applied Statistics*, vol. 4, no. 3, pp. 1311–1341, 2010.

[104] B.-M. Hodge and M. Milligan, "Wind Power Forecasting Error Distributions Over Multiple Timescales," in *2011 IEEE Power and Energy Society General Meeting*, 2011, pp. 1–8.

[105] S. Pelland, J. Remund, J. Kleissl, T. Oozeki, and K. De Brabandere, "Photovoltaic and Solar Forecasting: State of the Art," International Energy Agency (IEA), Tech. Rep. October, 2013.

[106] B. Wolff, J. Kühnert, E. Lorenz, O. Kramer, and D. Heinemann, "Comparing Support Vector Regression for PV Power Forecasting to a Physical Modeling Approach Using Measurement, Numerical Weather Prediction, and Cloud Motion Data," *Solar Energy*, vol. 135, pp. 197–208, 2016.

[107] J. Linssen, S. Bickert, and W. Hennings, *Netzintegration von Fahrzeugen mit elektrifizierten Antriebssystemen in bestehende und zukünftige Energieversorgungsstrukturen-Advances in Systems.* Jülich, Germany: Forschungszentrum Jülich GmbH, 2012.

[108] A. Kunith, R. Mendelevitch, A. Kuschmierz, and D. Göhlich, "Optimization of Fast Charging Infrastructure for Electric Bus Transportation - Electrification of a City Bus Network," in *IEEE 16th International Conference on Intelligent System Applications to Power Systems*, Montréal, Canada, 2016.

[109] F. Baouche, R. Billot, R. Trigui, and N. E. E. Faouzi, "Efficient Allocation of Electric Vehicles Charging Stations: Optimization Model and Application to a Dense Urban Network," *IEEE Intelligent Transportation Systems Magazine*, vol. 6, no. 3, pp. 33–43, 2014.

[110] A. Kunith, D. Göhlich, and R. Mendelevitch, "Planning and Optimization of a Fast Charging Infrastructure for Electric Urban Bus Systems," in *ICTTE*, Belgrade, Serbia, 2014.

[111] N. Hatziargyriou, J. A. Peças Lopes, K. Strunz, A. F. Raab, T. G. San Román, A. Gonzalez Bordagaray, E. Karfopoulos, A. Walsh, K. Kanellopoulos, C. Sanchez Tejerina, B. Díaz-Guerra Calderón, N. Hartmann, I. Momber, and M. Rivier, "Final Recommendations," Mobile Energy Resources In Grids Of Electricity (MERGE), Tech. Rep., 2012.

[112] W. Kempton and J. Tomić, "Vehicle-to-Grid Power Fundamentals: Calculat-

ing Capacity and Net Revenue," *Journal of Power Sources*, vol. 144, no. 1, pp. 268–279, 2005.

[113] L. Pieltain Fernández, T. Román, R. Cossent, C. Domingo, and P. Frias, "Assessment of the Impact of Plug-in Electric Vehicles on Distribution Networks," *IEEE Transactions on Power Systems*, vol. 26, no. 1, pp. 206–213, 2011.

[114] A. F. Raab, M. Ellingsen, and A. Walsh, "Learning from Electric Vehicle Field Tests," Mobile Energy Resources in Grids of Electricity (MERGE), Tech. Rep., 2011.

[115] C. Shao, X. Wang, X. Wang, C. Du, and B. Wang, "Hierarchical Charge Control of Large Populations of EVs," *IEEE Transactions on Smart Grid*, vol. PP, no. 99, pp. 1–1, 2015.

[116] K. Mets, R. D'hulst, and C. Develder, "Comparison of Intelligent Charging Algorithms for Electric Vehicles to Reduce Peak Load and Demand Variability in a Distribution Grid," *Journal of Communications and Networks*, vol. 14, no. 6, pp. 672–681, 2012.

[117] J. Zheng, X. Wang, K. Men, C. Zhu, and S. Zhu, "Aggregation Model-based Optimization for Electric Vehicle Charging Strategy," *IEEE Transactions on Smart Grid*, vol. 4, pp. 1058–1066, 2013.

[118] C. Shao, X. Wang, X. Wang, C. Du, and B. Wang, "Hierarchical Charge Control of Large Populations of EVs," *IEEE Transactions on Smart Grid*, vol. 7, no. 2, pp. 1147–1155, 2016.

[119] G. H. Mohimani, F. Ashtiani, A. Javanmard, and M. Hamdi, "Mobility Modeling, Spatial Traffic Distribution, and Probability of Connectivity for Sparse and Dense Vehicular ad hoc Networks," *IEEE Transactions on Vehicular Technology*, vol. 58, no. 4, pp. 1998–2007, 2009.

[120] C.-H. Ou, H. Liang, and W. Zhuang, "Investigating Wireless Charging and Mobility of Electric Vehicles on Electricity Market," *IEEE Transactions on Industrial Electronics*, vol. 62, no. 5, pp. 3123–3133, 2015.

[121] S. Shahidinejad, S. Filizadeh, and E. Bibeau, "Profile of Charging Load on the Grid Due to Plug-in Vehicles," *Smart Grid, IEEE Transactions on*, vol. 3, no. 1, pp. 135–141, 2012.

[122] S. Vagropoulos and A. Bakirtzis, "Optimal Bidding Strategy for Electric Vehicle Aggregators in Electricity Markets," *IEEE Transactions on Power Systems*, vol. 28, no. 4, pp. 4031–4041, 2013.

[123] I. Momber, A. Siddiqui, T. Gomez San Roman, and L. Soder, "Risk Averse Scheduling by a PEV Aggregator Under Uncertainty," *IEEE Transactions on Power Systems*, vol. 30, no. 2, pp. 882–891, 2015.

[124] T. Sousa, H. Morais, Z. Vale, P. Faria, and J. Soares, "Intelligent Energy Resource Management Considering Vehicle-to-Grid: A Simulated Annealing Approach," *IEEE Transactions on Smart Grid*, vol. 3, no. 1, pp. 535–542, 2012.

[125] R. J. Bessa and M. A. Matos, "Economic and Technical Management of an Aggregation Agent for Electric Vehicles: A Literature Survey," *European Transactions on Electrical Power*, vol. 22, no. 3, pp. 334–350, 2012.

[126] R. Bessa and M. Matos, "Global against Divided Optimization for the Participation of an EV Aggregator in the Day-Ahead Electricity Market. Part II: Numerical Analysis," *Journal on Electric Power Systems Research*, vol. 95, pp. 319–329, 2013.

[127] M. Ortega-Vazquez, F. Bouffard, and V. Silva, "Electric Vehicle Aggregator/System Operator Coordination for Charging Scheduling and Services Procurement," *IEEE Transactions on Power Systems*, vol. 28, no. 2, pp. 1806–1815, 2013.

[128] R. Bosshard and J. W. Kolar, "Inductive Power Transfer for Electric Vehicle Charging: Technical Challenges and Tradeoffs," *IEEE Power Electronics Magazine*, vol. 3, no. 3, pp. 22–30, 2016.

[129] R. J. Bessa, M. A. Matos, F. J. Soares, and J. A. P. Lopes, "Optimized Bidding of a EV Aggregation Agent in the Electricity Market," *IEEE Transactions on Smart Grid*, vol. 3, no. 1, pp. 443–452, 2012.

[130] R. J. Bessa and M. A. Matos, "Optimization Models for an EV Aggregator Selling Secondary Reserve in the Electricity Market," *Journal on Electric Power Systems Research*, vol. 106, pp. 36–50, 2014.

[131] X. Luo, S. Xia, and K. W. Chan, "A Decentralized Charging Control Strategy for Plug-In Electric Vehicles to Mitigate Wind Farm Intermittency and Enhance Frequency Regulation," *Journal of Power Sources*, vol. 248, pp. 604–614, 2014.

[132] S. Bending, M. Ferdowsi, S. Channon, and K. Strunz, "Specifications for EV-Grid Interfacing, Communication and Smart Metering Technologies, Including Traffic Patterns and Human Behaviour Descriptions," Mobile Energy Re-

sources for Grids of Electricity (MERGE), Tech. Rep., 2010.

[133] S. Göhlich, A. Kunith, and T. Ly, "Technology Assessment of an Electric Urban Bus System for Berlin." Southhampton, England: WIT Press, 2014.

[134] J. A. Peças Lopes, F. J. Soares, and P. M. R. Almeida, "Integration of Electric Vehicles in the Electric Power System," *Proceedings of the IEEE*, vol. 99, no. 1, pp. 168–183, 2011.

[135] Q. Gong, Y. Li, and Z. R. Peng, "Trip-Based Optimal Power Management of Plug-in Hybrid Electric Vehicles," *IEEE Transactions on Vehicular Technology*, vol. 57, no. 6, pp. 3393–3401, 2008.

[136] Z. Miao, L. Xu, V. R. Disfani, and L. Fan, "An SOC-Based Battery Management System for Microgrids," *IEEE Transactions on Smart Grid*, vol. 5, no. 2, pp. 966–973, 2014.

[137] K. Mamadou, E. Lemaire, A. Delaille, D. Riu, S. E. Hing, and Y. Bultel, "Definition of a State-of-Energy Indicator (SoE) for Electrochemical Storage Devices: Application for Energetic Availability Forecasting," *Journal of the Electrochemical Society*, vol. 159, no. 8, pp. A1298–A1307, 2012.

[138] C. Guenther, B. Schott, W. Hennings, P. Waldowski, and M. a. Danzer, "Model-based Investigation of Electric Vehicle Battery Aging by Means of Vehicle-to-Grid Scenario Simulations," *Journal of Power Sources*, vol. 239, pp. 604–610, 2013.

[139] W. Su, H. Rahimi-Eichi, W. Zeng, and M.-Y. Chow, "A Survey on the Electrification of Transportation in a Smart Grid Environment," *IEEE Transactions of Industrial Informatics*, vol. 8, no. 1, p. 10, 2012.

[140] M. Hayn, V. Bertsch, and W. Fichtner, "Electricity Load Profiles in Europe: The Importance of Household Segmentation," *Energy Research & Social Science*, vol. 3, pp. 30 – 45, 2014.

[141] B. Ketterer, U. Karl, D. Möst, and S. Ulrich, "Lithium-Ion Batteries: State of the Art and Application Potential in Hybrid-, Plug-In Hybrid- and Electric Vehicles," Karlsruhe Institute of Technology (KIT), Karlsruhe, Tech. Rep., 2009.

[142] R. Follmer, B. Lenz, B. Jesske, and S. Quandt, "Mobilität in Deutschland 2008 Tabellenband," Deutsches Zentrum für Luft- und Raumfahrt e.V. Institut für Verkehrsforschung, Berlin, Tech. Rep., 2008.

[143] P. Y. Kong and G. K. Karagiannidis, "Charging Schemes for Plug-In Hybrid Electric Vehicles in Smart Grid: A Survey," *IEEE Access*, vol. 4, pp. 6846–6875, 2016.

[144] O. J. Ibarra-Rojas, F. Delgado, R. Giesen, and J. C. Muñoz, "Planning, Operation, and Control of Bus Transport Systems: A Literature Review," *Transportation Research Part B: Methodological*, vol. 77, pp. 38–75, 2015.

[145] M. Hajesch, D. Misitano, G. Schmidt, M. Schwalm, P. Krams, and M. Meurer, "Klimaentlastung durch den Einsatz erneuerbarer Energien im Zusammenwirken mit emissionsfreien Elektrofahrzeugen," München, Tech. Rep., 2011.

[146] S. Bunte and N. Kliewer, "An Overview on Vehicle Scheduling Models," *Public Transport*, vol. 1, no. 4, pp. 299–317, 2009.

[147] I. Steinzen, V. Gintner, L. Suhl, and N. Kliewer, "A Time-Space Network Approach for the Integrated Vehicle- and Crew-Scheduling Problem with Multiple Depots," *Transportation Science*, vol. 44, no. 3, pp. 367–382, 2010.

[148] N. Brinkman, M. Wang, T. Weber, and T. Darlington, "Well-to-Wheels Analysis of Advanced Fuel/Vehicle Systems - A North American Study of Energy Use, Greenhouse Gas Emissions, and Criteria Pollutant Emissions," General Motors Corporation, Argonne National Laboratory, Air Improvement Resource, Inc., Tech. Rep., 2005.

[149] A. Tsolakis, A. Megaritis, M. Wyszynski, and T. K., "Engine Performance and Emissions of a Diesel Engine Operating on Diesel-RME (Rapeseed Methyl Ester) Blends with EGR (Exhaust Gas Recirculation)," *Energy*, vol. 32, no. 11, pp. 2072 – 2080.

[150] A. Raskin and S. Shah, *The Emergence of Hybrid Vehicles - Ending Oil's Strangehold on Transportation and the Economy.* New York, USA: Alliance-Bernstein, 2006.

[151] J. O. Estima and A. J. M. Cardoso, "Efficiency Analysis of Drive Train Topologies Applied to Electric/Hybrid Vehicles," *IEEE Transactions on Vehicular Technology*, vol. 61, no. 3, pp. 1021–1031, 2012.

[152] A. A. Pesaran and M. Keyser, "Thermal Characteristics of Selected EV and HEV Batteries," *Annual Battery Conference: Advances and Applications*, 2001.

[153] E. Mahnke and M. J., "Renews Spezial - Strom speichern," Agentur für Erneuerbare Energien, Tech. Rep., 2012.

[154] J. Drobnik and P. Jain, "Electric and Hybrid Vehicle Power Electronics Efficiency, Testing and Reliability," in *2013 World Electric Vehicle Symposium and Exhibition (EVS27)*, 2013, pp. 1–12.

[155] A. Emadi, Y. J. Lee, and K. Rajashekara, "Power Electronics and Motor Drives in Electric, Hybrid Electric, and Plug-In Hybrid Electric Vehicles," *IEEE Transactions on Industrial Electronics*, vol. 55, no. 6, pp. 2237–2245, 2008.

[156] S. Torzynski, D. Göhlich, D. Hahn, and M. Bryl-Radziemska, "Demonstration of an Electric Bus Fleet Operated on Line 204 with Inductive Charging System in Berlin (EBus Berlin)," Institut für Elektrische Anlagen und Energiewirtschaft, Tech. Rep., 2016.

[157] M. Ye, Z.-F. Bai, and B.-G. Cao, "Energy Recovery for Battery Electric Vehicles," *Proceedings of the Institution of Mechanical Engineers, Part D: Journal of Automobile Engineering*, vol. 222, no. 10, pp. 1827–1839, 2008.

[158] ZeEUS, "eBus Report: An overview of electric buses in Europe," International Association of Public Transport, Tech. Rep., 2016.

[159] G. E. Asimakopoulou, A. L. Dimeas, and N. D. Hatziargyriou, "Leader-Follower Strategies for Energy Management of Multi-Microgrids," *IEEE Transactions on Smart Grid*, vol. 4, no. 4, pp. 1909–1916, 2013.

[160] S. Dempe, V. Kalashnikov, G. A. Pérez-Valdés, and N. Kalashnykova, *Bilevel Programming Problems: Theory, Algorithms and Applications to Energy Networks*. Berlin, Heidelberg: Springer Berlin Heidelberg, 2015, pp. 1–20.

[161] Y. G. Rebours, D. S. Kirschen, M. Trotignon, and S. Rossignol, "A Survey of Frequency and Voltage Control Ancillary Services-Part I: Technical Features," *IEEE Transactions on Power Systems*, vol. 22, no. 1, pp. 350–357, 2007.

[162] C. Epe, J. Fuhrberg-Baumann, U. Herbst, M. Mermann, H. D. Kreye, U. Mahn, R. Mönnig, and U. Scherer, "DistributionCode 2007 - Regeln für den Zugang zu Verteilungsnetzen," Verband der Netzbetreiber, Tech. Rep., 2007.

[163] W. Bartels, N. Bruns, M. Elsner, U. Fährmann, C.-D. Gabel, A. Hettich, D. Lehmer, L. Stürmer, H. Vogt, and U. Wiedemann, "Technische Anschlussbedingungen für den Anschluss an das Mittelspannungsnetz," Bundesverband der Energie- und Wasserwirtschaft e.V. (BDEW), Tech. Rep., 2008.

[164] W. Bartels, F. Ehlers, K. Heidenreich, R. Hüttner, H. Kühn, T. Meyer,

T. Kumm, J.-M. Salzmann, H.-D. Schäfer, and K.-H. Weck, "Technische Richtlinie Erzeugungsanlagen am Mittelspannungsnetz," Bundesverband der Energie- und Wasserwirtschaft e.V. (BDEW), Tech. Rep., 2008.

[165] H. Berndt, M. Hermann, H. D. Kreye, R. Reinisch, U. Scherer, and J. Vanzetta, "TransmissionCode 2007 - Netz- und Systemregeln der deutschen Übertragungsnetzbetreiber," Verband der Netzbetreiber e.V., Tech. Rep., 2007.

[166] G. Joos, B. T. Ooi, D. McGillis, F. D. Galiana, and R. Marceau, "The Potential of Distributed Generation to Provide Ancillary Services," vol. 3, pp. 1762–1767 vol. 3, 2000.

[167] C. I. Chen and Y. C. Chen, "Intelligent Identification of Voltage Variation Events Based on IEEE Std 1159-2009 for SCADA of Distributed Energy System," *IEEE Transactions on Industrial Electronics*, vol. 62, no. 4, pp. 2604–2611, 2015.

[168] P. Moutis, P. S. Georgilakis, and N. D. Hatziargyriou, "Voltage Regulation Support Along a Distribution Line by a Virtual Power Plant Based on a Center of Mass Load Modeling," *IEEE Transactions on Smart Grid*, vol. PP, no. 99, pp. 1–1, 2016.

[169] D. Ranamuka, A. Agalgaonkar, and K. Muttaqi, "Online Voltage Control in Distribution Systems with Multiple Voltage Regulating Devices," *IEEE Transactions on Sustainable Energy*, vol. 5, no. 2, pp. 617–628, 2014.

[170] S. Toma, T. Senjyu, Y. Miyazato, A. Yona, K. Tanaka, and C. H. Kim, "Decentralized Voltage Control in Distribution System Using Neural Network," in *Power and Energy Conference, 2008. PECon 2008. IEEE 2nd International*, 2008, pp. 1557–1562.

[171] G. W. Kim and K. Lee, "Coordination Control of ULTC Transformer and STATCOM based on an Artificial Neural Network," *IEEE Transactions on Power Systems*, vol. 20, no. 2, pp. 580–586, 2005.

[172] F. A. Viawan, A. Sannino, and J. Daalder, "Voltage Control with On-load Tap Changers in Medium Voltage Feeders in Presence of Distributed Generation," *Electric Power Systems Research*, vol. 77, no. 10, pp. 1314–1322, 2007.

[173] T. Senjyu, Y. Miyazato, A. Yona, N. Urasaki, and T. Funabashi, "Optimal Distribution Voltage Control and Coordination with Distributed Generation," *IEEE Transactions on Power Delivery*, vol. 23, no. 2, pp. 1236–1242, 2008.

[174] A. Kulmala, S. Repo, and P. Jarventausta, "Coordinated Voltage Control in

Distribution Networks Including Several Distributed Energy Resources," *IEEE Transactions on Smart Grid*, vol. 5, no. 4, pp. 2010–2020, 2014.

[175] K. Muttaqi, A. Le, M. Negnevitsky, and G. Ledwich, "A Coordinated Voltage Control Approach for Coordination of OLTC, Voltage Regulator, and DG to Regulate Voltage in a Distribution Feeder," *IEEE Transactions on Industry Applications*, vol. 51, no. 2, pp. 1239–1248, 2015.

[176] M. El Moursi, H. Zeineldin, J. Kirtley, and K. Alobeidli, "A Dynamic Master/Slave Reactive Power-Management Scheme for Smart Grids with Distributed Generation," *IEEE Transactions on Power Delivery*, vol. 29, no. 3, pp. 1157–1167, 2014.

[177] M. Braun, "Technological Control Capabilities of DER to Provide Future Ancillary Services," *International Journal of Distributed Energy Resources*, vol. 3, no. 3, pp. 191–206, 2007.

[178] R.-H. Liang and C.-K. Cheng, "Dispatch of Main Transformer ULTC and Capacitors in a Distribution System," *IEEE Transactions on Power Delivery*, vol. 16, no. 4, pp. 625–630, 2001.

[179] Y. Liu, J. Bebic, B. Kroposki, J. de Bedout, and W. Ren, "Distribution System Voltage Performance Analysis for High-Penetration PV," in *Energy 2030 Conference*, Atlanta, USA, 2008, pp. 1–8.

[180] Q. Zhou and J. W. Bialek, "Generation Curtailment to Manage Voltage Constraints in Distribution Networks," *IET Generation, Transmission Distribution*, vol. 1, no. 3, pp. 492–498, 2007.

[181] X. Liu, A. Aichhorn, L. Liu, and H. Li, "Coordinated Control of Distributed Energy Storage System with Tap Changer Transformers for Voltage Rise Mitigation Under High Photovoltaic Penetration," *IEEE Transactions on Smart Grid*, vol. 3, no. 2, pp. 897–906, 2012.

[182] M. Juamperez, G. Yang, and S. B. KJÆR, "Voltage Regulation in LV Grids by Coordinated Volt-VAr Control Strategies," *Journal of Modern Power Systems and Clean Energy*, vol. 2, no. 4, pp. 319–328, 2014.

[183] H. Vu, P. Pruvot, C. Launay, and Y. Harmand, "An Improved Voltage Control on Large-Scale Power System," *IEEE Transactions on Power Systems*, vol. 11, no. 3, pp. 1295–1303, 1996.

[184] F. Bignucolo, R. Caldon, and V. Prandoni, "Radial MV Networks Voltage Regulation with Distribution Management System Coordinated Controller,"

Electric Power Systems Research, vol. 78, no. 4, pp. 634 – 645, 2008.

[185] J.-H. Choi and S.-I. Moon, "The Dead Band Control of LTC Transformer at Distribution Substation," *IEEE Transactions on Power Systems*, vol. 24, no. 1, pp. 319–326, 2009.

[186] M. S. Calovic, "Modeling and Analysis of Under-Load Tap-Changing Transformer Control Systems," *IEEE Transactions on Power Apparatus and Systems*, vol. PAS-103, no. 7, pp. 1909–1915, 1984.

[187] J. y. Park, S. r. Nam, and J. k. Park, "Control of a ULTC Considering the Dispatch Schedule of Capacitors in a Distribution System," *IEEE Transactions on Power Systems*, vol. 22, no. 2, pp. 755–761, 2007.

[188] F. A. Viawan and D. Karlsson, "Voltage and Reactive Power Control in Systems with Synchronous Machine-Based Distributed Generation," *IEEE Transactions on Power Delivery*, vol. 23, no. 2, pp. 1079–1087, 2008.

[189] R. Zimmerman, C. Murillo-Sánchez, and R. Thomas, "MATPOWER: Steady-State Operations, Planning, and Analysis Tools for Power Systems Research and Education," *IEEE Transactions on Power Systems*, vol. 26, no. 1, pp. 12–19, 2011.

[190] J. Faiz and B. Siahkolah, *Electronic Tap-Changer for Distribution Transforsmers*. Berlin, Germany: Springer, 2011.

[191] J. D. Hurley, L. N. Bize, and C. R. Mummert, "The Adverse Effects of Excitation System VAr and Power Factor Controllers," *IEEE Transactions on Energy Conversion*, vol. 14, no. 4, pp. 1636–1645, 1999.

[192] E. Demirok, P. C. González, K. H. B. Frederiksen, D. Sera, P. Rodriguez, and R. Teodorescu, "Local Reactive Power Control Methods for Overvoltage Prevention of Distributed Solar Inverters in Low-Voltage Grids," *IEEE Journal of Photovoltaics*, vol. 1, no. 2, pp. 174–182, 2011.

[193] T. Fawzy, D. Premm, B. Bletterie, and A. Goršek, "Active Contribution of PV Inverters to Voltage Control - from a Smart Grid Vision to Full-Scale Implementation," *e & i Elektrotechnik und Informationstechnik*, vol. 128, no. 4, pp. 110–115, 2011.

[194] P. N. Vovos, A. E. Kiprakis, A. R. Wallace, and G. P. Harrison, "Centralized and Distributed Voltage Control: Impact on Distributed Generation Penetration," *IEEE Transactions on Power Systems*, vol. 22, no. 1, pp. 476–483, 2007.

[195] A. Borghetti, M. Bosetti, S. Grillo, S. Massucco, C. A. Nucci, M. Paolone, and F. Silvestro, "Short-Term Scheduling and Control of Active Distribution Systems With High Penetration of Renewable Resources," *IEEE Systems Journal*, vol. 4, no. 3, pp. 313–322, 2010.

[196] K. Christakou, D. C. Tomozei, M. Bahramipanah, J. Y. L. Boudec, and M. Paolone, "Primary Voltage Control in Active Distribution Networks via Broadcast Signals: The Case of Distributed Storage," *IEEE Transactions on Smart Grid*, vol. 5, no. 5, pp. 2314–2325, 2014.

[197] K. Strunz, E. Abbasi, C. Abbey, C. Andrieu, U. Annakkage, S. Barsali, R. C. Campbell, R. Fletcher, F. Gao, T. Gaunt, A. Gole, N. Hatziargyriou, R. Iravani, G. Joos, H. Konishi, M. Kuschke, E. Lakervi, C.-C. Liu, J. Mahseredjian, F. Mosallat, D. Muthumuni, A. Orths, S. Papathanassiou, K. Rudion, Z. Styczynski, and S. C. Verma, "Benchmark Systems for Network Integration of Renewable and Distributed Energy Resources," CIGRE Task Force C6.04.02, Tech. Rep., 2014.

[198] M. Newborough and P. Augood, "Demand-Side Management Opportunities for the UK Domestic Sector," *IEE Proceedings - Generation, Transmission and Distribution*, vol. 146, no. 3, pp. 283–293, 1999.

[199] G. Wood and M. Newborough, "Dynamic Energy-Consumption Indicators for Domestic Appliances: Environment, Behaviour and Design," *Energy and Buildings*, vol. 35, no. 8, pp. 821 – 841, 2003.

[200] J. Fortmann, R. Pfeiffer, E. Haesen, F. van Hulle, F. Martin, H. Urdal, and S. Wachtel, "Fault-Ride-Through Requirements for Wind Power Plants in the ENTSO-E Network Code on Requirements for Generators," *IET Renewable Power Generation*, vol. 9, no. 1, pp. 18–24, 2015.

[201] G. Brauner, W. Glaunsinger, S. Bofinger, M. John, W. Magin, I. Pyc, S. Schüler, S. Schulz, U. Schwing, P. Seydel, and F. Steinke, "Erneuerbare Energie braucht flexible Kraftwerke - Szenarien bis 2020," VDE, Tech. Rep., 2012.

[202] F. Cziesla, E.-G. Hencke, A. Kather, D. Keller, and B. Rukes, "Fossil befeuerte Großkraftwerke in Deutschland - Stand, Tendenzen, Schlussfolgerungen," VDI, Tech. Rep., 2013.

[203] K.-D. Weßnigk, *Kraftwerkselektrotechnik*. Zittau, Germany: VDE Verlag, 1993.

[204] M. Hundt, R. Barth, N. Sun, H. Brand, and A. Voß, "Herausforderungen eines Elektizitätsversorgungssystems mit hohen Anteilen erneuerbarer Energien," Universität Stuttgart, Tech. Rep., 2010.

[205] A. Schröder, F. Kunz, J. Meiss, R. Mendelevitch, and C. von Hirschhausen, "Current and Prospective Costs of Electricity Generation until 2050," 2013.

[206] P. Götz, J. Henkel, T. Lenck, and K. Lenz, "Negative Strompreise: Ursachen und Wirkungen," Tech. Rep., 2014.

[207] K. Darrow, R. Tidball, J. Wang, and A. Hampson, "Catolog of CHP Technologies," U.S. Environmental Protection Agency, Tech. Rep., 2015.

[208] I. Pierre, F. Bauer, R. Blasko, N. Dahlback, M. Dumpelmann, K. Kainurinne, S. Luedge, P. Opdenacker, I. Pescador Chamorro, D. Romano, F. Schoonacker, and G. Weisrock, "Flexible generation: Backing up renewables," EURELECTRIC Renewables Action Plan, Tech. Rep., 2011.

[209] R. D. Corporation, "Assessment of Distributed Generation Technology Applications," Resourcen Dynamics Corporation, Tech. Rep., 2001.

[210] J. Conrad, C. Pellinger, and M. Hinterstocker, "Gutachten zur Rentabilität von Pumpspeicherkraftwerken," Forschungsstelle für Energiewirtschaft e.V., Tech. Rep., 2014.

[211] A. Meinzenbach, J. Haupt, P. Seidel, L. Schinke, T. Heß, and J. Werner, "Regionales Virtuelles Kraftwerk auf Basis der Mini- und Mikro-KWK Technologie," Technische Universität Dresden, Tech. Rep., 2015.

[212] C. Kost, J. Thomsen, T. Schlegl, S. Nold, and J. Mayer, "Studie - Stromgestehungskosten Erneuerbare Energien," Frauenhofer Institut für Solare Energiesysteme, Tech. Rep., 2012.

[213] F. Brachvogel, "Kraftwerksplanungen und aktuelle ökonomische Rahmenbedingungen für Kraftwerke in Deutschland," Bundesverband der Energie- und Wasserwirtschaft e.V. (BDEW), Tech. Rep. August, 2013.

[214] C. Kost, J. Mayer, J. Thomsen, N. Hartmann, C. Senkpiel, S. Philipps, S. Nold, S. Lude, and T. Schlegl, "Studie - Stromgestehungskosten Erneuerbare Energien," Frauenhofer Institut für Solare Energiesysteme, Tech. Rep., 2013.

[215] M. Kintner-Meyer, P. Balducci, C. Jin, T. Nguyen, M. Elizondo, V. Viswanatahn, X. Guo, and F. Tuffner, "Energy Storage for Power Sys-

tems Applications: A Regional Assessment for the Northwest Power Pool (NWPP)," Pacific Northwest National Laboratory, Tech. Rep. April, 2010.

[216] E. Fukushima, "Inside Cooperative Innovation: Development and Commercialization of Sodium-Sulfur Batteries for Power Storage," Tokyo, Japan, 2013.

[217] J. Brandhoff, C. Dürschner, A. Gutsch, C. Lichner, V. Quaschning, I. Röpcke, F. Schnorr, T. Tjaden, J. Weniger, O. Wollersheim, and M. Zerer, "Sind Sie bereit für die neue Energiewelt?" *pv magazine*, vol. 6, p. 83, 2015.

[218] D. Linden and T. Reddy, *Linden's Handbook of Batteries*, 4th ed. New York City, USA: McGraw-Hill Education, 2010.

[219] X. Liu, J. Wu, C. Zhang, and Z. Chen, "A Method for State of Energy Estimation of Lithium-Ion Batteries at Dynamic Currents and Temperatures," *Journal of Power Sources*, vol. 270, pp. 151 – 157, 2014.

[220] A. Thielmann, A. Sauer, M. Schnell, R. Isenmann, and M. Wietschel, "Technologie-Roadmap Stationäre Energiespeicher 2030," Fraunhofer-Institut für Systemund Innovationsforschung ISI, Tech. Rep., 2015.

[221] B. Nykvist and M. Nilsson, "Rapidly falling costs of battery packs for electric vehicles," Tech. Rep. 4, 2015.

[222] J. Weniger, J. Bergner, T. Tjaden, and V. Quaschning, "Dezentrale Solarstromspeicher für die Energiewende," HTW University of Applied Science, Tech. Rep., 2015.

[223] DENA, "DENA Grid Study II - Integration of Renewable Energy Sources in the German Power Supply System from 2015 - 2020 with an Outlook to 2025," German Energy Agency - Deutsche Energie-Agentur GmbH (DENA), Tech. Rep., 2011.

[224] M. Diagne, M. David, P. Lauret, J. Boland, and N. Schmutz, "Review of Solar Irradiance Forecasting Methods and a Proposition for Small-Scale Insular Grids," *Renewable and Sustainable Energy Reviews*, vol. 27, pp. 65–76, 2013.

[225] C. Monteiro, R. Bessa, V. Miranda, A. Botterud, J. Wang, and G. Conzelmann, "Wind Power Forecasting: State-of-the-Art 2009," Argonne National Laboratory, Tech. Rep., 2009.

[226] U. Focken, M. Lange, K. Mönnich, H.-P. Waldl, H. Beyer, and A. Luig, "Short-Term Prediction of the Aggregated Power Output of Wind Farms - A Statistical Analysis of the Reduction of the Prediction Error by Spatial Smoothing

Effects ," *Journal of Wind Engineering and Industrial Aerodynamics*, vol. 90, no. 3, pp. 231–246, 2002.

[227] E. Lorenz, J. Hurka, D. Heinemann, and H. G. Beyer, "Irradiance Forecasting for the Power Prediction of Grid-Connected Photovoltaic Systems," *IEEE Journal of Selected Topics in Applied Earth Observations and Remote Sensing*, vol. 2, no. 1, pp. 2–10, 2009.

[228] S. W. Smith, *The Scientist and Engineer's Guide to Digital Signal Processing*, 2nd ed. Kassel, Germany: California Technical Publishing, 1999.

[229] R. Perez, E. Lorenz, S. Pelland, M. Beauharnois, G. Van Knowe, K. Hemker, D. Heinemann, J. Remund, S. C. Müller, W. Traunmüller, G. Steinmauer, D. Pozo, J. A. Ruiz-Arias, V. Lara-Fanego, L. Ramirez-Santigosa, M. Gaston-Romero, and L. M. Pomares, "Comparison of Numerical Weather Prediction Solar Irradiance Forecasts in the US, Canada and Europe," *Solar Energy*, vol. 94, no. 6, pp. 305–326, 2013.

[230] M. V. Shcherbakov, A. Brebels, N. L. Shcherbakova, A. P. Tyokov, T. A. Janovsky, and V. A. Kamaev, "A Survey of Forecast Error Measures," no. Septemper, 2013.

[231] C. Reese, C. Buchhagen, and L. Hofmann, "Voltage Range as Control Input for OLTC-equipped Distribution Transformers," in *IEEE PES Transmission and Distribution Conference and Exposition (T D)*, Orlando, USA, 2012, pp. 1–6.

[232] C. Reese, C. Buchhagen, and L. Hofmann, "Enhanced Method for Voltage Range Controlled OLTC-equipped Distribution Transformers," in *IEEE Power and Energy Society General Meeting*, San Diego, USA, 2012, pp. 1–8.

[233] K. Alobeidli and M. El Moursi, "Novel Coordinated Secondary Voltage Control Strategy for Efficient Utilisation of Distributed Generations," *Renewable Power Generation, IET*, vol. 8, no. 5, pp. 569–579, 2014.

[234] J. Faiz and B. Siahkolah, "Differences between Conventional and Electronic Tap-Changers and Modifications of Controller," *IEEE Transactions on Power Delivery*, vol. 21, no. 3, pp. 1342–1349, 2006.

[235] P. Kundur, *Power System Stability And Control*, 1st ed., ser. EPRI power system engineering series. McGraw-Hill Education (India) Pvt Limited, 1994.

[236] A. J. Schwab, *Elektroenergiesysteme: Erzeugung, Transport, Übertragung und Verteilung elektrischer Energie*, 3rd ed. Springer-Verlag, 2012.

[237] M. Thomson, "Automatic Voltage Control Relays and Embedded Generation. I," *Power Engineering Journal*, vol. 14, no. 2, pp. 71–76, 2000.

[238] L. Heinhold and R. Stubbe, *Power Cables and Their Application*, 1st ed., ser. Power Cables and Their Application. Ann Arbor, USA: Siemens Aktiengesellschaft, 1993.

[239] T. Short, *Electric Power Distribution Handbook*, 2nd ed. CRC Press, 2014.

[240] W. Kersting, *Distribution System Modeling and Analysis*, 3rd ed. CRC Press, 2012.

[241] "The Authoritative Dictionary of IEEE Standards Terms, Seventh Edition," *IEEE Std 100-2000*, pp. 1–1362, 2000.

[242] B. Gao, G. K. Morison, and P. Kundur, "Voltage Stability Evaluation Using Modal Analysis," *IEEE Transactions on Power Systems*, vol. 7, no. 4, pp. 1529–1542, 1992.

[243] P. Anderson, A. Fouad, I. of Electrical, and E. Engineers, *Power System Control and Stability*, 2nd ed., ser. IEEE Press power engineering series. Ames, Iowa: Wiley-IEEE Press Home, 2003.

List of Figures

List of Tables

List of Symbols

Indexes:

fh	forecast horizon, e.g. da, id, rt	(h)
i, j, m, n	counter index	(-)
k	time step	(-)
k_{ini}	initial time step	(-)
k_{fin}	final time step	(-)

Sets:

H_{ts}	set of time steps k	(-)
H_{day}	set of n^{day} days	(-)
H_{time}	set of event-oriented timestamps e.g. $t^{\text{D},O}$ - departure time at origin	(-)
H_{res}	set of renewable technologies	(-)
H_{ces}	set of conventional technologies	(-)
H_{stor}	set of storage technologies	(-)
H_{typ}	set of unit types	(-)
H_{cl}	set of unit clusters	(-)
H_{gis}	set of locations L	(-)
H_{vl}	set of voltage levels	(-)
H_{cap}	set of installed capacities	(-)
H_{year}	set of years	(-)
H_{pev}	set of passenger electric vehicle models	(-)
H_{cev}	set of commercial electric vehicle models	(-)
H_{mstor}	set of electric vehicle models	(-)
H_{fleet}	index set containing one electric vehicle model	(-)
H_{ev}	disjoint set of H_{mstor} and H_{fleet}	(-)
H_{tariff}	set of charging tariffs	(-)
H_{prp}	set of driving purposes	(-)
$H_{\text{Q}^{\text{ctr}}}$	set of reactive power control modes	(-)
$H_{\text{T}^{\text{ctr}}}$	set of tap-changing transformer control modes	(-)
H_{bus}	index set of buses of network	(-)

$H_{\mathrm{ts}}^{\mathrm{T^{Q_m^{ctr}}}}$	set of time steps for move time of Q-control	(-)

Network related:

B'_{ph}	phase susceptance	(S/km)
C'	capacitive reactance, e.g. C'_{ph} - phase capacitive reactance	(S/km)
G'	line conductance, e.g. G'_{ph} - phase conductance	(S/km)
I	root mean square value of current e.g. I_1 - current of phase 1	(A)
R'	resistance, e.g. R'_{ph} - phase resistance	(Ω/km)
V	voltage magnitude, e.g. $V_{\mathrm{bus},i}$ - voltage of bus i	(V)
V_1,V_2	primary and secondary side voltage	(V)
$V_{2\mathrm{m}}$	voltage control signal e.g. $V_{2\mathrm{m}}^{\mathrm{sen}}$ - voltage control signal of the sensitive bus	(V)
V^{lb},V^{ub}	lower and upper voltage boundary magnitude e.g. $V^{\mathrm{lb,db}}$ - lower voltage boundary of dead band	(V)
X'	line reactance e.g. X'_{ph} - phase reactance	(Ω/km)
Y'	line admittance	(S/km)
Z'	line impedance	(Ω/km)

Energy related:

E_{d}, E_{g}	energy demand and generation e.g. E_{d}^{typ} - energy demand of $typ \in H_{\mathrm{typ}}$	(kWh)
$E_{\mathrm{d}}^{mstor,\mathrm{km}}$	energy demand of $mstor \in H_{\mathrm{mstor}}$	(kWh/km)
E_{r}	rated energy capacity e.g. E_{r}^{typ} - rated energy of $typ \in H_{\mathrm{typ}}$	(kWh)
$E^{\mathrm{CR}\pm}$	positive and negative control reserve energy e.g. $E_{\mathrm{BG},i}^{\mathrm{CR}+}$ - positive control reserve of balance group i	(kWh)
E^{em}	traded energy with energy market	(kWh)
$FLH_{year}^{typ,cnt}$	full load hours in certain year and country of $typ \in H_{\mathrm{typ}}$	(h)
P_{d}, P_{g}	power demand and generation e.g. P_{d}^{typ} - power demand of $typ \in H_{\mathrm{typ}}$	(kW)
P_{r}	rated power, e.g. P_{r}^{typ} - rated power of $typ \in H_{\mathrm{typ}}$	(kW)
$P^{\mathrm{ref},typ}$	reference power for $typ \in H_{\mathrm{typ}}$	(kW)
P^{em}	traded power with energy market	(kW)

$P^{\mathrm{CR}\pm}$	positive or negative control reserve power	(kW)
$P_{\mathrm{IM,BG}}$,$P_{\mathrm{EX,BG}}$	imported and exported power for balance group	(kW)
$\tilde{P}^{typ}_{\mathrm{d},fh}$, $\tilde{P}^{typ}_{\mathrm{g},fh}$	power demand and generation forecast	(kW)
$\tilde{P}^{\mathrm{lb},typ}$, $\tilde{P}^{\mathrm{ub},typ}$	lower and upper boundary for power forecast of $typ \in H_{\mathrm{typ}}$	(kW)
$\tilde{P}^{\mathrm{err},typ}_{fh}$	power forecast error of $typ \in H_{\mathrm{typ}}$	(kW)
pf^{typ}	power factor of $typ \in H_{\mathrm{typ}}$	(-)
Q	reactive power	(kVAr)
$Q^{\mathrm{ctr}}_{\mathrm{ramp}}$	characteristics of the Q-ramp function	(-)
S^{typ}_{d}	apparent power demand of $typ \in H_{\mathrm{typ}}$	(kVA)
SoE^{typ}	state of energy of $typ \in H_{\mathrm{typ}}$	(%)
γ	incremental change of the power factor	(-)

Optimization related:

$\boldsymbol{A}$, $\boldsymbol{B}$	coefficient matrices	(-)
$\boldsymbol{b}$, $\boldsymbol{b}^{typ}$	righthand side constraint conditions	(-)
$f(\boldsymbol{x})$	optimization function	(-)
LP	linear optimization problem	(-)
OB^{VPP}	objective function e.g. $OB^{\mathrm{VPP}}_{\mathrm{vc}}$ objective function for variable cost	(-)
$\boldsymbol{x}, \boldsymbol{y}$	optimization variables	(-)

Others:

C^{bid}	bidding capacity	(MW)
$c^{\mathrm{Q^{ctr}}}$, $c^{\mathrm{Q^{ctr}}}$	time constant for Q- and P-control	(s)
d	diameter	(m)
cnt	country	(-)
$\boldsymbol{CON}$	connectivity matrix with elements con	(-)
fh	forecast horizon	(h)
l	line length	(km)
$lon^{\mathrm{sph}}_i, lat^{\mathrm{sph}}_i$	spherical longitude and latitude coordinates	(°)
$lon^{\mathrm{crt}}_i, lat^{\mathrm{crt}}_i$	cartesian longitude and latitude coordinates	(km)
m^{OD}	mileage between origin and destination	(km)
m_k	discretized mileage per timestep	(km)
N	size of a statistical sample	(-)
n^{tap}	tap limit	(-)
R^{earth}	earth radius	(km)

$\boldsymbol{TRIP}$	trip matrix with elements $trip$	(-)
Δt	time increment	(h)
$t^{\mathrm{D},O}$	departure time at origin	(-)
$t^{\mathrm{A},D}$	arrival time at destination	(-)
T	time period	(h)
$T_{\mathrm{m}}^{\mathrm{T^{ctr}}}$, $T_{\mathrm{m}}^{\mathrm{Q^{ctr}}}$, $T_{\mathrm{m}}^{\mathrm{P^{ctr}}}$	move time of transformer control, Q-control and P-control	(s)
$T_{\mathrm{d}}^{\mathrm{T^{ctr}}}$, $T_{\mathrm{d}}^{\mathrm{Q^{ctr}}}$, $T_{\mathrm{d}}^{\mathrm{P^{ctr}}}$	delay time of transformer control, Q-control and P-control	(s)
typ	unit type	(-)
$\alpha^{\mathrm{Q^{ctr}}}$, $\alpha^{\mathrm{P^{ctr}}}$	output signal of voltage error	(-)
$\beta^{\mathrm{P^{ctr}}}$, $\beta^{\mathrm{P^{ctr}}}$	output signal of voltage error with time delay	(-)
ϖ^{em}	market prices	(EUR/kWh)
ϖ_{cp}	capacity price	(EUR/MW)
$\varpi_{\mathrm{vc}}^{typ}$	variable cost of $typ \in H_{\mathrm{typ}}$	(EUR/kWh)
$\varpi^{\mathrm{CR}\pm}$	internal control reserve cost	(EUR/kWh)
$\overline{\varpi}_{\mathrm{ep}}$	average weighted energy price	(EUR/kWh)
$\overline{\varpi}_{\mathrm{cp}}$	average weighted capacity price	(EUR/MW)
μ_{fh}^{typ}	mean values for $typ \in H_{\mathrm{typ}}$ in forecast horizon	(kW)
σ_{fh}^{typ}	standard deviations for $typ \in H_{\mathrm{typ}}$ in forecast horizon	(kW)

Indicators:

err_{fh}	forecast error, e.g. err_{fh}^{RMSE} root mean square error	(kW)
$\boldsymbol{J}$	Jacobian Matrix, e.g. $\boldsymbol{J}_{\mathrm{R}}$ - reduced Jacobian matrix	(-)
ghg_{CO2}^{typ}	green house gas emission of $typ \in H_{\mathrm{typ}}$	(gCO2/kWh)
$\varepsilon_{\mathrm{vc}}$	variable cost factor	(p.u.)
$\lambda^{\hat{\chi}_{FLH}}$	energy density	(p.u.)
$\lambda^{\mathrm{P^{ctr}}}$	slope characteristic of P-control	(1/MW)
$\lambda^{\mathrm{Q^{ctr}}}$	slope characteristic of Q-control	(1/MVAr)
$\lambda_{bus}^{\mathrm{Q-V}}$	slope characteristic of the Q-V-curve	(1/MVAr)
λ^{ur}	utilization rate	(%)
η^{mod}	energy conversion efficiency	(%)
Ξ_{lat}	conversion factor for latitude coordinates	(km/∘)
$\bar{\Xi}_{\mathrm{lon}}$	conversion factor for longitude coordinates	(km/∘)
Γ^{typ}	penetration rate of $typ \in H_{\mathrm{typ}}$	(%)
κ_{d}	coincidence factor	(%)

A. Appendix
Energy Market Characteristics of the German-Austrian Bidding Zone

A.1. Price Movements in Wholesale Spot Markets

The following analyses are based on information published by the European Energy Exchange and the European Power Exchange [1] for spot market auctions. More specifically, the contract and clearing sequences, as shown in Fig. 2.10, are specified by the delivery data of the German-Austrian bidding zone. The spot market products are characterized by the tendering period, 1-hour based average weighted prices with standard deviations, minimum, maximum and median prices. Table A.1 gives an overview of the resulting day-ahead auction prices in 2008-2014, which is traded daily at 12:00 with minimum volume increments of 0.1 MW for individual hours and 0.1 MW for blocks.

TABLE A.1.: Day-ahead characteristics of the European Power Exchange spot market EPEX SPOT of the German-Austrian bidding zone.

year	average price	std	min	max	med
	energy price (EUR/MWh)				
2008	65.76	28.65	-101.52	494.26	63.31
2009	38.85	19.40	-500.02	182.05	38.07
2010	44.49	13.98	-20.45	131.79	45.09
2011	51.12	13.59	-36.82	117.49	51.85
2012	42.60	18.69	-221.99	210.00	42.08
2013	37.59	16.64	-100.03	130.27	36.00
2014	32.76	12.77	-65.03	87.97	31.64

*) 1-hour based average weighted prices

[1] available at http : //www.epexspot.com

Table A.2 provides a summary of intraday auctions in 2008-2014, which is traded daily at 15:00 with minimum volume increments of 0.1 MW for individual quarter hours and traded for delivery the following day in 96 quarter hour interval. In addition, continuous trading for delivery on the same or the following day is possible and starts at 04:00 on the current day. The products are based on single hours, 15-minute periods or block of hours until 30 minutes before delivery begins.

TABLE A.2.: Intraday Characteristics of the European Power Exchange Spot Market EPEX SPOT of the German-Austrian bidding zone.

year	average price	std	min	max	med
	energy price (EUR/MWh)				
2008	63.51	29.75	-22.65	389.79	62.41
2009	38.92	25.02	-648.62	173.72	37.85
2010	58.59	20.51	-20.36	190.00	57.06
2011	50.72	16.27	-140.88	162.06	51.72
2012	43.59	19.97	-270.11	272.95	43.17
2013	38.42	17.98	-84.88	163.44	36.75
2014	33.01	13.71	-55.95	139.12	32.05

*) 1-hour based average weighted prices

A.2. Price Movements in Balancing Market

The products on the balancing markets consist of primary control (PCR), secondary control (SCR) and tertiary control reserve (TCR). Interruptible loads provide addition measures to maintain grid and system security since the amendment of the Energy Industry Act of 20 December 2012 and by means of the Ordinance on Interruptible Load Agreements of 28 December 2012. Beside the provision of primary, secondary and tertiary control reserve, the affected balancing responsible party is in charge for the compensation of remaining power imbalances after 60 minutes. Among others, this can be realized through the activation of additional reserve capacities of power plants or intraday tradings in the energy markets. The following analyzes are focused on the first three mentioned measures based on information published on the joint internet platform of transmission system operators in Germany [2]. Tertiary control reserve is procured since 1^{st} December 2006 as a joint tender, primary and secondary control reserve followed in 2007. The control reserve

[2]available at https : //www.regelleistung.net

products are characterized by the tendering period, activation time, average prices, standard deviations, minimum and maximum capacity and energy prices, as well as required volumes. The tender period for primary and secondary control reserve is one week, whereas it is one day for tertiary control reserve. The listed prices represent average weighted prices in order to enhance the comparability. The average weighted energy price $\overline{\varpi}_{\mathrm{ep}}$ and capacity price $\overline{\varpi}_{\mathrm{cp}}$ are defined as the quotient of total payments, consisting of single bid prices i. For example, the average weighted capacity price is calculated by:

$$\overline{\varpi}_{\mathrm{cp}} = \frac{\sum_{i=1}^{n^{\mathrm{bid}}} C_i^{\mathrm{bid}} \cdot \varpi_{\mathrm{cp},i}}{\sum_{i=1}^{n^{\mathrm{bid}}} C_i^{\mathrm{bid}}} \tag{A.1}$$

where n^{bid} represents the total number of bids consisting of single bidding capacity C_i^{bid} with the corresponding capacity prices $\varpi_{\mathrm{cp},i}$. The calculation in (A.1) also applies to determine the average weighted energy price, where n^{call} is defined as the total number of calls with the corresponding called energy E^{call} and energy prices ϖ_{ep} of individual control power suppliers. In case of three accepted bids A,B,C with single energy prices of 30 EUR/MWh, 70 EUR/MWh, 90 EUR/MWh and bidding capacity of 1 MW, 2 MW and 1 MW, the average weighted energy price for two calls of 1 MW and 3 MW is:

$$\begin{aligned} \overline{\varpi}_{\mathrm{ep}} &= \frac{(1\mathrm{MW} \cdot 30\frac{\mathrm{EUR}}{\mathrm{MWh}}) + (1\mathrm{MW} \cdot 30\frac{\mathrm{EUR}}{\mathrm{MWh}} + 2\mathrm{MW} \cdot 70\frac{\mathrm{EUR}}{\mathrm{MWh}})}{1\mathrm{MW} + 3\mathrm{MW}} \\ &= 50\mathrm{EUR/MWh} \end{aligned} \tag{A.2}$$

The calculation is based on the merit order and reflects the order of the short-run marginal costs.

Primary Control Reserve: Short term frequency deviations are compensated through the activation of primary control reserve within 30 seconds and is available for a period of 15 minutes. The tendering period changed from monthly (m) to weekly (w) tenders on 26th June 2011. Due to shorter tender periods and joint tender, the required control reserve volume dropped in 2011, as shown in Fig. A.1. Control power suppliers have to provide both positive and negative control reserve. The activated and provided active and reactive power is not separately measured by the transmission system operator and therefore not reported in Table A.3.

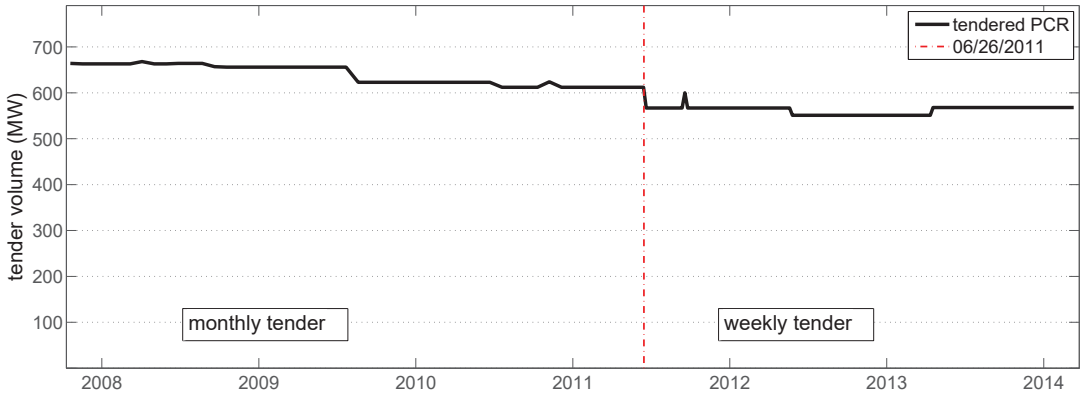

Fig. A.1.: Primary control reserve $PCR^{+/-}$ annual tender volume from 2008 to 2014.

Within the considered years, the deviation of minimum and maximum annual prices vary considerably with a maximum value of 19,995.00 EUR/MW in 2012.

TABLE A.3.: Primary control reserve characteristics $PCR^{+/-}$ of German electricity balancing market.

year	average price	std	min	max	average required control reserve (MW)
	capacity price*) (EUR/MW)				
2008	3,438.57	684.04	2,370.52	5,889.57	663.75
2009	3,893.51	256.05	3,347.36	5,600.00	656.08
2010	3,350.51	189.56	3,068.26	3,997.50	623.00
2011 (m)	3,103.05	450.76	2,527.93	7,338.71	642.28
2011 (w)	3,749.14	363.56	2,975.00	4,363.00	569.64
2012	2,771.45	698.48	1,925.00	19,995.00	567.62
2013	2,960.59	508.82	2,098.00	9,253.00	551.33
2014	3,513.77	706.88	2,542.00	8,744.00	568.00

*) 1-week based average weighted prices

Secondary Control Reserve: The secondary control reserve is used for medium term stabilization and is activated after system failures longer than 30 seconds, fully activated after 5 minutes and available for a period of 4 hours. In addition there are two separate time slices, namely peak hours from 8 am to 8 pm on weekdays, and off-peak hours in the remaining time of the week, including public holidays and weekends. Control power suppliers can provide both positive SCR^{+} and/or negative SCR^{-} secondary control reserve. The prices listed in Table A.4 and Table A.5 correspond to the weekly based average weighted capacity prices and called capacities.

TABLE A.4.: Secondary control reserve SCR^+ capacity and energy price characteristics of the electricity balancing market.

time slices	peak	off-peak	peak	off-peak
year	**capacity price***) (EUR/MW)		**capacity demand***) (MW)	
2008	1,326.30	799.76	2,983.33	2,983.33
2009	1,090.06	682.79	2,846.58	2,853.50
2010	829.64	829.07	2,402.33	2,447.17
2011 (m)	451.98	713.66	2,169.00	2,205.00
2011 (w)	444.52	1,145.80	2,088.08	2,088.08
2012	108.72	315.53	2,082.19	2,082.19
2013	540.77	731.73	2,115.48	2,115.48
2014	468.08	807.23	2,052.10	2,052.10
year	**energy price***) (EUR/MWh)		**called energy***) (MWh)	
2008	120.62	77.86	113.31	61.40
2009	102.89	80.77	82.88	68.34
2010	97.43	93.19	134.68	122.45
2011 (m)	104.00	100.18	80.57	57.46
2011 (w)	95.56	88.29	46.64	34.23
2012	107.49	111.91	66.43	56.50
2013	85.50	78.29	47.32	33.83
2014	78.16	71.84	40.52	29.23

*) 1-week based average weighted prices and quantity

The demand of secondary control reserve dropped in 2011 after the change of the tendering period from monthly to weekly biddings. Despite the constant demand of secondary control reserve after 2011, the average annual capacity prices remain unsteady and fluctuate between 109 EUR/MW and 541 EUR/MW for peak hours and between 316 EUR/MW and 1,146 EUR/MW for off-peak hours. The annual average energy prices dropped for peak hours and remained almost at the same level for off-peak hours. Note, negative prices indicate payments of the transmission system operator to the control power supplier. Positive prices indicate payments of the control power supplier to the transmission system operator. The movement of the energy prices of negative secondary control reserve show the complexity of the balancing market and is influenced by several factors, such as the current power demand and supply, cross-border exchanges, partial blackouts, tender specifications and even the legal framework and politics.

TABLE A.5.: Secondary control reserve SCR^- capacity and energy price characteristics of the electricity balancing market.

time slices	peak	off-peak	peak	off-peak
year	**capacity price**$^{*)}$ (EUR/MW)		**capacity demand**$^{*)}$ (MW)	
2008	243.24	885.00	2,403.33	2,403.33
2009	153.00	1,420.56	2,189.50	2,217.83
2010	172.14	2,469.97	2,214.42	2,223.67
2011 (m)	285.91	1,444.50	2,115.17	2,176.00
2011 (w)	694.44	1,653.41	2,060.35	2,063.62
2012	536.27	1,419.39	2,117.31	2,117.31
2013	787.58	1,165.31	2,074.52	2,074.48
2014	348.09	529.46	1,980.15	1,980.15
year	**energy price**$^{*)}$ (EUR/MWh)		**called energy**$^{*)}$ (MWh)	
2008	-10.55	-2.86	97.78	139.42
2009	-4.81	-0.86	134.97	138.94
2010	-9.60	-4.45	132.14	122.76
2011 (m)	-14.04	-1.50	97.67	125.41
2011 (w)	-15.91	-9.41	114.40	122.26
2012	-12.61	-2.87	68.57	78.40
2013	-12.48	-0.42	55.90	56.50
2014	9.73	17.46	44.64	46.79

*) 1-week based average weighted prices and quantity

Tertiary Control Reserve: The tertiary control reserve is used for medium term stabilization to cope with significant or systematic imbalance in the control area and/or resolve major congestion problems. The control reserve product offers flexibilities to control power suppliers because of longer activation times, structure of shorter time slices, lower minimum bid ranges and bid pooling possibilities of power plant capacities. The control reserve is fully activated after 15 minutes and replaces the secondary control reserve to stabilize the network frequency. The tender is separated in six time slices, 4 hours each. Control power suppliers can provide both, positive TCR^+ and/or negative TCR^- tertiary control reserve. The prices listed in Table A.6 and Table A.7 correspond to the daily based average weighted capacity and energy prices. The capacity prices for positive tertiary control reserve declined substantially between 2007 and 2014, with different price characteristics concerning the time slices.

TABLE A.6.: Tertiary control reserve TCR^{+} capacity and energy price characteristics of the electricity balancing market.

time slices	0 - 4	4 - 8	8 - 12	12 - 16	16 - 20	20 - 24
year	**capacity price***) (EUR/MW)					
2008	4.29	13.05	40.90	28.95	29.33	13.42
2009	2.55	4.83	19.21	13.51	11.98	4.58
2010	0.50	2.15	9.08	5.55	6.82	2.56
2011	0.35	1.15	1.97	1.75	1.64	1.22
2012	0.41	1.71	3.71	3.25	6.07	2.46
2013	0.71	1.92	5.35	4.21	6.36	4.60
2014	0.17	1.09	3.33	2.23	3.75	2.50
year	**energy price***) (EUR/MWh)					
2008	160.89	215.91	305.40	336.97	284.70	184.43
2009	226.89	137.09	157.06	149.51	166.54	212.88
2010	89.80	111.09	190.44	182.81	160.47	141.47
2011	128.09	150.91	217.33	237.57	206.73	217.55
2012	254.78	206.21	197.65	172.98	197.11	208.01
2013	95.92	155.63	208.96	157.78	182.55	161.98
2014	108.49	137.70	203.25	184.43	168.46	168.60

*) 4-hour based average weighted prices

The movement of capacity and energy prices traded for negative tertiary control reserve are comparable to the price characteristics of the positive tertiary control reserve. However, there are significant price differences in the individual time slices. While the capacity prices of positive control reserve are low in the time slices from 0-8 and high in the time slices from 8-24, the capacity prices follow almost the reverse order for the negative control reserve and indicates a negative correlation. The energy prices increase and change from negative to positive prices. In such cases, the control power suppliers of tertiary control reserve paid for lowering the generation of power plants or activation of additional loads.

TABLE A.7.: Tertiary control reserve TCR^{-} capacity and energy price characteristics of the electricity balancing market.

time slices	0 - 4	4 - 8	8 - 12	12 - 16	16 - 20	20 - 24
year	**capacity price***) (EUR/MW)					
2008	27.46	27.88	1.47	1.39	1.42	1.95
2009	70.75	70.04	13.98	14.64	13.50	16.54
2010	33.31	32.90	2.25	2.33	2.23	3.68
2011	38.34	38.64	5.00	5.99	5.95	10.36
2012	23.30	23.73	6.51	7.04	6.53	6.21
2013	35.86	33.62	17.02	25.38	18.65	13.42
2014	25.07	23.58	12.90	16.08	12.14	10.69
year	**energy price***) (EUR/MWh)					
2008	-0.48	-0.33	-1.57	-1.94	-1.83	-0.73
2009	6.72	7.14	-3.70	-3.44	-4.13	-3.36
2010	0.72	-1.84	-3.51	-1.32	-7.56	-3.53
2011	11.77	20.00	10.25	0.33	-2.42	0.39
2012	67.67	70.93	94.37	71.30	41.94	72.54
2013	60.41	149.71	108.36	80.70	46.78	46.29
2014	35.83	48.22	49.02	48.98	40.74	31.09

*) 4-hour based average weighted prices

B. Appendix

Power Plant Portfolio Parameter Tables

B.1. List of Existing Power Plants

TABLE B.1.: Composition of power plant portfolios in Germany for 1990 and 2014 by unit types, installed capacity and numbers.

	1990	2014*)			
	> 20 MW	> 20 MW	10-20 MW	< 10 MW	total
unit type	**installed capacity**$^{*)}$ (GW)				
nuclear	25.09	12.07	-	-	12.07
lignite	28.67	22.92	0.08	0.01	23.01
hard coal	32.60	27.50	0.07	-	27.57
gas	17.17	27.38	0.85	0.14	28.37
renewables*)	1.42	73.98	8.46	0.48	82.93
other	16.72	17.47	0.23	0.01	17.72
total	121.67	181.33	9.69	0.64	191.66
	1990	2014*)			
	>20 MW	>20 MW	10-20 MW	<10 MW	total
unit type	**numbers**$^{*)}$				
nuclear	27	9	-	-	9
lignite	152	73	6	1	80
hard coal	161	111	4	-	115
gas	140	193	62	26	281
renewables*)	38	316	601	95	1012
other	172	125	14	4	143
total	690	827	687	126	1,660

*) tabulated numbers representing the sum clustered values per federal state and source of energy, e.g. wind farm with several single wind power plants.

B.2. Indicating Power Plant Characteristics

TABLE B.2.: Characteristics of controllable power plant technologies.

power plant technology	start-up time, cold	start-up time, warm	ramp rate*)	minimum power generation*)	control range	start-up cost**) 5)6)
	(h)	(h)	(%P_r/min)	(%P_r)	(%P_r)	(EUR/MW)
nuclear	< 24	1 - 4 2)3)	2 / 5 / 10 2)4)	60 / 50 / 40 4)	60 - 90	35 / - / -
lignite	9 - 15	1 - 3 2)4)	1 / <u>2.5</u> / 4	60 / <u>50</u> / 40	60 - 90	112 / 73 / 62
hard coal	6 - 8	2 - 4	1.5 / <u>4</u> / 6	40 / <u>25</u> / 20	40 - 90	137 / 91 / 96
combined cycle	2 - 4 2)	0.5 - 1.5 2)	2 / <u>4</u> / 8	50 / <u>40</u> / 30	50 - 90	117 / 83 / 57
gas turbine	< 0.5	< 0.25	8 / <u>12</u> / 15	50 / <u>40</u> / 20	50 - 90	24 / 21 / 17
cogeneration	0.003 - 72 7)	0.02 - 0.2 11)	2 - 3 8) / - / -	- / - / -	-	- / - / -
diesel generator	0.03 9)	-	5 - 10 8) / - / -	- / - / -	-	- / - / -
pump storage	0.1 8)	0.1 8)	40 8) / - / -	15 8) / - / -	15 - 90	12 10) / - / -

*) usual / <u>state of the art</u> / potential for optimization

**) cold start / warm start / hot start

Basic data of Table B.2 are derived from 1) [201] and further amendments abstracted from 2) [202], 3) [203], 4) [204], 5) [205], 6) [206], 7) [207], 8) [208], 9) [209], 10) [210] and 11) [211]. The values of minimum load are conditioned by emission limit values for NOx and CO during permanent operation in case of nuclear, lignite, hard coal, combined cycle and gas turbine power plants. In case of cogeneration, diesel generator or pump storage systems minimum load as well as control range are subjected to the respective power plant technologies or internal module composition.

B.3. Site Location Based Full Load Hours

TABLE B.3.: Indicating site location based power generation per 1 MW of wind and photovoltaic power plants.

wind power plants (2-5 MW)		full load hours	power generation 'per 1 MW'
geographical area	technology / details	(h/a)	(MWh/a)
Germany	inland	1,300	1,300
Germany	near-shore/windy location	2,000	2,000
Germany	atlantic coast	2,700	2,700
Germany	near-shore (short distance)	2,800	2,800
Germany	near-shore (average distance)	3,200	3,200
Germany	near-shore (long distance)	3,600	3,600
Germany	excellent location	4,000	4,000
pv-standard modules		solar radiation 'opt. tilt angle'	power generation 'per 1 MW'
geographical area	technology / details	(kWh/m^2/a)	(MWh/a)
Germany	north	1,100	900
Germany	central/east	1,200	1,000
Germany	south	1,300	1,100
France	south	1,700	1,400
Spain	south	2,000	1,600
Africa	north	2,500	2,000

*) values correspond to elaborations according to [15, 212, 213] and supplementary additions.

C. Appendix
Unified Unit Models and Characteristics

For the set of the introduced unit types H_{typ} in Table 3.1 as part of the unified model architecture of the Virtual Power Plant, the following elaborations specify the integrated unit models. Indicating the amount of energy provided by distinct power plant portfolios and for comparison reasons of the generation and load profiles, a reformulation of the full load hours calculated in (2.2) is presented. The normalized profiles are further investigated by means of the normalized energy density $\lambda^{\hat{\chi}^{\text{norm}}_{FLH}}$ which is defined with $\|\boldsymbol{\lambda}^{\hat{\chi}_{FLH}}\|_\infty = \max\left(|\lambda_1^{\hat{\chi}_{FLH}}|, |\lambda_2^{\hat{\chi}_{FLH}}|, \ldots, |\lambda_{n^{\text{day}}}^{\hat{\chi}_{FLH}}|\right)$ as follows:

$$\lambda_d^{\hat{\chi}^{\text{norm}}_{FLH}} = \frac{\lambda_d^{\hat{\chi}_{FLH}}}{\|\boldsymbol{\lambda}^{\hat{\chi}_{FLH}}\|_\infty} \qquad \forall d \in H_{\text{day}} \ . \tag{C.1}$$

Let $\lambda_d^{\hat{\chi}_{FLH}} = \sum_{k \in H_{\text{ts}}} P^{typ}_{\text{g},k,d} \cdot \Delta t \ \forall k \in H_{\text{ts}}$ be the cumulated energy equivalents for each day and $H_{\text{day}} = \{1, 2, \ldots, d, \ldots, n^{\text{day}}\}$ the total days considered. The corresponding set of incremental time steps $H_{\text{ts}} = \{k_{\text{ini}}, \ldots, k_{\text{fin}}\}$ is defined by the initial k_{ini} and final k_{fin} time steps.

C.1. Wind and Photovoltaic Power Plants

The unit models for wind and photovoltaic power plants are summarized in Table C.1, which represent onshore and offshore wind turbines, as well small up to large free-standing photovoltaic power plants. The variable cost are obtained from [212, 214] while the greenhouse gas emissions are assumed to be zero. The unit models are assigned with different generation profiles as shown in Fig. C.1. The generation profiles are normalized to the base of the total rated power and subdivided into hourly-based average profiles for comparison reasons. The rated power serves as scaling factor to model power plant portfolios with different sizes of renewable energy sources.

TABLE C.1.: Wind and photovoltaic power plant models differentiated by the attributes plurality of the installed capacity, specific variable cost and greenhouse gas emissions.

unit type	unit model	P_{r}^{typ} (MW)	$\varpi_{\mathrm{vc}}^{typ}$ (EUR/kWh)	ghg_{CO2}^{typ} (gCO2/kWh)
wind	small onshore	0.5	0.110	0
wind	medium onshore	1	0.080	0
wind	large onshore	3	0.050	0
wind	large offshore	5	0.140	0
pv	small roof-mounted	0.01	0.170	0
pv	medium roof-mounted	0.04	0.150	0
pv	large roof-mounted	0.1	0.120	0
pv	large free-standing	0.5	0.090	0

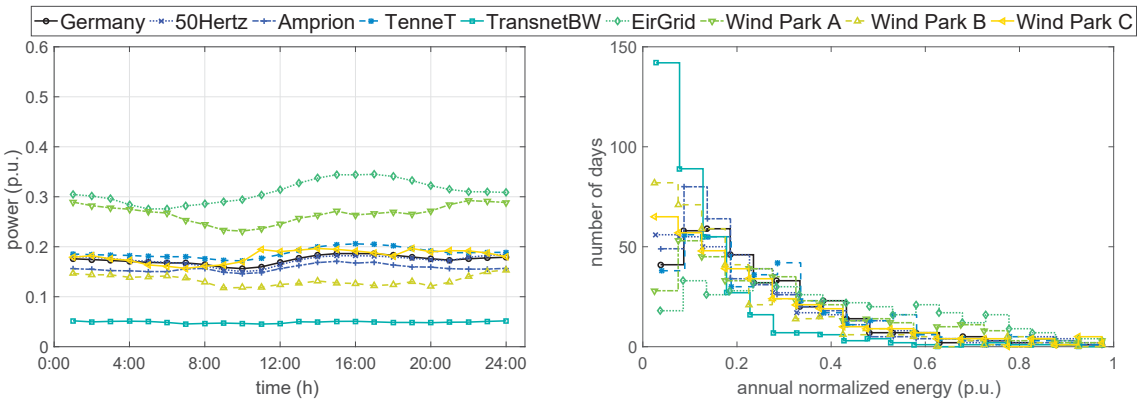

(a) hourly-based average profiles

(b) probability distribution

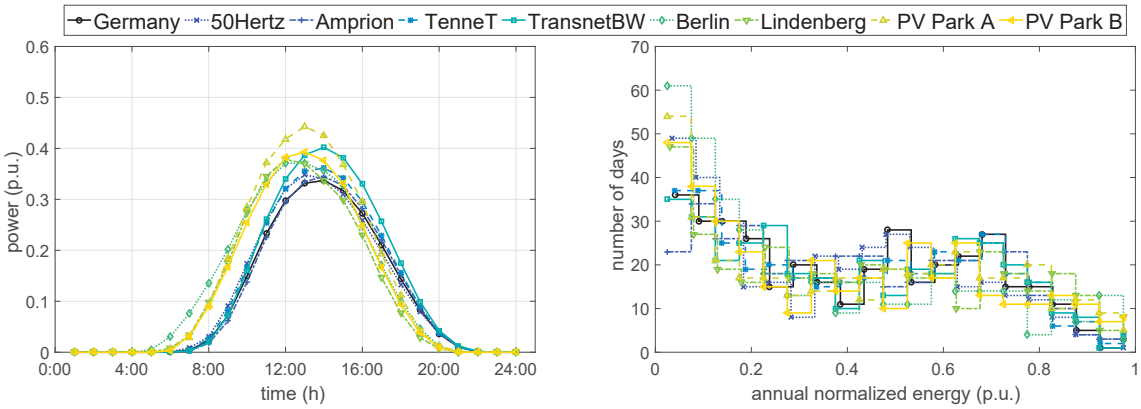

(c) hourly-based average profiles

(d) probability distribution

Fig. C.1.: Characteristics of generation profiles for wind and photovoltaic power plants for different site locations/areas specified by the (a),(c) hourly-based average profiles and (b),(d) probability distribution of the normalized energy density $\lambda_d^{\hat{\chi}_{FLH}^{\mathrm{norm}}}$.

Figure C.1a gives the obtained hourly-based average profiles of highly aggregated unit clusters, referring to control areas (50Hertz, Aprion, TenneT, TransnetzBW) and an entire country (Germany), as well as site locations of wind parks (Wind Park

A, Wind Park B, Wind Park C, EirGrid Wind Generator). Analogously, Fig. C.1c shows the generation profiles for photovoltaic power plants but located at different site locations (PV Park A, PV Park B, Lindenberg, Berlin). For example, from wind power plants located in the TransnetBW control area it can be seen that the hourly-based average profile are smoother and have smaller values compared to site locations of single wind parks which indicates the probability of the coincidence for the power generation. Further differences can be observed in the probability distribution of the energy density as shown in Fig. C.1b and Fig. C.1d. The probability distribution is a result of applying (C.1). The result indicates that the more the curve is skewed to the right, the higher the expected energy provided per day.

C.2. Combined Heat and Power and Distributed Generators

Controlled power generation includes combined heat and power and distributed generator units with combustion engines. The characteristics of the unit type specific models is derived from the GEMIS 4.9 database and are detailed in Table C.2.

TABLE C.2.: Combined heat and power and distributed generator unit models differentiated by the attributes plurality of the installed capacity, variable cost and greenhouse gas emissions.

unit type	unit model	P_{r}^{typ} (MW)	$\varpi_{\mathrm{vc}}^{typ}$ (EUR/kWh)	ghg_{CO2}^{typ} (gCO2/kWh)
dg	small biogas	0.05	0.045	9.44
dg	small jatrophaoil	0.5	0.241	8.21
dg	medium diesel	5	0.083	836.30
dg	large diesel	20	0.071	716.83
chp	small naturalgas	0.018	0.151	615.64
chp	medium jatrophaoil	0.1	0.588	10.57
chp	small biogas	0.5	0.141	5.52
chp	large fueloil	1	0.113	271.55

The combustion engines are assumed to be fired with fuel oil, jatropha oil, generic diesel or natural gas. Hence, the specific greenhouse gas emissions vary between $ghg_{\mathrm{CO2}}^{typ} = [8.21 - 836.30]$ gCO2/kWh. The controlled generation units are considered in the energy management algorithm for the provision of firm capacity and functions as secure back-up capacity in joint market operations.

C.3. Stationary Battery Systems

Three distinct unit models for battery technologies are considered, as highlighted in Fig. C.2. The characteristics are derived from information provided by [215–217] and further databases [1]. The red line in Fig. C.2 gives the E-rate, which expresses the ratio of charging/discharging power and the rated energy capacity [218].

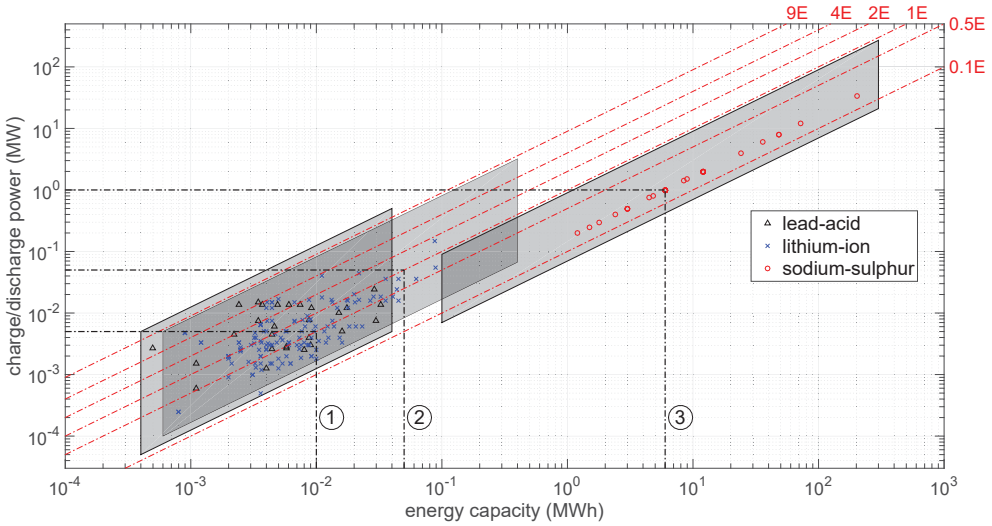

Fig. C.2.: Ragone chart of battery technologies based on database including 34 lead-acid (Pb), 154 lithium-ion (Li-Ion) and 41 sodium-sulphur (NaS) battery systems.

The normalized value of the energy capacity defines the state of energy SoE^{stor} and indicates the remaining available energy of the battery [137, 219]. In case of charging/discharging processes, the available energy capacity at a specific subsequent time step is modeled in the form of

$$SoE^{stor}_{k+1} = \begin{cases} SoE^{stor}_{k} + \frac{P^{\mathrm{stor}}_{\mathrm{d},k} \cdot \Delta t}{E^{typ}_{\mathrm{r}}} \cdot \eta^{mod}, & \text{charging mode} \\ SoE^{stor}_{k} - \frac{P^{\mathrm{stor}}_{\mathrm{g},k} \cdot \Delta t}{E^{typ}_{\mathrm{r}}} \cdot \frac{1}{\eta^{mod}}, & \text{discharging mode} \\ SoE^{stor}_{k}, & \text{otherwise.} \end{cases} \tag{C.2}$$

Table C.3 summarized the assigned model attributes and gives the rated charging/discharging power P^{typ}_{r} and efficiencies $\eta^{mod} \in \{\eta^{\mathrm{char}}, \eta^{\mathrm{dis}}\}$ of the corresponding specific battery technologies. For simplicity, the efficiency for charging/discharging processes is assumed to be equal. The attributed variable costs are derived from future scenarios for battery systems and consider a wide range of application purposes and installation settings [220, 221]. The values reflect optimum prices to model grid parity with the remaining unit types.

[1] available on http : //www.energie − datenbank.eu

TABLE C.3.: Stationary battery system unit models differentiated by the attributes plurality of the installed capacity, specific variable cost and charging/discharging efficiencies.

unit type	unit model	$P_{\mathrm{r}}^{typ}/E_{\mathrm{r}}^{typ}$ (MW/MWh)	$\varpi_{\mathrm{vc}}^{typ}$ (EUR/kWh)	η^{mod} (%)
bat	lead-acid	0.005/0.010	0.06	90
bat	lithium-ion	0.050/0.050	0.07	95
bat	sodium-sulphur	1.000/6.000	0.04	85

The first unit model denotes lead-acid (Pb) battery systems, which are typically used within smart household systems or in combination with small photovoltaic power plants [222]. The second unit model is derived from a review of lithium-ion (Li-Ion) battery systems, usually integrated in smart grid environments [35, 46]. The unit model for sodium-sulphur (NaS) battery systems with high rated charging/discharging power is typically used in combination with large wind or photovoltaic parks. Through the definition of the same model attributes, several extensions can be performed, for example to integrate pumped-storage systems as additional unit models.

C.4. Industrial, Commercial and Household Load Units

Fully-controlled loads are modeled as part of flexible industrial processes, such as refiners used in paper factories. These are operated between 60 % and 80 % of the maximum load and can provide significant demand-side management potential for several hours [223]. The flexible industrial processes are modeled by the assigned maximum positive and negative $P_{\mathrm{max}}^{\mathrm{CR}^{\pm}}$ control reserve as listed in Table C.4. Partly-controlled loads are represented by three distinct unit models, referring to anonymized intra-urban depots and office buildings with load shifting potentials. These unit models are defined by uncontrolled power demand and additional flexibilities for the provision of positive and negative control reserve. The maximum power demand $P_{\mathrm{d,max}}^{typ}$ and annual energy demand $E_{\mathrm{d,r}}^{typ}$ are examples and used as scaling factors to simulate different loading conditions. Non-controlled loads are modeled with six unit models, representing commercial and household load units. Depending on the annual energy demand $E_{\mathrm{d,r}}^{typ}$, load profiles are assigned either with historical measured data or approximated with standard load profiles as summarized in Fig. C.3. An example of which is given in Fig. C.3a by means of the hourly-based average profiles.

TABLE C.4.: Industrial, commercial and household load unit models differentiated by the attributes plurality of the installed capacity, reserve capacity, annual energy demand and specific variable cost.

unit type	unit model	$P^{typ}_{\mathrm{d,max}}$ (MW)	$P^{\mathrm{CR}^+}_{\mathrm{max}}$ (MW)	$P^{\mathrm{CR}^-}_{\mathrm{max}}$ (MW)	$E^{typ}_{\mathrm{d,r}}$ (MWh)	$\varpi^{typ}_{\mathrm{vc}}$ (EUR/kWh)
ind	paper factory	15	15	15	90,000	0.0445
ind	intra-urban depot A	0.50	0.20	\	1,000	0.0519
ind	intra-urban depot B	0.25	\	0.05	837	0.0519
ind	office building	0.15	0.03	0.03	250	0.0610
hh	private (H0)	0.80	\	\	3	0.0772
hh	general (G0)	1.20	\	\	5	0.0744
hh	workday (G1)	3.43	\	\	7	0.0744
hh	evening peak (G2)	2.26	\	\	9	0.0744
hh	continuous (G3)	1.70	\	\	11	0.0744
hh	weekend (G6)	4.48	\	\	15	0.0741

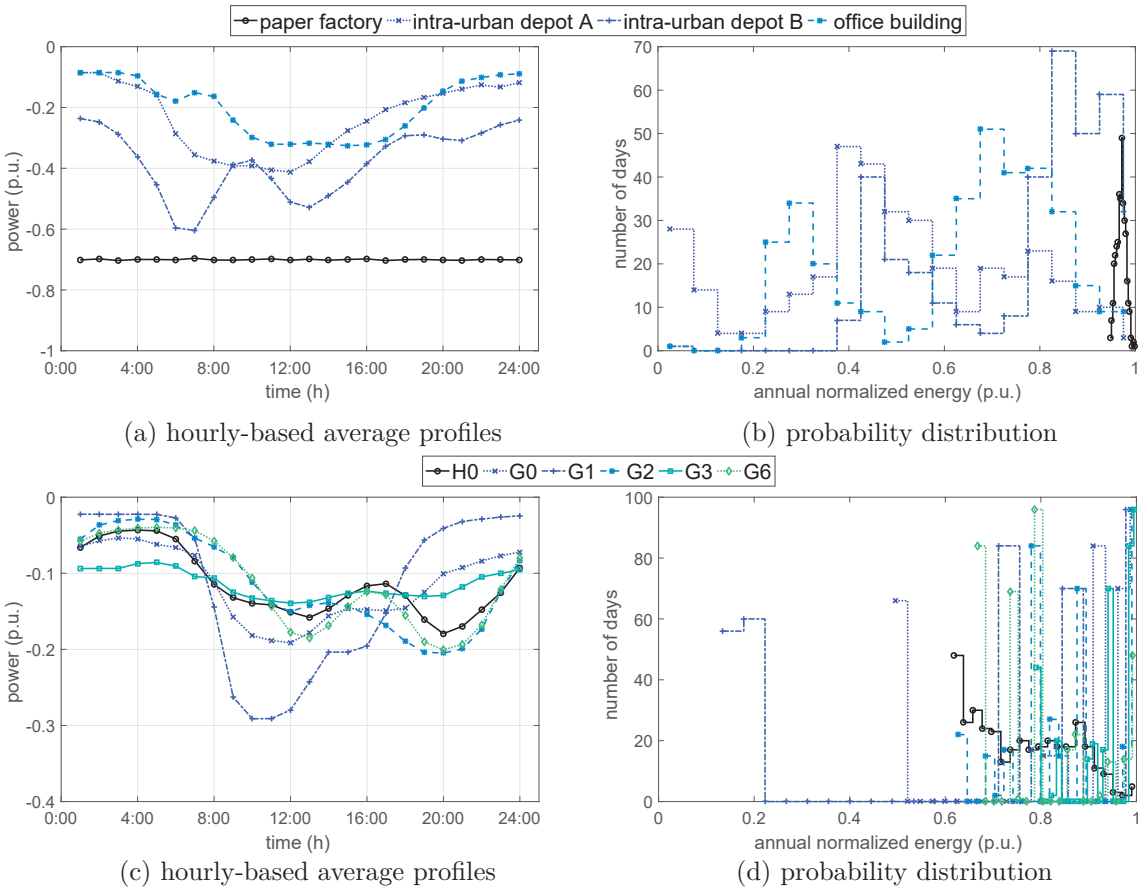

(a) hourly-based average profiles

(b) probability distribution

(c) hourly-based average profiles

(d) probability distribution

Fig. C.3.: Characteristics of load profiles for industrial, commercial and household load units for different site locations/areas specified by the (a),(c) hourly-based average profiles and (b),(d) probability distribution of the normalized energy density $\lambda_d^{\hat{\chi}^{\mathrm{norm}}_{FLH}}$.

Reflecting the load patterns of the customers with lower annual energy demand, the used standard load profiles are taken from the German Association of Energy and Water Industries for modeling the load characteristics of household and commercial load units and are depicted in Fig. C.3c. The highly aggregated average profiles represent numerous individual loads [140]. Typically, the standard load profiles are normalized based on the annual energy demand which serves as scaling factor to vary the loading conditions in the power plant portfolio. Fig. C.3b and Fig. C.3d show the evaluation of the probability distribution of the energy density which are calculated in (C.1) to indicate the expected energy demand per day.

D. Appendix

Synthetic Forecast Profiles and Uncertainties

The forecast model uses uniform and normal distribution function to synthetically generate forecast profiles with defined forecast errors. The distribution functions and model variables are schematically illustrated in Fig. D.1. The forecast horizon fh reflects the trading period and clearing sequence of the day-ahead and intraday market operations and ranges from 15-minutes, several hours up to multiple days.

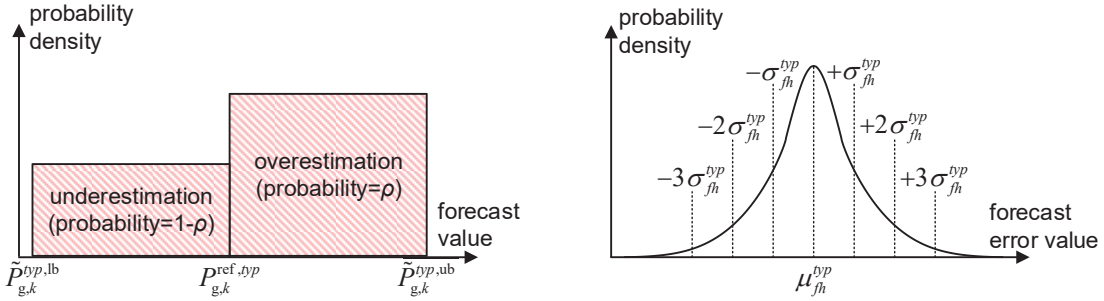

(a) uniform distribution (b) normal distribution

Fig. D.1.: Modeling of forecast errors with standard distribution functions through the application of (a) uniform distribution function and (b) normal distribution function.

The generation of forecast values with uniform distribution is calculated in (D.1). The ranges for overestimation and underestimation are defined by the probabilities ρ and $1-\rho$, respectively.

$$f(P_{\mathrm{g},k}^{\mathrm{ref},typ} \mid \tilde{P}_{\mathrm{g},k,fh}^{\mathrm{lb},typ}, \tilde{P}_{\mathrm{g},k,fh}^{\mathrm{ub},typ}) = \begin{cases} \dfrac{\rho}{\tilde{P}_{\mathrm{g},k,fh}^{\mathrm{ub},typ} - P_{\mathrm{g},k}^{\mathrm{ref},typ}} & \text{overestimation} \\ \dfrac{1-\rho}{P_{\mathrm{g},k}^{\mathrm{ref},typ} - \tilde{P}_{\mathrm{g},k,fh}^{\mathrm{lb},typ}} & \text{underestimation} \end{cases} \tag{D.1}$$

First, random numbers are generated from the continuous uniform distributions. $\tilde{P}_{\mathrm{g},k,fh}^{\mathrm{lb},typ}$ denotes the lower and $\tilde{P}_{\mathrm{g},k,fh}^{\mathrm{ub},typ}$ the upper forecast boundaries. Under consideration of the unit type specific power generation $P_{\mathrm{g},k}^{\mathrm{ref},typ}$, the calculation is as follows:

$$\tilde{P}_{\mathrm{g},k,fh}^{\mathrm{lb},typ} = \begin{cases} P_{\mathrm{g},k}^{\mathrm{ref},typ} - \Delta\tilde{P}_{fh,\min}^{\mathrm{err},typ} & \text{if } P_{\mathrm{g},k}^{\mathrm{ref},typ} > \Delta\tilde{P}_{fh,\min}^{\mathrm{err},typ} \\ 0 & \text{otherwise} \end{cases} \tag{D.2}$$

$$\tilde{P}^{\mathrm{ub},typ}_{\mathrm{g},k,fh} = \begin{cases} P^{\mathrm{ref},typ}_{\mathrm{g},k} + \Delta\tilde{P}^{\mathrm{err},typ}_{fh,\max} & \text{if } P^{\mathrm{ref},typ}_{\mathrm{g},k} + \Delta\tilde{P}^{\mathrm{err},typ}_{fh,\max} < P^{typ}_{\mathrm{r}} \\ P^{typ}_{\mathrm{r}} & \text{otherwise} \end{cases} \tag{D.3}$$

$\Delta\tilde{P}^{\mathrm{err},typ}_{fh,\min}$ and $\Delta\tilde{P}^{\mathrm{err},typ}_{fh,\max}$ refer to unit type specific minimum and maximum forecast errors. Next, (D.4) calculates the forecast values of the power generation.

$$\tilde{P}^{typ}_{\mathrm{g},k,fh} = \begin{cases} unifrnd\ (P^{\mathrm{ref},typ}_{\mathrm{g},k}, \tilde{P}^{\mathrm{ub},typ}_{\mathrm{g},k,fh}) & \text{overestimation} \\ unifrnd\ (\tilde{P}^{\mathrm{lb},typ}_{\mathrm{g},k,fh}, P^{\mathrm{ref},typ}_{\mathrm{g},k}) & \text{underestimation} \end{cases} \tag{D.4}$$

The generation of forecast values with normal distribution is defined by (D.5), which uses the mean value μ^{typ}_{fh} and standard deviation σ^{typ}_{fh}.

$$f(P^{\mathrm{ref},typ}_{\mathrm{g},k} \mid \mu^{typ}_{fh}, \sigma^{typ}_{fh}) = \frac{1}{\sigma^{typ}_{fh}\sqrt{2\pi}} \cdot e^{-\left(\frac{P^{\mathrm{ref},typ}_{\mathrm{g},k} - \mu^{typ}_{fh}}{2\sigma^{typ}_{fh}}\right)^2} \tag{D.5}$$

The corresponding forecast values for power generation are calculated in (D.6). In case of $P^{\mathrm{ref},typ}_{\mathrm{g},k} - normrnd\ (\mu^{typ}_{fh}, \sigma^{typ}_{fh}) < 0$, the forecast values for power generation is set to $\tilde{P}^{typ}_{\mathrm{g},k,fh} = 0$. Otherwise, if $P^{\mathrm{ref},typ}_{\mathrm{g},k} + normrnd\ (\mu^{typ}_{fh}, \sigma^{typ}_{fh}) > P^{typ}_{\mathrm{r}}$, the forecast values for power generation are set to $\tilde{P}^{typ}_{\mathrm{g},k,fh} = P^{typ}_{\mathrm{r}}$.

$$\tilde{P}^{typ}_{\mathrm{g},k,fh} = \begin{cases} P^{\mathrm{ref},typ}_{\mathrm{g},k} + normrnd\ (\mu^{typ}_{fh}, \sigma^{typ}_{fh}) & \text{overestimation} \\ P^{\mathrm{ref},typ}_{\mathrm{g},k} - normrnd\ (\mu^{typ}_{fh}, \sigma^{typ}_{fh}) & \text{underestimation,} \end{cases} \tag{D.6}$$

D.1. Generation of Synthetic Forecast Profiles

The unit type specific forecast errors are calculated (D.7) and denote the uncertainties related to the intermittent power generation. $\tilde{P}^{typ}_{\mathrm{g},k,fh}$ refer to forecast values for power generation and $P^{\mathrm{ref},typ}_{\mathrm{g},k}$ to values of the historical measured data.

$$\Delta\tilde{P}^{\mathrm{err},typ}_{k,fh} = \tilde{P}^{typ}_{\mathrm{g},k,fh} - P^{\mathrm{ref},typ}_{\mathrm{g},k} \tag{D.7}$$

The forecast profiles are evaluated by (D.8), using standard equation of the statistic mean absolute error err^{MAE} and root mean square error err^{RMSE}.

$$err^{\mathrm{MAE}}_{fh} = \frac{1}{|H_{\mathrm{ts}}|} \cdot \sum_{k=k_{\mathrm{ini}}}^{k_{\mathrm{fin}}} |\Delta\tilde{P}^{\mathrm{err},typ}_{k,fh}| \qquad err^{\mathrm{RMSE}}_{fh} = \sqrt{\frac{1}{|H_{\mathrm{ts}}|} \cdot \sum_{k=k_{\mathrm{ini}}}^{k_{\mathrm{fin}}} (\Delta\tilde{P}^{\mathrm{err},typ}_{k,fh})^2} \tag{D.8}$$

Additionally, the normalized root mean square error err^{NRMSE} is used as an indicating parameter for the evaluation of the forecast accuracy. The normalized values obtained by (D.9) uses the same model variables.

$$err_{fh}^{\mathrm{NRMSE}} = \frac{\sqrt{\frac{1}{|H_{\mathrm{ts}}|} \cdot \sum_{k=k_{\mathrm{ini}}}^{k_{\mathrm{fin}}} (\Delta \tilde{P}_{k,fh}^{\mathrm{err},typ})^2}}{P_{\mathrm{r}}^{typ}} \tag{D.9}$$

Table D.1 summarizes typical values reported in [97–106] for wind and photovoltaic power plants. The values differ as various forecasting methods are used, e.g. persistence forecasts for forecast horizons of 0.25h [224, 225]. Further, the forecast accuracy for single units might be lower compared to aggregated units in geographical areas due to the smoothing effect [226, 227].

TABLE D.1.: Normalized root mean square error $err_{fh}^{\mathrm{NRMSE}}$ values serve as measure of forecast accuracy for wind and photovoltaic power plants in different time periods.

unit type	$err_{0.25\mathrm{h}}^{\mathrm{NRMSE}}$ (p.u.)	$err_{1\mathrm{h}}^{\mathrm{NRMSE}}$ (p.u.)	$err_{2\mathrm{h}}^{\mathrm{NRMSE}}$ (p.u.)	$err_{4\mathrm{h}}^{\mathrm{NRMSE}}$ (p.u.)	$err_{24\mathrm{h}}^{\mathrm{NRMSE}}$ (p.u.)
wind	0.013 - 0.020	0.016 - 0.030	0.026 - 0.035	0.034 - 0.060	0.049 - 0.068
pv	0.006 - 0.024	0.017 - 0.039	0.027 - 0.042	0.037 - 0.047	0.046 - 0.070

Complementary to the tabulated values, historical forecast data from the German transmission system operator [1] are analyzed and the input parameter for the introduced distribution functions determined. According to (D.9), the input parameters are normalized by the rated power P_{r}^{typ} to obtain the mean values μ_{fh}^{typ} and standard deviations σ_{fh}^{typ}. The resulting values for day-ahead and intraday operation are summarized in Table D.2 and Table D.3, respectively. For simplification, the unit type specific minimum and maximum forecast errors $\Delta \tilde{P}_{fh,\min}^{\mathrm{err},typ} = \Delta \tilde{P}_{fh,\max}^{\mathrm{err},typ} = \mu_{fh}^{typ} + 3 \cdot \sigma_{fh}^{typ}$ are assumed to be equal.

TABLE D.2.: Initial mean value μ_{fh}^{typ} and standard deviation σ_{fh}^{typ} for normal distribution, and minimum $\Delta \tilde{P}_{fh,\min}^{\mathrm{err},typ}$ and maximum $\Delta \tilde{P}_{fh,\max}^{\mathrm{err},typ}$ forecast errors for generation of forecast profiles with uniform distribution in day-ahead operation.

unit type	$\mu_{24\mathrm{h}}^{typ}$ (GW)	$\sigma_{24\mathrm{h}}^{typ}$ (GW)	P_{r}^{typ} (GW)	$\mu_{24\mathrm{h}}^{typ}$ (p.u.)	$\sigma_{24\mathrm{h}}^{typ}$ (p.u.)	$\Delta \tilde{P}_{24\mathrm{h},\min}^{\mathrm{err},typ}$ (p.u.)	$\Delta \tilde{P}_{24\mathrm{h},\max}^{\mathrm{err},typ}$ (p.u.)
wind	0.193	0.575	12	0.016	0.048	0.160	0.160
pv	0.020	0.237	5	0.004	0.047	0.145	0.145

The intraday forecast parameters are estimated by applying the ratio between day-ahead and intraday forecasts to the above mentioned normalized root mean square

[1] available on http : //www.50hertz.com

TABLE D.3.: Initial mean value μ_{fh}^{typ} and standard deviation σ_{fh}^{typ} for normal distribution, and minimum $\Delta\tilde{P}_{fh,\min}^{\mathrm{err},typ}$ and maximum $\Delta\tilde{P}_{fh,\max}^{\mathrm{err},typ}$ forecast errors for generation of forecast profiles with uniform distribution in intraday operation.

unit type		μ_{fh}^{typ} (p.u.)		σ_{fh}^{typ} (p.u.)		$\Delta\tilde{P}_{fh,\min}^{\mathrm{err},typ}$ (p.u.)		$\Delta\tilde{P}_{fh,\max}^{\mathrm{err},typ}$ (p.u.)	
	fh:	1h	0.25h	1h	0.25h	1h	0.25h	1h	0.25h
wind		0.0052	0.0042	0.0157	0.0127	0.0522	0.0424	0.0522	0.0424
pv		0.0015	0.0005	0.0174	0.0061	0.0536	0.0189	0.0536	0.0189

errors. As an example, the ratio $\frac{err_{0.25\mathrm{h}}^{\mathrm{NRMSE}}}{err_{24\mathrm{h}}^{\mathrm{NRMSE}}}$ is assumed to be $\frac{0.013}{0.049}$ for the prediction of the intraday forecast of wind power plants with 0.25h forecast horizon. Based on the method of linear regression, the forecast values for power generation $\tilde{P}_{\mathrm{g},k,fh}^{typ}$ are calculated iteratively as a function of the previous forecast value $\tilde{P}_{\mathrm{g},k-1,fh}^{typ}$ with defined limitations of power deviations, e.g. up to $\pm 5\%$. Finally, the forecast profiles are smoothed using moving average filtering functions [228].

D.2. Forecast Error Evaluation

For evaluation purposes, the intermittent power generation of wind and photovoltaic power plants is modeled with the introduced methodology. Through heuristic and iterative stochastic adjustments of the initial input parameters in Table D.2 and Table D.3, the forecast accuracies as summarized in Table D.4 are obtained. It is shown that both probability density functions are capable to generate forecast profiles within the range of realistic forecast accuracies.

TABLE D.4.: Average normalized root mean square errors $err_{fh}^{\mathrm{NRMSE}}$ for day-ahead and intraday operations generated with uniform and normal distribution functions.

unit type	distribution function	$err_{0.25\mathrm{h}}^{\mathrm{NRMSE}}$ (p.u.)	$err_{1\mathrm{h}}^{\mathrm{NRMSE}}$ (p.u.)	$err_{24\mathrm{h}}^{\mathrm{NRMSE}}$ (p.u.)
wind	$unifrnd$	0.016	0.027	0.067
	$normrnd$	0.016	0.028	0.066
pv	$unifrnd$	0.014	0.029	0.069
	$normrnd$	0.014	0.029	0.070

An example of which is given in Fig. D.2, where the red solid line illustrates the forecast profile for the day-ahead operation, while the black dashed and blue solid line show the forecast profiles for the intraday operation. The ratio of the calculated forecast errors err_{fh}^{MAE} and err_{fh}^{RMSE} are shown below. The bisecting line denotes the

ratio $\frac{err_{fh}^{\mathrm{RMSE}}}{err_{fh}^{\mathrm{MAE}}} = 1$ and indicates perfect matching without exaggerated errors. By applying the root mean square error calculation, the forecast errors and outliers are weighted more strongly than small errors because of the square of differences [229, 230].

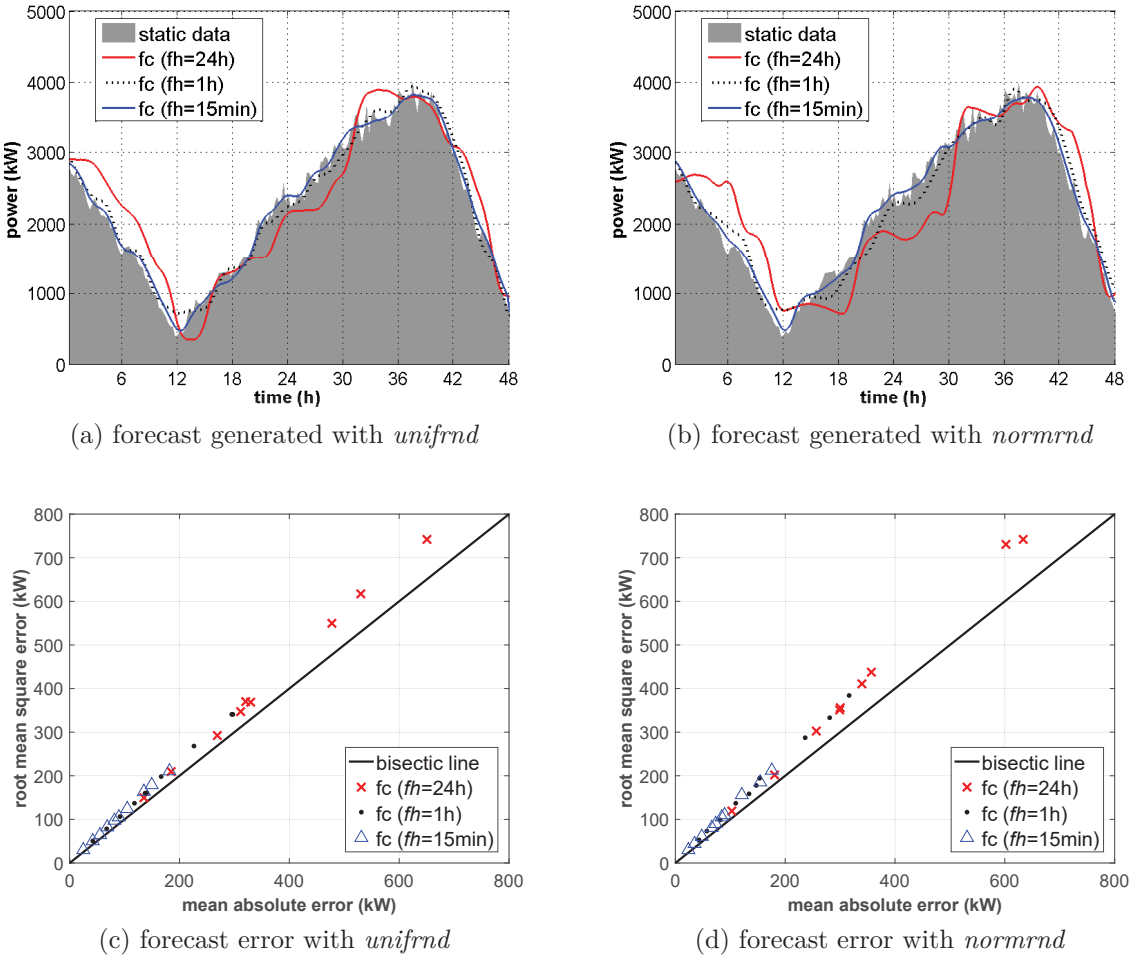

(a) forecast generated with *unifrnd*

(b) forecast generated with *normrnd*

(c) forecast error with *unifrnd*

(d) forecast error with *normrnd*

Fig. D.2.: Comparison of forecast profiles and errors modeled with uniform and normal distribution function for two 3 MW onshore wind power plants.

As indicated by the values of err_{fh}^{RMSE} over err_{fh}^{MAE}, the forecast profiles modeled with the uniform probability density function show lower sensitivity towards exaggerating outliers compared to forecast error based on normal distribution function with similar forecast accuracies. Therefore, the uniform probability density function is selected in the Virtual Power Plant model to generate the forecast profiles for the intermittent power generation of wind and photovoltaic power plants.

E. Appendix
Extended European 20 kV Distribution Network Benchmark

The CIGRE Task Force C6.04.02. established several benchmark systems that serve as test systems for the integration of distributed and renewable energy sources in different power systems. The benchmark modeling methodology of the European 20 kV distribution network benchmark is derived from a physical medium voltage network in southern Germany, which supplies a small town and the surrounding rural area. The number of buses was reduced to enhance user friendliness and flexibility while maintaining the realistic character of the network [197]. Through sensitivity analysis, critical power system buses are identified and the voltage stability of the power system evaluated. Additional generators and tap-changing transformer are included in order to investigate the impacts of under- and over-voltage conditions during power system operations. In the following, the power system architecture and essential model characteristics are briefly discussed. The load distribution is derived from real-data sets of load profiles and is incorporated in a software optimization tool to obtain solutions for a multi-temporal optimum power flow calculation. The generation profiles of the integrated conventional generators are optimized in order to obtain the lowest-cost generation dispatch while realizing near optimum network conditions.

E.1. Network Topology with Distributed and Renewable Energy Sources

The network topology of the extended European 20 kV distribution network benchmark is shown in Fig. E.1. The two feeder sections are characterized by residential and industrial/commercial loads. The primary sub-transmission high voltage system is modeled as slack bus with a rated voltage of $V_{1\mathrm{r}} = 110\,\mathrm{kV}$. The distribution feeders with a rated voltage of $V_{2\mathrm{r}} = 20\,\mathrm{kV}$ are connected through HV/MV transformers. According to operational features and in order to satisfy security requirements, both feeder sections can be operated in radial and/or meshed structures by means of con-

figuration switches/circuit breakers $S1$, $S2$, and $S3$. Each feeder section includes numerous laterals with corresponding load profiles for each bus. However, the load characteristics can be changed and additional system devices, conductor types and tap-changing transformers implemented.

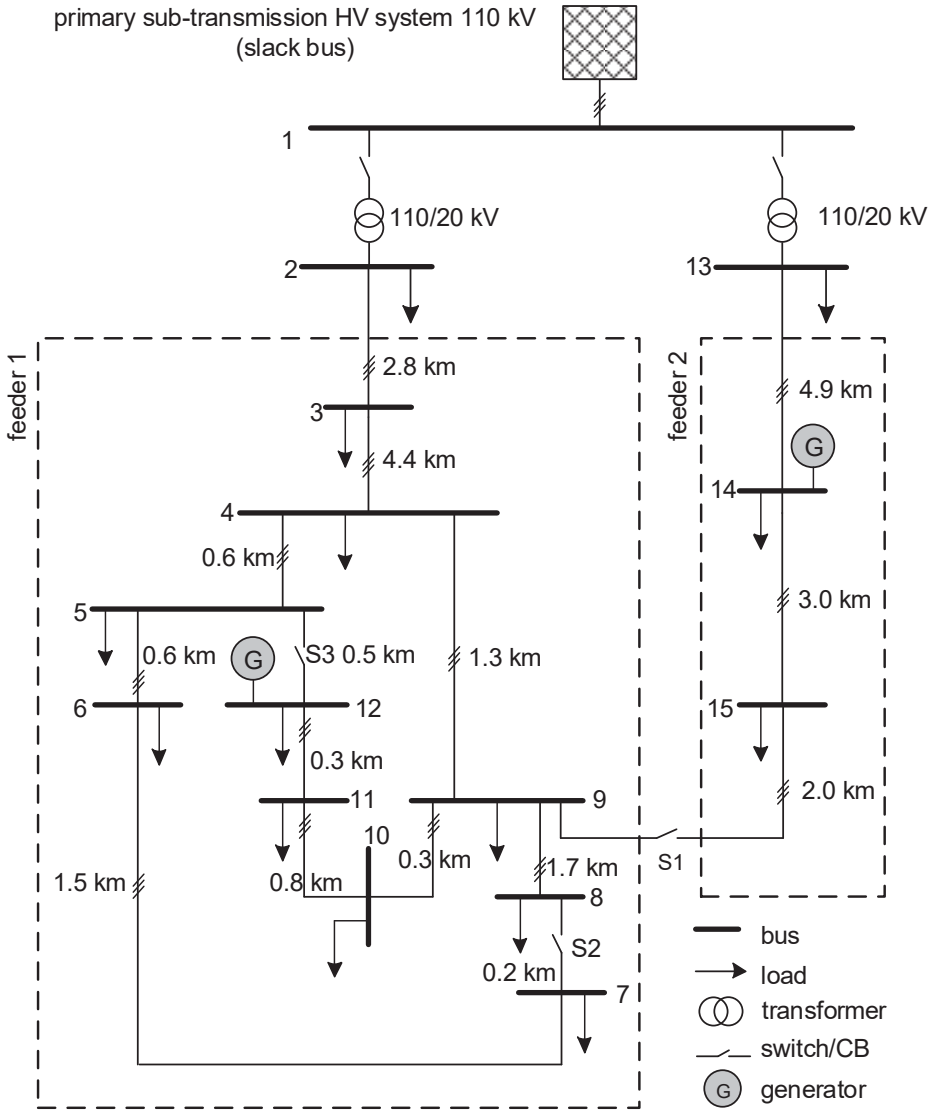

Fig. E.1.: Network topology of extended European 20 kV distribution network benchmark model with residential and industrial/commercial feeder sections.

In order to investigate voltage control methods with multiple power sources and system devices, additional distributed, renewable and mobile energy sources are integrated. These units and unit clusters are categorized in three subcategories with different configurations and locations as illustrated in Fig. E.2. Bus 10, 11 and 13 are modeled as residential load areas and equipped with a certain amount of combined heat and power plants, bio-diesel generators and photovoltaic power plants as shown in Fig. E.2a. Feeder 2 is defined as industrial area, as depicted in Fig. E.2c, with corresponding industrial loads. The renewable energy resources,

which refer to wind power plants and photovoltaic power plants, are integrated at bus 5, 6, 7, 8 and 12 as shown in Fig. E.2b.

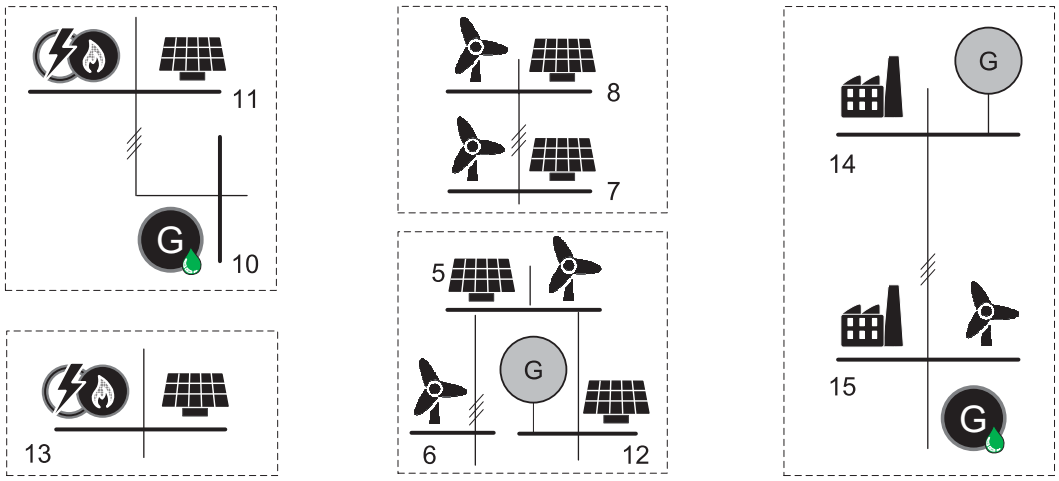

(a) residential (b) renewable (c) industrial

Fig. E.2.: Configuration and location of Virtual Power Plant coordinated units and unit clusters in the extended European 20 kV distribution network benchmark model.

With the presence of the additional distributed, renewable and mobile energy sources which are coordinated within the Virtual Power Plant, the original residential and industrial load distribution are modified.

E.2. Network Model with Tap-Changing Transformer

Instead of fixed voltages from the primary or secondary side of the sub-station, additional voltage measurements can be used to mitigate steady-state voltage variations under consideration of high penetration of renewable energy sources. Among those voltage measurements, the utilization of tap-changing transformer is assessed. This allows the system operator to change the power system voltage depending on power system conditions. Two types of tap-changing transformer can be implemented for the mitigation of long-term and short-term voltage variations in distribution networks:

- off-load tap-changing: corresponds to the 110 kV primary side rated voltage V_{1r} with ± 5 % in 2.5 % increment turns ratio $\Delta\bar{n}_1$ to meet long-term variation due to (i) load growth, (ii) system expansion, or (iii) seasonal changes
- on-load tap-changing: corresponds to the 20 kV secondary side rated voltage V_{2r} with ± 10 % in 0.625 % increment turns ratio $\Delta\bar{n}_2$ to meet frequent load changes due to short-term variations

The tap positions are limited to a minimum $n_{\min}^{\text{tap}}$ and maximum $n_{\max}^{\text{tap}}$ tap position. In order to reduce frequent tap operations, different tap-changing transformer control methods can be integrated [231–233]. For the purpose of modeling the control method in steady-state analysis, distinct voltage ranges are defined and measurements from remote buses as input parameter used for the controller of the on-load tap-changing transformer. Figure E.3a shows a simplified equivalent circuit of the on-load tap-changing transformer and Fig. E.3b the corresponding equivalent π-circuit model.

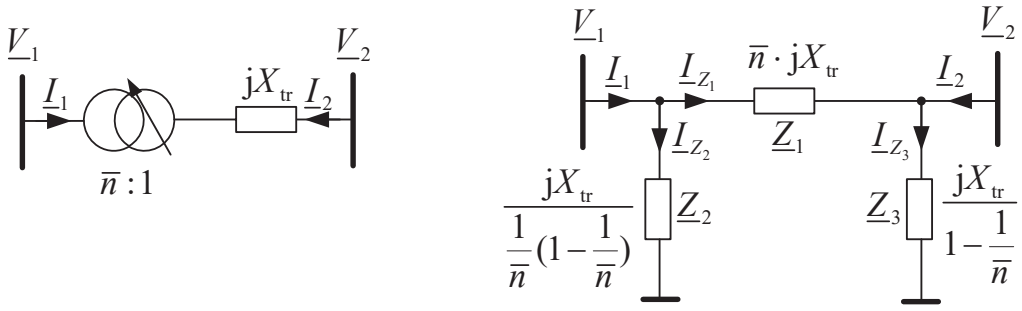

(a) circuit model (b) equivalent π-circuit model

Fig. E.3.: Representation of on-load tap-changing transformer for steady-state analysis in Matlab/Matpower with (a) sub-station circuit model and (b) equivalent π-circuit model.

The mathematical model of the on-load tap-changing transformer is formulated by (E.1) as the relationship between the current $\underline{I}$ and voltage $\underline{V}$ of the transformer. For small values of the transformer resistance $R_{\text{tr}} \ll X_{\text{tr}}$, the transformer impedance can be expressed by $\underline{Z}_{\text{tr}} = \mathrm{j}X_{\text{tr}}$. Then, the ideal transformer is eliminated by using three variable impedances $\underline{Z}_1 - \underline{Z}_3$ with off-nominal turns ratio $\bar{n}$, which allows the simulation and changes of tap positions in steady-state analysis.

$$\begin{cases} \underline{I}_1 = \dfrac{\underline{Y}_{\text{tr}}}{\bar{n}} \cdot (\dfrac{\underline{V}_1}{\bar{n}} - \underline{V}_2) \\ \underline{I}_2 = \underline{Y}_{\text{tr}} \cdot (\underline{V}_2 - \dfrac{\underline{V}_1}{\bar{n}}) \end{cases} \Rightarrow \begin{cases} \underline{V}_1 = X_{\text{tr}} \cdot \bar{n} \left[\dfrac{1}{1 - \dfrac{1}{\bar{n}}} \cdot \underline{I}_1 + (\underline{I}_1 - \underline{I}_2) \right] \\ \underline{V}_2 = X_{\text{tr}} \cdot \left[\bar{n}(\underline{I}_2 - \underline{I}_1) + \dfrac{1}{1 - \dfrac{1}{\bar{n}}} \cdot \underline{I}_2 \right] \end{cases} \tag{E.1}$$

The equivalent π-circuit of on-load tap-changing transformer can be derived from the second part of (E.1) and is a representative model of a two-winding transformer. Subscript 1 refers to the primary and 2 to the secondary side of the sub-station. Alternatively, line drop compensation can be applied where the voltage on the secondary side of the transformer and the load current are monitored to simulate the voltage drop along the feeder [185]. Figure E.4 shows the functional block diagram

of the implemented transformer control scheme. According to [186, 190], a (i) dead band element, (ii) time element, (iii) tap limit element and (iv) motor unit is considered for the control concept.

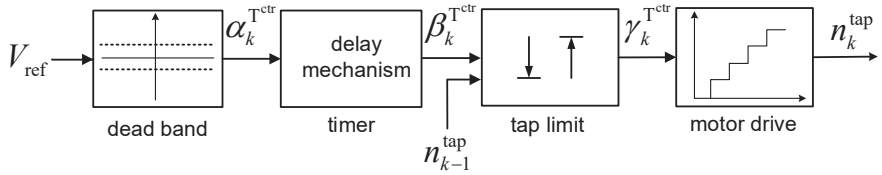

Fig. E.4.: T-control flow chart for on-load tap-changing transformers modeled with a dead band elements, tap limit elements, delay time elements, and motor drive element.

The increment turns ratio $\Delta\bar{n}_2$ of the transformer model correspond to a change of the tap position number n^{tap} by one step and is calculated by

$$\Delta\bar{n}_2 = \frac{V_2|_{n_{\text{max}}^{\text{tap}}} - V_{2\text{r}}}{n_{\text{max}}^{\text{tap}} \cdot V_{2\text{r}}} \tag{E.2}$$

$V_2|_{n_{\text{max}}^{\text{tap}}}$ defines the voltage magnitude at the secondary side of the sub-station at the maximum tap position $n_{\text{max}}^{\text{tap}}$, while $V_{2\text{r}}$ refers to the rated voltage of the secondary side. In order to prevent oscillations, the power system condition is evaluated within the dead band element through the determination of the voltage deviation $\Delta V = |V_{\text{ref}} - V_{2\text{r}}|$. The output signal $\alpha_k^{\text{T}^{\text{ctr}}}$ indicates the voltage limit exitation for each time step and is defined as follows:

$$\alpha_k^{\text{T}^{\text{ctr}}} = \begin{cases} +1, & \text{if } V_{\text{ref}} > V^{\text{lb,db}} \\ -1, & \text{if } V_{\text{ref}} < V^{\text{ub,db}} \\ 0, & \text{otherwise} \end{cases} \tag{E.3}$$

Then, $\alpha_k^{\text{T}^{\text{ctr}}}$ is forwarded to the delay element. Within the timer element, the output signal $\beta_k^{\text{T}^{\text{ctr}}}$ is calculated by (E.4). Here, the time parameter $c_k^{\text{T}^{\text{ctr}}}$ is compared to the defined delay time $T_{\text{d}}^{\text{T}^{\text{ctr}}}$ to avoid activation-deactivation cycles. The time parameter changes as specified by (E.5).

$$\beta_k^{\text{T}^{\text{ctr}}} = \begin{cases} +1, & \text{if } c_k^{\text{T}^{\text{ctr}}} \leq T_{\text{d}}^{\text{T}^{\text{ctr}}} \\ -1, & \text{if } c_k^{\text{T}^{\text{ctr}}} \geq -T_{\text{d}}^{\text{T}^{\text{ctr}}} \\ 0, & \text{otherwise} \end{cases} \tag{E.4}$$

$$c_k^{\mathrm{T^{ctr}}} = \begin{cases} c_{k-1}^{\mathrm{T^{ctr}}} + 1\mathrm{s}, & \text{if } \alpha_k^{\mathrm{T^{ctr}}} = +1 \text{ and } c_{k-1}^{\mathrm{T^{ctr}}} \geq 0\mathrm{s} \\ c_{k-1}^{\mathrm{T^{ctr}}} - 1\mathrm{s}, & \text{if } \alpha_k^{\mathrm{T^{ctr}}} = -1 \text{ and } c_{k-1}^{\mathrm{T^{ctr}}} \leq 0\mathrm{s} \\ 0, & \text{otherwise} \end{cases} \tag{E.5}$$

The delay mechanism is reset in case the voltage limit excitation at the bus changes. The tap limit element restricts the tap-changer within the defined minimum tap position and maximum tap position $n_{\mathrm{min}}^{\mathrm{tap}} \leq n_k^{\mathrm{tap}} \leq n_{\mathrm{max}}^{\mathrm{tap}}$. In case the tap-changer reaches the tap limit, the actual tap position number remains. The delay time $T_{\mathrm{d}}^{\mathrm{T^{ctr}}}$ is used for the first tap movement to prevent unnecessary tap-changes caused by transient and short-term voltage variations. Alternatively, the delay time characteristics can be modeled as function of the delay time of the first movement [234]. Here, the transformer control behave inversely proportional to the voltage deviation with a regulator dead band and allows the introduction of intentional delay time between consecutive tap movements [235]. Finally, the tap position changes with constant move times $T_{\mathrm{m}}^{\mathrm{T^{ctr}}}$ through the adjustment of the turns ratio $\bar{n}$ as calculated by (E.6), with γ_k^{tap} as the output signal of the tap limit element.

$$\bar{n}_{\mathrm{k}} = \bar{n}_{k-1} + \gamma_k^{\mathrm{tap}} \cdot \Delta\bar{n}_2 \quad \text{with} \quad \gamma_k^{\mathrm{T^{ctr}}} = \begin{cases} +1, & \text{if } \beta_k^{\mathrm{T^{ctr}}} = +1 \\ -1, & \text{if } \beta_k^{\mathrm{T^{ctr}}} = -1 \\ 0, & \text{otherwise} \end{cases} \tag{E.6}$$

The adjustment of the tap-changer position within the motor element is expressed by the increment turns ratio $\Delta\bar{n}_2$. The control concept is applied to the on-load tap-changing transformers, which are modeled with the parameters as listed in Table E.1.

TABLE E.1.: Equivalent transformer parameters with corresponding impedance $\underline{Z}_{\mathrm{tr}}$ and rated apparent power S_{r} capacity.

from bus	to bus	connection*)	$V_{1\mathrm{r}}$ (kV)	$V_{2\mathrm{r}}$ (kV)	$\underline{Z}_{\mathrm{tr}}$ (Ω)	S_{r} (MVA)
1	2	3-ph Ynd	110	20	$0.016 + \mathrm{j}1.92$	25
1	13	3-ph Ynd	110	20	$0.016 + \mathrm{j}1.92$	25

*) realized with 3-phase wye-delta and neutral solidly grounded.

The transformer impedance $\underline{Z}_{\mathrm{tr}}$ refers to the primary side of the sub-station where the transformer resistance R_{tr}^* and reactance X_{tr}^* are calculated by (E.7). The electrical quantities are represented in the per unit system and are normalized to the base apparent power S_{base}.

$$R^*_{\mathrm{tr}} = \frac{R_{\mathrm{tr}}}{Z_{\mathrm{base}}} \quad \text{and} \quad X^*_{\mathrm{tr}} = \frac{X_{\mathrm{tr}}}{Z_{\mathrm{base}}} \quad \text{with} \quad Z_{\mathrm{base}} = \frac{V^2_{2\mathrm{r}}}{S_{\mathrm{base}}} \tag{E.7}$$

In case of transformer maintenance or failures, parallel operation of the transformers positioned adjacently and feeding the same bus can supply the feeder sections without interruption to meet the $n-1$ criterion [236]. Therefore, parallel tap-changing transformers need to be at same ratio and same polarity when operating to improve the voltage performance [237]. Basically, the following configurations can be considered

- sub-station 1: three transformers (A,B,R), where A and B can be operated with 100% of the rated capacity, while R as the third transformer serves as reserve
- sub-station 2: two transformers (A,B) are operated with lower capacity utilization $< 50\%$ of the rated capacity.

As a simplification, the presented network model includes representative sub-station transformer models without parallel operations. The two feeder sections with substations are connected to the primary sub-transmission system. The initial tap position is arbitrarily assumed to be 10 and 5 for the tap-changing transformer at feeder section 1 and section 2, respectively. While feeder section 2 is supplied by overhead lines, the remaining buses in feeder section 1 are interconnected by underground cables. The geometry and conductor type of the overhead lines is designated using international notation as specified in IEC 61089. The tabulated values of the phase conductor diameter d_{c}, geometric mean radius GMR, direct current resistance per phase unit length R'_{dc}, and alternating current resistance per phase unit length R'_{ac} are given as conductor parameters, obtained from IEC 61597 [197]. The line types and constants used for overhead lines are listed in Table E.2. The conductor identification number (ID 1) refers to bare conductors made of aluminum, with or without steel reinforcement.

TABLE E.2.: Specifications of overhead lines with conductor parameters and characteristics for the geometry and conductor type.

cond. ID	type	stranding	cross-sectional area	d_{c}	GMR	R'_{dc} at 20 °C	R'_{ac} at 50 °C
			(mm^2)	(cm)	(cm)	(Ω/km)	(Ω/km)
1	A1	7	63	1.02	0.370	0.4545	0.5100

The designated values and conductor types can also be replaced with normative ref-

erences for aluminum conductor types AL1 or AL1/ST1A steel-reinforced according to DIN EN 50182. Conductor types for underground cables are designated using the German DIN VDE notation for underground cables. Values of d_c, R'_{dc}, and R'_{ac} are obtained from [238] with stranding and geometric mean radius from [239]. Table E.3 provides the associated conductor constants for underground cables. The conductor identification number (ID 2) refers to underground cables with cross-linked polyethylene round, stranded aluminum conductors and copper tape shields.

TABLE E.3.: Specifications of underground cables with conductor parameters and characteristics for the geometry and conductor type.

cond. ID	type	stranding	cross-sectional area	d_c	GMR	R'_{dc} at 20 °C	R'_{ac} at 90 °C
			(mm^2)	(cm)	(cm)	(Ω/km)	(Ω/km)
2	NA2XS2Y	19	120	1.24	0.480	0.253	0.338

Specification on the thickness of insulation, outer jacket, tape shield, and overall diameter of conductor are provided in [197] to calculate the geometry and distances between phase conductors. In order to determine the phase resistance R'_{ph}, reactance X'_{ph} and susceptance B'_{ph}, the modified Carson's equations are obtained as further detailed in [197] and [240], respectively. Figure E.5 exemplary describes the single-phase equivalents used in the network model. Here, it is assumed that the power system is operated as a three phase balanced system.

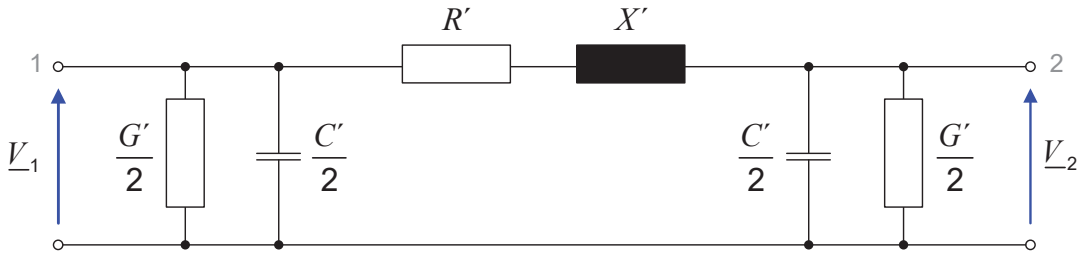

Fig. E.5.: Simplified equivalent π-circuit model diagram.

The conductance G'_{ph} specifies the leakage current on the surface of the overhead lines and the dielectric losses in the solid insulation of the underground cables. The electrical quantities are used for the calculation of the admittance $\underline{Y}'$ according (E.8). For $G'_{ph} \ll B'_{ph}$, $\underline{Y}'$ can be simplified as a function of the angular frequency ω dependent on the capacitive reactance C'_{ph}.

$$\underline{Y}' = \mathrm{j}\omega C'_{ph} \quad \text{with} \quad \underline{Y}' = G'_{ph} + \mathrm{j}B'_{ph} = 0 + \mathrm{j}\omega C'_{ph} \quad \text{and} \quad \underline{Z}' = \frac{1}{\mathrm{j}\omega C'_{ph}} \tag{E.8}$$

In order to determine the rated power capacity $S_{\mathrm{r}}^{\mathrm{A,B,C}}$ of the integrated system devices, the effective values of the rated base voltage $V_{2\mathrm{r}}$ and the maximum current carrying capacity $I_{\mathrm{ph,max}}$ of the respective conductors is calculated

$$S_{\mathrm{r}}^{\mathrm{A,B,C}} = V_{2\mathrm{r}} \cdot I_{\mathrm{ph,max}} \cdot \sqrt{3} \tag{E.9}$$

where A refers to long term rating, B to short term rating and C to emergency rating. For simplification the ratings are considered to be equal. The conductor attributes are transformed into the per unit system by applying (E.7) and are summarized in Table E.4. The tabulated line lengths l_{br} can be modified with respect to predetermined voltage ranges.

TABLE E.4.: Equivalent conductor parameters per phase unit length.

from bus	to bus	R'	X'	B'	$S_{\mathrm{r}}^{\mathrm{A,B,C}}$	l_{br}	cond. ID *)
		(p.u.)	(p.u.)	(p.u.)	(MVA)	(km)	
1	2	0.0040	0.4800	0.00E+00	25.00	-	3
1	13	0.0040	0.4800	0.00E+00	25.00	-	3
2	3	0.1253	0.1788	1.90E-04	11.10	2.82	2
3	4	0.1253	0.1788	1.90E-04	11.10	4.42	2
4	5	0.1253	0.1788	1.90E-04	11.10	0.61	2
5	6	0.1253	0.1788	1.90E-04	11.10	0.56	2
6	7	0.1253	0.1788	1.90E-04	11.10	1.54	2
7	8	0.1253	0.1788	1.90E-04	11.10	0.24	2
8	9	0.1253	0.1788	1.90E-04	11.10	1.67	2
9	10	0.1253	0.1788	1.90E-04	11.10	0.32	2
10	11	0.1253	0.1788	1.90E-04	11.10	0.77	2
11	12	0.1253	0.1788	1.90E-04	11.10	0.33	2
12	5	0.1253	0.1788	1.90E-04	11.10	0.49	2
4	9	0.1253	0.1788	1.90E-04	11.10	1.30	2
13	14	0.1275	0.0915	1.27E-05	9.35	4.89	1
14	15	0.1275	0.0915	1.27E-05	9.35	2.99	1
15	19	0.1275	0.0915	1.27E-05	9.35	2.00	1

*) conductor ID refers to: (1) overhead line, (2) underground cable, (3) transformer.

For further steady-state analysis in Matlab/Matpower, the introduced transformer and conductor parameters may be replaced and the branch matrix modified, accordingly.

E.3. Load Model with Distributed Time-Varying Load Demand

The loads served in the distribution system are characterized by residential and industrial/commercial loads. With respect to permissible operating limits, the rate of utilization λ_k^{ur} is calculated in every time step k by (E.10). The factor expresses the ratio of the served apparent power demand $S_{\mathrm{d},k}$ in relation to the rated apparent power S_{r} of the respective system device.

$$\lambda_k^{\mathrm{ur}} = \frac{S_{\mathrm{d},k}}{S_{\mathrm{r}}} = \frac{\sqrt{P_{\mathrm{d},k}^2 + Q_{\mathrm{d},k}^2}}{S_{\mathrm{r}}} \qquad \forall k \in H_{\mathrm{ts}} \ . \tag{E.10}$$

The load demand is decomposed into the sum of active $P_{\mathrm{d},k}$ and reactive $Q_{\mathrm{d},k}$ power demand. The loading conditions are modeled via hourly based load coincidence factors $\boldsymbol{\kappa}_{\mathrm{d}}$ as summarized in Table E.5.

TABLE E.5.: Hourly based load coincidence factors $\boldsymbol{\kappa}_{\mathrm{d}}^{\mathrm{red}}$ and $\boldsymbol{\kappa}_{\mathrm{d}}^{\mathrm{ind}}$ for residential and industrial/commercial loads.

time (h)	1	2	3	4	5	6	7	8	9	10	11	12
$\boldsymbol{\kappa}_{\mathrm{d}}^{\mathrm{red}}$	0.21	0.18	0.18	0.18	0.24	0.40	0.64	0.64	0.65	0.68	0.60	0.73
$\boldsymbol{\kappa}_{\mathrm{d}}^{\mathrm{ind}}$	0.32	0.28	0.30	0.36	0.47	0.60	0.88	1.00	0.98	0.99	0.79	0.84
time (h)	13	14	15	16	17	18	19	20	21	22	23	24
$\boldsymbol{\kappa}_{\mathrm{d}}^{\mathrm{red}}$	0.70	0.56	0.50	0.45	0.66	0.85	0.88	0.82	0.67	0.60	0.40	0.25
$\boldsymbol{\kappa}_{\mathrm{d}}^{\mathrm{ind}}$	0.86	0.86	0.86	0.80	0.54	0.48	0.45	0.41	0.39	0.36	0.33	0.32

Table E.6 provides the values of the coincident maximum load $S_{\mathrm{d,max}}$ for each bus as reported in [197]. The power factor denotes the ratio of the maximum active and apparent power demand at each bus. Accordingly, the load distribution of the active power demand $P_{\mathrm{d},k}$ for each time step can be calculated as follows

$$\boldsymbol{P}_{\mathrm{d},k} = \left(\boldsymbol{S}_{\mathrm{d,max}}^{\mathrm{red}} \circ \boldsymbol{pf}_{\mathrm{d}}^{\mathrm{red}}\right) \cdot \boldsymbol{\kappa}_{\mathrm{d},k}^{\mathrm{red}} + \left(\boldsymbol{S}_{\mathrm{d,max}}^{\mathrm{ind}} \circ \boldsymbol{pf}_{\mathrm{d}}^{\mathrm{ind}}\right) \cdot \boldsymbol{\kappa}_{\mathrm{d},k}^{\mathrm{ind}} \quad \forall k \in H_{\mathrm{ts}} \tag{E.11}$$

where $\boldsymbol{S}_{\mathrm{d,max}}^{\mathrm{red}}$ and $\boldsymbol{S}_{\mathrm{d,max}}^{\mathrm{ind}}$ denote the residential and industrial maximum loads, and $\boldsymbol{pf}_{\mathrm{d}}^{\mathrm{red}}$ and $\boldsymbol{pf}_{\mathrm{d}}^{\mathrm{red}}$ the corresponding power factors. Using the tabulated values in steady-state analysis, the maximum rates of utilization is $\|\lambda^{\mathrm{ur}}\|_\infty \leq 0.7$ and the power system voltages remain in acceptable limits in each load level.

In order to model more critical time-varying voltage variations in the power system, the load characteristics are adjusted while the total coincident maximum loads remain the same. Also the power factors as listed in Table E.6 remain unchanged, but have a significant impact on the voltage characteristics [235, 241].

TABLE E.6.: Load characteristic and adjustments of the European 20 kV distribution network benchmark with residential $S^{\text{red}}_{\text{d,max}}$ and industrial $S^{\text{ind}}_{\text{d,max}}$ coincident maximum loads.

bus ID	original values		adjusted values		power factor	
	$S^{\text{red}}_{\text{d,max}}$	$S^{\text{ind}}_{\text{d,max}}$	$S^{\text{red}}_{\text{d,max}}$	$S^{\text{ind}}_{\text{d,max}}$	$pf^{\text{red}}_{\text{d}}$	$pf^{\text{ind}}_{\text{d}}$
	(MVA)	(MVA)	(MVA)	(MVA)	(p.u.)	(p.u.)
1	0.00	0.00	0.00	0.00	0.00	0.00
2	15.30	5.10	3.30	2.10	0.98	0.98
3	0.00	0.00	2.00	0.00	0.00	0.00
4	0.29	0.27	1.29	0.27	0.97	0.85
5	0.45	0.00	0.45	0.00	0.97	0.00
6	0.74	0.00	0.74	0.00	0.97	0.00
7	0.57	0.00	2.57	0.50	0.97	0.00
8	0.00	0.09	1.00	2.59	0.00	0.85
9	0.61	0.00	2.61	0.00	0.97	0.00
10	0.00	0.68	2.00	1.68	0.00	0.85
11	0.49	0.08	2.49	0.08	0.97	0.85
12	0.34	0.00	0.34	0.00	0.97	0.00
13	15.30	5.28	6.30	3.28	0.98	0.95
14	0.00	0.04	4.00	1.04	0.00	0.85
15	0.22	0.39	5.22	0.39	0.97	0.85
SUM	34.29	11.92	34.29	11.92		

E.4. Power System Sensitivity Analysis and Voltage Stability Evaluation

To identify sensitive and critical buses in the network model and to assess the effect of active and reactive power adjustments on voltage stability, sensitivity analysis derived from Q-V characteristics and V-P characteristics are performed. The results are obtained from power flow analysis performed in Matlab/Matpower and summarized in Fig E.6. The obtained curves show the highest slopes and represent the change of the voltage magnitude ΔV at the bus that is most sensitive to

active ΔP or reactive power ΔQ changes. In comparison, the curves with the lowest slopes are less sensitive to the same power changes. The Q-V characteristics and V-P characteristics of the remaining buses are between the identified extreme curves. At lower voltage values, the voltage drops fast as the load demand increases. The power flow solution fails to converge beyond this limit and indicates the voltage instability of the power system. Hence, the operating points above the critical points represent satisfactory operating conditions [235]. Therefore, the highest power generation or load demand at each bus should be beyond the limiting rated capacities of the considered power system devices, e.g. conductor parameters for overhead lines. In combination with the associated voltage ranges between 0.94 p.u. $<$ V $<$ 1.04 p.u., the operation area is defined as shown in Fig. E.6a and highlighted with grey rectangles.

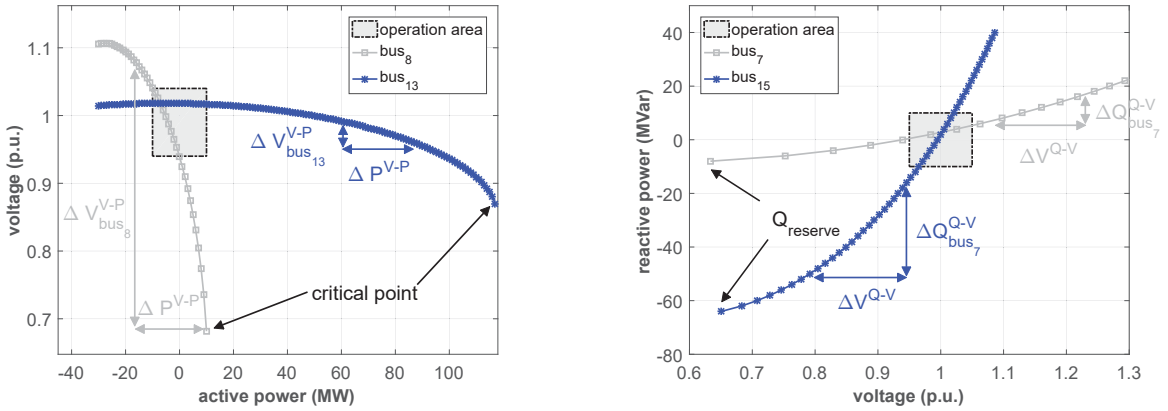

(a) V-P characteristics

(b) Q-V characteristics

Fig. E.6.: Voltage stability analysis with (a) V-P characteristics and (b) Q-V characteristics of the European 20 kV distribution network benchmark.

For the determination of the Q-V characteristics, the active power demand is kept constant, and the voltage stability is evaluated under consideration of the incremental relationship between reactive power and voltage magnitudes at each bus. This method allows to examine the requirements for the provision of reactive power compensation. Although the obtained V-P characteristics and Q-V characteristics are appropriate for voltage stability analysis, there are limitations by the use of power flow calculations, which may not converge. In that case, the use of the Q-V sensitivity is proposed by [242]. The derivation of the Q-V characteristics calculated by (E.12) indicates the voltage stability at each bus.

$$\begin{bmatrix} \Delta \boldsymbol{P} \\ \Delta \boldsymbol{Q} \end{bmatrix} = \begin{bmatrix} \boldsymbol{J}_{\mathrm{P}\theta} & \boldsymbol{J}_{\mathrm{PV}} \\ \boldsymbol{J}_{\mathrm{Q}\theta} & \boldsymbol{J}_{\mathrm{QV}} \end{bmatrix} \cdot \begin{bmatrix} \Delta \boldsymbol{\theta} \\ \Delta \boldsymbol{V} \end{bmatrix} \tag{E.12}$$

The deviations of the active power P, reactive power Q, voltage magnitude V,

and voltage angle θ are associated for each bus of the power system. With $\Delta P = 0$, (E.12) can be rewritten in the reduced Jacobian matrix $\boldsymbol{J}_{\mathrm{R}}$ as follows:

$$\boldsymbol{J}_{\mathrm{R}} = (\boldsymbol{J}_{\mathrm{QV}} - \boldsymbol{J}_{\mathrm{Q}\theta} \cdot \boldsymbol{J}_{\mathrm{P}\theta}^{-1} \cdot \boldsymbol{J}_{\mathrm{PV}}). \tag{E.13}$$

The $i-$ th diagonal element of $\boldsymbol{J}_{\mathrm{R}}^{-1}$ is the Q-V sensitivity $\lambda_{\mathrm{bus}_i}^{\mathrm{Q-V}}$, where the reciprocal value of $\lambda_{\mathrm{bus}_i}^{\mathrm{Q-V}}$ represents the slope of the Q-V curve. Positive values of the Q-V sensitivity indicate stable operation areas, whereas small and negative values correspond to unstable operation areas. Hence, the relationship between the Q-V sensitivity and Q-V characteristics can be described by

$$\Delta \boldsymbol{Q} = \boldsymbol{J}_{\mathrm{R}} \Delta \boldsymbol{V} \qquad \text{, with} \qquad \frac{1}{\lambda_{\mathrm{bus}_i}^{\mathrm{Q-V}}} = \frac{\Delta Q_{\mathrm{bus}_i}^{\mathrm{Q-V}}}{\Delta V_{\mathrm{bus}_i}^{\mathrm{Q-V}}}. \tag{E.14}$$

The Q-V characteristics obtained from the power flow calculations can be summarized by (E.15). For example, with a given change of the voltage magnitude $\Delta \boldsymbol{V}^{\mathrm{Q-V}}$, the results indicate that more incremental reactive power $\Delta \boldsymbol{Q}^{\mathrm{Q-V}}$ is required at bus 15.

$$\lambda_{\mathrm{bus}_{15}}^{\mathrm{Q-V}} \leq \lambda_{\mathrm{bus}_i}^{\mathrm{Q-V}} \leq \lambda_{\mathrm{bus}_7}^{\mathrm{Q-V}} \tag{E.15}$$

Furthermore, it is shown that bus 7 has less reactive power reserves with 10 MVar compared to bus 15 with 50 MVar. This indicates that bus 7 requires less reactive power compensation to maintain the bus voltages within the stipulated limits. In case that the feeder sections are operated in radial structure, bus 7 is set as sensitive bus for feeder section 1 and bus 15 as sensitive bus for feeder section 2. These buses are defined as references buses for transformer control using load drop compensation. In case that the structure of the power system changes the sensitive bus has to be redetermined. In summary, the results show that the network model can be operated in stable conditions as the Q-V sensitivity is positive at each bus and within the defined operation areas.

E.5. Generation Model and Generation Dispatch

The generation profiles of the conventional and controllable generators are determined through solving the optimal power flow problem. The calculations consider the selection of the lowest-cost generation dispatch for a set of generators H_{gen} , and is constrained by individual generator limits while fulfilling power system con-

straints, e.g. power capacity rating of power system devices, power limits of generation or voltage limits of buses. According to [189], the generation dispatch is modeled with a number of data points for piecewise linear generator cost and a total cost function. The cost of each generator is based on the active power generation per MW in EUR/h and reactive power generation per MVar in EUR/h. The cost function for the active power generation $f(p)$ is defined by the coordinates (p_1, f_1), (p_2, f_2) and (p_3, f_3). The same applies to the cost function of reactive power generation. The objective function is a summation of individual polynomial cost functions f_{P}^i and f_{Q}^i of active and reactive power injections and defined by

$$\min_{\theta,V,P_{\mathrm{g}},Q_{\mathrm{g}}} \sum_{i \in H_{\mathrm{gen}}} \left(f_{\mathrm{P}}^i(p_{\mathrm{g}}^i) + f_{\mathrm{Q}}^i(q_{\mathrm{g}}^i) \right). \tag{E.16}$$

The extended European 20 kV distribution network benchmark includes two controllable generators in order to provide local power in each feeder section. Table E.7 summarizes the defined generator characteristics with startup, shutdown and cost function specifications. The values have been extracted from the IEEE-9 bus system [243], whereby the currency is changed to EUR.

TABLE E.7.: Location of conventional and controllable generators and characteristics with cost function specifications of the IEEE-9 bus system.

bus ID	$P_{\mathrm{g,max}}$ (MW)	$Q_{\mathrm{g,max}}$ (MVar)	startup (EUR)	shutdown (EUR)	cost function coordinates (EUR/h per MW)		
1*)	50	50	1,500	0	0.1100	5.0	150
12	10	7.5	2,000	0	0.0850	1.2	600
14	5	3.75	3,000	0	0.1225	1.0	335

*) slack bus

The maximum active power generation $P_{\mathrm{g,max}}$ is set to 10 MW and 5 MW, respectively. Further, the maximum power output of the generators are limited by the maximum reactive power generation $Q_{\mathrm{g,max}}$ and the defined power factors of the generators and set to $pf = 0.8$ in per unit.